THE REACTIONS OF n-OCTANE ON SUPPORTED PLATINUM CATALYSTS

THESIS

SUBMITTED FOR THE DEGREE

OF

DOCTOR OF PHILOSOPHY

OF THE

UNIVERSITY OF GLASGOW

BY

JAMIE MACLIVER ROY, BSc

DEPARTMENT OF CHEMISTRY

JANUARY, 1992

ProQuest LLC.
789 East Eisenhower Parkway
P.O. Box 1346
Ann Arbor, MI 48106 – 1346

TO MUM AND DAD

ACKNOWLEDGEMENTS

I would like to express my thanks to Professor G. Webb, my supervisor and to Dr. M. Day, my industrial supervisor, for proposing the topic for this thesis and for their advice and cooperation during the last four years.

Thanks also to everyone in Surface Chemistry for their good company over the years and to the staff of the mechanical and electronic workshops for their invaluable technical assistance. Special thanks are due to Dr. Mark Keane for his proof reading of this work. In addition, I would like to thank everyone in the Micromeritics Laboratory at ICI Wilton for their help during my industrial visits.

I am indebted to the Science and Engineering Research Council and ICI Chemicals and Polymers Division for the award of a CASE studentship.

Finally, I would like to thank my Mother and Father for their great support and encouragement.

CONTENTS

CHAPTER FOUR - EXPERIMENTAL

CHAPTER FIVE - RESULTS

CHAPTER SIX - DISCUSSION

SUMMARY

The reaction of n-octane with hydrogen on 0.9% w/w Pt/γ-alumina/Cl^- (GHI), 0.3% w/w Pt/γ-alumina/Cl^- (EUROPT 3) and 0.3% w/w Pt - 0.3% w/w Re/γ-alumina/Cl^- (EUROPT 4) has been investigated. Catalyst activity, selectivity and stability were determined using a microcatalytic reactor under realistic reforming conditions of moderate pressure (110 psig) and high temperature (450-500°C).

Each of the EURO catalysts has been extensively characterised by temperature - programmed reduction (TPR), carbon monoxide chemisorption, transmission electron microscopy, physical adsorption of nitrogen and mercury porosimetry, the GHI catalyst was investigated using the latter two techniques only, having been partially characterised in an earlier study.

The TPR profile for EUROPT 3 indicates that precalcination of the catalyst at high temperature leads to a strong interaction between the metal oxide and the support, whilst comparison of the TPR profiles for EUROPT 3 and EUROPT 4 shows that, in the case of EUROPT 4, simaltaneous reduction of the platinum and rhenium components occurred, the latter at a lower temperature than would be expected for rhenium alone, possibly implying an interaction between the two metals. With the EURO catalysts, the hydrogen uptakes were consistent with complete reduction from Pt^{4+} and Re^{7+}.

The carbon monoxide adsorption capacities of EUROPT 3 and EUROPT 4 were very similar suggesting that no CO adsorption occurred on the Re component of

the latter. From saturation CO coverages Pt dispersions of 81.2% and 83.3% were obtained for EUROPT 3 and EUROPT 4 respectively and an average metal particle size of 1.5 nm calculated for EUROPT 3, this small particle size being consistent with the failure to observe any metal particles in the freshly reduced catalysts by transmission electron microscopy.

Nitrogen physical adsorption and mercury porosimetry measurements showed that all three catalysts had a mesoporous structure with a narrow distribution of pore sizes. Not surprisingly, since the same support material was used, the BET areas of EUROPT 3 and EUROPT 4 were similar (193.2 and 195.8 $m^2 g^{-1}$ respectively) and were approximately twice that for the GHI catalyst (95.5 $m^2 g^{-1}$).

In the reaction of n-octane on the two monometallic catalysts, GHI and EUROPT 3, the activity of the latter, as determined by the overall n-octane conversion, was much greater, in line with its higher metal dispersion, larger alumina surface area and more extensive activation procedure. Products due to hydrocracking, hydrogenolysis, isomerisation and aromatisation were formed over each catalyst, although the orders of selectivities were different over the two. Thus, with the GHI catalyst, the selectivities decreased in the order, aromatisation > hydrocracking > hydrogenolysis > isomerisation. An increase in isomerisation activity together with a decrease in hydrocracking activity, observed with increased time-on-stream, is interpreted in terms of coke deposition on the alumina support, together with a loss of support chloride. The observed decrease in hydrogenolysis activity with increased catalyst usage is ascribed to coke deposition on the metal function. With EUROPT 3 at 500°C, the selectivites were in the order, aromatisation > hydrocracking >

isomerisation > hydrogenolysis. Coke deposition was greater on EUROPT 3 than on the GHI catalyst and the decline in the yield of aromatic products with time-on-stream is attributed to increasing coke deposition on the metal component of EUROPT 3.

Comparison of the results obtained for the reaction of n-octane on EUROPT 3 and EUROPT 4 clearly shows that the incorporation of rhenium results in important changes in product yields and selectivities. EUROPT 4 is characterised by a high selectivity for hydrogenolysis. This, together with the observation of a lower coking rate on EUROPT 4, compared with EUROPT 3, is taken as a clear demonstration of the active role that rhenium plays in attenuating coke formation by catalysing the fission and hydrogenation of coke precursors. At 500°C, the order of selectivities over EUROPT 4 was:

aromatisation > hydrocracking > hydrogenolysis > isomerisation,

whilst at 450°C, after 20 hours-on-stream, the order was:

aromatisation > hydrogenolysis > isomerisation > hydrocracking

In conclusion, the results obtained in the present study show the importance of platinium dispersion, presence of rhenium and of catalyst acidity in determining the coking characteristics and, hence, the activities and selectivities for various products from the reaction of n-octane with hydrogen.

CHAPTER ONE

INTRODUCTION

CHAPTER ONE

INTRODUCTION

1.1 CATALYTIC REFORMING

1.1.1 Industrial Significance

Catalytic reforming is one of the principal petroleum refining processes and has developed over the last four decades to the point where it is now one of the most important industrial applications of catalysis.

With the exception of ethanol, in use in a few countries only, almost all fuels used today in modern internal combustion engines are formulated around high octane bases resulting from catalytic reforming. With the development of the petrochemicals industry reforming has also become the favoured process in most refineries for producing hydrogen and aromatics, in particular, benzene, toluene and xylenes. These aromatics are subsequently used in the manufacture of a diverse range of valuable oil-based products such as plastics, paints, detergents and dyes (1).

The hydrocarbon feedstock used in the reforming process is referred to by the generic term "naptha". Naptha fractions are composed of hydrocarbons with boiling points in the approximate temperature range 40-200°C and contain a mixture of paraffins, aromatics and napthenes (fully hydrogenated 5- and 6-membered ring compounds). The exact chemical composition of napthas varies widely between different geographical sources of crude oil. Although the aromatic concentration rarely exceeds 20% by volume the napthene content can vary from 10 to 70% (2). Table 1.1 presents a detailed analysis of two reforming feedstock napthas; feedstock a) is a paraffinic Middle East crude and feedstock b) is a napthenic Nigerian crude (3).

	Paraffins	Napthenes	Aromatics
Feedstock a)			
C_5	-	-	-
C_6	5.49	2.30	0.41
C_7	16.83	5.80	3.18
C_8	21.38	8.27	6.80
C_9	17.26	5.95	3.08
C_{10}	2.59	0.63	-
Total	63.55	22.95	13.47
RON = 50			
Feedstock b)			
C_5	0.16	0.27	-
C_6	3.31	5.78	0.20
C_7	6.13	14.24	1.20
C_8	9.79	14.47	3.54
C_9	3.89	17.14	4.29
C_{10}	3.59	11.17	0.88
Total	26.81	63.07	10.10
RON = 66			

Table 1.1 - Detailed analysis of two reforming feedstocks by weight % (3).

Feed napthas are further characterised by their sulphur, nitrogen and trace metal contents. The most important source of napthas is from the fractional distillation of crude oil; thermal and catalytic hydrocracking processes remain a secondary source.

Despite the importance of the petrochemicals industry it still only accounts for approximately 10% of all crude oil used (1). The primary use for oil has always been as a fuel, particularly for transportation. The requirement for high octane fuels is due, therefore, to the use of high compression, spark ignition, internal combustion engines and their predominance in today's developed world.

The octane rating of a fuel is a measurement of its anti-knock properties under compression and prior to spark ignition. The octane number is quantitative and indicates the ability of a hydrocarbon mixture or pure hydrocarbon to resist detonation under a rise in temperature due to compression (knocking). The fuel being tested is assigned an octane number based on comparative performance tests in a standardised motor engine using a standardised fuel. When the motor rotates at 600 rpm the octane number is defined as the Research Octane Number (RON); this corresponds to the volume percent of iso-octane (2,2,4-trimethyl pentane) that is blended with n-heptane to match the performance of the sample fuel. Iso-octane is assigned a value of 100 RON on an arbitrary scale while n-heptane has a value of 0. When a sample fuel's octane number exceeds 100, tetra ethyl lead is added to iso-octane to improve the reference. Typically today's internal combustion engines require a high octane fuel of between 92 and 98 RON (3).

Figure 1.1 shows the relationship between research octane number and various low molecular weight hydrocarbons (1,4).

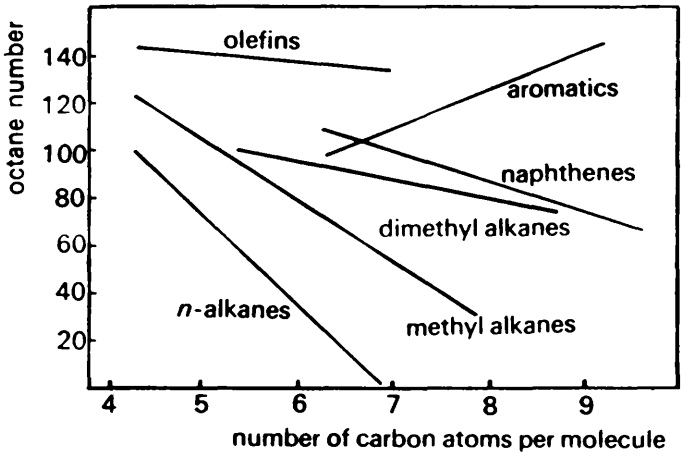

Figure 1.1 Octane number as a function of chemical composition.

It is apparent from figure 1.1 that the octane number of the paraffins increases with 1) the degree of branching 2) the degree of unsaturation and 3) their transformation into aromatics. With the exception of aromatic hydrocarbons the octane number decreases with increasing carbon number or molecular weight. High concentrations of olefins in fuels are known to cause engine fouling problems. Consequently, despite their high anti-knock ratings, their production is undesired.

It is primarily the formation of aromatics, whose research octane number is always above 100, that causes the largest increase in the octane rating of naptha feedstocks. This is achieved by the dehydrocyclisation of paraffins and by the dehydrogenation of napthenes. An increase in the concentration of iso-paraffins and a commensurate decrease in their overall molecular weight further contributes, albeit

to a more modest degree, to an improvement in product research octane number. The specific aim of catalytic reforming is therefore to produce aromatic hydrocarbons as selectively as possible while decreasing the overall molecular weight to a limited extent.

Industrial reforming is typically carried out in the temperature range 480-530°C. Reaction pressures may vary between 10 and 35 atmospheres (5). The exact conditions used depends upon several factors including the feedstock composition and the product requirements.

1.1.2 Reforming Catalysts

Reforming catalysts are bifunctional in nature. In other words the catalyst has both an acidic and a metallic function, each contributing independently to the major reactions. In addition to catalysing hydrogenation and dehydrogenation reactions, reforming catalysts also catalyse hydrocarbon rearrangements of a type commonly observed in acid catalysis.

The first commercial catalytic naptha reforming process was introduced in the early 1940's. The molybdenum or chromium oxide-alumina catalysts employed, incorporated both catalytic functions on the surface of the metal oxide (6). Following extensive investigations which focussed on the hydrogenation-dehydrogenation properties of selected transition metals, several new classes of hydrocarbon conversion catalysts were developed. These catalysts consisted of a metal such as platinum,

palladium, iridium or rhodium supported on an acidic oxide such as silica-alumina or alumina. It was demonstrated that platinum offered the best combination of availability and catalytic activity for the preferred hydrocarbon hydrogenation-dehydrogenation reaction (7). In addition, the platinum based catalysts were shown to possess far superior selectivity, activity and maintenance of activity than that of the chromium and molybdenum based oxides. Accordingly, the metal oxide catalysts were replaced in the early 1950's by the new bifunctional platinum-alumina systems.

The monometallic platinum-alumina catalyst is usually prepared by impregnation of a very pure alumina with an aqueous solution of hydrochloric and chloroplatinic acid (H_2PtCl_6). The relative quantities of alumina and chloroplatinic acid are chosen such that a catalyst with, typically, between 0.2 and 1% platinum by weight is produced. The loading of platinum is a compromise between the basic cost of the metal, the intrinsic hydrogenation-dehydrogenation activity of the metal and its capacity to maintain that activity in use. The impregnated alumina is then activated by a series of carefully controlled drying, calcination and reduction steps.

The platinum is supported on the alumina surface as very small crystallites which are usually in the size range 80-100 Å diameter (8). Crystallite size is known to be affected by the calcination and reduction steps. Crystallite size growth during calcination, for example, is associated with the formation of volatile platinum chlorides from the metal salt. The platinum salts are believed to be carried from small to large crystallites by a vapour transport mechanism (8,9). Work by Guenin et al. (10) has demonstrated that hydrogen pressure also plays a role in determining

crystallite size; in particular, reduction at low hydrogen pressures leads to smaller metal crystallites.

Near uniform distribution of the metal is achieved by the activation process and dispersion, as measured by electron microscopy and selective chemisorption of hydrogen or carbon monoxide, is typically close to 1.

Acid catalysed reactions on the bifunctional catalyst are associated with sites on the surface of the alumina support. Alumina is an aluminum oxide; a member of a class of binary oxides in which the oxygen ions have a close packed structure. Aluminas are characterised by high surface areas (150-500 m^2/g) and may be prepared by flame hydrolysis of crystallised aluminum hydroxides and aluminum chlorides or, more commonly, by precipitation and thermal ageing of colloidal gels. The colloidal gel method of preparation is preferred as the product surface area and porosity is readily adjusted by appropriate choice of gelation conditions. Aluminas exist in several allotropic forms and their exact structure is related to the method of preparation (8). The favoured materials for reforming catalysts are η - and γ-alumina. The crystallographic structure of both materials is a defect lattice of the spinel type. The η - and γ-alumina allotropes are distinguished by the distribution of the cations in tetrahedral and octahedral sites created by the cubic close packed oxygen (11). Due to the economic simplicity of its manufacture and high thermal stability the most widely used form is γ-Al_2O_3 (3).

Uncalcined alumina surfaces are terminated by a near monolayer coverage of

hydroxyl groups, the presence of which is well established and has been demonstrated by deuterium exchange and infra-red spectroscopic studies (12,13). The hydroxylated aluminum oxide surface is not strongly acidic and is more amphoteric in nature. It was demonstrated by Parry (14) in the early 1960's that the hydroxyl groups do not contribute significantly as a source of Brønsted acidity. Parry's conclusion was based on infra-red spectra of adsorbed ammonia and pyridine on the surface of γ-Al_2O_3. No adsorption bands due to ammonium or pyridinium ions, anticipated if protonic acid sites were present, were observed.

A variety of surface groups are formed when hydroxylated aluminas are activated by outgassing or calcination. The most significant change which occurs is the removal of most hydroxyl groups. The residual hydroxyl groups are still non-acidic but now exist in a variety of coordination sites. Peri reported that about 67% of the surface hydroxyl content was removed by heating γ-Al_2O_3 at approximately 500°C; this value increased to 90% when the temperature was raised to 670°C (13). The removal of hydroxyl groups from the surface involves a condensation reaction between two neighbouring hydroxyl groups and leads to the elimination of water. The process leaves an oxide ion in the outermost surface layer and an exposed, incompletely coordinated aluminum ion in the layer below; this exposed cation is electron-deficient and behaves as a Lewis acid site.

Pure activated aluminas are therefore weakly acidic and are capable of catalysing skeletal isomerisation reactions typical of carbonium ion chemistry. Pines and Haag (15),using indicator tests, confirmed that the source of acid activity in

γ-Al_2O_3 consisted of Lewis rather than Brønsted acid sites.

The acidity of hydroxyl groups on the surface of γ-Al_2O_3 can be greatly enhanced by the incorporation of small amounts of chlorine which is normally introduced in the form of alkyl or hydrogen halides. The surface of γ-Al_2O_3 in reforming catalysts normally contains 0.1 - 1% chlorine by weight (8). The interaction of electron-withdrawing chloride ions with hydroxyl groups is believed to be responsible for the promotion of surface acidity on alumina. The close proximity of the chloride species draws electrons from the O-H bond, thereby increasing the Brønsted acidity of the group. An infra-red study by Tanaka and Ogasawara (16) demonstrated that chemisorption of HCl on γ-Al_2O_3 does form Brønsted acid sites as well as non-acidic OH groups. Spectra of chemisorbed pyridine were examined before and after the alumina had been exposed to gaseous HCl. The formation of the 1545-cm^{-1} adsorption band due to the pyridinium ion was assumed to be diagnostic of the creation of Brønsted acid sites in the chlorinated product. It is apparent that the acidity of a hydroxyl group on the surface may be progressively increased as more of the OH groups surrounding it are replaced by Cl^- ions. This was confirmed by Tanaka and Ogasawara in the same study. Measurements of but-1-ene isomerisation, a typical acid catalysed reaction, over deuterated alumina samples with varying chlorine contents showed that initial rates of double-bond isomerisation and hydrogen-deuterium exchange increased as the chlorine level increased.

The preparation of alumina-supported reforming catalysts involves heating to high temperatures (500-600°C) and the presence of Lewis acid sites resulting from

dehydroxylation reactions is readily envisaged. Lewis acid sites on the surface of the γ-Al_2O_3, associated with incompletely coordinated aluminum ions, are also likely to be enhanced by the presence of neighbouring, electron withdrawing chloride ions (17).

In the case of chlorinated alumina surfaces therefore, both Brønsted and Lewis acid sites may be active in promoting hydrocarbon conversion reactions. The importance of each source of acidity is difficult to quantify. However, the relative contribution of each would appear to be related to both the extent of surface hydroxyl coverage and the level of chlorine content. The chlorine content of a reforming catalyst is maintained at its optimum level during operation by adding chlorinated hydrocarbons to the liquid feed (18).

The first generation monometallic platinum-alumina catalysts dominated naptha reforming during the 1950's and 1960's. However, the metallic function of the catalyst was found to be greatly improved by the addition of a second metal and in 1968 Chevron obtained the patent for the addition of rhenium (19). The new Pt-Re catalyst very quickly became a commercial success and accounted for an estimated 90% of all industrial reforming operations by the mid 1970's (20). Despite the introduction in recent years of new bimetallic catalysts such as Pt-Ir/Al_2O_3 and Pt-Sn/Al_2O_3, the original Pt-Re system remains the most widely used catalyst in this branch of petrochemistry (21).

The superiority of Pt-Re/Al_2O_3 to Pt/Al_2O_3 for the catalytic reforming of petroleum napthas was well demonstrated on the announcement of its discovery (19).

The advantages of the new bimetallic Pt-Re/Al_2O_3 catalyst included a much improved activity maintenance and a higher reformate yield under steady-state industrial reforming conditions.

Pt-Re/Al_2O_3 catalysts generally contain an amount of rhenium comparable to the amount of platinum present. A typical catalyst loading is 0.3% by weight of each metal (5). The most common method of preparation is by impregnation of alumina with an aqueous solution of hydrochloric, chloroplatinic and perrhenic (Re_2O_7) acids. Following impregnation the catalyst is dried and then activated by a series of calcination and reduction steps.

The physical and chemical nature of rhenium in the catalyst has been the focus of much investigation. Particular attention has been paid to establishing the valence state of rhenium and whether or not it is alloyed with platinum in the reduced catalyst. Johnson and LeRoy (22) proposed that rhenium is present as a highly dispersed oxide, such as ReO_2, supported on the surface of the alumina. A series of platinum-rhenium catalysts, prepared by impregnation of η - and γ-alumina with aqueous solutions of chloroplatinic acid and ammonium perrhenate, were studied by these workers; platinum and rhenium contents ranged from 0.31 to 0.66% by weight and 0.20 to 1.18% by weight, respectively. Hydrogen consumption during reduction of the catalysts at 482° was measured volumetrically. In addition, X-ray diffraction studies of the catalyst were undertaken after the alumina had been removed by treatment with a solution of fluoboric acid. The measured hydrogen consumption was equivalent to

reduction of platinum (IV) to the metal and of rhenium from the +7 to the +4 oxidation state. X-ray diffraction data on the metallic residue revealed no evidence for rhenium metal or platinum-rhenium alloy formation.

In contrast, a study on rhenium-alumina catalysts indicated that rhenium was completely reduced to the metal by hydrogen at temperatures of 400-450°C (23). Two possible explanations were proposed to account for the different results. Webb (23) noted that the rhenium content of the catalysts could play a role in determining the extent of reduction since the interaction of non-noble metal oxides with the support would be stronger at low concentrations. The influence of the presence of water in the hydrogen was also considered. The experiments of Johnson and LeRoy were conducted in a static system, with water, produced by the reduction process, presumably being absorbed by the alumina support. Webb used a system employing recirculating hydrogen from which water was removed by a liquid nitrogen trap.

Subsequent experiments, using chemisorption, electron spin resonance and temperature-programmed reduction, confirmed the results of Webb and showed a change in oxidation state of rhenium from +7 to 0 (24-26). Results obtained from temperature-programmed reduction studies further suggested that the properties of alumina supported platinum-rhenium catalysts depend on the method of preparation. The results of McNicol (26), for example, indicated that the reduction of rhenium in Pt-Re/Al_2O_3 samples is catalysed by the platinum and that this effect depends on the degree of hydration of the alumina support. When the catalyst has been dried at low temperatures (ca. < 250°C) both metals are reduced together and show a single low

temperature peak in the TPR profile between 250 and 300°C. In samples that have been predried at higher temperatures, rhenium reduction is retarded and the TPR profile contains at least two peaks; one at a temperature characterisitc of monometallic Pt/Al_2O_3 and one at a temperature characteristic of monometallic Re/Al_2O_3 (27).

TPR peaks in the sample predried at higher temperatures were assigned to the different metals by comparison with similar monometallic catalysts. The temperatures corresponding to the maximum reduction rates of the monometallic catalysts Pt/Al_2O_3 and Re/Al_2O_3 depend upon several factors including metal loading, oxidation temperature, heating rate, and hydrogen pressure. The reduction rates of both Pt/Al_2O_3 and Re/Al_2O_3, for example, are positive in hydrogen pressure (28). In general Pt/Al_2O_3 and Re/Al_2O_3 oxidised at 500-550°C exhibit a TPR peak at ca. 275 and 550°C respectively. After oxidation at 300°C or less the maxima in hydrogen uptake are lowered to ca. 150 and 350°C respectively. The implication is that higher oxidation temperatures enhance interaction of the metal oxides with the support (27). On the basis of these results the high temperature reduction peak for bimetallic catalysts predried at ca. 500°C was assigned to rhenium and the low temperatures peak to platinum.

Three different proposals have been made to explain the contrasting TPR profiles obtained for $Pt\text{-}Re/Al_2O_3$ catalysts dried at different temperatures:

1) The degree of hydration influences the ease of reduction of the metal oxide;

2) The degree of hydration influences the rate of hydrogen spillover;

3) The degree of hydration influences the mobility of Re_2O_x.

Isaacs and Petersen (27) dismissed the first proposal after observing that the degree of hydration did not significantly affect the reduction of either Pt/Al_2O_3 or Re/Al_2O_3. The oxidation temperature in the calcination step and not the drying temperature was the important factor in determining the rate of reduction of the monometallic catalysts.

The second explanation for the two forms of TPR profile was based upon the theory of activated hydrogen spillover. Atomic hydrogen, produced by dissociative adsorption of molecular hydrogen on the reduced platinum, migrates by way of the alumina support to the rhenium precursor. As water is known to be a necessary co-catalyst for hydrogen spillover (29), the difference in the reducibility of rhenium with drying temperature may be due to variations in water content of the support. However, calculations based on kinetic data, obtained by Kramer and Andre (30), implied that insufficient active hydrogen is generated under these conditions. More recently, Mieville (31) presented a mechanism which required only sufficient active hydrogen to reduce a small portion of the rhenium oxide. It was proposed by the author that the rhenium nuclei thus created subsequently catalysed the reduction of the remaining oxide. Reduction of rhenium and platinum oxide precursors at separate sites on the surface of the alumina support is implicit in the hydrogen spillover mechanism.

The catalysed reduction of rhenium has been rationalised by Isaacs and Petersen (27), Bolivar et al. (28) and Wagstaff and Prins (32) by assuming a high mobility of hydrated Re_2O_x species. Following migration to hydrogen covered platinum centres, reduction of rhenium and subsequent alloying with platinum takes

place immediately. For catalysts predried at higher temperatures dehydroxylation hinders surface migration of Re_2O_x. It was concluded that the platinum exhibited much less interaction with the rhenium under these conditions resulting in at least two TPR peaks and by implication no formation of a bimetallic alloy.

It is apparent that the extent to which rhenium is alloyed to platinum is highly dependent on the precise nature of the catalyst thermal pretreatment. This observation would account, to some extent, for the controversy still existing as to the degree of alloying of the metallic components in $Pt\text{-}Re/Al_2O_3$. The degree of alloying in bimetallic reforming catalysts has also been investigated by using catalytic probes or structure sensitive reactions which are susceptible to the composition of the active metal sites in the catalyst. Jossens and Peterson (33), investigating the effect of rhenium addition to platinum catalysts on reactions related to reforming, demonstrated that the rate for toluene dealkylation, methylcyclopentane ring opening and long term self-deactivation by methylcyclohexane all decreased. In contrast the rates for production of benzene from methylcyclopentane and of toluene from methylcyclohexane and the rate of short term self-deactivation by methylcyclohexane were unchanged. The former reactions are believed to be structure sensitive while the latter are not, suggesting that rhenium directly affects platinum, as would be expected for Pt-Re alloy in which the metal surface would be divided into small ensembles of adjoining platinum and rhenium atoms.

Bolivar et al. (34) in an earlier study showed that the catalytic properties of a bimetallic $Pt\text{-}Re/Al_2O_3$ catalyst, in which platinum and rhenium were both reduced

to the metallic state, differed from the predicted additive behaviour of pure platinum and pure rhenium. The authors explained their results by assuming the presence of not only "pure" atoms of platinum and rhenium but also platinum and rhenium atoms electronically modified by the presence of the other metal. The catalyst used was reduced in flowing hydrogen at 500°C after a low temperature drying step and had previously been characterised using several techniques including infra-red spectroscopy of chemisorbed carbon monoxide. Features corresponding to linearly adsorbed carbon monoxide on platinum and rhenium shifted frequency and the relative intensity of the band corresponding to carbon monoxide multiply adsorbed on platinum increased. Since the same effects were seen earlier for Ni-Cu/SiO_2, where alloy formation was explicitly established, it was concluded that observation of these band shifts for Pt-Re/Al_2O_3 provided indirect evidence for alloy formation (25).

Similarly, a recent study by Ponec and co-workers (21), investigating the reaction of 2,2-dimethylbutane on Pt-Re/Al_2O_3, confirmed the "non additive" catalytic behaviour of the system. It was found that addition of rhenium to platinum resulted in a small decrease in hydrogenolysis, despite the fact that rhenium itself is an active hydrogenolytic agent.

In contrast to the above-mentioned evidence for formation of Pt-Re alloy, an infra-red study of adsorbed carbon monoxide and nitric oxide on Pt, Re and Pt-Re/Al_2O_3 catalysts revealed no spectral features for the bimetallics that could not be the result of a combination of features observed for the monometallics (35). Reforming experiments undertaken by Bertolacini and Pellet (36) provided further

evidence against the possibility of alloy formation in the working catalyst. A mixed bed of monometallic platinum and rhenium on separate pellets was observed to perform similarly to co-supported platinum and rhenium pellets. Moreover, postanalysis of the mechanical mixture established that no metal transfer had taken place. On the basis of these results the authors concluded that alloy formation, if it occurred, was not necessary for the reforming catalyst to benefit from rhenium addition. Microanalysis by energy-dispersive X-ray spectroscopy in a scanning transmission electron microscope and surface analysis by ion scattering spectroscopy have also indicated that rhenium is not significantly associated with platinum, but rather is widely dispersed on the surface of the alumina support (37).

Few of the above studies have addressed the role of sulphur, though it is standard industrial practice to sulphide the catalyst before use. Sulphur is a commonly encountered impurity in naptha feedstocks and can readily react with platinum atoms in monometallic reforming catalysts effectively blocking the metal sites. Because this can cause complete loss of activity sulphur concentrations must be carefully controlled (38). Similarly, bimetallic Pt-Re catalysts are also known to be susceptible to sulphur and feedstock sulphur contents of less than ca. 1ppm have been specified in the patent literature (39).

Despite the poisoning effect of sulphur on reforming catalysts, the addition of small quantities of sulphur improves their performance. A low concentration of sulphur in the feed or in a pretreatment gas can selectively diminish the initial hydrogenolysis hyperactivity associated with Pt-Re/Al_2O_3 catalysts. In addition, it is

well established that catalyst coke formation (Section 1.2) is attenuated during reforming. thereby improving yield stability (40,41). Sulphiding Pt/Al_2O_3 causes similar changes in behaviour (38). Sulphur is therefore a selective poison which, when used in a controlled manner, modifies the intrinsic properties of the metal. Several different sulphur compounds may be applied to catalyst pretreatment, including thiophene and hydrogen sulphide. In all cases the catalysts undergo a final high temperature reduction step in a hydrogen atmosphere. Under these conditions the deposited sulphur is either removed as hydrogen sulphide or retained on the catalyst surface. This strongly bound or "irreversible" sulphur remains on the metal function of the catalyst during industrial reforming (42).

In the case of monometallic Pt/Al_2O_3 several possible mechanisms have been proposed to account for the beneficial effects of controlled sulphur addition. In the sulphurisation of platinum, it is now generally accepted that the number of large ensembles of adsorbing surface atoms is significantly lowered (43). This geometric effect, in turn, reduces hydrogenolysis and, it is claimed, the formation of hydrogen-deficient carbonaceous residues. Both are demanding reactions that require an ensemble of several atoms for each active site (44, 108) (Section 1.1.4). Parera and co-workers (45) have suggested that modification of the platinum selectivity may be attributed to the influence of an electronic transfer from platinum to sulphur. The strong chemical bond formed with sulphur changes the chemical bonding of platinum with other adsorbates and hence alters catalyst selectivity. In a later paper the same authors considered that both electronic and geometric effects acted together in influencing selectivity changes (46). When considering the possibility of a geometric

effect it should be noted that alloying platinum with catalytically inactive atoms such as gold, tin and lead has a similar effect to that of sulphurisation (47).

In the modification of platinum with rhenium the combined effect of rhenium and sulphur is essential. Bimetallic Pt-Re catalysts offer a superior performance to monometallic platinum catalysts only when sulphided. Rhenium, due to its lower electron affinity, adsorbs sulphur more strongly than platinum. The majority of rhenium and only a portion of the platinum is therefore in the sulphided state in modified Pt-Re/Al_2O_3 catalysts (48,49). The undesired contribution of rhenium, increasing the formation of lower molecular weight paraffins by hydrogenolysis, is effectively tempered by the addition of sulphur to the catalyst. If a Pt-Re alloy is formed during reduction the sulphided rhenium atom may also be considered as an inert diluent; the size of surface metal atom ensembles is reduced and certain undesired reactions are selectively poisoned (50).

1.1.3 Thermodynamic Considerations in Catalytic Reforming

Catalytic reforming of petroleum napthas includes the following major hydrocarbon reactions:

1) Dehydrogenation of cyclohexanes to aromatics

2) Dehydroisomerisation of alkylcyclopentanes to aromatics

3) Dehydrogenation of paraffins to olefins

4) Dehydrocyclisation reactions

5) Isomerisation of n-paraffins to iso-paraffins

6) Hydrocracking and hydrogenolysis reactions.

The above reactions occur over bifunctional reforming catalysts to varying degrees. The extent to which each takes place depends upon several factors including the nature of the catalyst, the composition of the hydrocarbon feedstock and the reaction conditions.

The most important single reaction in the reforming of petroleum napthas is dehydrogenation. The conversion of napthenes to aromatics is one of the primary Research Octane Number upgrading reactions. In addition, the dehydrogenation of paraffins and cycloparaffins to the corresponding olefins provides reactive intermediates for subsequent cyclisation, isomerisation and acid-catalysed hydrocracking reactions (section 1.1.4).

Of all the reactions encompassed by catalytic reforming the dehydrogenation of cyclohexanes to aromatics occurs the most rapidly. Napthene dehydroisomerisation and isomerisation reactions also occur readily but nonetheless at a slower rate than that of cyclohexane dehydrogenation. Dehydrocyclisation and hydrocracking proceed at much lower rates and are the limiting reactions in typical reforming operations (5).

Table 1.2 lists the average heats of reaction and thermodynamic equilibrium constants determined for various reactions of C_6 hydrocarbons (51). The heats of reaction vary only slightly with the number of carbon atoms in the molecule and these may be taken as representative of the reforming reaction. The equilibrium constant, K, is defined as the ratio of the partial pressures of the products to reactants expressed

in atmospheres at 500°C.

Table 1.2 Thermodynamic Data on Reactions of C_6 Hydrocarbons.

Reaction	K	ΔH_R kJ/mole
Cyclohexane → Benzene + $3H_2$	6×10^5	221
Methylcyclopentane → Cyclohexane	0.086	-16.0
n-Hexane → Benzene +$4H_2$	0.78×10^5	266
n-Hexane → 2-Methylpentane	1.1	-5.9
n-Hexane → 3-Methylpentane	0.76	-4.6
n-Hexane → 1-Hexene + H_2	0.037	130

Some reactions, such as dehydrogenation of paraffins, are mildly endothermic . Others, such as the dehydrogenation of napthenes or the dehydrocyclisation of paraffins, are highly endothermic. Isomerisation reactions and dehydroisomerisation reactions (eg. the conversion of methylcyclopentane to benzene) are very slightly exothermic.

Because the dehydrogenation of cyclohexane and the dehydrocyclisation of n-hexane are endothermic and result in a net increase in the number of molecules, their equilibrium is favoured by as high a temperature and as low a hydrogen partial pressure as possible; thus optimising the yield of aromatic hydrocarbons.

In a similar manner the dehydrogenation of paraffins to olefins is favoured by the same conditions. The concentration of olefinic hydrocarbons remains very low

under typical reforming conditions and therefore makes no significant contribution to the improvement in octane rating. However, the extent of olefin formation is important in determining the rates of those reactions that proceed via olefinic intermediates. This matter will be discussed in more detail in the following section.

Isomerisation reactions are pressure independent and the equilibria vary only slightly with temperature due to the small heats of reaction. In the equilibria between n-hexane and the methylpentanes, 2-methlypentane is the favoured isomer over 3-methylpentane as would be predicted by statistical considerations. Thermodynamics predict that approximately 30-35% of the total hexane isomers at 500°C should be dimethylbutanes. However, this is not observed in practice and it has been suggested that a strong kinetic barrier opposes the formation of doubly branched isomers (6).

Hydrogenolysis and hydrocracking reactions, where carbon-carbon bonds are broken and subsequently hydrogenated, are very exothermic and highly favoured by thermodynamics (8). In practise, the reactions are limited only by kinetic factors. Since reforming reactions which produce hydrogen, especially aromatisation, predominate over those which consume hydrogen, such as hydrogenolysis and hydrocracking, the process is a net hydrogen producer.

On the basis of the above discussion and considering the slight influence of isomerisation on the overall octane number the reforming reaction should be operated at high temperature and the lowest possible hydrogen pressure. Under such conditions the preferred dehydrogenation and dehydrocyclisation reactions are favoured.

However, these conditions also favour coke formation resulting in catalyst deactivation. As a result, economic considerations dictate that catalytic reforming is operated at ca. 500°C and pressures in excess of 10 atmospheres.

1.1.4 Mechanistic and Kinetic Considerations

Under the influence of a bifunctional catalyst the hydrocarbon reactions in catalytic reforming typically proceed through a number of sequential steps. The dehydrogenation of paraffins to olefins and napthenes to aromatics is catalysed by the metal function. The metal function also catalyses hydrogenolysis reactions and contributes to dehydrocyclisation and isomeration. The acid function of the catalyst, in the form of halogenated alumina, catalyses isomerisation, cyclisation, dehydroisomeration and hydrocracking reactions via a carbonium ion mechanism. Unsaturated hydrocarbons act as key intermediates in much of the reaction network. The classical reaction scheme proposed by Mills et al. (52), describing the reforming of C_6 hydrocarbons, is shown in figure 1.2. Such a scheme, though incomplete, gives a good qualitative description of the overall phenomena observed in catalytic reforming.

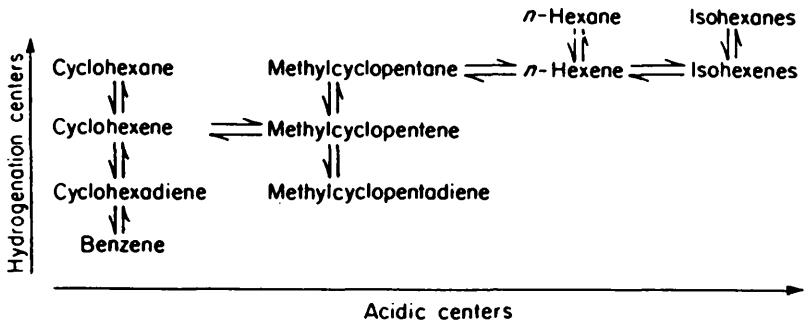

Figure 1.2 Reaction paths in Catalytic Reforming of C_6 Hydrocarbons (52)

Reactions drawn parallel to the y-axis in figure 1.2 occur at the hydrogenation-dehydrogenation centres and reactions drawn parallel to the x-axis occur at the acidic centres of the catalyst. According to this mechanism, the reactant (n-hexane) is first dehydrogenated on the metal to give hexene. The hexene migrates to a neighbouring acid centre where it is converted into a secondary carbonium ion by the addition of a proton. The carbonium ion undergoes skeletal rearrangement, returns a proton to the acid support and is desorbed as iso-hexene. Subsequent migration to the metal function where the olefin intermediate is absorbed and hydrogenated gives the product, iso-hexane. Alternatively, the secondary carbonium ion can react through a similar sequence of steps, this time involving a ring closure mechanism, to form methylcyclopentane, a precursor for both cyclohexane and benzene formation.

Weisz and Swegler (53), in a series of experiments involving n-heptane isomerisation, demonstrated the independent action of the metal and acidic centres of the bifunctional catalyst. The reaction was investigated separately over SiO_2-Al_2O_3

(acidic function) and platinum on a non-acidic support such as carbon or SiO_2 (hydrogenation-dehydrogenation function). Conversion was found to be negligible in each case. However, when mechanically distinct but mixed particles of SiO_2-Al_2O_3 and Pt/SiO_2 were studied significant conversion was observed. Because of the presence of gas phase diffusioned limitations, reducing the particle size resulted in increased conversion. In the limit, a mechanical mixture of 5μm particles of Pt/SiO_2 and SiO_2-Al_2O_3 gave the same conversion as SiO_2-Al_2O_3 impregnated with platinum.

It is worthwhile considering the isomerisation reaction in catalytic reforming in order to further substantiate the bifunctional nature of the supported metal catalysts and to illustrate the reaction kinetics. The kinetics of isomerisation are best illustrated by referring to a specific example. The isomerisation of n-pentane was investigated by Sinfelt and co-workers (54) over platinum on alumina at low conversion levels. Rate measurements were determined in a flow system at 372°C in the presence of hydrogen at total pressures of between 7.7 and 27.7 atmospheres. The rate was found to be independent of total pressure and increased with an increasing n-pentane to hydrogen ratio in the range of hydrogen pressures commonly used in reforming. The kinetic data was interpreted in terms of a reaction proceeding on the two catalyst functions via the following mechanism:

$$n\,C_5 \rightleftharpoons n\,C_5^{=} + H_2 \quad (1)$$

$$n\,C_5^{=} \rightarrow i\,C_5^{=} \quad (2)$$

$$H_2 + i\,C_5^{=} \rightleftharpoons i\,C_5 \quad (3)$$

For a typical reforming catalyst, reaction (2) is assumed to be slow and reactions (1)

and (3) are assumed to be close to equilibrium (54). If the rate of reaction is assumed to be proportional to the concentration of adsorbed olefin on acid sites, then the rate of reaction is given by

$$r = k' [n\ C_5^=]_{ads} \quad (4)$$

where $[n\ C_5^=]_{ads}$ represents the concentration of n-pentenes adsorbed on the acid function and k' is a rate constant. Based on the assumption that equilibrium is established in equation (1), the concentration of n-pentenes ($n\ C_5^=$) in the gas phase is given by

$$(n\ C_5^=) = K_1 (n\ C_5) / (H_2) \quad (5)$$

where K_1 is an equilibrium constant, ($n\ C_5$) is the concentration of gas phase n-pentane and (H_2) is the concentration of gas phase hydrogen. If we assume also that equilibrium is established between n-pentene in the gas phase and n-pentene adsorbed on the acid sites then the equilibrium can be represented by the equation

$$[n\ C_5^=]_{ads} = K_2 (n\ C_5^=)^n \quad (6)$$

where n has a value between 0 and 1 and K_2 is an adsorption coefficient. After substitution of equations (5) and (6) into equation (4) the rate equation is given by

$$r = k [(n\ C_5) / (H_2)]^n \quad (7)$$

where $k = k'K_2K_1^n$. The rate of reaction is therefore obtained in terms of the n-pentane and hydrogen partial pressures. This expression states that the isomerisation rate is independent of total pressure and dependent only on the ratio of the n-pentane partial pressure to the hydrogen partial pressure. The observed reaction kinetics are indeed consistent with equation (7) and provide good supporting evidence for the mechanism illustrated in figure 1.2. Further support for the above kinetic analysis was presented by Sinfelt and co-workers when they reported that the rate of isomerisation of pent-1-ene on Pt-free promoted alumina (no hydrogenation-dehydrogenation function) was in close agreement with that for n-pentane isomerisation on a bifunctional reforming catalyst (54).

The assumption in equations (1) and (3) that the hydrogenation-dehydrogenation reactions are close to equilibrium is in good agreement with the experimental evidence. It has been shown that for platinum contents greater than 0.1% by weight, sufficient metal surface area is available to maintain an equilibrium concentration of olefin intermediate in both the n-heptane isomerisation and methylcyclopentane dehydroisomerisation reactions (55). Reforming catalysts typically contain between 0.2 and 1% platinum by weight implying that equilibrium concentrations of olefins should be reached. The occurrence of equilibrium concentrations of olefins has indeed been measured during reforming operations (56).

The independence of isomerisation rate on platinum content above a certain level indicates that the formation of olefin intermediate is not a limiting factor in the reaction. In addition, the similar rate of n-pentane isomerisation on Pt/Al_2O_3-Cl and

n-pentene skeletal isomerisation on Pt-free promoted alumina clearly show that the rate-limiting step in bifunctionally catalysed isomerisation is on the acid centres of the catalyst. This is the usual situation in paraffin and napthene isomerisation reactions under typical reforming conditions.

However, it is now accepted that the skeletal rearrangement of hydrocarbons may also occur on the metal function alone (57,58). The available data on commercial reforming operation indicates that the purely metal catalysed contribution is significant although not great. Weisz and Swegler (53), for example, estimated that between 10 and 15% of n-heptane isomerisation could be attributed to the metal.

Two basic mechanisms have been proposed to account for skeletal isomerisation of hydrocarbons on platinum. The first metal-catalysed paraffin isomerisation mechanism involves a bond-shift rearrangement. Anderson and Avery (59), in an attempt to explain the skeletal isomerisation of saturated hydrocarbons, studied the influence of hydrocarbon geometry on the reaction. Based on studies comparing the reactions of ethane, n-butane, iso-butane and neopentane, the authors proposed a bond-shift mechanism involving an α α γ - triadsorbed intermediate bonded to two adjoining platinum atoms. In the case of neopentane, isomerisation can be visualized as involving adsorption on the metal surface through the carbon atoms at the 1 and 3 positions (A), transformation to a short lived bridged intermediate (B) in which C_2 has been rehybridised to sp^2 and subsequent isomerisation and desorption to form 2-methylpentane (C):

(A) (B) (C)

In contrast, Rooney et al. proposed a mechanism, based on hydrogen-deuterium exchange studies, involving metallocarbonium ions (60). Formation of the intermediate involved interaction of the metal dπ orbital and the pπ orbitals of the carbon resulting in a lowered energy barrier for the methyl group shift. In the conversion of iso-butane to n-butane the following structures were envisaged:

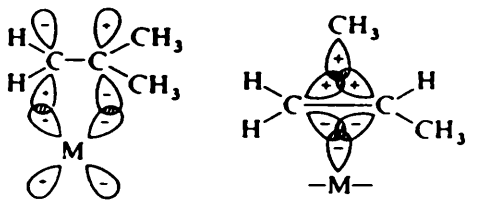

Rooney et al. drew attention to the very close parallel between this mechanism on a monometallic site and a metallaenzyme rearrangement.

The second metal-catalysed paraffin isomerisation mechanism proceeds via formation of a cyclic five-membered ring (8,61). The reaction sequence may be represented as three consecutive steps:

1) 1,5 dehydrocyclisation to form an adsorbed cyclopentane intermediate;

2) Desorption of the ring species can occur allowing for readsorption through different carbon atoms or, alternatively, the intermediate cyclic hydrocarbon may displace the points of attachment to the metal without desorption;

3) Ring cleavage, followed by desorption of the isomeric product.

Step 2) allows the ring to be opened at a different position from where it was closed and accounts for skeletal isomerisation. Figure 1.3 illustrates the reaction scheme for C_6 paraffin isomeration on a metal surface.

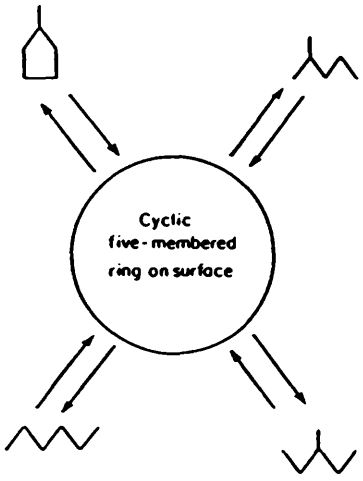

Figure 1.3 Reaction scheme for isomerisation of C_6 paraffin on a metal surface (8).

Gault found that the cyclic mechanism of isomerisation allowed for two types of ring opening and that the contribution of each was related to platinum particle size (61). Step (3) in the reaction sequence above was investigated separately by studying the hydrogenolysis of methylcyclopentane. Non-selective hydrogenolysis of the

cyclopentanic intermediate, in which the chances of rupturing the five C-C bonds of the ring were approximately equal, was observed on Pt-Al_2O_3 catalysts of low metal loading, i.e. small platinum particles. At higher metal loadings (> 2% Pt) an almost selective rupture of the C-C bonds was found (Figure 1.4).

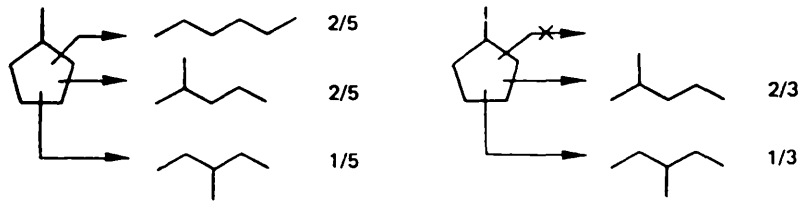

Figure 1.4 Non-selective and Selective Hydrogenolysis illustrating the relative quantities of observed products (61)

The relative importance of bond-shift and cyclic isomerisation reactions has been determined using ^{13}C - radiotracer techniques. Supported metal particle size was shown to be critical in determining which mechanism prevailed. For 2-methylpentane-2-^{13}C, isomerisation to give 3-methylpentane proceeded almost exclusively by the cyclic mechanism on well dispersed Pt crystallites (~12Å). On larger Pt crystallites (~180Å) the bond-shift mechanism was predominant (57).

The dehydrocyclisation reaction of paraffins is similar to isomerisation since it can occur on the metal alone or via a bifunctionally catalysed reaction pathway. In the bifunctionally catalysed reaction scheme (Figure 1.2) the dehydrocyclisation of, for example, n-hexane, proceeds via formation of n-hexene on the platinum sites

followed by cyclisation of the intermediate olefin to methyl-cyclopentane on the acidic support. Similarly, conversion to methylcylopentene followed by isomerisation yields the six membered ring structure, cyclohexene. The cyclohexene may then return to the hydrogenation-dehydrogenation sites on the catalyst where, depending on reaction conditions, it can either be hydrogenated to form cyclohexane or further dehydrogenated to form benzene.

Sinfelt and Rohrer (62), investigating the dehydrocyclisation of n-hexane on a 0.3% by weight platinum-alumina catalyst, found that the major product at low conversion was methylcyclopentane rather than benzene or cyclohexane. Their results strongly indicated that the preferred reaction mechanism for n-hexane dehydrocyclisation involved formation of a cyclic five-membered ring intermediate.

The effect of hydrogen partial pressure on the kinetics of n-heptane dehydrocyclisation on a Pt/Al_2O_3 catalyst was also investigated by Sinfelt et al. (63). No dehydrocyclisation was detected in the absence of hydrogen. In the presence of hydrogen the rate of dehydrocyclisation was found to increase with increasing hydrogen pressure until a given point. Thereafter the rate decreased as the hydrogen pressure further increased. The change in the nature of the hydrogen pressure dependence was interpreted as follows: at low hydrogen pressures, the metal sites became covered with carbonaceous residues resulting in the reaction rate being limited by the dehydrogenation activity of the catalyst. Increasing the hydrogen pressure resulted in the beneficial removal of such surface residues, freeing platinum sites and increasing the overall rate of dehydrocyclisation. Above a certain hydrogen pressure,

however, the rate did not continue to increase. The formation of olefins was no longer the rate controlling step and the overall reaction became limited by the cyclisation of olefins on the acidic centres of the catalyst. Any further increase in hydrogen pressure served only to attenuate the concentration of the olefin intermediate at equilibrium and hence decreased the rate of dehydrocyclisation. Similar behaviour has been observed in the isomerisation reaction at pressures greater than those normally used in reforming and has been interpreted in the same manner (63).

In addition to the bifunctionally catalysed dehydrocyclisation mechanism, there is evidence for a monofunctional pathway involving dehydrogenation and cyclisation on the metal. Sinfelt and co-workers (55) observed that the rate of n-heptane dehydrocyclisation increased significantly when the metal content of a Pt/Al_2O_3 catalyst was increased from 0.1 to 0.6% by weight. The increase in rate was not directly proportional to platinum content but the results did indicate that the rate of dehydrocyclisation was not solely determined by an acid site controlled bifunctional mechanism. The dependence of alkane dehydrocyclisation rate on platinum surface area and hence platinum content was further substantiated by Silvestin et al. (64), who investigated the production of ring compounds from n-heptane at commercial reforming temperatures and pressures. Using platinum supported on carbon (non-acidic) and platinum-alumina catalysts in conjunction with selective poisoning of the metal cyclisation function using thiophene, the authors estimated that the monofunctional and bifunctional cyclisation contributions were of about equal importance.

Dehydrocyclisation activity on monofunctional supported catalysts has also been reported by Dautzenberg and Platteeuw (65) and Davis (66). Since bifunctional catalysis on the non-acidic catalysts was assumed to be eliminated, the dehydrocyclisation activity was attributed to platinum metal alone. Davis reported evidence for direct (1,6) - ring closure of straight chain paraffins. Similarly, the aromatic products obtained from the dehydrocyclisation of C_8 - and C_9 - paraffins, catalysed by a non-acidic platinum catalyst at atmospheric pressure and 482°C, were those predicted for direct C_6 cyclisation (67). In contrast, Gault and co-workers have postulated a 5-membered ring closure of the paraffin followed by ring enlargement over non-acidic platinum catalysts (61, 68).

In addition to a platinum catalysed dehydrocyclisation route, Dautzenberg and Platteeuw (65) have also suggested a second mechanism in which hexatriene, formed on the platinum, subsequently undergoes a gas phase cyclisation reaction to form benzene. When the high hydrogen partial pressures typical of industrial catalytic reforming are considered, it is apparent that this route is probably not an important source of dehydrocyclisation activity.

Two types of reaction involving carbon-carbon bond scission in the presence of hydrogen are hydrogenolysis and hydrocracking; both reactions occur to a significant extent in catalytic reforming.

Hydrogenolysis involves only the metal component of the catalyst and leads to the formation of methane along with smaller amounts of ethane. Hydrocarbon

hydrogenolysis on metal catalysts has been studied extensively and particular attention is drawn to a review by Sinfelt (69). The mechanism of hydrogenolysis is reasonably well established and the reaction appears to be initiated by chemisorption of adjacent carbon atoms on adjacent metal sites. Hydrocarbon adsorption on the metal surface involves rupture of carbon-hydrogen bonds. The hydrogen-deficient surface species, multiply bonded to the metal, then undergoes carbon-carbon bond scission. This is followed by a rehydrogenation of the intermediates, producing methane and a paraffin from the second fragment. The following sequence of reaction steps is used to explain many of the results from mechanistic and kinetic studies on ethane hydrogenolysis:

$$C_2H_6 \rightleftharpoons C_2H_5\,(ads) + H\,(ads)$$

$$C_2H_5\,(ads) + H\,(ads) \rightleftharpoons C_2H_x\,(ads) + a\,H_2(g)$$

$$C_2H_x\,(ads) + H\,(ads) \rightarrow CH_y\,(ads) + CH_z\,(ads)$$

$$CH_y\,(ads) + CH_z\,(ads) \xrightarrow{H_2} CH_4\,(g)$$

where the quantity a is equal to (6-X)/2. The species C_2H_5 and H are considered to be singly bonded to the metal surface, whereas C_2H_x, CH_y and CH_z are multiply bonded. Ethane hydrogenolysis is visualised as proceeding via a 1,2 adsorbed intermediate. In contrast, Anderson and Avery (70), studying the hydrogenolysis of neopentane (which, due to its structure is unable to adsorb as a 1,2 species) proposed that the hydrogenolysis of higher molecular weight paraffins involved 1,3 adsorbed intermediates.

It has been demonstrated that the catalytic activities of metals for ethane

hydrogenolysis vary as a function of their position within the periodic table (69,71). Thus, beginning with rhenium and proceeding in the direction of increasing atomic number to platinum, hydrogenolysis activity reaches a maximum value at osmium. Platinum is seven orders of magnitude less active than osmium. A similar pattern of activity is observed from ruthenium to palladium in the second transition series. Despite attempts to relate hydrogenolysis activity to percentage d-character this criterion alone does not adequately describe the catalytic activity of transition metals for hydrogenolysis. The relatively low hydrogenolysis activity of platinum combined with its established dehydrogenation activity makes it the preferred choice of metallic species in reforming catalysts.

With regard to platinum, it is generally accepted that hydrogenolysis is a demanding reaction, e.g. experimental evidence shows that large ensembles of group VIII metal atoms are beneficial (44, 72). Information about the size of metal-atom ensembles required to catalyse the hydrogenolysis reaction has been inferred from alloying platinum with inactive atoms such as gold, tin and lead. Very dilute Pt-Au alloys have been prepared in which the metal surface is almost pure gold (73, 74). It was observed that under such conditions the isomerisation reaction alone was catalysed, suggesting a single atom site for this reaction. Hydrogenolysis reactions were found to require significantly larger site ensembles. Blakely and Somorjai (75) have proposed that the hydrogenolytic sites on platinum are kinks and furthermore that these sites are preferred by the atoms of a second metal (or sulphur). The hydrogenolysis activity is therefore selectively poisoned in this way.

The second type of reaction that involves carbon-carbon bond scission is termed hydrocracking and occurs on the acidic sites of the catalyst support. Bifunctional catalysis is involved in the mechanism and olefins are regarded as key intermediates. In this sense hydrocracking is similar to isomerisation except that the olefin undergoes a fragmentation reaction rather than a skeletal rearrangement. The hydrocracking mechanism is understood to require the formation of a carbonium ion as the first step in the reaction (76). This is facilitated by the formation of olefins on the metal surface of the catalyst. Such olefinic hydrocarbons readily react with a proton from the acidic support to produce a carbonium ion. The next step in the catalytic cracking of paraffins is the decomposition of the carbonium ion. The empirically observed rule (77), referred to as the beta-rule, states that the carbon-carbon bond scission occurs at the position one carbon atom away from the hydrogen-deficient carbon atom. The beta-rule is the rule of least rearrangement since it involves the shifting of electrons only:

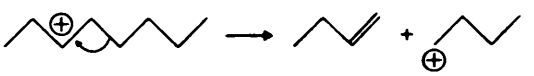

The cracking produces an α-olefin and a new hydrogen-deficient species. The new carbonium ion is converted to a more stable secondary configuration by a simple proton shift. The secondary carbonium ion undergoes further cleavage at the beta-position and the cracking may proceed until a carbonium ion which cannot yield fragments of three or more carbon atoms is produced.

A characteristic feature of catalytic cracking is the formation of large amounts of iso-paraffins. The formation of light iso-paraffins in the products is readily explained by a rearrangement of the secondary carbonium ion prior to cracking:

Saturated paraffins predominate among the cracked products because the olefins formed are hydrogenated on the metal component of the catalyst.

1.2 DEACTIVATION OF REFORMING CATALYSTS

Coke deposition is one of the most important causes of catalyst deactivation and is an important technological and economic problem in petroleum refining and in the petrochemicals industry. In commercial reforming the activity of any reforming catalyst gradually decreases with the formation of coke. Here, the term coke or carbon is used to define the carbonaceous materials formed on the catalyst surface. In addition, the presence of coke deposits on the surface of reforming catalysts is associated with significant changes in reaction selectivity. The loss of catalyst activity and modification of catalyst selectivity is manifested by a lowering of the reformate octane number and a decrease in hydrogen yield.

In order to maintain the same anti-knock qualities in the reformate product the

average operating temperature is gradually increased. Though effective, this remedy is relatively short term as there are upper limits on plant operating temperatures. Increasing temperatures also favour undesirable side reactions such as hydrocracking and hydrogenolysis which have high activation energies (3).

Commercial catalysts are operated for many thousands of hours and are known to accumulate high steady-state levels of carbonaceous deposits which may be as much as 20% by weight (78). These carbonaceous deposits are irreversibly transformed into graphitic coke that block the metal sites and plug the porous support, rendering the catalyst inactive.

Plant shutdown is required and the catalyst is subjected to an expensive regeneration process in order to restore its initial activity. The regeneration process involves burning of the accumulated coke under carefully regulated conditions. The catalyst is returned to commercial operation following readjustment of its chlorine and sulphur levels (8). A more recent development of the process is a moving bed system that enables the catalyst to circulate between the reactors and regeneration equipment allowing for continuous regeneration. Development of such a system has enabled each catalyst grain to be regenerated more than 50 times (3).

1.2.1 Chemical and Physical Characterisation of Coke Deposits

Several experimental techniques have been used to characterise the location, composition and structure of coke deposits on bifunctional reforming catalysts. One

of the simplest and most widely used techniques is the removal of coke by gasification with oxygen. The technique, referred to as temperature programmed oxidation (TPO) allows the location of coke deposited on the reforming catalyst to be distinguished. Using fresh catalyst as a reference and oxygen as the dynamic gas the heat produced by the combustion of the coke is measured as a function of temperature by differential thermal analysis. The resultant thermograms show two well defined zones of coke combustion (79-81).

Parera et al. (79) in a study comparing coke deposition on chlorinated alumina (acidic function only) and bifunctional platinum-alumina, demonstrated that the burning at ca. 300°C corresponds to coke on the metallic function and that the burning at ca. 500°C corresponds to coke on the acidic function. The catalysts were coked by Parera and co-workers at atmospheric pressure and 500°C using n-hexane or methylcyclopentane as feedstock. Similar results were reported by Barbier et al. (80) after investigating coke obtained from cyclohexane on Pt/Al_2O_3. In a more recent paper by Querini, Figoli and Parera (120), the coke concentration corresponding to each function on a commercial reforming catalyst was determined by TPO as a function of time-on-stream. Using several model hydrocarbon feedstocks (n-hexane, n-heptane and a mix of n-pentane and cyclohexane) the authors established that there was an initial rapid deposition of coke on the metal for the first few days only, thereafter it remained constant. In contrast, coke on the acid sites increased during the whole run (ca. 200 days).

Chromatographic analysis of the combustion gases (CO_2 and H_2O) from TPO

experiments on Pt/Al_2O_3 allowed Parera and co-workers (79) to determine the hydrogen to carbon ratios for the different zones of coke burning. Specific H/C ratios were not reported by the authors but it was observed that the combustion zone on the acidic function corresponded to a more polymerised deposit. The results of Parera and co-workers are in accordance with those of Barbier (81) who compared the H/C ratio of coke deposited on pure Pt and pure Al_2O_3-Cl catalysts. Both catalysts were coked at 400°C using a cyclopentane and 10% cyclopentene feedstock. Coke on the platinum was reported to have a H/C ratio of 1.05 whereas coke on the Al_2O_3-Cl was more dehydrogenated and had a lower H/C ratio of 0.5. Furthermore, Barbier reported that the C/H stoichiometric ratio varied with time-on-stream, an effect that has been termed coke ageing. Barbier noted that the average H/C ratio of coke deposited on a bifunctional reforming catalyst decreased from 0.70 to 0.39 after 10 hours on-stream. Following comparison with the H/C values for crude oil (1.1 - 1.6) and of coals (0.6 - 0.8) Barbier concluded that the structure of coke was between that of polyaromatics and coals.

Biswas, Gray and Do (82) have further demonstrated the existence of two types of coke on the metal surface of reforming catalysts. Using thermal gravimetric analysis (TGA) a standard Pt/Al_2O_3 catalyst, previously coked by a cyclohexane feedstock, was analysed under a hydrogen atmosphere. The authors showed that, at the analysis temperatures used, coke removal from the acid sites would be negligible. Any weight loss recorded was therefore exclusive to the metal sites of the catalyst. The removal of coke was reported to occur in two distinct phases. The first type of coke, easily removed by hydrogen, was termed reversible; the second type of coke,

more resistant to hydrogen removal, was termed irreversible or graphitic coke. The phenomenon of reversible and irreversible coke on hydrocarbon conversion catalysts has been proposed by a number of authors (83, 84). Single crystal studies by surface scientists have verified these coke types, the reversible coke being hydrogenated surface species (H/C ratio 1.5 - 2.0) and the other being graphitic in nature (H/C ratio ca. 0.2) (85, 86). Biswas, Gray and Do (82) noted that the graphitic coke was favoured by high temperatures and low partial pressures and increased with time-on-stream, corresponding with the drop in catalyst activity.

Parmaliani et al. (87) used IR analysis to study the structure of coke deposits obtained by methylcyclohexane dehydrogenation over $Pt/\gamma Al_2O_3$ / honeycomb reforming catalysts. The IR spectra of the coke deposits revealed four absorption bands at 1420-1470, 2860-2890, 2930-2940 and 2960-2980cm^{-1} which correspond to stretching of CH bonds in CH_2 and CH_3 groups. Two absorption bands at 1490 and 1590cm^{-1} were attributed to characteristic stretching of aromatic rings and a further absorption band at 3020cm^{-1} was attributed to the stretching of CH bonds in unsaturated aromatic compounds. The results indicated that carbonaceous residues on the surface of the catalyst investigated consisted of mono- and polycyclic aromatic rings connected by aliphatic and alicyclic adjuncts.

Beltramini and co-workers (88) used an accelerated deactivation test in conjunction with a commercial naptha feedstock to coke a monometallic Pt/Al_2O_3 catalyst. Partial coke extraction with various organic solvents enabled these workers to characterise the soluble coke using GC-MS and NMR-H. The proton NMR spectra

of the extracted coke showed two zones, one corresponding to aliphatic protons and the other, at higher shifts, corresponding to protons associated with condensed aromatic centres. The authors determined that alkylic appendages joined to the aromatic rings were mainly CH_3 or C_2H_5. No olefins were detected although protons associated with saturated carbons in acanapthene or indene-type structures were observed. In addition, the authors noted that the region corresponding to aromatic protons signals included hydrogens attached to unsaturated five carbon atom rings. Approximately 60 compounds were detected in the soluble coke GC-MS spectra. Among the more important compounds recognised were napthene, indene and acanapthenic structures. The largest compounds detected contained up to four condensed aromatic rings.

The non-soluble coke fraction was analysed by X-ray diffraction (XRD) after destroying the Al_2O_3 support with concentrated HCl . X-ray diffraction results showed the existence of poorly organised structures separated by 3.4 Å . The higher separation between planes found in non-soluble coke compared with graphite (3.34Å) was attributed to the presence of five carbon atom rings or alkylic chains joined to the rings. A similar study by Barbier and co-workers (89), investigating unextractable carbonaceous residues with XRD, showed that the deposits on Pt/Al_2O_3 coked with cyclopentane were composed of a pseudo-graphitic phase with large aggregates of graphite. Whilst reaction temperatures were reported to have no apparent effect on the chemical nature of the deposited coke, in contrast with the previously cited work of Biswas, Gray and Do (82), it was noted that an increase in reaction pressure promoted the graphitisation of coke on the support.

Auger electron spectroscopy (AES) combined with hydrogen thermal desorption was employed by Davis, Zaera and Somorjai (90) to investigate the nature of coke overlayers deposited during the reaction of various hydrocarbons on a variety of platinum single crystal faces. Auger electron spectroscopy was used to determine the surface carbon to surface platinum ratio, whilst temperature programmed hydrogen desorption provided a quantitative measure of the hydrogen content. The H/C stoichiometry of the residues was observed to range between 1.6 at 300°C and 1.0 at 405°C in agreement with the results of Biswas and co-workers (82). The authors observed that these chemical compositions were intermediate between those of polyacetylene (H/C = 1.0) and polyethylacetylene (H/C = 1.5). Further investigation by Davis et al. using AES in conjunction with carbon-monoxide to quantify uncovered platinum sites, revealed that the morphology of the coke deposit varied continuously from two dimensional at low reaction temperature to three dimensional at higher temperatures (> 300°C).

Espinat et al. (91) have shown that Raman spectroscopy is an especially valuable technique for coke characterisation. Raman spectroscopy studies of coked Pt/Al_2O_3-Cl catalysts enabled the authors to determine the relative amounts of nondesorbed heavy polyaromatics (pregraphitic coke, spectral band at 1355cm^{-1}) and graphitic coke (spectral band at 1600cm^{-1}). The technique has established that, even with 0.3 wt % carbon, there are already organised carbonaceous structures, thus proving that the formation of localised graphitic aggregates takes place early in the reaction.

1.2.2 Mechanism of Coke Formation

Various mechanisms have been proposed to account for coke formation on the surface of reforming catalysts (88, 90, 92-97, 99). All involve an initial step of dehydrogenation and formation of unsaturated hydrocarbons. The unsaturated species retained on the catalyst surface subsequently undergo a series of condensation and polymerisation reactions producing extensive deposits of hydrogen-deficient carbonaceous material.

Carbonaceous residues formed on acidic oxides are known to be different from those formed on metals (section 1.2.1). It is generally believed that coke formation on the acidic function of reforming catalysts proceeds via polymerisation of olefinic material. The following mechanism involving carbonium ions produced from olefins has been proposed by Trimm (92):

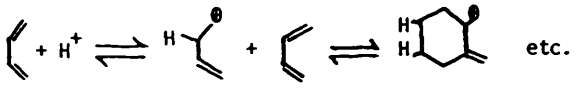

Parera and co-workers (88) have proposed a Diels-Alder type condensation mechanism, catalysed by Lewis acid sites, to account for coke formation. This mechanism emphasises the role of five carbon-atom ring structures as particularly effective coke precursors. Indene was regarded as an important intermediate because of its reactive cyclopentadiene nucleus. Condensation of indene with a further molecule of cyclopentadiene gives benzindene or fluorene. Benzindene also has a terminal five carbon atom ring and condensation can either continue linearly or by a

spiral mechanism as shown below:

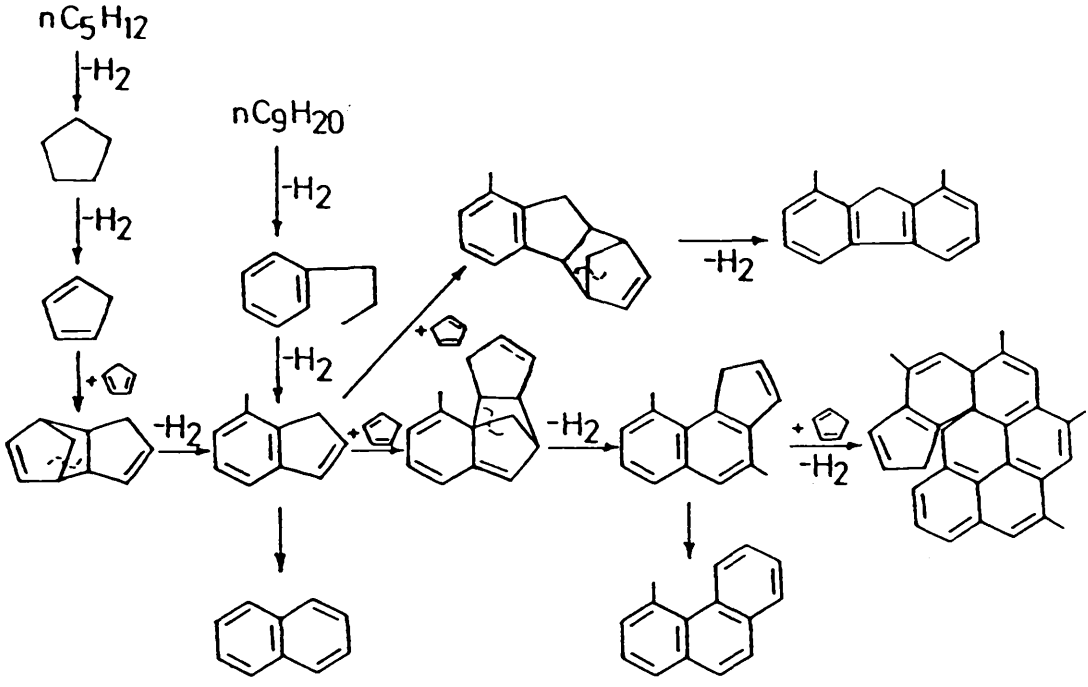

The importance of catalyst acidity in hydrocarbon conversion catalysts with respect to the rate of coke deposition has been demonstrated by several authors (93, 94). Van der Waals (94), for example, established that during the cracking of anthracene the amount of carbon deposited on silica-alumina was 23 times higher than that accumulated on non-acidic silica.

Coking of the metal component in bifunctional reforming catalysts is a dynamic process in which partially hydrogenated carbonaceous species are produced, migrate across the surface to a nucleation site, and there grow to form a deposit (90). A typical model proposed for coke production on platinum is shown in figure 1.5.

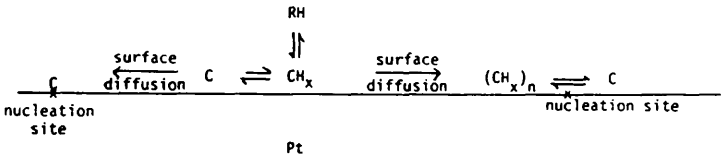

Figure 1.5 Model for the production of carbon on platinum (95).

A series of fragmentation reactions and successive dehydrogenation reactions leads to the formation of carbon atoms. More toxic coke deposits are formed by the combination of these atoms or partially dehydrogenated intermediates. Possible factors influencing the process are the production and dehydrogenation of intermediates, the migration of these intermediates (or carbon) to a nucleation site, the nature of such sites and the growth and subsequent reactions of the deposits on these sites. Removal of hydrogen leads to restructuring of the deposits to a more graphitic form, a reorganisation that can also be induced by increasing temperature. The deposits decrease the available metal surface area by a masking process and appear to form almost instantly as the reaction commences (90). Davis and Somorjai (90) have demonstrated that platinum single-crystal surfaces do not appear to be altered either structurally or electronically by the existence of the carbon deposit.

Maire, Luck and Aeinjach (96) favour a polyene mechanism for coke formation on platinum in which gas phase dimerisation of carbenes is believed to produce olefins which in turn give rise to polyolefins. Carbene addition to adsorbed polyolefins

creates polycyclic residues or pregraphitic coke which is subsequently dehydrogenated to form irreversible graphitic coke. In contrast, Levintar and co-workers (97), studying petroleum naptha reforming on Pt/Al_2O_3, have suggested the following scheme for coke laydown:-

naptha → dienes → resins + asphaltenes → carboids

It is generally accepted that the coke precursor molecules are not normal components of the naptha feedstock, but occur as reaction intermediates, generated by dehydrogenation reactions on the catalyst surface. Thus, for example, Bertolacini and Pellet (36) demonstrated that an intimate mechanical mixture of Pt/Al_2O_3 and Re/Al_2O_3 had a greater resistance to coke deposition than either monometallic Pt/Al_2O_3 or Pt/Al_2O_3 followed, further upstream, by Re/Al_2O_3. The results of Betrolacini and Pellet were attributed to the ability of rhenium in the physical mixture to remove the coke precursor molecules by hydrogenolysis. As the displacement of the Re/Al_2O_3 upstream of the Pt/Al_2O_3 coincided with the removal of the beneficial effect of rhenium it is apparent that the coke precursors were formed over the Pt/Al_2O_3 catalyst and were not contained in the actual hydrocarbon feedstock. Similarly, Wojciechowski et al. (98), following analysis of experimental results obtained by cracking typical oil feedstocks, showed that coke was not a primary product of the reaction but rather was a product of secondary reactions arising from the primary products. Since the only primary products that were quantitively different from the feed in the experiment were olefins, it was inferred that coke formation was attributable to these.

In view of the practical importance of reforming catalyst deactivation by carbonaceous residues it is of interest to know which of the functions, acid or metal, controls coke formation. According to some authors coke formation can be attributed to acid sites (8, 98, 99) whilst others favour the metal function (82, 100) or a combination of both metallic and acidic sites (92).

Gates, Katzer and Schuit (8) reported that poisoning begins on the metal with the formation of olefinic species and aromatics. These precursors slowly form coke on the metal, but may also be transported by gas-phase diffusion and surface migration to the acid sites of the catalyst where they form more resistant coke. According to the authors the long-term deactivation in reforming may be attributed to this second type of coke formation. Shum, Butt and Sachtler (100) have questioned these results and propose a deactivation mechanism controlled by the metal function. The conversion of n-hexane on previously coked Pt/Al_2O_3 catalyst, physically mixed with either fresh Al_2O_3 (acidic function) or fresh Pt/SiO_2 (metallic function), was investigated by these workers. It was observed that the addition of Pt/SiO_2 caused a significant increase in dehydrocyclisation. In contrast, the addition of Al_2O_3 caused no significant change. It was concluded from these results that the metal function controlled dehydrocyclisation and was therefore, the critical function of a reforming catalyst. Consequently, the long-term deactivation of reforming catalysts, involving loss of dehydrocyclisation activity, was attributed to the poisoning of the metal function by carbonaceous residues. Biswas and co-authors (82) in their review on reforming catalysts support the views of Shum et al. and state that it is unacceptable to consider only acidic site coking mechanisms. According to these authors the

overall deactivation of octane improvement in reforming is controlled by the alteration in nature or graphitisation of carbonaceous residues located on metal sites.

However, Margitfalvi and co-workers (99), on the basis of results obtained on the deactivation of Pt/Al_2O_3 and different $Pt\text{-}Sn/Al_2O_3$ catalysts, claim that such statements should be revised. The loss of activity and selectivity changes observed by Margitfalvi et al. were attributed to the alteration in the ratio of unpoisoned metallic to acidic sites. Furthermore, their results showed that coke formation on the Al_2O_3 support was responsible for the rapid deactivation of reforming catalysts and that the support should not be considered as an inert coke reservoir.

1.2.3 Effect of Operating Conditions on Formation of Catalyst Coke

Operating conditions have an extremely important influence on the amount of coke deposited on reforming catalysts. The rate of formation is affected by several factors including pressure, temperature, hydrogen/hydrocarbon reactant ratio and feedstock composition. Other aspects which influence coke fouling of the catalyst include factors such as the chlorine content, sulphur content, metal loading, metal dispersion and the composition of the metallic phase of the catalyst.

When considering the preferred reactions in catalytic reforming exclusively in terms of thermodynamics, it is apparent that it would be best to operate at the lowest possible hydrogen pressure (section 1.1.3). However, it is well established that the rate of catalyst coking and hence deactivation is greatly favoured under such

conditions. (2, 8, 82, 92). Low hydrogen pressures encourage the formation of highly unsaturated coke precursors on the catalyst surface. In addition the conversion of pregraphitic carbonaceous residues to toxic graphitic coke is greatly accelerated (82). With increasing hydrogen pressure the catalyst surface is partially cleaned of carbonaceous residues. Both surface migration of hydrogen absorbed on the metal and spillover of hydrogen to the support are responsible for the availability of activated atomic hydrogen, which removes carbon or coke producing precursors (8,82,95). The net accumulation of coke on the surface of reforming catalysts is, therefore, a balance between coke formation and coke removal.

Biswas et al. (82) used the concept of reversible and irreversible (graphitic) coke to explain the attainment of a "steady-state" level of carbonaceous deposit on the platinum surface after the first few hours of operation. Although there was no discernable increase in metal coke levels over the reformer cycle, acid site coke was observed to increase continuously during the same time. Biswas and co-workers noted that the initial deposition of coke in the presence of hydrogen was reversible in nature. The presence of a steady level of coke on the metal was therefore attributed to the rate of reversible coking on the metal being equivalent to the rate of cleaning of reversible coke by hydrogen. It was proposed that long-term deactivation of the catalyst was due to the rate of change of "metal site" coke to graphite being greater than the rate of cleaning of graphitic coke by hydrogen. The fast cleaning of reversible coke has been postulated to occur by catalytic hydrogenation, while the slower removal of graphitic coke occurs by catalytic hydrogasification (101).

Figoli and co-workers (102), studying the relationship between operational conditions and coke formation on a Pt/Al_2O_3 catalyst, concluded that there was a critical value of pressure below which coke deposition was particularly severe. Using TPO it was established that at pressures lower than 7.6 atmospheres coke deposited on the support was more stable and difficult to remove. In the same study, Figoli and co-workers also investigated the influence of the hydrogen to naptha molar ratio. As when the effect of pressure was considered, the authors were able to identify a critical value for the hydrogen to naptha molar ratio of approximately 3, below which coke formation was particularly severe.

In general, high hydrogen pressures suppress coke formation on the catalyst. At the same time, however, it is necessary to use high temperatures to shift the equilibrium constant and composition to favour the dehydrogenation of napthenes and obtain the desired aromatic products. In commercial reforming both the total pressure and hydrogen to naptha molar ratio are fixed at a predetermined level. Temperature is therefore the only possible operating variable for maintaining the catalyst activity. Increasing temperature, however, also increases the rate at which coke is formed (95, 101, 102). The optimum conditions of temperature and pressure during reformer operation are arrived at by making a series of compromises between the desire to reduce the rate of catalyst deactivation and the desire to attain high yields of aromatic products, thus keeping constant the octane number of the reformate.

The influence of feedstock composition on the rate of catalyst deactivation has been noted in several studies. Zhorov et al., for example, demonstrated that certain

hydrocarbon structures have a particularly high coking effect (103). Various hydrocarbons were assessed and classified by these workers according to their coke forming effectiveness. The order of coking efficiency was found to be as follows, where cyclohexane, taken as reference, was given a coefficient of 1:

> Cyclopentadiene (670) > indane (250) > methylcyclopentane (130) > n-nonane (41) > n-hexane (35) > ethylbenzene (23) > benzene (3) > cyclohexane (1)

Cooper and Trimm (104) obtained similar results when investigating the coking of Pt/Al_2O_3 with various hydrocarbons, each having six carbon atoms. Beltramini et al. (105) compared the coke forming tendency of several pure hydrocarbons including napthenes, aromatics and normal paraffins. It was found that coke formation was not directly related to molecular weight, although there was higher coke deposition for paraffins containing seven carbon atoms or more, but was more strongly influenced by hydrocarbon structure or those of their principal products.

A common feature noted in all of the above studies was the potency of the C_5 ring structure towards formation of coke. As discussed in section 1.2.2 this has been attributed by Parera and co-workers (88) to a Diels-Alder type condensation mechanism.

The composition and structure of reforming catalysts plays a major role in determining catalyst stability and activity. Both platinum content and dispersion, for

example, have been shown to influence the rate of coke deposition. Franck and Martino (106) report that for two Pt/Al_2O_3 catalysts of 0.35 and 0.60% Pt by weight, coked under identical conditions, the catalyst with higher metal loading was more stable by 20-30%. A similar relationship between metal loading and coke deposition has been noted by other authors (80).

As to the effect of metal dispersion on the rate of coking, it is accepted that small platinum particles (high dispersion) show greater resistance to deactivation than do larger particles (106, 107). Barbier and co-workers, for example, investigated the coking of a series of Pt/Al_2O_3 catalysts using TPO to quantify the coke deposits on the metal surface (107). It was shown that catalysts with a low metal dispersion were more sensitive to auto-deactivation than were equivalent well dispersed catalysts. Lankhorst et al. (108) considered that the greater activity and selectivity maintenance of well dispersed Pt/SiO_2 catalysts was indicative of a reduced rate of coke deposition. The greater stability of highly dispersed Pt/SiO_2 was attributed to the increased number of low coordination edge or corner atoms present in smaller crystallites. This is in agreement with the proposal of Barbier et al. (107) that large platinum crystallites increase the coke reaction rate due to their ability to stabilise cyclopentadiene coke precursors. Taken together with the observations of Somorjai and Blakely (109) that corner sites are the longest surviving during coking of platinum crystallites, these results suggest that coke is deposited preferentially on high coordination number metal atoms such as those found in crystallite planes or large metal ensembles.

Regarding chlorine on the surface of reforming catalysts, its presence is

essential in modifying the acidity of the Al_2O_3 support (Section 1.1.2). Several workers have also commented on the importance of chlorine in promoting the transportation of dissociatively adsorbed hydrogen from Pt to Al_2O_3 (87, 110). This phenomenon, known as hydrogen spillover, has been accredited with reducing the rate of coke formation through rehydrogenation of unsaturated coke precursors on the support. An excess of chlorine, however, is known to promote both hydrocracking and to increase the rate of formation of carbonaceous deposits. Parera and co-workers (111) have shown that the amount of coke on a reforming catalyst is at a minimum when the chlorine content is in the range 0.7-0.9% by weight, in agreement with industrial practise. This represents an optimum level of chlorine on the catalyst surface, balancing the rate of hydrogen spillover and the rate of catalyst deactivation through coking.

Since the introduction of bimetallic reforming catalysts the most popular view to explain their characteristic catalytic behaviour has been that of alloy formation (section 1.1.2). Indeed the beneficial effect of the high dispersion of monometallic platinum (reduced ensemble size) could explain the role of additive such as Re, Ir or Sn which could divide the larger platinum ensembles into smaller ones, thus inhibiting the coking reaction (50, 111). The lower coke formation on bimetallic catalysts has also been ascribed to the ability of Re or Ir to destroy coke precursors by hydrogenolysis (36, 112). Barbier, Churin and Marecot (113), in a recent study on the coking of Pt-Re/Al_2O_3 and Pt-Ir/Al_2O_3 catalysts, confirmed that both additives resulted in a lower rate of coke deposition. Whilst agreeing with the suggestion that both Re and Ir induced the transformation of coke precursors to paraffins the authors also

noted that the decrease in coke formation was associated with a modification of the nature of the deposits, which on average were more dehydrogenated. Furthermore, it was demonstrated that at high pressure, coke was deposited mainly on the support in Pt-Re and Pt-Ir catalysts, consequently preventing deactivation of the metal. In view of these results the authors have suggested that an explanation of the improved performance of Pt-Re and Pt-Ir catalyst simply in terms of dilution of large platinum ensembles by Re or Ir is insufficient.

Another explanation for the beneficial effects of bimetallic Pt-Re is given by Parera et al. (46) who suggest that Re reduces the dehydrogenation efficiency of Pt, thus reducing coke formation. On the other hand Margitfalvi and co-workers (114) have proposed that Re increases the amount of hydrogen available through a spillover mechanism. Hydrogen-consuming reactions like hydrogenolysis are therefore increased and coke formation is decreased. Burch and Mitchell (115) take the view that Pt-Re and Pt-Sn are more suitable than Pt in hydrogenating dienes into alkenes, which are less active for the formation of coke precursors. It is emphasised in the latter study that any conclusions are based on results at atmospheric pressure only and that different mechanisms may operate at higher pressure.

As discussed in section 1.1.2, the beneficial properties of Pt-Re/Al_2O_3 are observed only after presulphurisation. Shum, Butt and Sachtler (111), after extensive studies on the sulphiding of both mono- and bimetallic reforming catalysts, have concluded that Pt-Re alloy particles are responsible for the catalytic properties of Pt-Re/Al_2O_3. However, the differences in performance between sulphided Pt/Al_2O_3 and

sulphided Pt-Re/Al_2O_3 are attributed to the combined action of rhenium and sulphur. In addition to rationalising changes in selectivity in terms of reduced ensemble size the authors propose a model to explain the enhanced activity maintenance of Pt-Re(S)/Al_2O_3. It is suggested that the reduced rate of coke formation on the catalyst may be attributed to protruding sulphur atoms adsorbed on the surface rhenium atoms. Shum, Butt and Sachtler assert that these impede the reorganisation of hydrogen-deficient carbonaceous residues into toxic graphitic coke, thereby improving catalyst stability.

1.2.4 Effect of Deposited Coke on Reforming Reactions

In addition to causing loss of catalyst activity, it is well established that the presence of coke deposits are influential in determining catalyst selectivity (102, 116-120). It is apparent from the preceding section that the coking of reforming catalysts is a complicated phenomenon. Similarly, when we consider the changes observed in catalyst selectivity it is evident that the effect of coke deposition is far from simple.

The ability of coke deposits to change catalyst selectivity has been demonstrated by Christoffel and Paál (116). According to these workers both fresh and partly deactivated Pt/Al_2O_3 catalysts lose isomerisation and hydrogenolysis activity during reaction with methylcyclopentane. Dehydrogenation activity, however, remains unchanged. In accordance with these results Barbier (117) has reported that, with various hydrocarbons on Pt/Al_2O_3, the hydrogenolysis reaction is the most sensitive to coke deposition, whereas hydrogenation and dehydrogenation reactions are

essentially unaffected. Christoffel and Paál (116) also observed that the formation of carbonaceous deposits favoured metal-catalysed bond-shift skeletal rearrangements in preference to the cyclic mechanism of isomerisation. The authors attributed this to the dilution of the larger metal ensembles, required in the latter mechanism, by surface carbon. The results of Beltramini and Trimm (118) provided evidence for the selective loss of both hydrogenolysis and hydrocracking activity with increasing coke content. However, in contrast with Christoffel and Paál (116), Beltramini and Trimm report that the isomerisation selectively of their Pt/Al_2O_3 catalyst increased with time. In addition, Figoli and co-workers (102) have established from naptha reforming studies, that increasing coke content induces a selective loss of dehydrocyclisation activity.

A more recent study by Beltramini and Trimm (119) has indicated that the main benefit in using bimetallic reforming catalysts originates in their ability to control not only coke deposition but also those sites on which the coke is deposited. Thus, for example, in the reaction of n-heptane on $Pt\text{-}Re/Al_2O_3$, undesired hydrocracking reactions were rapidly deactivated by coke formation. On the other hand, desired isomerisation and aromatisation reactions were observed to increase in importance with catalyst deactivation. Parera et al. (120), investigating the reforming of n-heptane on a $Pt\text{-}Re/Al_2O_3$ catalyst under commercial conditions, have also observed that conversion to paraffins with six or fewer carbon atoms decreases with time, whilst isomerisation selectively increases. Contrary to the results of Beltramini and Trimm (119), aromatisation selectivity was reported to decrease with increased coking.

In conclusion, coke deposits can alter the selectivity of bifunctional reforming catalysts by showing different toxicities towards the reactions taking place. On the metal function of the catalyst coke settles preferentially on the hydrogenolysis sites accounting for the significant losses in hydrogenolysis activity observed. On the alumina support, the coke is deposited on the sites of greatest acidity, thereby inhibiting reactions such as hydrocracking and dehydrocyclisation.

CHAPTER TWO

OBJECTIVES

2 OBJECTIVES OF THE PRESENT WORK

The work described in this thesis comprises of a detailed study of the reaction of n-octane and hydrogen on $Pt/\gamma\text{-}Al_2O_3/Cl^-$ and $Pt\text{-}Re/\gamma\text{-}Al_2O_3/Cl^-$ catalysts using a continuous flow microreactor technique. The main objectives were to determine the influence of catalyst composition and structure on activity, selectivity and stability, with particular reference to: i) the effect of platinum loading and dispersion on coking characteristics; ii) the effect of catalyst support variations on coking characteristics and iii) the role that rhenium plays when used to modify the behaviour of Pt/Al_2O_3 reforming catalysts.

To this end the following studies have been undertaken using 0.9% w/w $Pt/\gamma\text{-}Al_2O_3/Cl^-$, 0.3% w/w $Pt/\gamma\text{-}Al_2O_3/Cl^-$ and 0.3% w/w Pt-0.3% w/w $Re/\gamma\text{-}Al_2O_3/Cl^-$:-

a) Temperature-programmed reduction

b) Static and pulse carbon monoxide chemisorption

c) Nitrogen physisorption

d) Mercury porosimetry

e) Transmission electron microscopy

f) Neutron activation analysis

g) n-Octane reforming at high pressure

h) Quantitative surface carbon analysis of spent catalysts.

CHAPTER 3

CATALYST CHARACTERISATION

3.1 CATALYST PREPARATION AND REDUCTION

Three supported platinum catalysts, CK 303, CK 433 and GHI were investigated in this study. Both CK 303 and CK 433 are commercial catalysts and were manufactured by Akzo Chemie Ketjen. Catalysts CK 303 and CK 433 use the same high purity γ-alumina support (CK 300, Akzo Chemie Ketjen) and are more commonly known as EUROPT 3 and EUROPT 4. Although details on the preparation of these catalysts are not supplied by the manufacturer, it has been reported that commercial precursors are probably calcined at ca. 500°C (27).

EUROPT 3 is monometallic and contains 0.3% platinum by weight. EUROPT 4 is bimetallic and contains 0.3% platinum and 0.3% rhenium by weight. Both catalysts are chlorinated and each contain 0.95% chlorine by weight. The catalysts are supplied as cylindrical pellets about 1/16" in diameter and 1/4" long.

The third catalyst, GHI, was prepared at ICI Billingham as part of a joint research project undertaken by Glasgow University, Hull University and ICI Chemicals and Polymers Limited. The GHI catalyst used Degussa Aluminium Oxide C as a support and was prepared by the incipient wetness technique. The support was impregnated with an aqueous solution of chloroplatinic acid (H_2PtCl_6) consistent with a platinum loading of approximately 1.0% by weight. The impregnated alumina was then dried at 80°C for 24 hours in flowing nitrogen. Following the drying procedure the catalyst powder was pressed at a pressure of 5 tonnes. The tablets formed were carefully crushed and then sieved; the particles with diameters between 180 and

500 μm being retained for use.

The platinum and chlorine content of unreduced samples of GHI catalyst were determined respectively by atomic adsorption spectroscopy and neutron activation analysis as part of the GHI study (121). Table 3.1 summarises the platinum and chlorine content for each catalyst used in this study.

Table 3.1: Catalyst Platinum and Chloride Content

	GHI	EUROPT 3	EUROPT 4
Platinum Content (wt.%)	0.9	0.3	0.3
Rhenium Content (wt.%)	0	0	0.3
Chlorine Content (wt.%)	1.28	0.95	0.95

Catalysts EUROPT 3 and EUROPT 4 were activated using a standard technique. The technique used, unless stated otherwise, was as follows:-

i) Calcination

Heat to 400°C at 5° min^{-1} in flowing air (60ml min^{-1}). Hold at 400°C for 4 hours then cool to room temperature in air.

ii) Flushing

Switch to helium flow (60 ml min^{-1}). Hold for 1 hour at room temperature.

iii) Reduction

Switch to hydrogen flow (60ml min^{-1}) and heat to 400°C at 5° min^{-1}. Hold at 400°C for 2 hours.

Similarly, a standard reduction technique was used for the GHI catalyst. The reduction procedure was as follows:-

i) The catalyst was held at ambient temperature for 30 minutes in flowing hydrogen (25ml min^{-1}).

ii) The catalyst was then heated to 300°C at 10° min^{-1} in flowing hydrogen (25ml min^{-1}) and held at this temperature for 1 hour.

3.2 CHARACTERISATION OF FRESH CATALYSTS

An understanding of the physical and chemical characteristics of a catalyst is invaluable when investigating its reaction chemistry. A wide range of analytical techniques were therefore used to establish a detailed knowledge of the catalysts' physiochemical properties. Freshly prepared catalysts were characterised in terms of their metal dispersion, specific surface areas, pore attributes and temperature-programmed reduction profiles. Errors, where calculated on the results, are quoted as the standard deviation on the mean. Except where stated otherwise, the work described in the following sections of this chapter was carried out in the laboratories of ICI Wilton.

3.2.1 Temperature-Programmed Reduction

The technique of temperature-programmed reduction (TPR) was used to characterise the reduction process associated with each catalyst. This sensitive technique involves measuring the hydrogen consumption due to reduction of the metal oxide surface while the catalyst sample is heated up with linear temperature-programming. The technique is very susceptible to the presence of species in a reducible form and has been extensively applied to the study of supported metal catalysts (122).

A conventional temperature-programmed reduction apparatus was used similar to that described by Robertson et al. (123). The equipment used consisted of several gas supply lines capable of delivering a choice of synthetic air, helium or 5% v/v hydrogen in argon and a reactor section comprising a quartz tube (1/4" o.d.) placed horizontally in an insulated furnace connected to a linear temperature programmer. A calibrated thermal conductivity detector was connected to a chart recorder for measurement and display of hydrogen consumption.

Helium, synthetic air and 5% v/v hydrogen in argon were purified by passing through molecular sieve "gas clean moisture filters" (Chrompack Ltd.). TPR profiles were measured at a total pressure of 1 atmosphere. The gas emerging from the reactor was dried by passing through a solid carbon dioxide-acetone trap before entering the thermal conductivity detector. A sample weight of approximately 0.5 g was used; the desired particle size of 425-850 μm was obtained by crushing and sieving the catalyst.

A standard programme for the calcination and temperature-programmed reduction of EUROPT 3 and EUROPT 4 was used. This was adapted from the technique detailed in section 3.1. The standard programme involved three steps:-

i) Calcination

Heat to 400°C at 5° min^{-1} in flowing air (60ml min^{-1}). Hold at 400°C for 4 hours then cool to room temperature in air.

ii) Flushing

Switch to helium flow (4 litres $hour^{-1}$). Hold for 1 hour at room temperature.

iii) Reduction

Switch to 5% hydrogen flow in argon (10ml min^{-1}) and heat to 550°C at 10° min^{-1}. Hold at 550°C for 1 hour.

Typical TPR profiles for EUROPT 3 and EUROPT 4 are shown in figure 3.1 and figure 3.2 respectively. A summary of the number of TPR peaks and the temperatures of peak maxima is present in Table 3.2.

Table 3.2: Temperature Corresponding to Peak Maximum for EUROPT 3 and EUROPT 4

	Number of Peaks	Temperature of Peak Maximum (°C)						
EUROPT 3	5	243	340	550	550	550	-	-
EUROPT 4	7	260	340	395	415	550	550	550

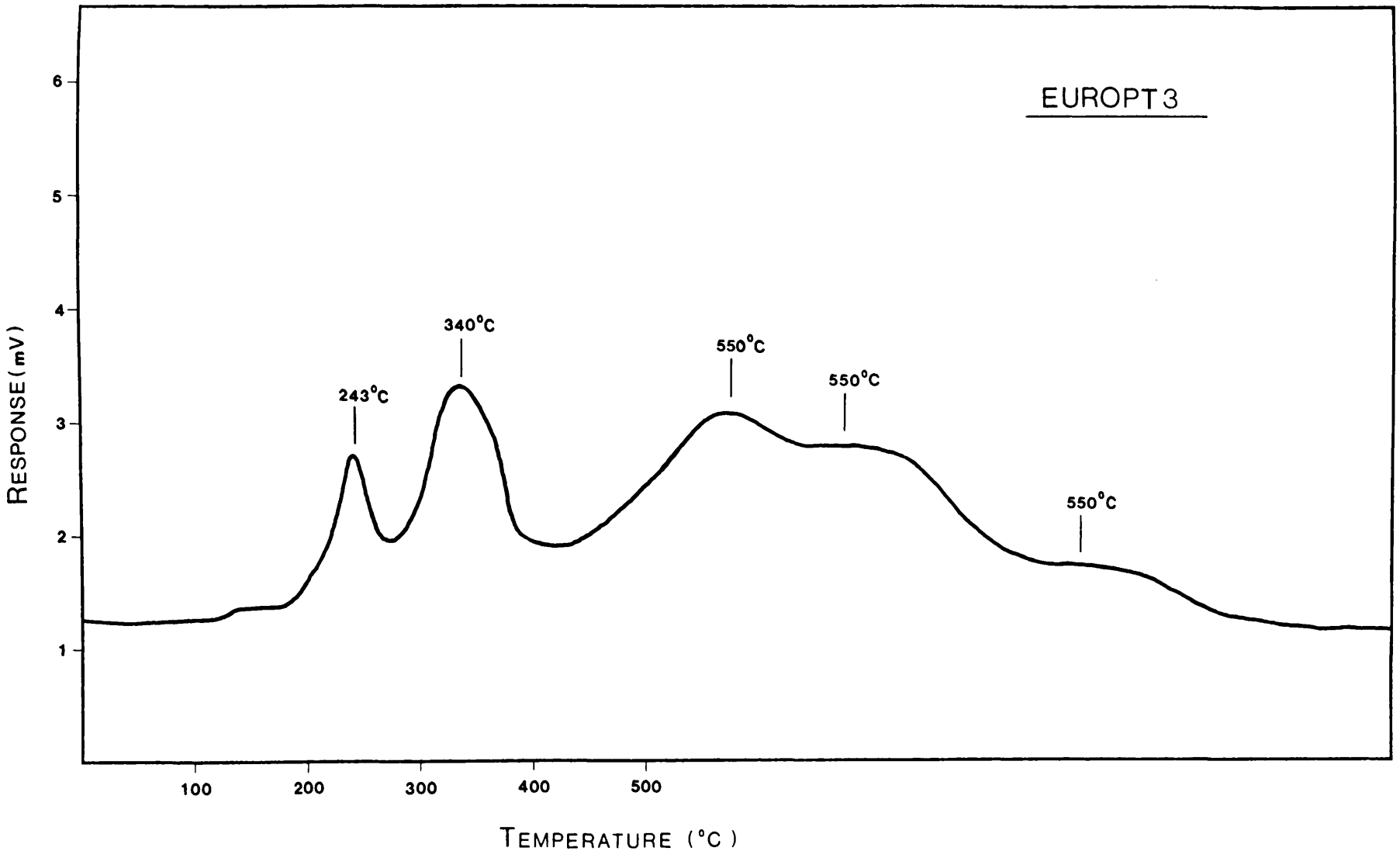

Figure 3.1 - Typical TPR Profile for Catalyst EUROPT3.

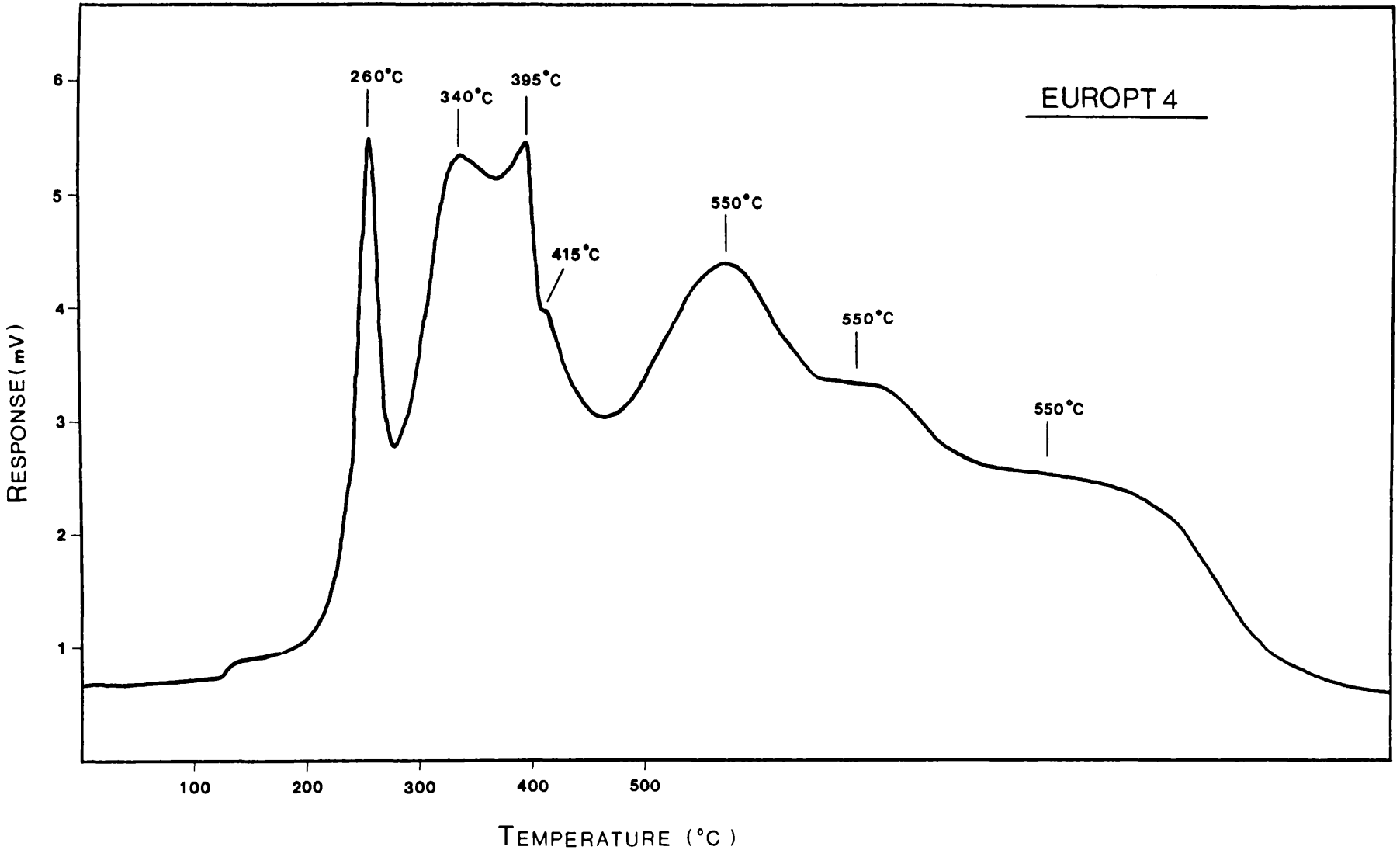

Figure 3.2 - Typical TPR Profile for Catalyst EUROPT4.

Thermal conductivity detector response for hydrogen consumption was calibrated using approximately 0.005 g samples of high purity CuO wire (BDH Ltd). Total hydrogen uptakes for the TPR were measured by tracing the associated peak area, carefully cutting out the area and weighing it to 4 decimal places. By comparison with the calibrated CuO reduction peak the volume of hydrogen associated with the supported metal reduction process could be calculated. Table 3.3 compares the experimental hydrogen consumption with the theoretical hydrogen consumption for EUROPT 3 and EUROPT 4. Hydrogen uptake was calculated for $Pt^{4+} \rightarrow Pt^{0}$ and $Re^{7+} \rightarrow Re^{0}$ where appropriate.

Table 3.3: Hydrogen Uptake During TPR

	Experimental (μmol/g)	Calculated (μmol/g)
EUROPT 3	42 44	31
EUROPT 4	101 100	87

Temperature-programmed reduction profiles for the monometallic GHI catalyst were determined in previous work (121). The catalyst samples were reduced using the standard technique detailed in section 3.1. The TPR profile was reported to show a single peak with a maximum at 227 ± 5°C. No data was available on hydrogen uptake for the reduction procedure.

3.2.2 Pulse-Flow Carbon Monoxide Chemisorption

On completion of the temperature-programmed reduction procedure the catalyst samples EUROPT 3 and EUROPT 4 were further characterised by pulse-flow chemisorption of carbon monoxide. Following reduction the catalyst was maintained at 550°C in a helium flow of 4 L $hour^{-1}$. After flushing with helium for 1 hour the catalyst sample was cooled to room temperature. The adsorbate gas was admitted to the reduced catalyst by injecting 20 μl pulses into the helium carrier-gas stream. The volume of carbon monoxide was chosen such that a number of pulses would be completely consumed by the catalyst. The quantity of gas required to achieve saturation coverage of irreversibly adsorbed carbon monoxide was then calculated.

Assuming that carbon monoxide forms a linearly bound species with platinum we may determine the total number of exposed platinum atoms and hence the metal dispersion. Given that the cross sectional area of a platinum atom is 8.9 A^2 (124,125), the metal surface area per gram of catalyst, Sc, is calculated according to the equation:-

$$Sc = n_{co} \times N_A \times 8.9 \times 10^{-20} \quad \text{.....(1)}$$

Where N_A = Avogadros number

n_{co} = moles of carbon monoxide adsorbed at STP per gram of catalyst

Sc = m^2/g catalyst

Similarly, we may calculate the metal surface area, S_M, per gram of platinum:-

$$S_M = \frac{N_A \sigma R}{M} \qquad \text{.....(2)}$$

Where N_A = Avogardros number

σ = platinum cross sectional area

M = molecular weight of platinum

R = the ratio of carbon monoxide molecules adsorbed per platinum atom

The platinum crystallites were envisaged as being regular cubes with 5 faces exposed to the gas, the sixth in contact with the support. Electron micrographs of platinum catalysts suggest a roughly spherical crystallite shape. However the volume/surface ratio is constant for spheres and cubes (126). Hence the metal area of an amount of catalyst containing 1 gram of platinum is given by:-

$$S_M = \frac{5 \times 10^3}{l\rho} \qquad \text{.....(3)}$$

Where l = edge length of the cube in nm.

ρ = density of platinum

The edge length of the platinum crystallite may then be calculated using the value of metal surface per gram of platinum determined from equation (2). The face diagonal or mean diameter of the crystallite is readily calculated using Pythagoras's Theorem.

Metallic rhenium is also known to adsorb carbon monoxide in a linear form (25). The calculations outlined above are therefore applicable to the monometallic platinum

catalysts only. The results from pulse-flow carbon monoxide chemisorption on EUROPT 3 and EUROPT 4 are presented in table 3.4 and, where appropriate, in table 3.5. The results reported in tables 3.4 and 3.5 for catalyst GHI were determined in previous work (127).

Table 3.4: Determination of Metal Dispersion from Pulse CO Chemisorption

	EUROPT 3	EUROPT 4	GHI
Volume of CO (μl) Ads. .g^{-1} Catalyst (20°C)	300.2 ±2.8	308.1 ±5.4	790.2 ±43.1
No. of CO Molecules Ads. .g^{-1} Catalyst	7.5×10^{18}	7.7×10^{18}	2.0×10^{19}
No. of Metal Surface Atoms .g^{-1} Catalyst	7.5×10^{18}	7.7×10^{18}	2.0×10^{19}
No. of Bulk Metal Atoms .g^{-1} Catalyst	9.3×10^{18}	1.9×10^{19}	2.7×10^{19}
Metal Dispersion (%)	81.2	40.7	72.0

Table 3.5: Determination of Specific Platinum Surface Area and Mean Platinum Crystallite Diameter from Pulse CO Chemisorption

	EUROPT 3	GHI
No. of Pt Surface Atoms g^{-1} Catalyst	7.5×10^{18}	2.0×10^{19}
Platinum Surface Area (m^2 g^{-1} Catalyst)	0.7	1.8
Metal Surface Area (m^2 g^{-1} Platinum)	223.1	197.8
Crystallite Face Diagonal	1.5 nm	1.7 nm

3.2.3 Static Carbon Monoxide Chemisorption

Static carbon monoxide chemisorption experiments were performed using a Micromeritics Digisorb 2800 instrument. The Digisorb 2800 is a fixed volume instrument that uses a volumetric technique for chemisorption measurements. After pretreatment and evacuation of the catalyst, a known quantity of adsorbate is introduced into the system. When adsorption equilibrium is attained over the catalyst, the remaining gas in the system can be calculated from the pressure and the known volume of the system. The free volume in the catalyst sample tube and in the manometric part of the apparatus is determined using a non-adsorbable gas such as helium.

In practice, the amount of gas adsorbed is measured at increasing pressures with the catalyst maintained at a constant temperature. If a typical Langmuir-type adsorption isotherm is obtained, it is easy to intrapolate the isotherm to zero pressure. Two isotherms are usually established for the catalyst under investigation. The first

isotherm is a measure of total adsorption on the sample; the second, obtained after evacuation, is a measure of physical adsorption. The difference between the two gives the isotherm due to strongly adsorbed carbon monoxide only, as this material is untouched by the evacuation procedure. The intercept on the ordinate for the chemisorption isotherm is taken as the amount of gas required to form a unimolecular coverage on the metal of the sample.

Catalysts EUROPT 3 and EUROPT 4 were analysed using the Digisorb 2800 instrument. Each catalyst sample was dried at 120°C in an oven for 4 hours, transferred to the sample tube and then calcined and reduced using the standard technique described in section 3.1. Prior to the analysis the reduced catalyst was evacuated for 1 hour at 20°C and a pressure of 3×10^{-4} Torr. A sample size of ca. 0.5g was used in all experiments. Tables 3.6 and, where appropriate, 3.7 present the results for static carbon monoxide chemisorption on the two catalysts. Metal dispersion, surface areas and crystallite face diagonals were calculated from the volume of carbon monoxide adsorbed on each catalyst in exactly the same manner as described in the previous section.

Table 3.6 Determination of Metal Dispersion from Static CO Chemisorption

	EUROPT 3	EUROPT 4
Volume of CO (μl) Ads. g^{-1} Catalyst (20°C)	243.1 ± 1.4	244.0 ± 1.5
No. of CO Molecules Ads. g^{-1} Catalyst	6.5×10^{18}	6.6×10^{18}
No. of Metal Surface Atoms. g^{-1} Catalyst	6.5×10^{18}	6.6×10^{18}
No. of Bulk Metal Atoms $.g^{-1}$ Catalyst	9.3×10^{18}	1.9×10^{19}
Metal Dispersion (%)	70.5	34.6

Table 3.7 Determination of Specific Platinum Surface Area and Mean Platinum Crystallite Diameter from Static CO Chemisorption

	EUROPT 3
No. of Pt Surface Atoms $.g^{-1}$ Catalyst	6.5×10^{18}
Platinum Surface Area ($m^2 .g^{-1}$ Catalyst)	0.6
Metal Surface Area ($m^2 .g^{-1}$ Platinum)	194.0
Crystallite Face Diagonal	1.7 nm

3.2.4 Surface Area and Pore Structure Analysis

3.2.4.1 Surface Area Measurement

A Micromeritcs Digisorb 2600 Physisorption Analyser was used to determine the specific areas of catalysts EUROPT 3, EUROPT 4 and GHI. After outgassing the catalyst sample to remove any physically adsorbed material a volumetric procedure was used to determine the quantity of nitrogen gas adsorbed at liquid nitrogen temperature (77.4K). A known quantity of nitrogen gas was admitted to a confined volume containing the adsorbent. The volume of gas adsorbed at the equilibrium pressure was the difference between the volume of gas admitted and that required to fill the dead space at the equilibrium pressure. An adsorption isotherm was constructed point-by-point by the admission of successive charges of gas, allowing sufficient time for equilibrium at each point. Using this technique an isotherm for nitrogen physical adsorption was established on each adsorbent. Figures 3.3 (a) to 3.3 (c) show typical isotherms for catalysts EUROPT 3, EUROPT 4 and GHI respectively.

The Digisorb 2600 instrument used the conventional BET method for determining surface area. The BET theory is an extension of the Langmuir model of monolayer physical adsorption on surfaces to multilayer adsorption. Adsorption in the first layer is assumed to take place on a surface of uniform site energy. Multilayer adsorption then occurs on the first layer of molecules and approaches infinite thickness as the equilibrium vapour pressure approaches saturation vapour pressure ($p \rightarrow p^0$). Summation of the amount adsorbed in all layers gives the isotherm equation:

$$\frac{V}{V_m} = \frac{C\ p/p^0}{(1-p/p^0)[1 + (C-1)p/p^0]} \qquad \text{.....(4)}$$

Where V = the volume of gas adsorbed at the equilibrium relative pressure, p/p^0.

V_m = the value of V at monolayer coverage.

C = constant related to the heat of adsorption into the first layer and the heat of condensation of the adsorbate. The value of C determines the shape of the isotherm.

p^0 = the saturation vapour pressure.

The BET equation is usually expressed in the form:-

$$\frac{p}{V(p^0-p)} = \frac{1}{V_mC} + \frac{(C-1)p}{(V_mC)p^0} \qquad \text{.....(5)}$$

The plot of $p/V(p^0-p)$ against p/p^0 should therefore be a straight line with slope = $(C-1)/V_mC$ and intercept = $1/V_mC$. Solution of these two simultaneous equations gives V_m and C. The linearity of the BET plot is severely restricted - usually to within the p/p^0 range of 0.05 to 0.30. The lower and upper limits in the Digisorb 2600 calculation are set conservatively at 0.05 and 0.21. Figure 3.4 shows the linear BET plots derived from the corresponding isotherms for catalysts EUROPT 3, EUROPT 4 and GHI.

The second stage in the BET method is the calculation of the specific surface area, A_{sp}, from the value of V_m. The specific surface area is:-

$$A_{sp} = \frac{z\, a_m}{w} \qquad \text{.....(6)}$$

Where z = the number of molecules of adsorbate in the monolayer.

a_m = the cross sectional area of the adsorbate molecule.

w = sample weight.

It is assumed that for a given adsorbate and temperature the cross sectional area, a_m, remains constant and independent of the nature of the adsorbent. The Digisorb 2600 calculation used a value for the cross sectional area of the adsorbed nitrogen molecule of 0.162 nm^2. A catalyst sample weight of approximately 0.5g was used in each analysis and samples were dried at 120°C for 4 hours before each run. The outgassing procedure involved heating at 120°C under high vacuum (10^{-4} Torr) for 16 hours.

The specific surface areas and values of C determined for each catalyst were as shown in table 3.8.

Table 3.8 Specific Surface Areas and Values of C Calculated for each Catalyst

	Catalyst Surface Area (m^2/g)	Value of C
EUROPT 3	193.2 ± 0.8	81.0 ± 1.0
EUROPT 4	195.8 ± 0.5	88.0 ± 1.0
GHI	95.5	98.5

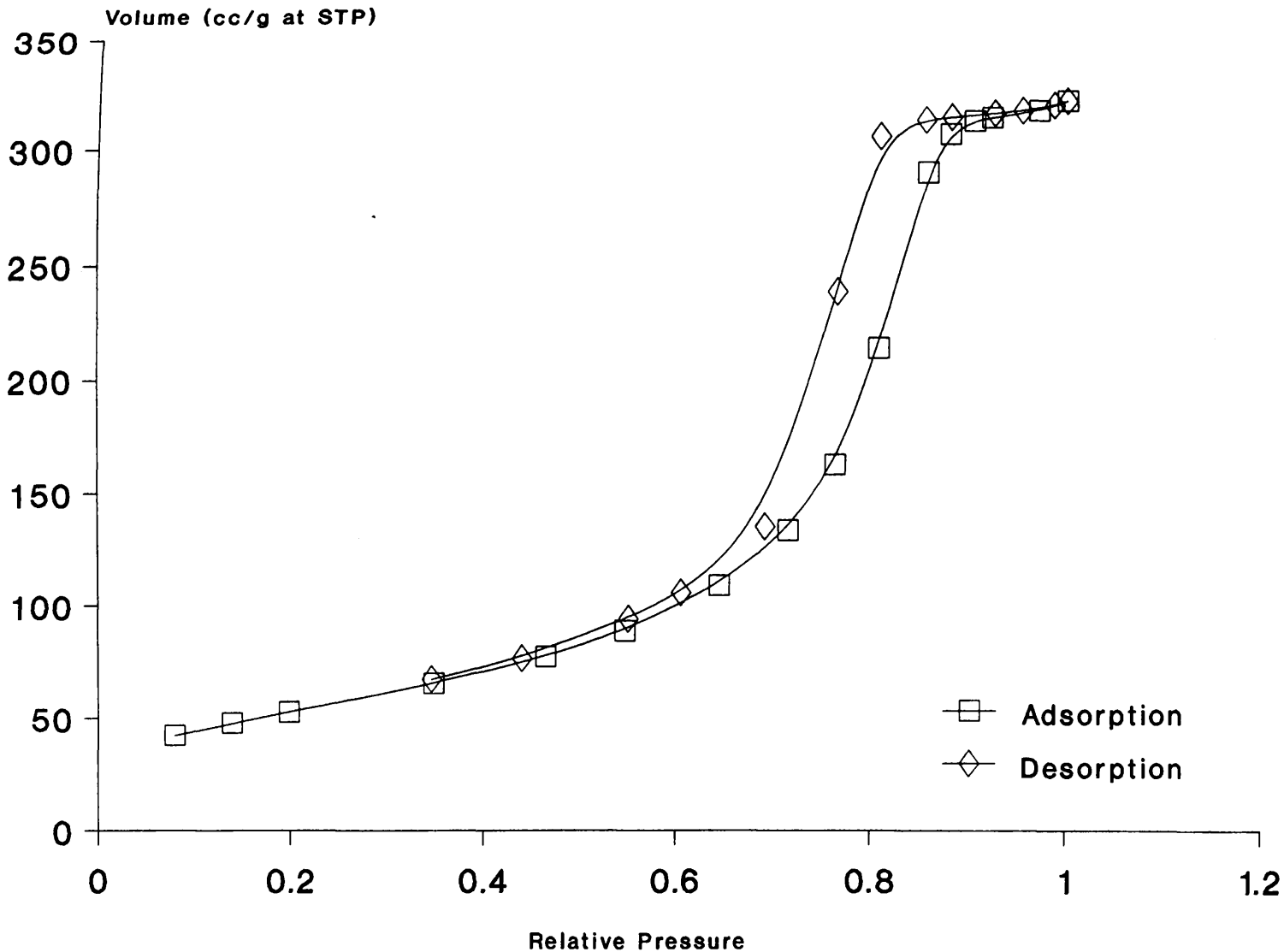

Figure 3.3(a)-Typical Isotherm for Nitrogen Physisorption on Catalyst EUROPT3

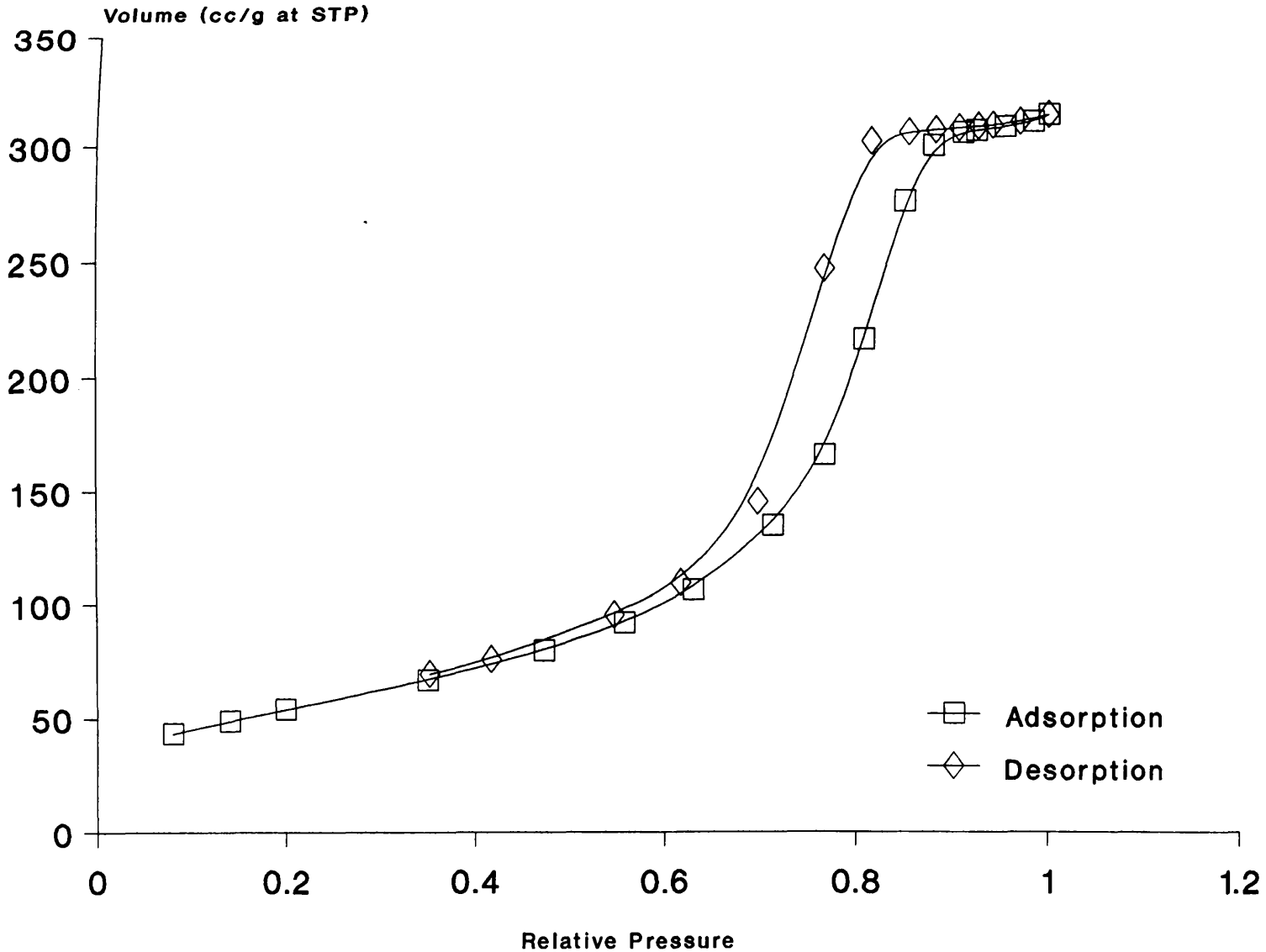

Figure 3.3(b)-Typical Isotherm for Nitrogen Physisorption on Catalyst EUROPT4

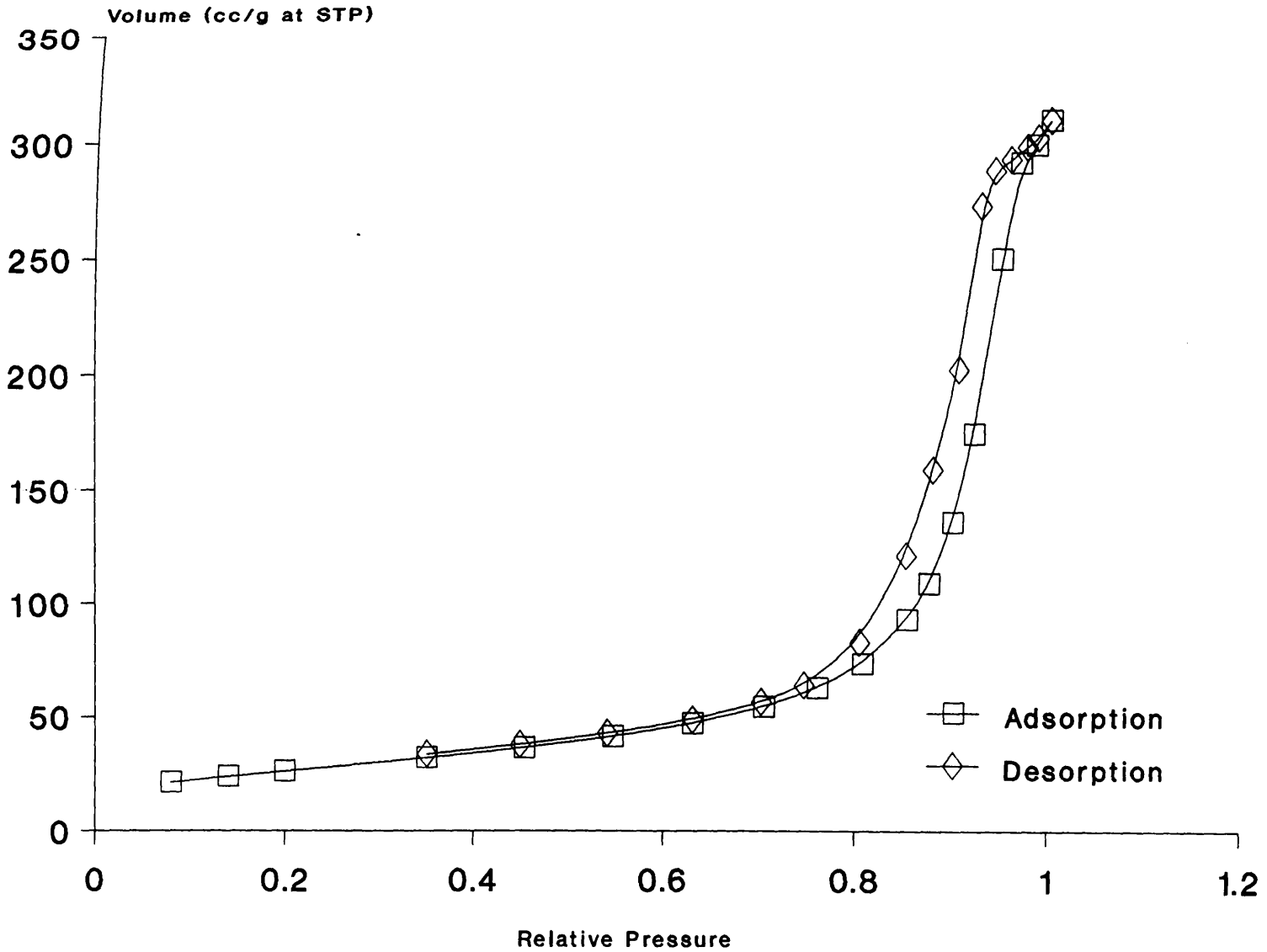

Figure 3.3(c) - Typical Isotherm for Nitrogen Physisorption on Catalyst GHI.

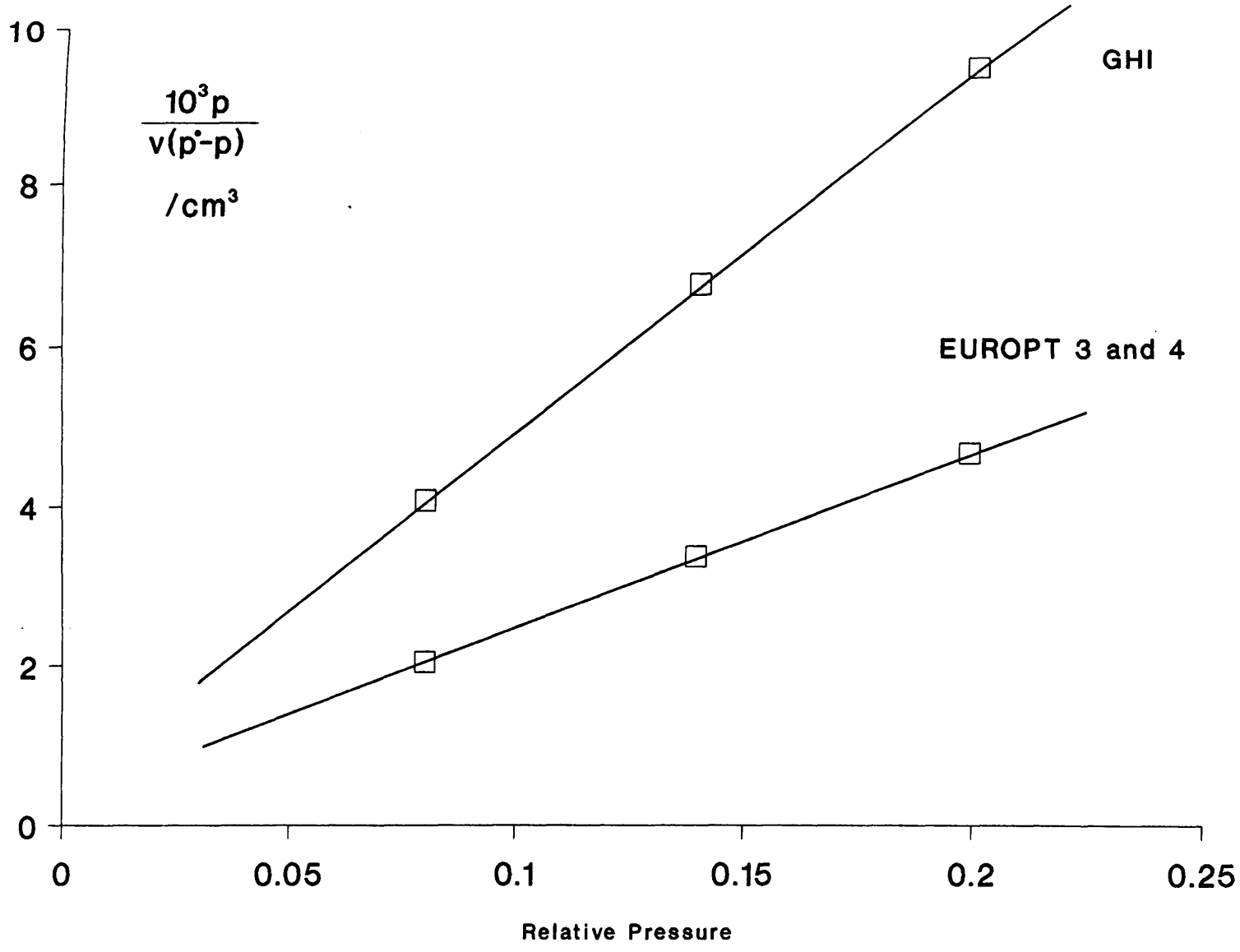

Figure 3.4 - Linear BET Plots for Catalysts EUROPT3, EUROPT4 and GHI.

3.2.4.2 Pore Volume and Pore Area Distribution

An important method for the measurement of pore size distribution is the analysis of the hysteresis in physical adsorption isotherms. The initial portion of type IV isotherm adsorption is restricted to a thin layer of adsorbate on the walls. Following this, at the inception of the hysteresis loop capillary condensation commences in the finest pores. Wider and wider pores are filled as the pressure is progressively increased until at the saturation pressure the entire system is full of condensate. Hysteresis is observed in the isotherm due to the condensation and evaporation processes occurring at different relative pressures. In general the desorption branch of an isotherm is used to relate the amount of adsorbate lost in a desorption step to the average size of pore emptied in the step. A pore loses its condensed liquid adsorbate, known as the core or capillary of the pore, at a particular relative pressure related to the core radius by the Kelvin equation. The mesopore size is usually calculated with the aid of the Kelvin equation in the form:-

$$\ln (p/p^0) = \frac{2\gamma V_L}{r_k RT} \qquad \text{.....(7)}$$

Where r_k = mean radius of the hemispherical meniscus associated with a cylindrical pore.

γ = the condensed liquid surface tension.

V_L = the molar volume of the condensed liquid.

After the core has evaporated in the desorption step, a layer of adsorbate remains on

the walls of the pore. The thickness of this layer is calculated for a particular relative pressure from the Halsey equation:-

$$t_i = m \left[\frac{n}{\text{In } (p/p^0)} \right]^x \qquad \text{.....(8)}$$

Where t_i = adsorbed layer thickness

m = monolayer thickness

n = the Halsey equation numerator

x = the Halsey exponent

This layer becomes thinner with successive pressure drops, so that the measured volume of gas desorbed in a step is composed of the volume of the cores evaporated in that step plus the volume desorbed from pore walls of pores whose cores have been evaporated in previous steps. Barrett, Joyner and Halenda developed the method (known as the BJH method) which incorporates these ideas (128). The procedure used to calculate pore volume and pore area distribution in the Digisorb 2600 instrument is based on an implementation of the BJH method. Several assumptions are made in the calculations: the surface is clean and uniform; the pores are straight; cylindrical and non-intersecting and the volume of gas adsorbed external to the pores is negligible. Figures 3.5(a) to 3.5(c) show the pore area distributions calculated by the Digisorb 2600 instrument for catalysts EUROPT 3, EUROPT 4 and GHI respectively.

The total cumulative pore volume calculated by the BJH method can be compared with the liquid equivalent of the maximum volume adsorbed. This value is determined by multiplying the value of the volume physically adsorbed at a relative

pressure near saturation by the density conversion factor. Assuming that all this liquid resides in pores gives a second measure of the samples total volume. Good agreement between these two values indicates that the assumptions used in the BJH calculation are valid. The maximum volume adsorbed and cumulative pore volume calculated for each catalyst were as shown in table 3.9. The results from catalyst GHI are of particular interest as the support, aluminium oxide C, is reported by the manufacturers to have a non-porous structure (129).

Table 3.9 Calculated Pore Volumes for Catalysts

	Cumulative Pore Volume (cc/g)	Maximum Volume Adsorbed (cc/g)
EUROPT 3	0.505 ± 0.001	0.500 ± 0.001
EUROPT 4	0.490 ± 0.002	0.485 ± 0.002
GHI	0.462	0.481

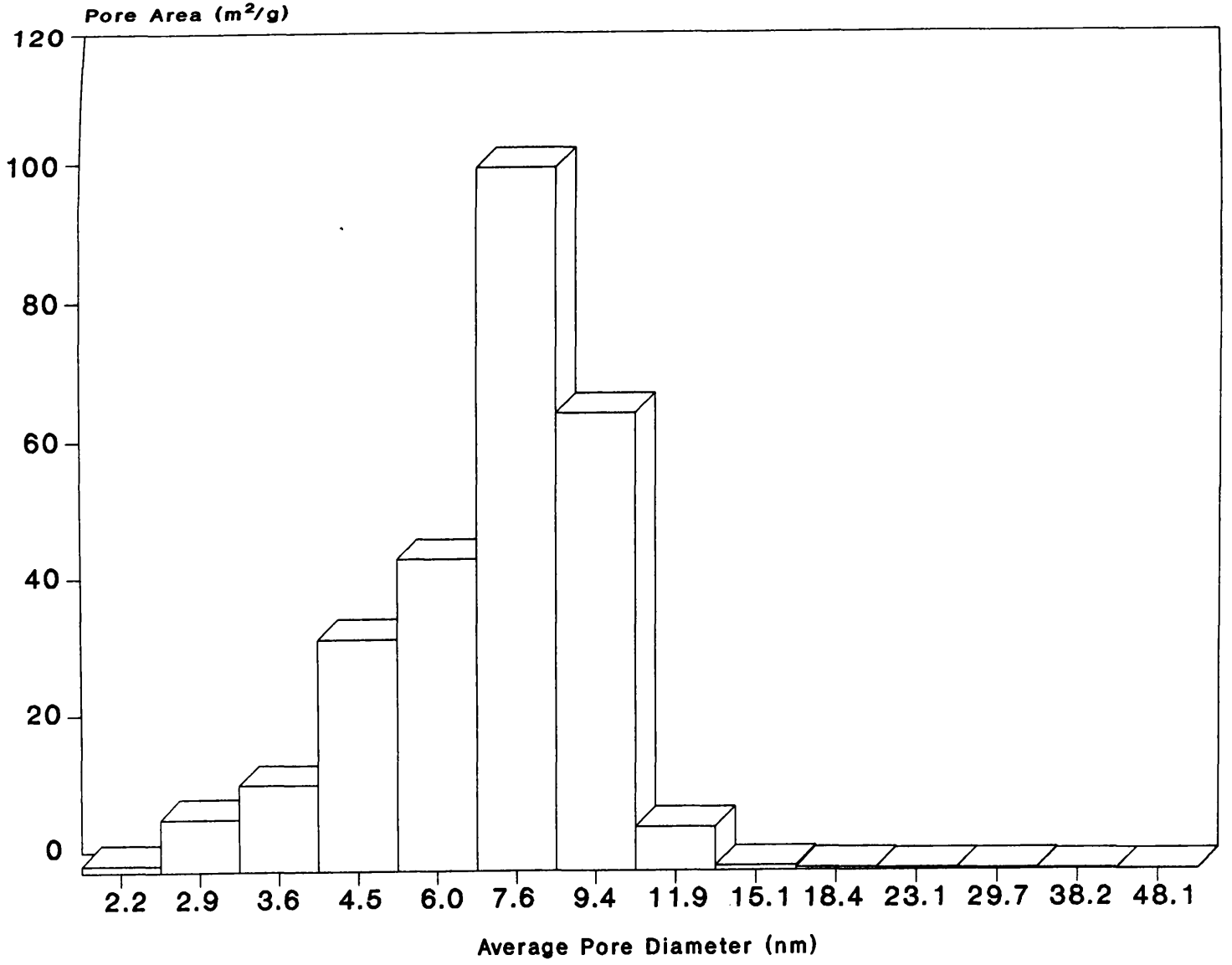

Figure 3.5(a) - Pore Area Distribution Calculated for Catalyst EUROPT3.

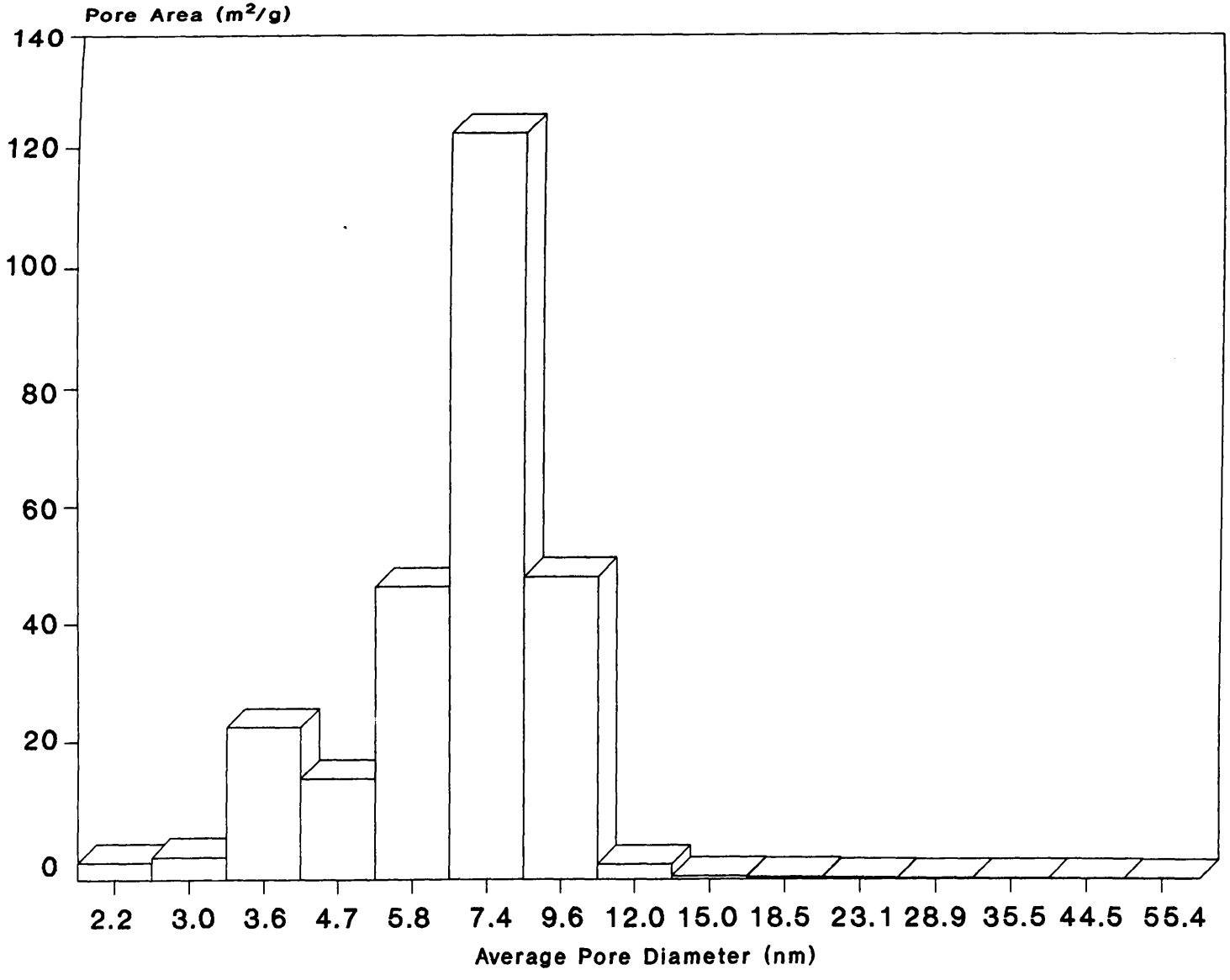

Figure 3.5(b) - Pore Area Distribution Calculated for Catalyst EUROPT4.

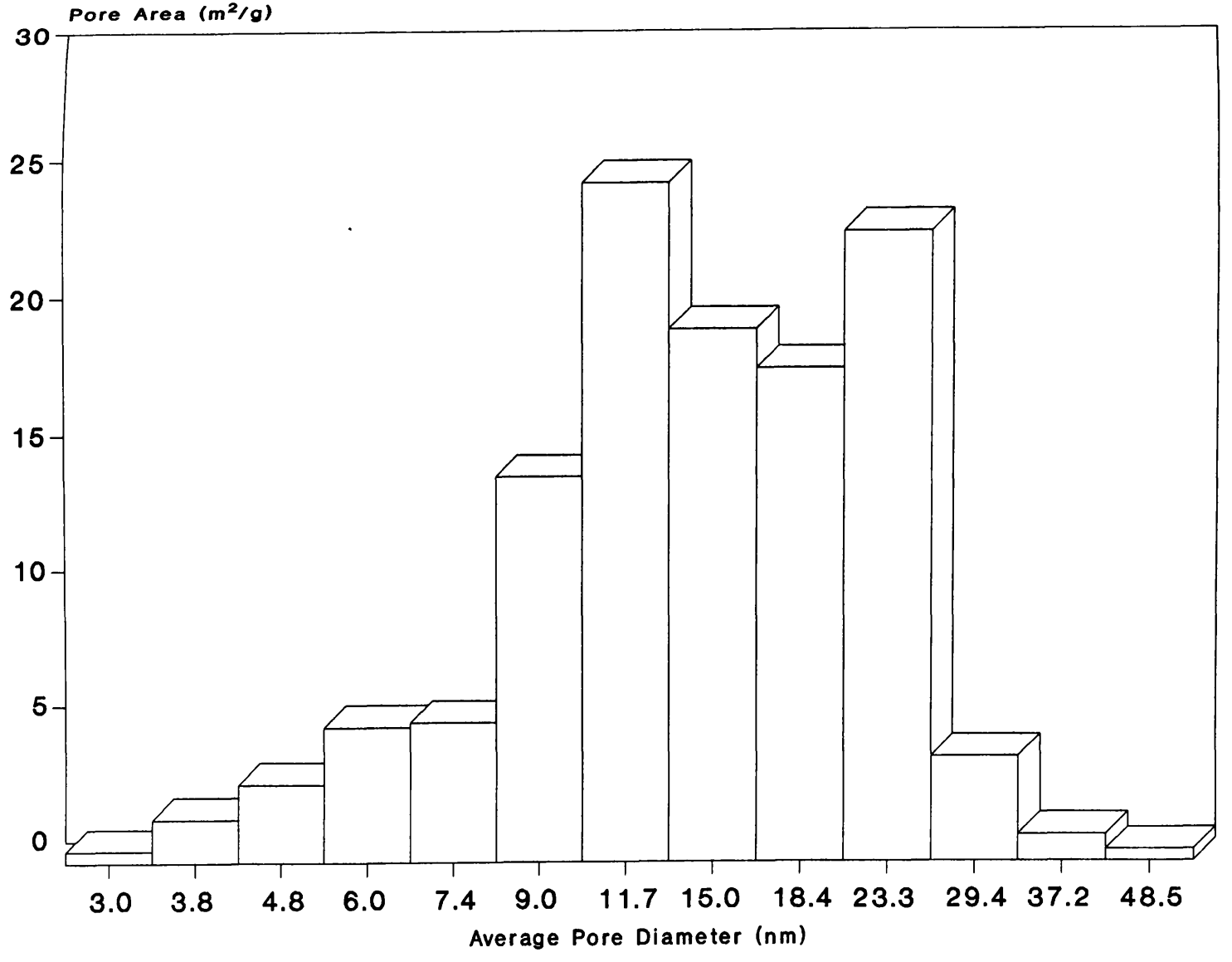

Figure 3.5(c) - Pore Area Distribution Calculated for Catalyst GHI.

3.2.5 Mercury Porosimetry

The contact angle, θ, of mercury with the surface of solids is greater than 90° and hence the mercury meniscus is convex. An excess pressure is therefore required to force liquid mercury into the pores of a solid. The technique of mercury porosimetry involves measuring the extent of mercury penetration in the evacuated solid as a function of the applied pressure. The saturation intrusion volume of mercury is taken as a measure of the total pore volume of the solid.

The determination of pore radii from mercury porosimetry is based upon the Washburn equation:-

$$r_p = \frac{2\gamma \cos\theta}{\Delta P} \qquad \text{.....(9)}$$

Where r_p = the radius of the pore, assumed to be cylindrical

ΔP = the excess pressure required to force liquid mercury into the pores.

γ = the surface tension of the penetrating liquid.

θ = the contact angle (140° for mercury).

The work, dW, required to force a volume, dV, of mercury into the pore of a solid may be related to the work required to form an area, dA, of mercury-solid interface. The relationship is expressed in the following equation:-

$$dW = \gamma \cos\theta \, dA = -PdV \qquad \text{.....(10)}$$

Integration of equation (10) over the range of the mercury penetration curve gives an expression for the surface area, A, of the pore walls:-

$$A = -(\gamma \cos \theta)^{-1} \int_{V\,min}^{V\,max} P\,dV \qquad \text{.....(11)}$$

In common with the physical adsorption of inert gases on porous solids mercury porosimetry demonstrates hysteresis. The interpretation of hysteresis in mercury porosimetry is, perhaps, more difficult than with capillary condensation. One widely accepted explanation for reproducible hysteresis is based on the "ink bottle" model of pore structure. The pressure required to force mercury into a pore having a narrow neck, of radius r_n, will be

$$P_n = \frac{2\gamma \cos \theta}{r_n}$$

Mercury cannot leave the body of the pore, radius r_w, until the pressure has fallen to P_w, given by

$$P_w = \frac{2\gamma \cos \theta}{r_w}$$

From the definition of an "ink bottle" pore shape r_n is less than r_w. The pressure, P_n, for intrusion will therefore be greater than that for extrusion, P_w, and hysteresis will be observed. Non-closure of hysteresis loops in mercury porosimetry is attributed to entrapment of liquid mercury in the pore structure of the solid.

EUROPT 3 and EUROPT 4 catalysts were prepared from the same commercial alumina, CK 300, as described in section 3.1. It was therefore decided to investigate the pore structure of the support common to both catalysts. The pore structure of the alumina support, CK 300, and catalyst GHI were characterised by mercury porosimetry using a Micromeritics Autopore 9200 instrument.

Samples of CK 300 alumina and catalyst GHI, each weighing approximately 0.5g, were outgassed for 4 hours in an oven at 120°C. The samples were loaded into the Autopore 9200 penetrometer sample chambers and then evacuated to a pressure of 4.5×10^{-2} Torr. The applied pressure on the penetrometer mercury columns was then increased progressively from approximately 0.5 psia to approximately 60,000 psia.

The cumulative intrusion volume of mercury for each sample was recorded at each of the successive intermediate pressure values. Figures 3.6(a) and 3.6(b) show the plots of cumulative volume versus applied pressure for CK 300 and GHI respectively. Plots of incremental volume versus applied pressure for CK 300 and GHI are shown in figures 3.7(a) and 3.7(b) respectively.

The total pore volume, total pore area and average pore diameter values for CK 300 alumina and catalyst GHI were calculated from the mercury intrusion results and are given in table 3.10. The total pore volume and surface area results are in good agreement with those determined by nitrogen adsorption (Tables 3.8 - 3.9).

Table 3.10 **Pore Characteristics of CK 300 Alumina and Catalyst GHI**

	CK 300	GHI
Total Pore Volume (cm^3/g)	0.540 ± 0.004	0.452 ± 0.012
Total Pore Area (m^2/g)	203.7 ± 1.0	93.6 ± 0.3
Average Pore Diameter (nm)	10.62 ± 0.05	19.32 ± 0.53

Figures 3.8(a) to 3.8(c) are plots of cumulative pore volume versus average pore diameter for nitrogen adsorption compared with mercury porosimetry in the intrusion mode. Results for catalysts EUROPT 3, EUROPT 4 and GHI are shown in figures 3.8(a) to 3.8(c) respectively. A close agreement in results for the two different techniques indicates that the catalysts have a regular pore structure and that the assumptions made in the mercury porosimetry are valid.

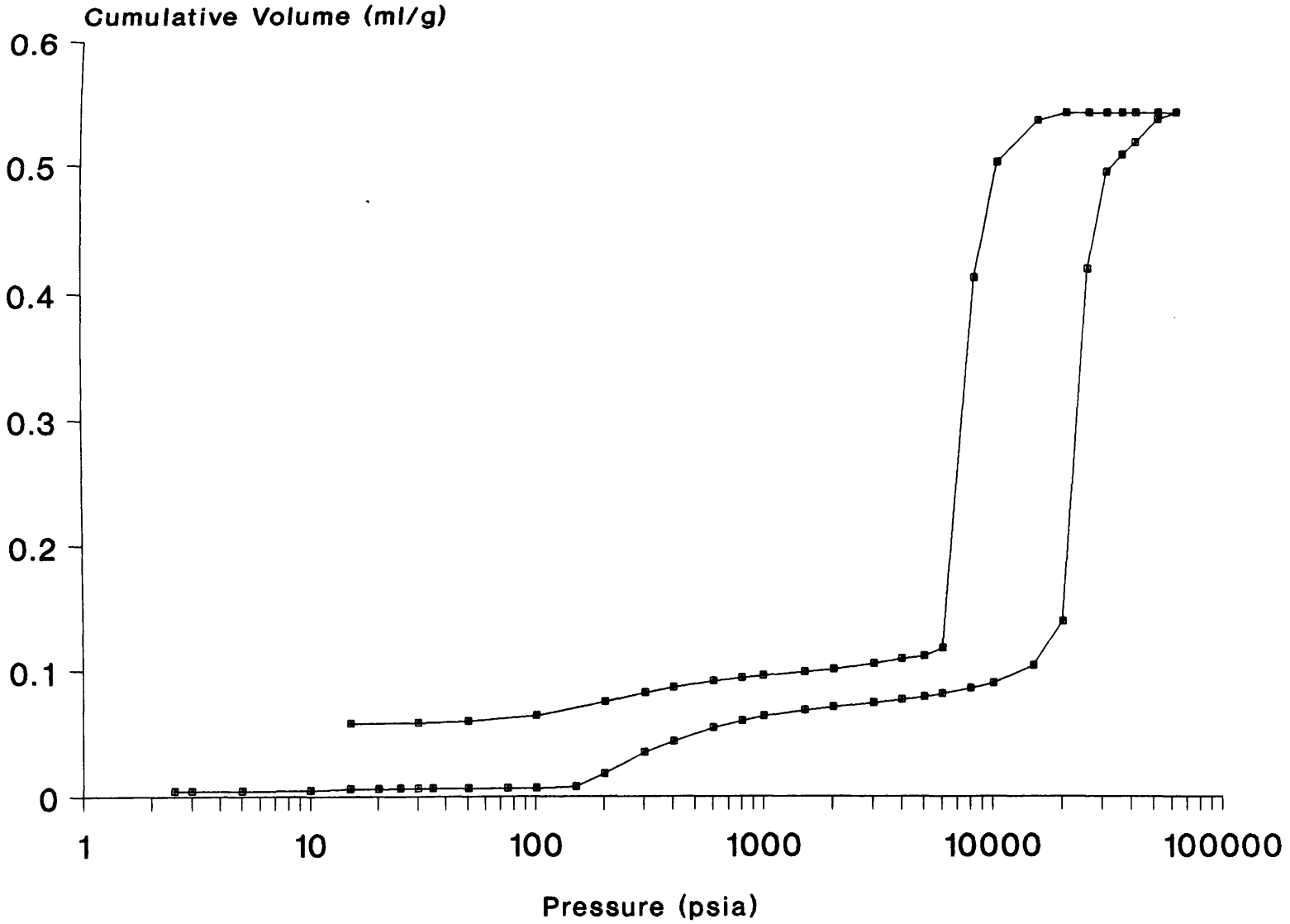

Figure 3.6(a) - Cumulative Mercury Intrusion Volume versus Applied Pressure for Alumina Support CK300.

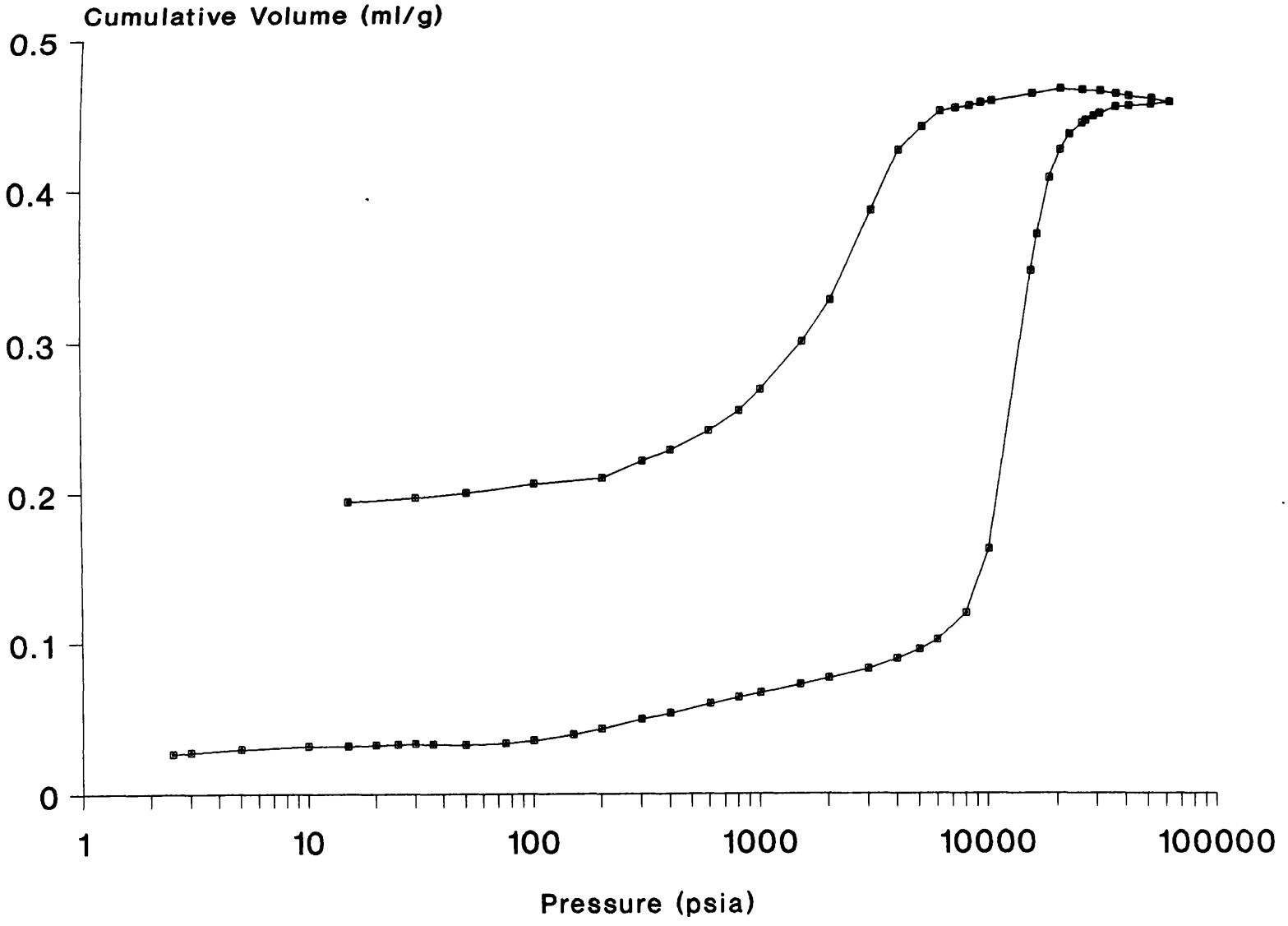

Figure 3.6(b) - Cumulative Mercury Intrusion Volume versus Applied Pressure for Catalyst GHI.

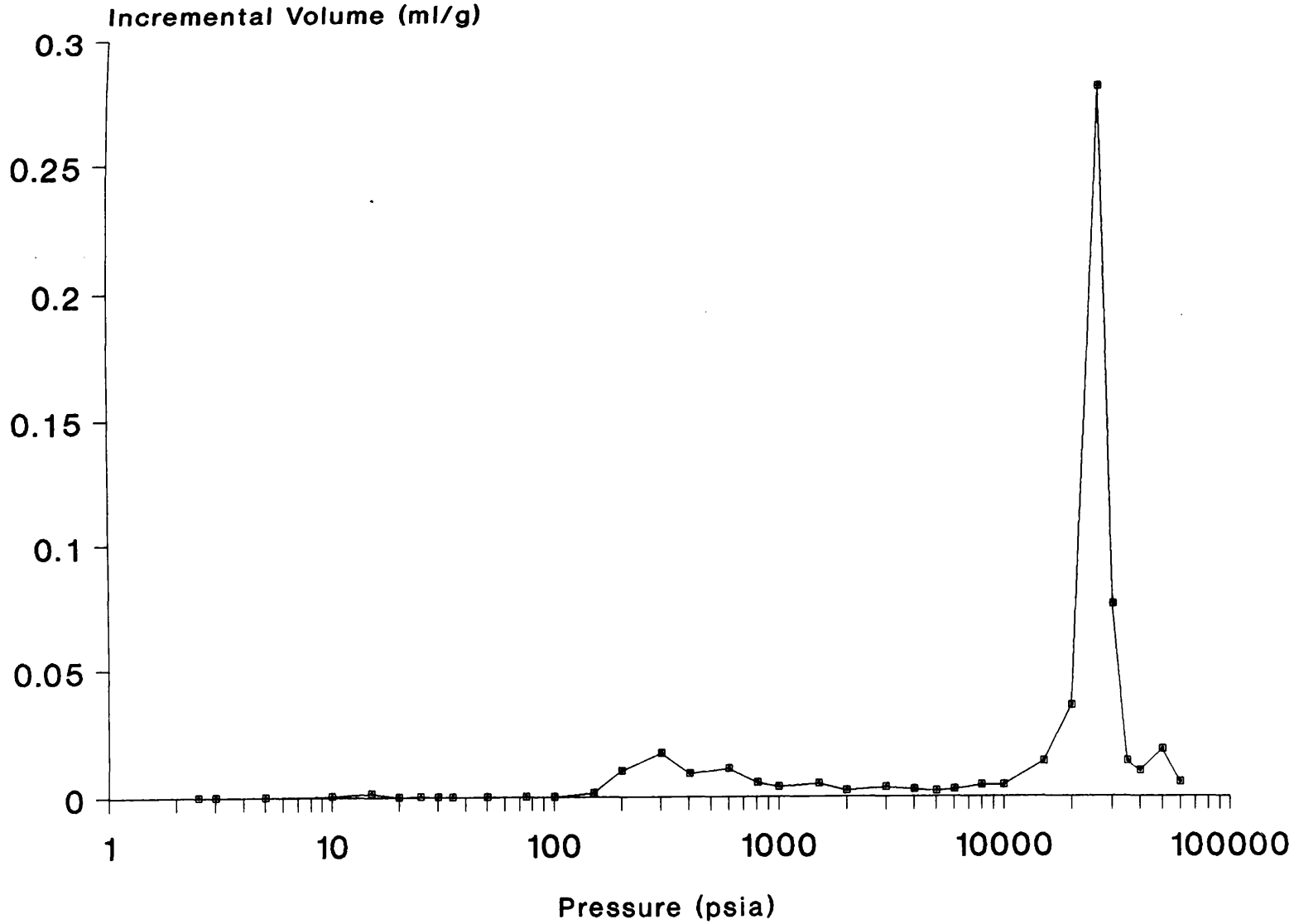

Figure 3.7(a) - Incremental Mercury Intrusion Volume versus Applied Pressure for Alumina Support CK300.

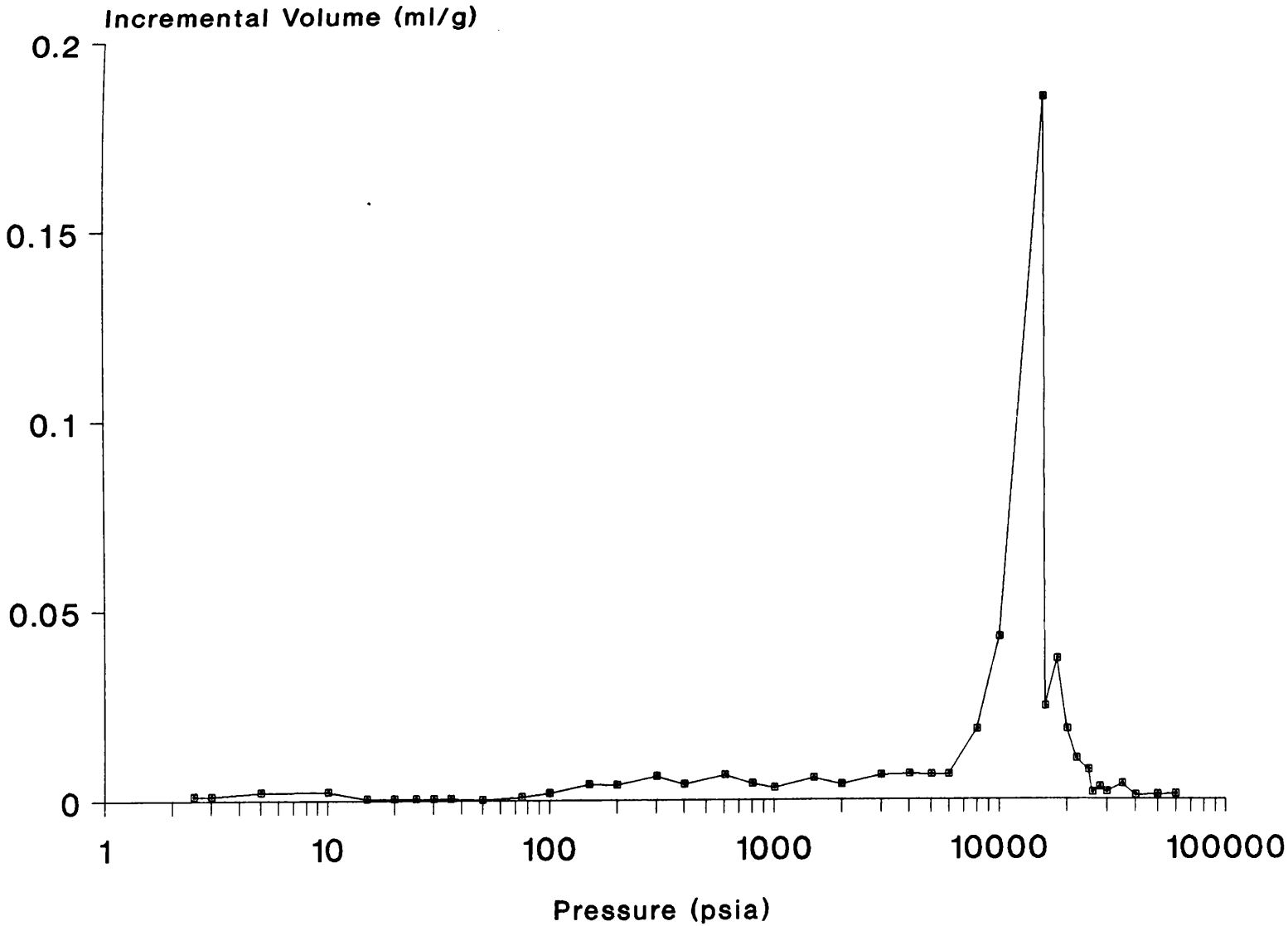

Figure 3.7(b) - Incremental Mercury Intrusion Volume versus Applied Pressure for Catalyst GHI.

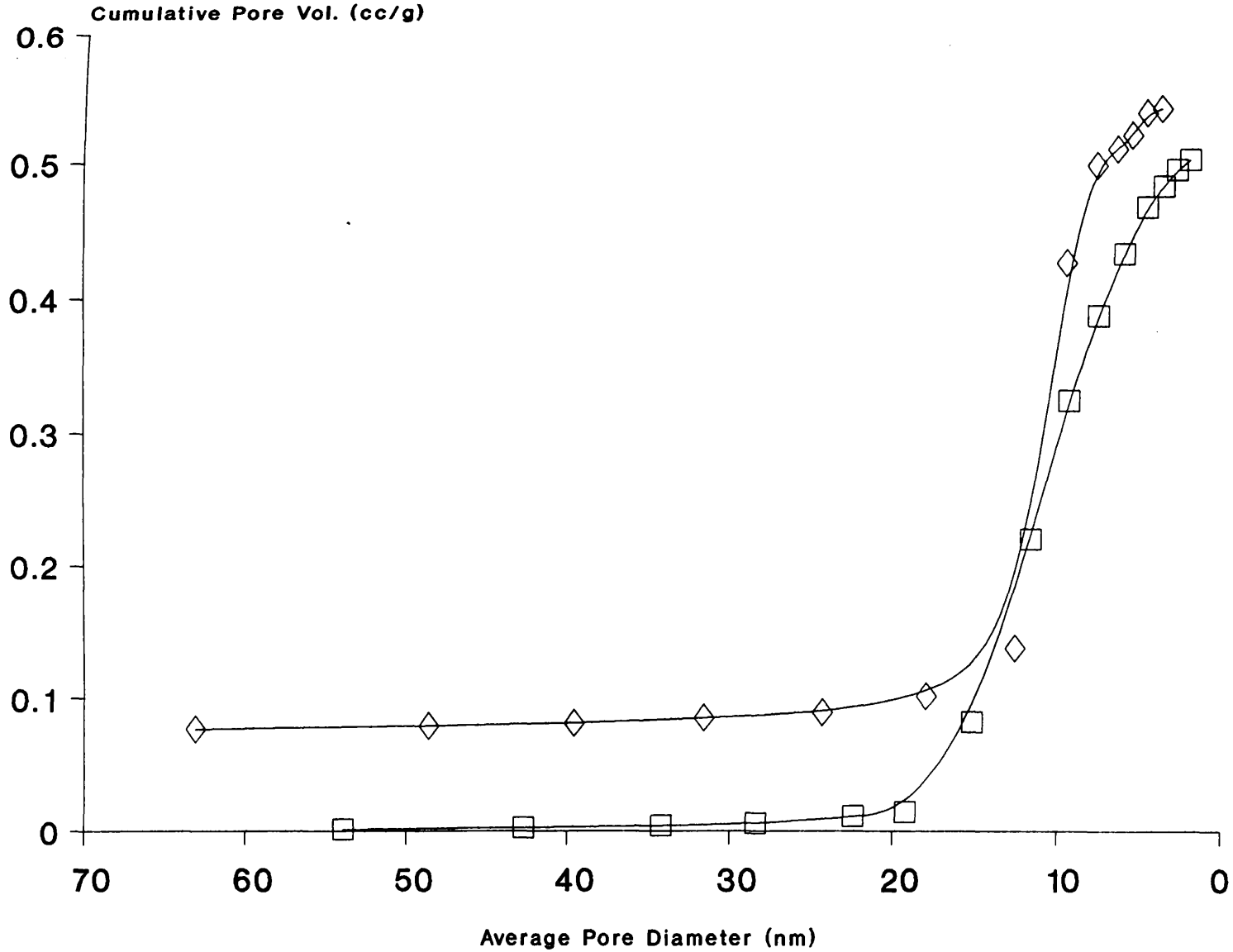

Figure 3.8(a) - Cumulative Pore Volume versus Average Pore Diameter for Catalyst EUROPT3, where □ Represents Nitrogen Adsorption and ◇ Represents Mercury Intrusion.

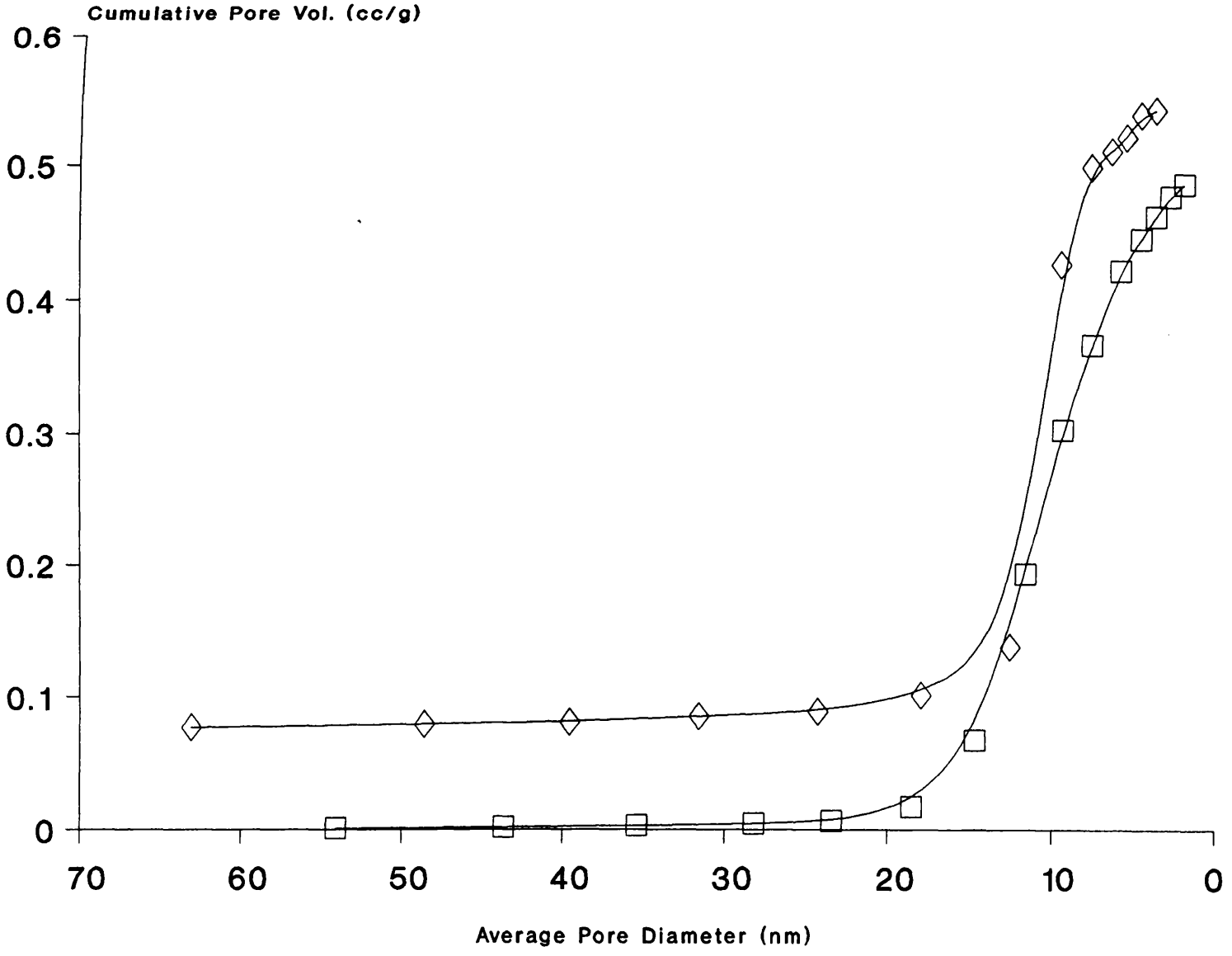

Figure 3.8(b) - Cumulative Pore Volume versus Average Pore Diameter for Catalyst EUROPT4, where □ Represents Nitrogen Adsorption and ◇ Represents Mercury Intrusion.

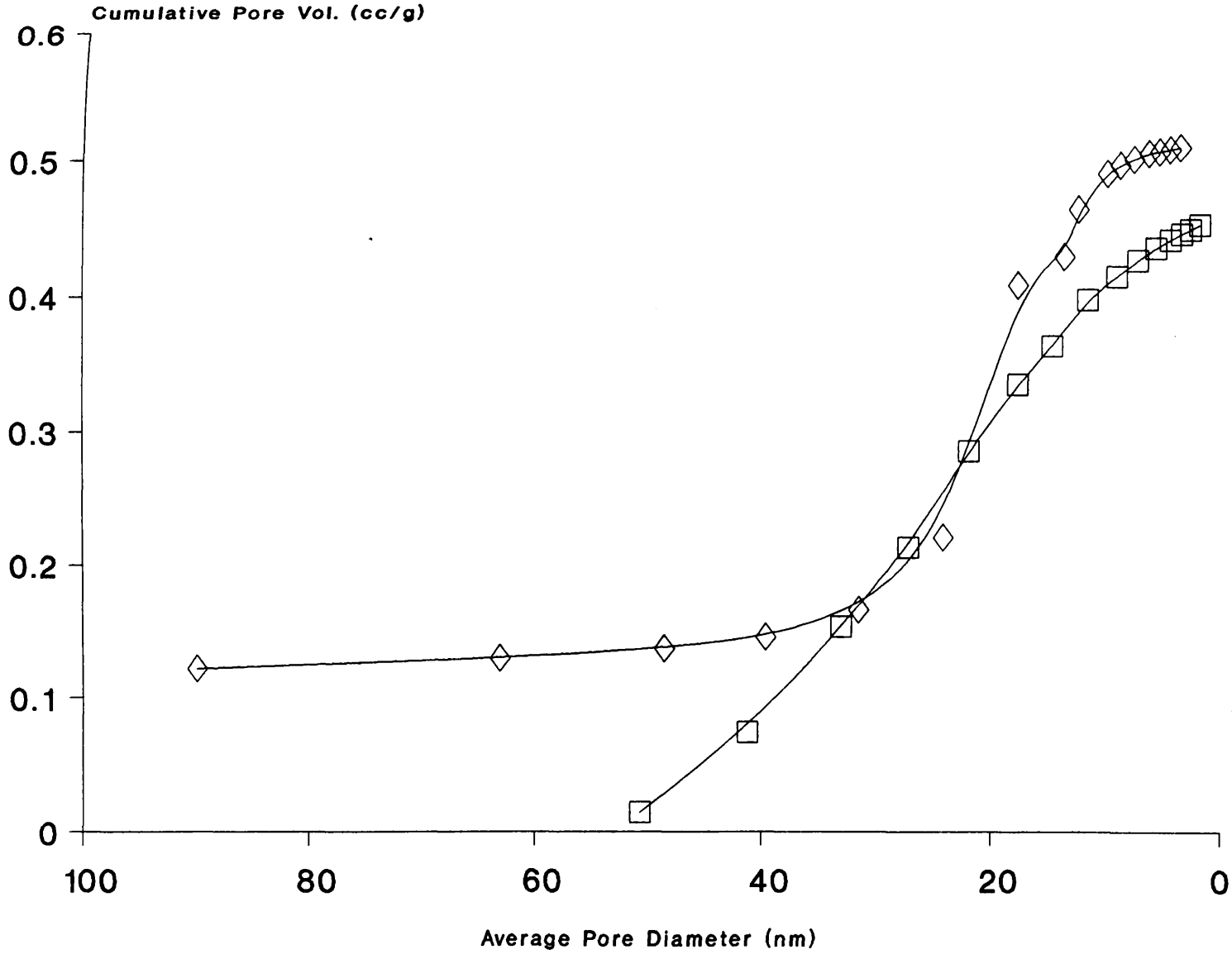

Figure 3.8(c) - Cumulative Pore Volume versus Average Pore Diameter for Catalyst GHI, where □ Represents Nitrogen Adsorption and ◇ Represents Mercury Intrusion.

3.2.6 Transmission Electron Microscopy

Transmission electron microscopy measurements were made using a Jeol 1200X high resolution electron microscope. Samples of EUROPT 3 and EUROPT 4 were reduced using the standard procedure detailed in section 3.1. Following reduction the samples were ground and suspended in distilled water. A drop of the suspension was then deposited on a carbon coated copper grid. Electron micrographs were taken at a magnification of 120,000. No metal particles could be observed on the micrographs of EUROPT 3 reflecting the low metal loading and dispersion calculated. Similarly, no metal particles could be observed on micrographs of EUROPT 4.

Results from a previous electron microscopy study on the GHI catalyst indicate a fairly narrow particle size distribution with most particles under 5nm in size (127).

3.3 ANALYSIS OF SPENT CATALYSTS

On completion of each reforming experiment samples of the used catalyst were recovered from the reactor tube and analysed for surface carbon and residual chlorine content using the techniques described below.

3.3.1 Neutron Activation Analysis

Neutron activation analysis (NAA) involves the capture of neutrons by the nuclei of the substance to be analysed. Neutron capture is immediately followed by emission of a gamma ray whose energy is equal to the kinetic energy of the neutron plus the neutron binding energy. The chemical elements being analysed with a sample are identified by their characteristic gamma radiation spectrum.

Irradiation is accomplished by placing the sample in an intense flux of thermal neutrons for a length of time sufficient to produce a measurable amount of the desired isotope. The determination is based on the following equation:-

$$R = mM^{-1}N \Phi \sigma E (1 - e^{\lambda t}) \quad \text{.....(12)}$$

Where Φ = neutron flux

σ = capture cross section of target nuclide

λ = decay constant of γ-emitting nuclide

t = irradiation time

E = efficiency of detector

R = counting rate at end of irradiation

m = mass of sample

N = Avogadro number

M = atomic weight of element analysed.

By comparing the ^{38}Cl activities of the catalyst samples at the end of the irradiation

period with those of a standard sample, the specific weights of chlorine in spent samples of EUROPT 3, EUROPT 4 and GHI were obtained. Results from the analysis are referred to, where appropriate, in the following chapters.

3.3.2 Surface Carbon Analysis

Samples of spent catalyst were analysed for surface carbon using a combustion technique. The surface carbonaceous residues on each catalyst were converted to carbon dioxide by pyrolysis in an oxygen rich atmosphere. A quantitative measure of carbon dioxide production was provided by on-line analysis in a calibrated gas chromatogram. The volume of carbon dioxide produced was used to determine the % weight of carbon originally present on each catalyst. Spent samples of EUROPT 3, EUROPT 4 and GHI were analysed in this manner. As with the residual chlorine contents determined by NAA, the results from surface carbon analysis are referred to, where appropriate, in the following chapters.

CHAPTER 4

EXPERIMENTAL

4.1 THE MICROCATALYTIC REFORMING SYSTEM

4.1.1 Introduction

Experiments in order to determine catalytic activity, selectivity and stability were performed in a high pressure microreactor designed and constructed during the initial stages of the project. The system was constructed almost entirely of stainless steel and was capable of operating at temperatures up to 500°C and pressures of up to 140 psig.

The high pressure system was designed for continuous flow studies and consisted of three sections:

i) The feed system;

ii) The reactor system;

iii) The analytical system.

A simplified diagram of the system is shown in Figure 4.1.

4.1.2 Overview

The microreactor was constructed such that a continuous flow of n-octane and hydrogen could be established. The two gaseous reactants were blended prior to contacting the catalyst charge maintained at the desired reaction temperature and pressure. Gaseous reaction products were vented to atmospheric through both a coarse

and a fine restrictor (see section 4.1.2.1). The reaction products were sampled at regular intervals by means of a heated gas sampling valve situated downstream of the fine restrictor. The sampled product was analysed using a packed column gas chromatography technique.

4.1.2.1 Restrictors

A most important feature of the microreactor design was the use of restrictors in both the feed and reactor sections. These components were critical in maintaining the stability of reactant and product flow rates. A restrictor is essentially a device which regulates the flow of gas and which is suitable for use under high pressure operation. Constructed from a section of calibrated crimped tubing; a restrictor, due to its design, experiences equal internal and external pressures. Thus, the possibility of distortion of the calibrated restriction, which would disturb the stability of the reactant flow across it, is avoided.

Flow across a calibrated restrictor is dependent upon two factors. These are, respectively, the differential pressure across the restriction and the temperature of the unit. Evidently, a higher pressure will result in a higher gas flow. Conversely, a higher temperature will decrease flow. Figure 4.2 illustrates a typical restrictor.

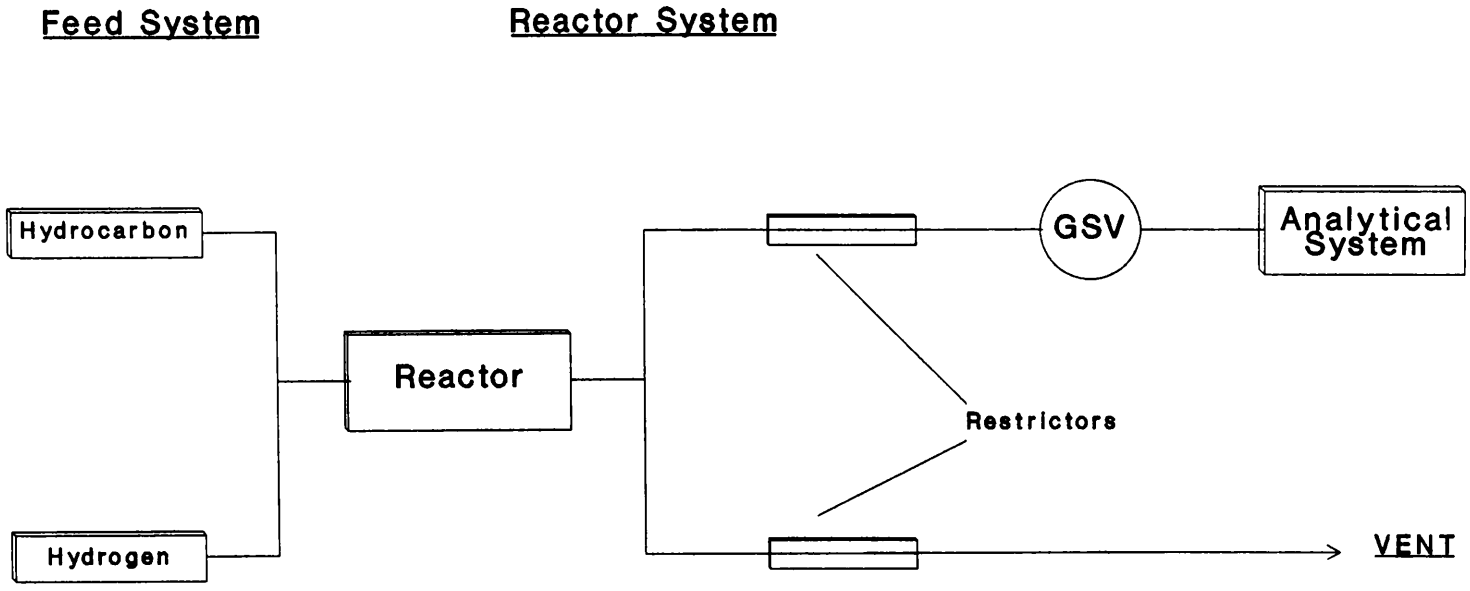

Figure 4.1 - Simplified Diagram of Reformer System.

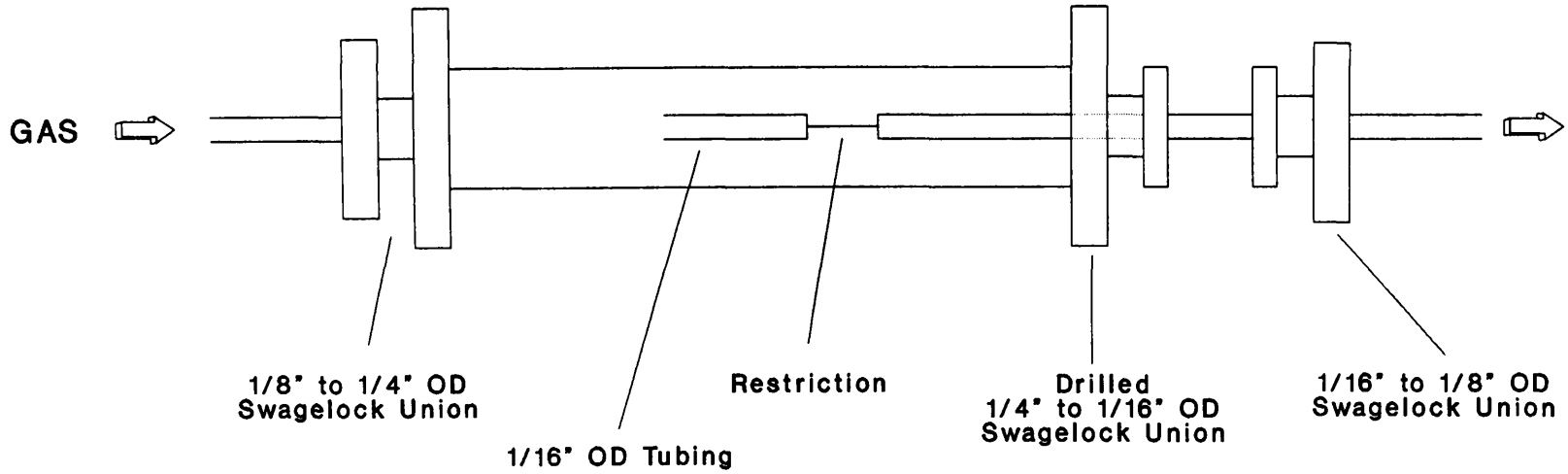

Figure 4.2 - Schematic Diagram of a Restrictor.

4.1.3 The Feed System

The microreactor feed system incorporated two sections each designed to deliver a constant, regulated flow of gaseous n-octane and hydrogen respectively. A schematic diagram of the feed system is shown in Figure 4.3.

Before any reforming operation the n-octane feed reservoir was detached and filled. The reservoir was a stainless steel 150 cc Whitey sample cylinder capable of holding pressures up to 1800 psig. The reservoir was then reconnected to the line using high pressure Swagelock couplings. With isolation valve 3 closed and isolation valve 2 open the n-octane feed system was then pressurised. Cylinder nitrogen (Harris 2 stage cylinder head, model no. 96) was directed towards the n-octane feed by setting valve 1 in the required position. The regulated pressure over the n-octane feed was then raised slowly to the desired value by means of the Brooks ELF pressure regulator (Model 8607). Nitrogen pressure was measured using a Budenberg gauge (0-300 psig) (Fig. 4.3.A).

Upon opening valve 3 the liquid n-octane was directed, via 1/16" stainless steel tubing, to a vapourisation/restriction unit. See figure 4.4. This unit was designed in such a manner that n-octane issued from the narrow bore tubing as a fine spray. The tubing within the vapouriser was enclosed by a furnace, the temperature of which was held at ca. 300°C, well in excess of the boiling point of n-octane (125-127°C); the n-octane was therefore instantly vapourised. A Cr/Al thermocouple (Type K, RS Components Ltd) positioned in contact with the 1/16" tubing outlet monitored the

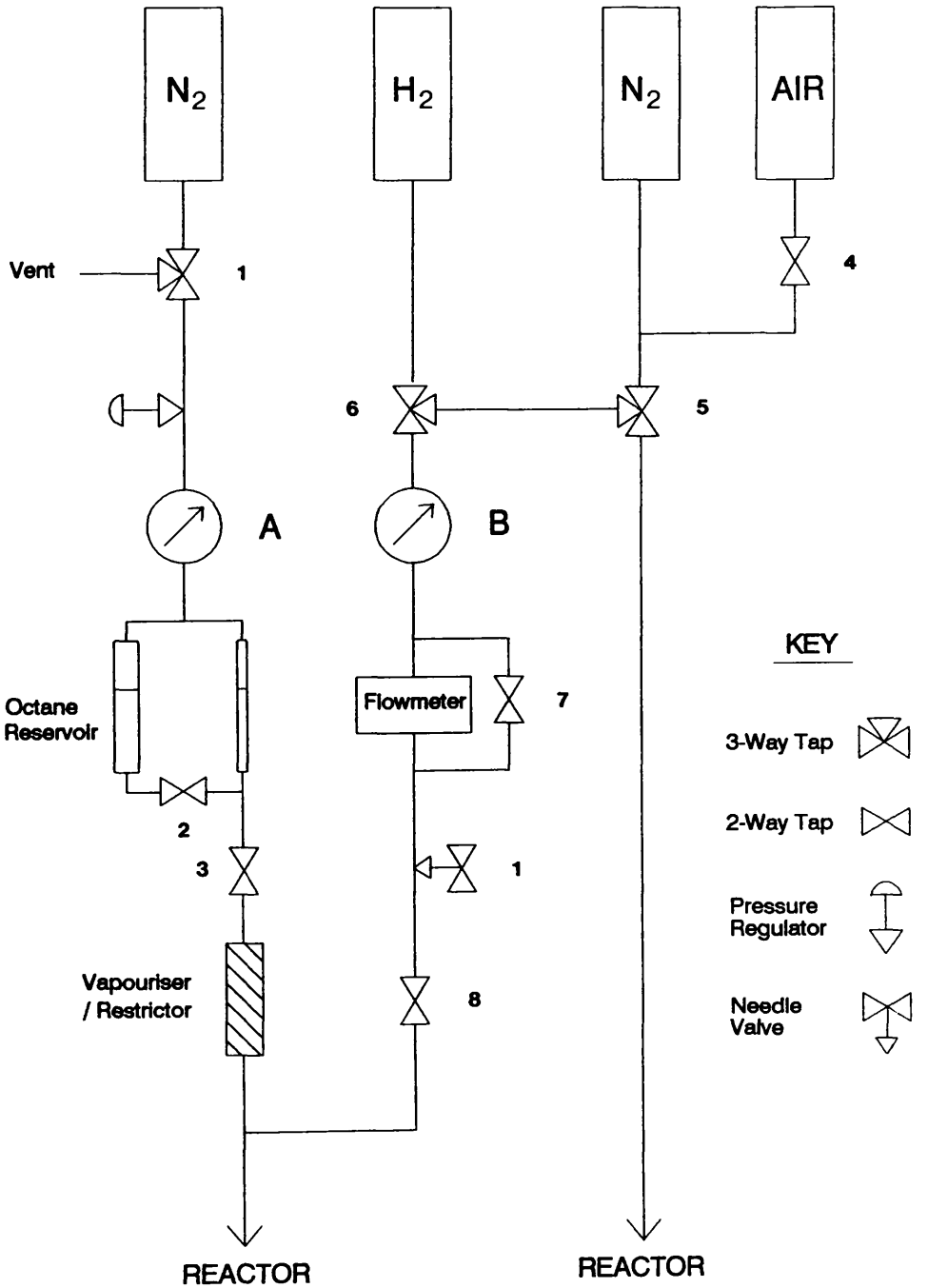

Figure 4.3 - Reactor Feed System.

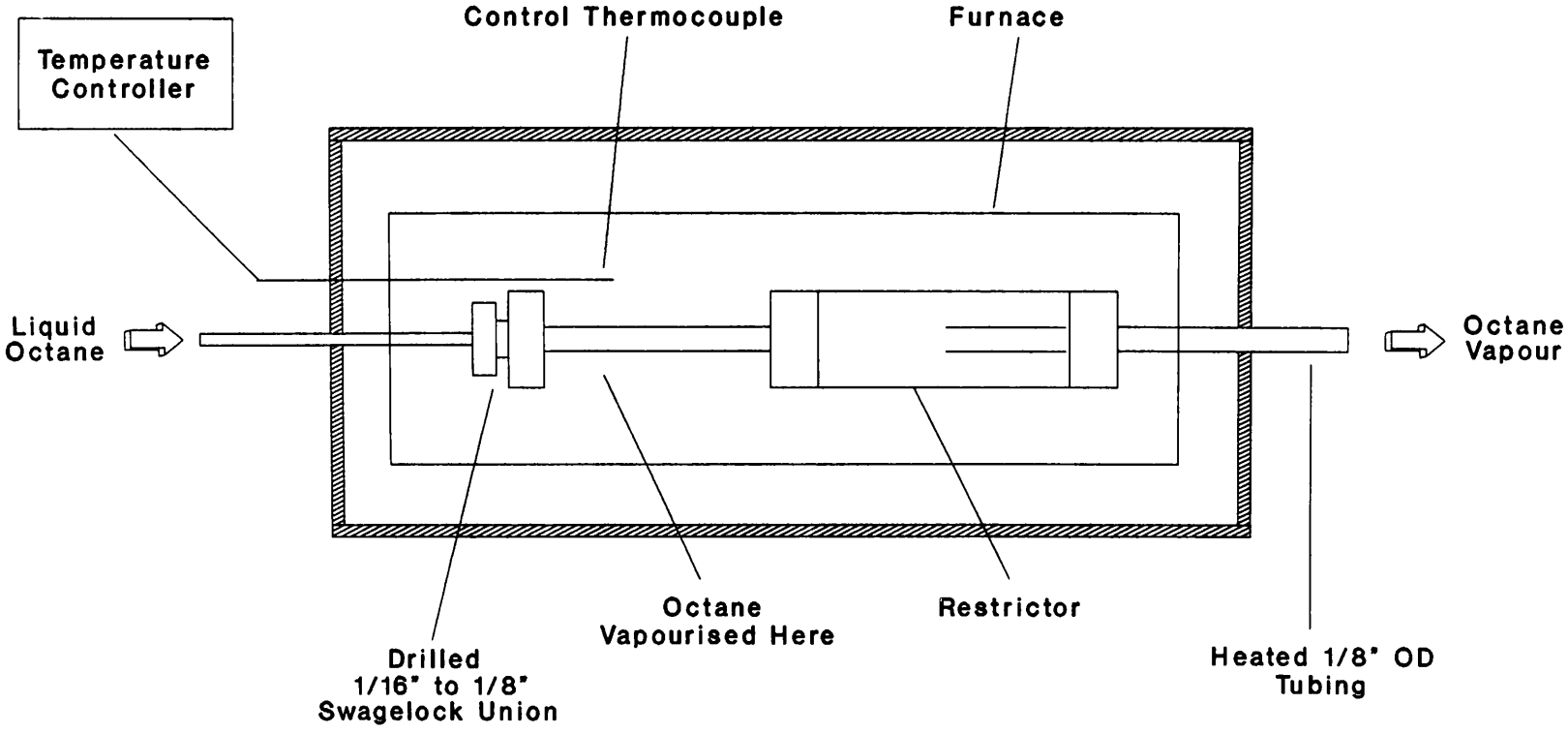

Figure 4.4 - Octane Vapourisation / Restrictor Unit.

temperature. The temperature was maintained by a West Gardian temperature control unit (Model no. Q3M) in conjunction with an Anglicon PR13 energy controller. (Heater controller designed by Rockhurst Group, Billingham, Cleveland).

Following vapourisation the n-octane was driven through the restrictor and entered the reactor section of the microreformer. The vapourisation/restrictor unit was enclosed by Duratech insulating board (dimensions 12¾" x 4½" x 2¾") and packed with glass wool in order to minimise heat loss. The tubing carrying gaseous n-octane from this unit was maintained at high temperature (ca. 170°C) using Electrothermal heating tape; thus ensuring that no n-octane condensed. The temperature of the n-octane feed line was controlled by a Variac transformer connected to the heating tape and was monitored by a Cr/Al thermocouple.

A most important feature of the hydrocarbon feed system was that the n-octane flow rate could be readily measured with a high degree of precision. This was achieved by using a graduated ¼" o.d. sightglass (Bibby co., pyrex borosilicate capillary tubing) situated parallel to the octane reservoir. This system was designed in such a manner that, with isolation valve 2 open and the n-octane feed under pressure, the level of liquid n-octane in the sightglass mirrored that in the stainless steel reservoir. Both the sightglass and the reservoir experienced identical pressures. Total n-octane flow to the vapouriser was therefore the sum of the two contributory flows from the reservoir and sightglass.

Flow measurements were taken by isolating the n-octane reservoir using valve

2. All the hydrocarbon was now drawn from that which was contained in the sightglass. The overall flow was unaffected by this operation. Under these circumstances the n-octane meniscus within the sightglass was observed to descend with time. Given the internal diameter of the sightglass tube, the volume of n-octane displaced with time may be calculated. After each flow measurement the n-octane reservoir was reinstated by opening valve 2.

A calibration graph for the n-octane feed system is shown in Figure 4.5, each point representing the mean value of at least three flow measurements at each respective pressure.

4.1.3.1 Hydrogen Feed System

The second section of the feed system was again designed to deliver a constant flow of metered gas towards the reactor. A schematic diagram of the gas feed system is shown in Figure 4.3.

A single stage brass regulator (BOC model no. 52B) was used to accurately control hydrogen pressure. With valve 6 set at the required position, hydrogen gas could be directed through the flowmeter. After ensuring that the Whitey 2 way tap (valve 8) was in the closed position and that the bypass facility on the flowmeter was open (valve 7), the gas feed system was set at the required delivery pressure. The delivery pressure was measured on a standard Budenburg gauge (0-300 psig) (Fig. 4.3.B).

With the bypass on the flowmeter closed and valve 8 opened, the hydrogen flow was directed through the reactor. The hydrogen flow was controlled using a fine metering needle valve (Hoke Millimite Valve, Model no. 131562B) situated between the flowmeter and valve 8. Gas flow was measured using a U-tube capillary flowmeter (Fig 4.6). With the bypass valve closed the gas stream was directed across a Nupro fine metering needle valve (Model no. SS-SS4) adjusted to a suitable fixed setting. This created a small pressure differential across the two arms of the U-tube manometer which was partially filled with dodecane. This pressure differential, Δp, resulted in the dodecane columns assuming different levels, Δh. Changing the gas flow resulted in the dodecane columns adopting a new Δh value. The relationship between absolute flow and the difference in height of the columns was established.

The flowmeter was calibrated against a graduated bubble flowmeter. A plot of hydrogen flow versus flowmeter response, Δh, is shown in figure 4.7.

It should be noted that the bypass valve was closed only when flowrates were being measured. The valve was held open at all other times thus ensuring that no sudden pressure changes emptied the U-tube of dodecane. This was particularly relevant when initially pressurising the line.

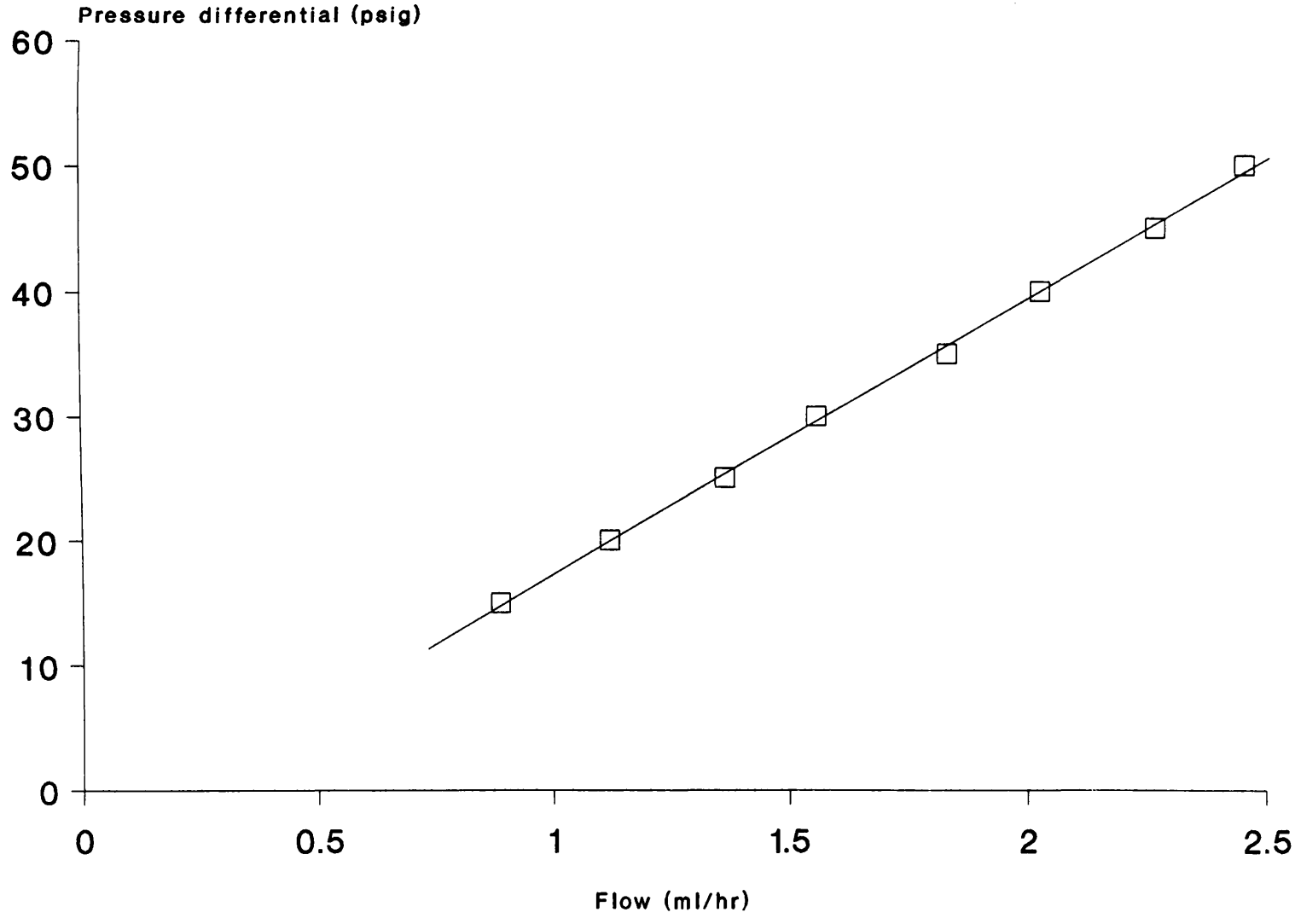

Figure 4.5 - Octane Flow versus Pressure Differential Across Feed Restrictor.

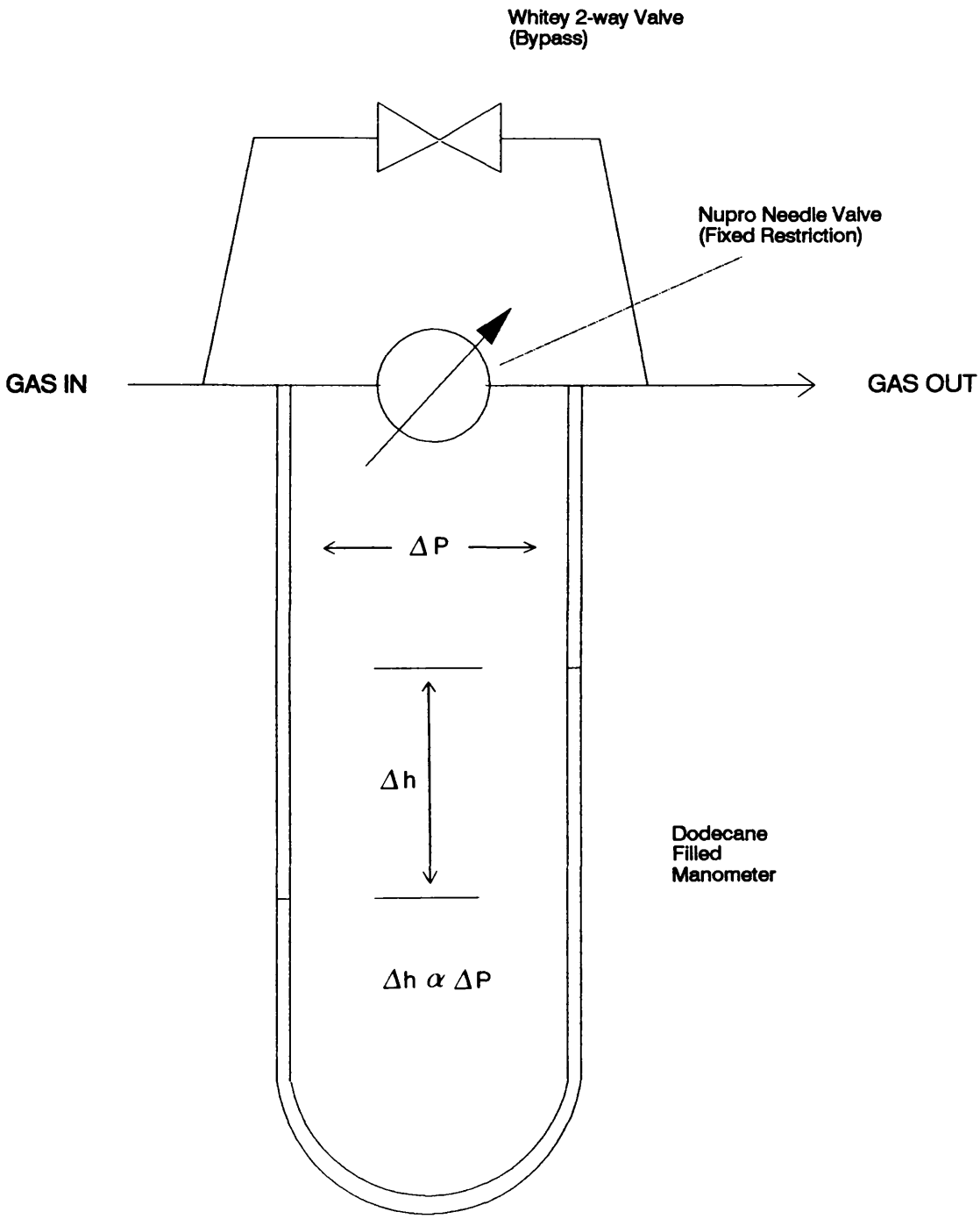

Figure 4.6 - Schematic Diagram of Gas Flowmeter.

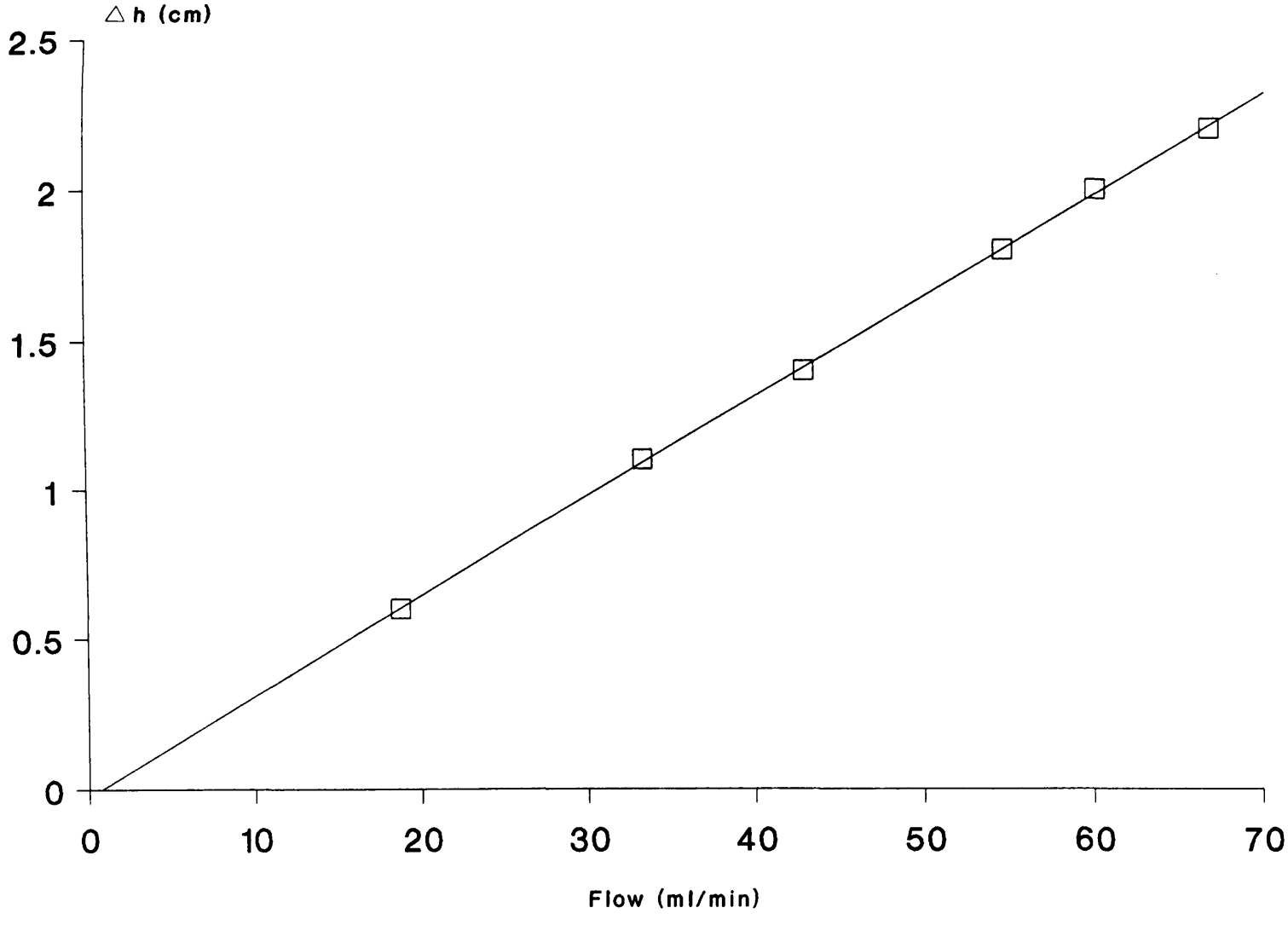

Figure 4.7 - Hydrogen Flow versus Flowmeter Response, △ h.

4.1.3.2 Air and Nitrogen Gas Feed

In addition to hydrogen, the gas feed system was capable of delivering a choice of a further 2 gases, in this case, nitrogen and air. This facility was used during the activation of catalyst charges using the standard technique detailed in section 3.1. Nitrogen gas was also used to flush the system after a reforming run. Nitrogen pressure was controlled using a Harris 2 stage regulator (Model no. 96). Air pressure was controlled using a BOC single stage regulator (Model no. 52B).

The desired gas was directed towards the feed system by manipulation of valves 4, 5 and 6 (Fig 4.3). Gas flow was measured using the technique outlined above. Figures 4.8 and 4.9 show plots of nitrogen and air flow respectively versus the flowmeter response.

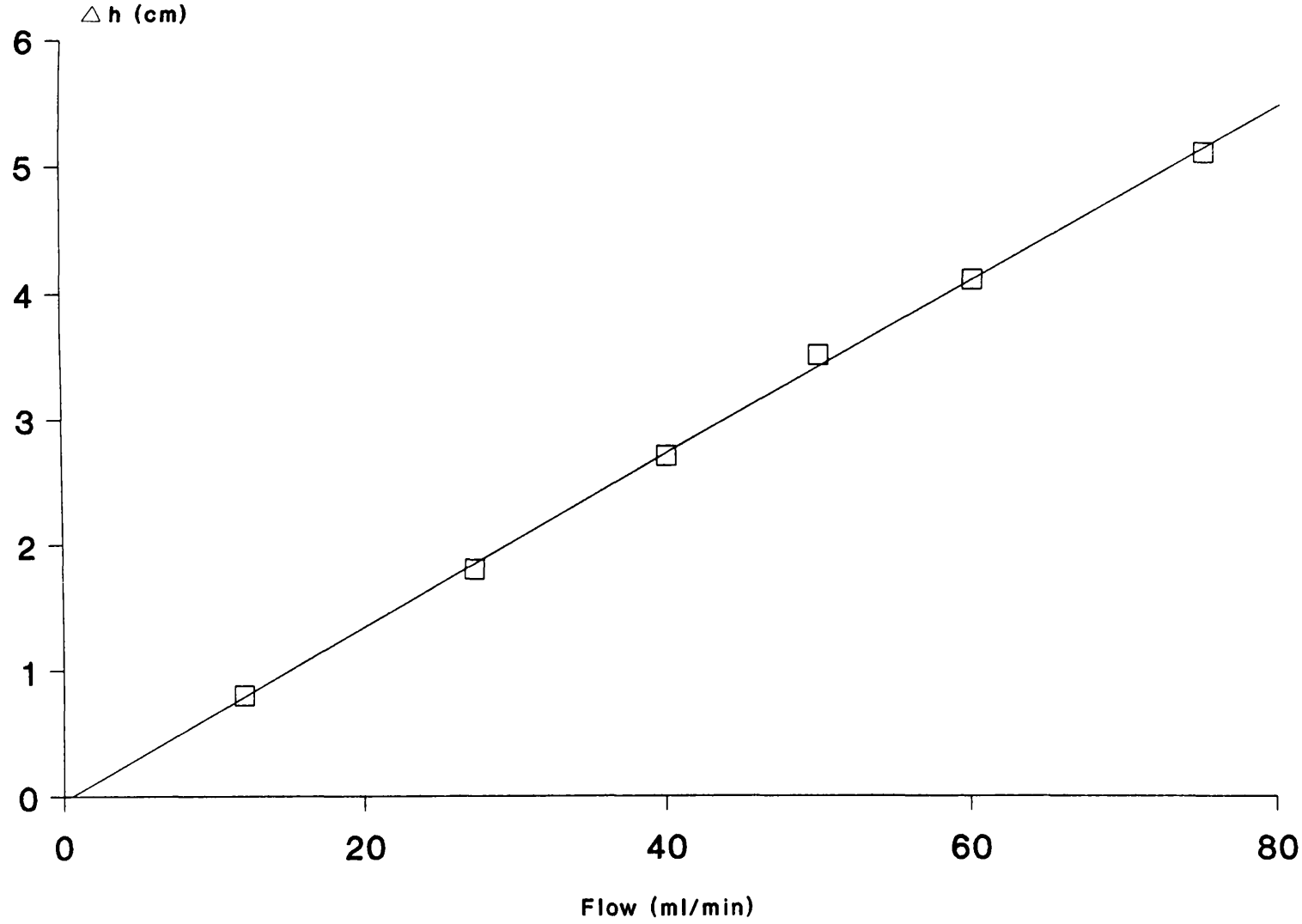

Figure 4.8 - Nitrogen Flow versus Flowmeter Response, △ h.

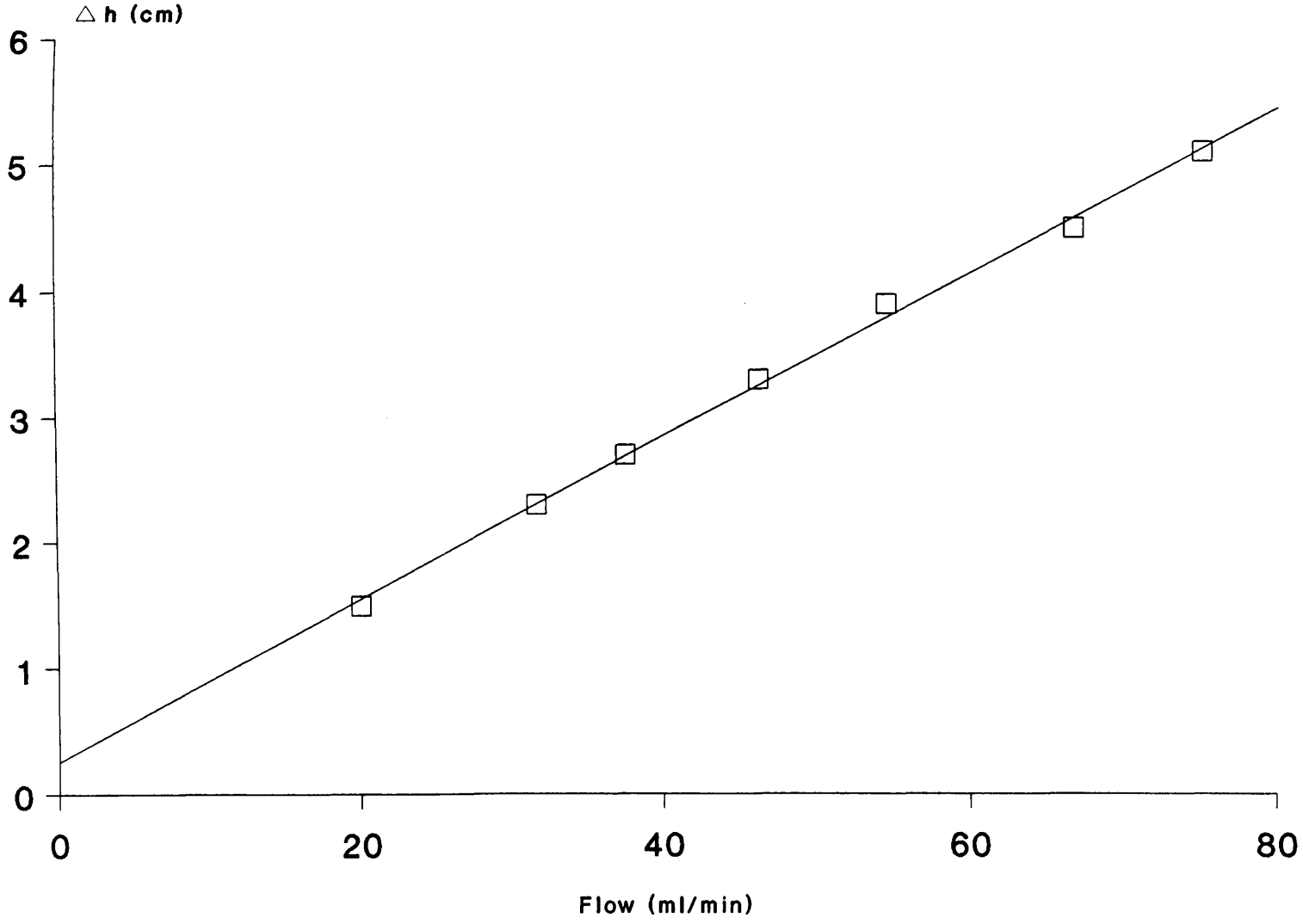

Figure 4.9 - Air Flow versus Flowmeter Response, △ h.

4.1.4 The Reactor System

A diagram of the reactor system is shown in Figure 4.10.

4.1.4.1 The Furnace

The furnace consisted of a cylindrical block of ceramic pyrophyllite (diameter 7cm, length 22.5cm) wound with Ni/Cr alloy heating wire. This in turn was enclosed by ¼" Duratech insulting board. Dead space between the Duratech board and the ceramic block was filled with Vermiculite chips in order to minimise heat loss. The reactor and bypass tubes were 30cm sections of 0.4cm i.d. glass lined stainless steel tubing (S.G.E. Ltd). Glass lined tubing was used as the surface of stainless steel has established catalytic activity at high temperature.

Catalyst samples, held in position by glass wool plugs, were placed in a central isothermal section in the reactor tube. The furnace was placed in a vertical configuration, such that the reactants were in downflow to preserve the packing of the catalyst bed. Furnace temperature was monitored using a Cr/Al thermocouple connected to a 6 channel digital thermometer (Gulton Europe Ltd, Type 4F4LH/120AF). The thermocouple was positioned in a drilled hole adjacent to the location of the catalyst charge in the reactor tube. An F.G.H. temperature programmer (Model no. K-P200) in conjunction with a 10A solid state relay was used to accurately control the furnace temperature.

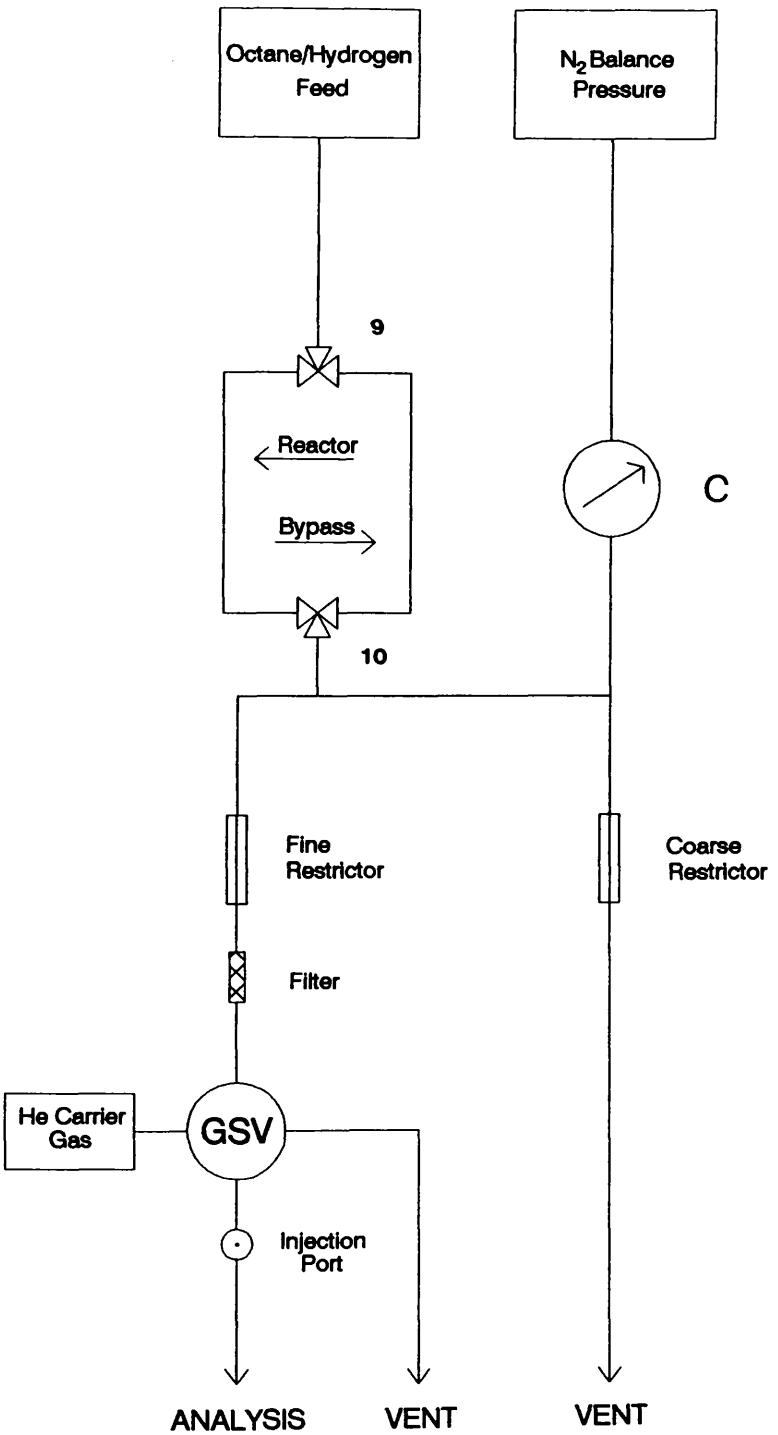

Figure 4.10 - Reactor System.

Switching between the reactor and bypass tubes was carried out using valves 9 and 10 (Fig. 4.10). The elevated temperatures in this section of the system necessitated that these taps were high temperature models; Whitey 3 way taps (Models' no. SS-83XTS4), with a temperature rating of 230°C, were therefore used.

The bypass tube was situated parallel to the reactor tube and was identical to it in all respects except that it contained no catalyst. During reforming studies the bypass enabled the desired hydrogen and n-octane flow rate to be established before the diversion of the reactant stream over the catalyst. The bypass tube also enabled blank experiments to be performed in situ. Such experiments gave an indication of any residual activity in the reactor.

4.1.4.2 Tubular Plug Flow Reactors, Heat and Mass Transfer Considerations

As detailed in the previous section a tubular plug flow reactor was used for this study. The reactor was operated in a continuous flow mode such that reactant concentration varied with axial position in the catalyst bed.

One of the main disadvantages of using tubular reactors concerns the difficulty in eliminating diffusion constraints through the catalyst bed. It is of importance in any microreactor study that the observed product distributions are not influenced by either axial or radial mass and heat transfer limitations. It is well established that in reaction tubes of small diameter, gas phase reactant molecules display laminar flow only.

Mixing of the gas phase proceeds through the radial diffusion of gas molecules from the centre of the catalyst charge to the reactor wall and vice versa.

The rate of this radial diffusion can be described by the following expression:-

$$t = (dT)^2/8dR$$

where t = time taken for gas phase molecule to travel from the centre of the tube to the wall.

dT = tube diameter

dR = radial diffusivity

Therefore as the tube diameter becomes smaller the rate of the radial mixing increases.

It has been further demonstrated that axial diffusion is insignificant if the ratio of the length of the catalyst bed to particle size is of the order of 100 or more (130). The dimension of the reactor vessel (0.4cm i.d.) and of the catalyst bed (length 5.5cm, particle size 180-500μm. Minimum ratio = 110) are therefore commensurate with the with the elimination of mass transfer limitations within the system.

Heat transfer within reaction vessels of small diameter occurs by convection in which the gas phase molecules themselves transport the heat. Heat transfer is, therefore, as rapid as mass transfer. Hence, even in the presence of exothermic and endothermic reactions the temperature gradient across a diameter of the catalyst bed is likely to be negligible.

A further deviation from ideal performance may occur if the reactant stream bypasses some of the catalyst. The catalyst particle size (180-500μm) was chosen to minimize this effect.

4.1.4.3 Reactor Pressure Control

The microreactor in this study was designed to operate at pressures in excess of atmospheric. High pressures within the system were achieved by using two parallel restrictors (see section 4.1.2.1) situated downstream of the reactor bed. Following catalyst reduction the desired reaction pressure was initially set using nitrogen gas. The nitrogen gas was drawn from the gas feed system described in section 4.1.3.2 and shown in figure 4.3.

Having set the pressure at the desired level, gaseous n-octane and hydrogen were allowed to flow through the reactor. The gas stream eluting from the reactor was split into two fractions by a T junction. The nitrogen line was connected to the reactor system after this T junction and before the coarse restrictor. Consequently the nitrogen vented only through this restrictor. Three gases now contributed towards the total pressure within the system, i.e. nitrogen, hydrogen and n-octane. A corollary at this system was that the total flow through the coarse and fine restrictors was greater than that of the combined n-octane and hydrogen feed. If this condition was met, the reactor pressure remained unchanged as the introduction of the feed gases produced a corresponding abatement in the contribution of the nitrogen to the absolute pressure. Reactor pressure was monitored using a Budenberg gauge (0-300 psig) (Figure 4.10.C).

4.1.4.4 Heating of the Reactor System

In order to avoid condensation of gaseous hydrocarbon it was necessary to ensure that all tubing in the reactor system was maintained at elevated temperatures. The reactor system shown in figure 4.10 was supported on a sheet of stainless steel. All exposed tubing situated behind this sheet was enclosed by a heated box. This was constructed from ¼" Duratech insulting board (dimensions 14" x 26" x 4"). Attached to the inside rear panel of this enclosure was a coiled 6'6", 200W heating element (Hedin Cartridge Heaters Ltd) and two fan outlets. Baffles fitted over the fans (Stemshire UK Ltd, Models' no. 73012005) ensured that heated air was constantly circulated and an even temperature distribution achieved. The temperature within the heated box was maintained at 140°C by a 10A Electrothermal power regulator.

4.1.4.5 Gas Sampling

The product gas stream was sampled at regular intervals by a "Valco" 8 port high temperature gas sampling valve (Model no. 8T). This valve was situated after the fine restrictor (Figure 4.10) and heated by the enclosure described in the previous section. Effluent gas was ultimately vented to the atmosphere. The two sample loops were therefore at atmospheric pressure and a temperature of 140°C.

A 7 micron in-line filter (Nupro F series) was fitted before the gas sampling valve in order to prevent any extraneous particles fouling the precision valve mechanism. A schematic diagram of the gas sampling valve is shown in figure 4.11.

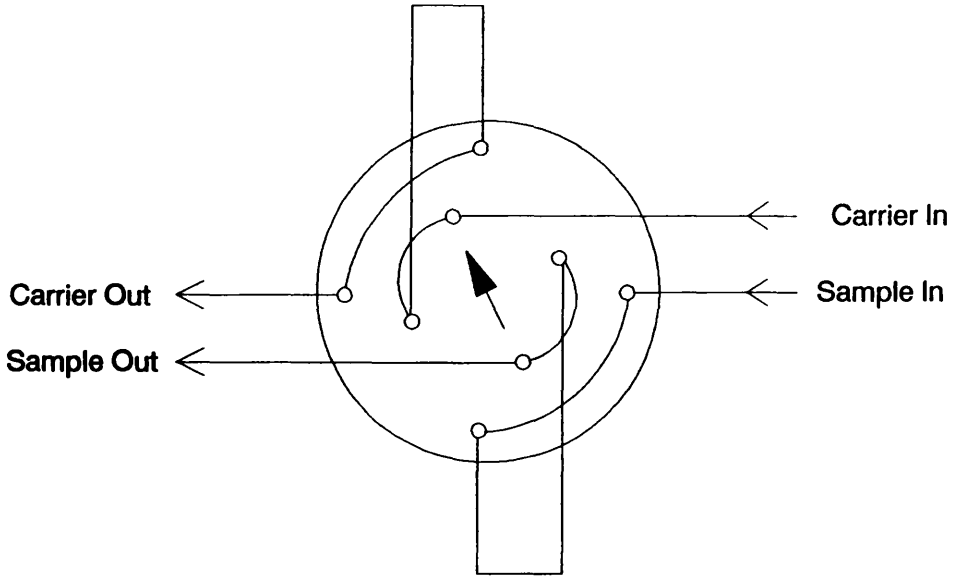

Position A

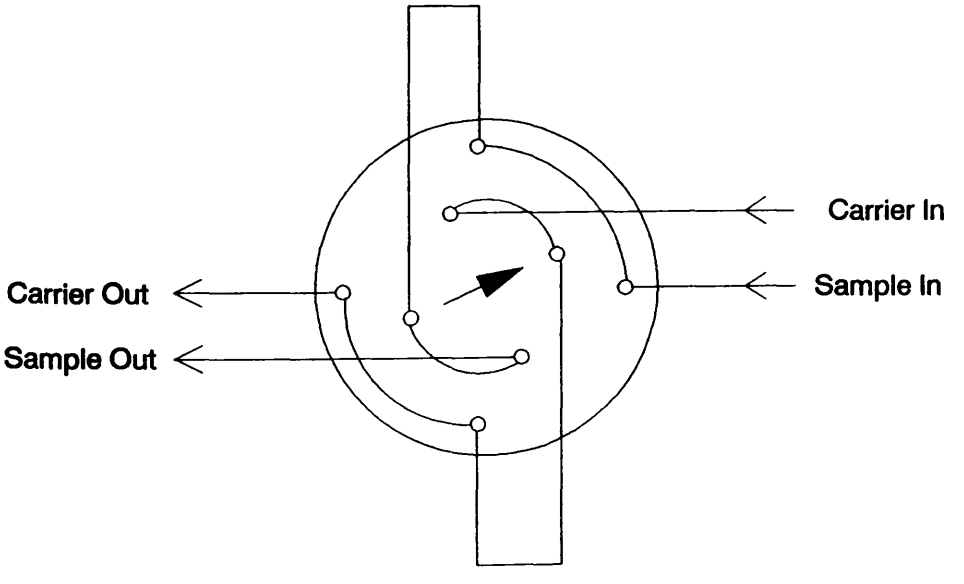

Position B

Figure 4.11 - Schematic Diagram of Gas Sampling Valve.

4.1.5 The Analytical System

A schematic diagram of the analytical system is shown in Figure 4.12.

4.1.5.1 Gas Chromatographic Analysis

Analysis of n-octane reformate products required a system that would allow quantitative separation of a wide variety of hydrocarbons. The hydrocarbons produced ranged from light aliphatic gases through napthenes and medium aliphatics, present as both normal and branched isomers, to aromatic species such as mixed xylenes.

It was decided to build an analytical system based upon a method established by ICI for the resolution of mixtures of paraffins, napthenes and aromatics. The acronym PNA is used to refer to the system. Sample injection was by the heated "Valco" sample valve described in section 4.1.4.5. Helium was used as a carrier gas.

In essence the PNA system involved the separation of aromatic hydrocarbons from the paraffins and naphenes. Non-aromatic hydrocarbons were resolved, according to hydrocarbon number and bulk hydrocarbon type, by a combination of 5A and 13X molecular sieves. Molecular sieves 5A and 13X are alumina silicate frameworks characterised by a uniform pore size distribution. Activated molecular sieves differ from other adsorbent types in that they only accept molecules or parts of molecules which fit within their micropores; that is they exhibit shape selectivity. Adsorbed molecules can subsequently be removed from the pores by heating. The

most significant difference between 5A and 13X molecular sieve is pore size (5Å versus 13Å).

4.1.5.2 PNA System Operation

Helium carrier gas flow was initially directed through the 13X trap and 5A/13X column. The trap, at ambient temperature, was enclosed by a tubular glass furnace and the 5A/13X column was held at 150°C in a PU4500 chromatographic oven (Philips Ltd). The TCEP column used for aromatic separation was isolated at this stage my means of the 6 port switching valve (Negretti and Zambra, Model no. 195-001).

The sample was injected and allowed to elute via the CEF column until all the non-aromatics had reached the 13X molecular sieve. As the molecular sieve was at ambient temperature all the paraffins with the exception of methane were "trapped". Methane was therefore the first hydrocarbon to be detected. The first aromatic component, benzene, was at this point reaching the end of the CEF column. Before benzene could proceed towards the trap the 6-port Negretti Zambra valve was switched to direct all aromatics to the TCEP column. Elution of aromatics was complete within 25 minutes, during which time the non-aromatics were held in the 13X molecular sieve. Unfortunately separation of meta- and para-xylenes could not be achieved on the TCEP column. Figure 4.13 shows a typical chromatogram of aromatic reformate products.

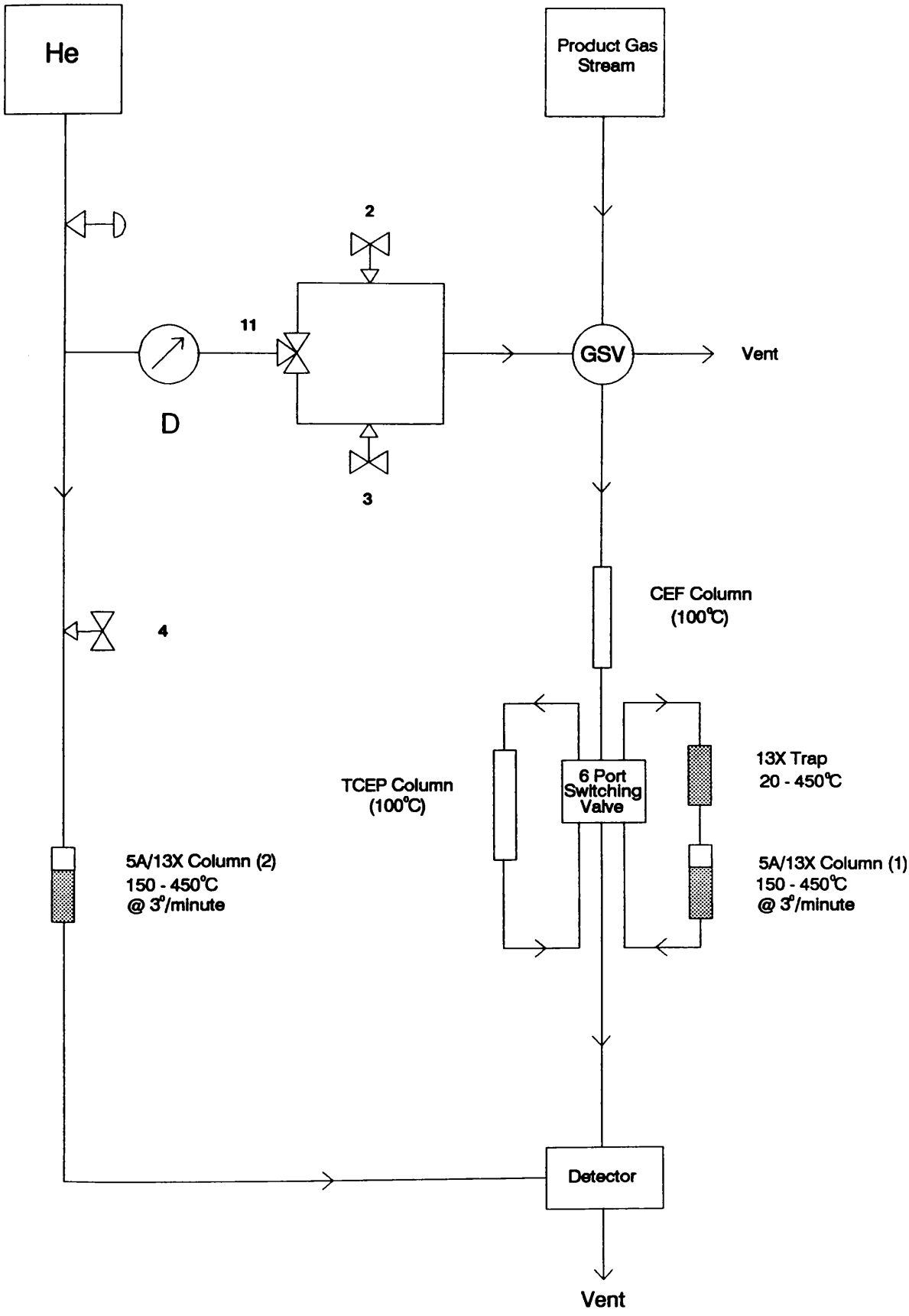

Figure 4.12 - Analytical System.

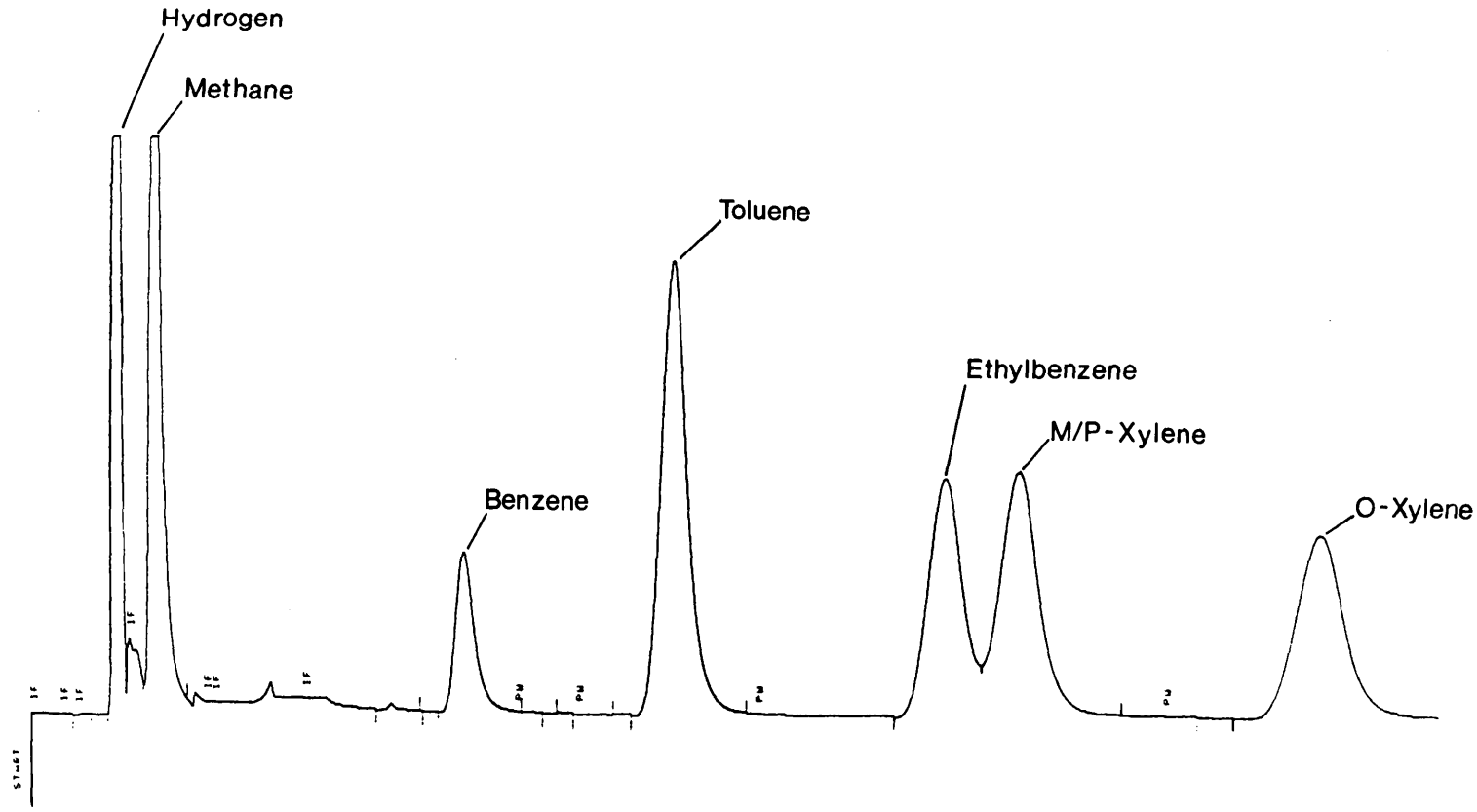

Figure 4.13 - Typical Chromatogram of Methane and Aromatic Reformate Products

The CEF column, the TCEP column and the 6 port switching valve were held at an isothermal temperature of 90°C by a Perkin Elmer F11 oven.

Following detection and measurement of the aromatics the 6-port Negretti Xambra valve was switched to allow flow through the 5A/13X column. Both the molecular sieve columns were held at their initial temperatures for a further 10 minutes allowing ethane to elute. The 13X trap was now heated as rapidly as possible (ca. 2 minutes) to 450°C whilst the 5A/13X column was maintained at 150°C. After 15 minutes the trap was switched off and allowed to cool to room temperature, all the non-aromatics having been displaced onto the 5A/13X column. The 13X trap was heated by a West Gardian temperature control unit (Model no. Q3M) used in conjunction with an Anglican PR13 energy controller.

The 5A/13X column was then ramped at 3° min^{-1} to 450°C and was maintained at this temperature until all paraffins were eluted. Raising the temperature at the optimum rate of 3°C min^{-1} allowed the adsorbed hydrocarbons to be removed sequentially in order of increasing carbon number. The different sorption energies of napthenes and paraffins on the 13X molecular sieve resulted in their separation. Similarly, iso and normal paraffins were resolved on the 5A molecular sieve.

Figure 4.14 shows a typical chromatogram of paraffin reformate products.

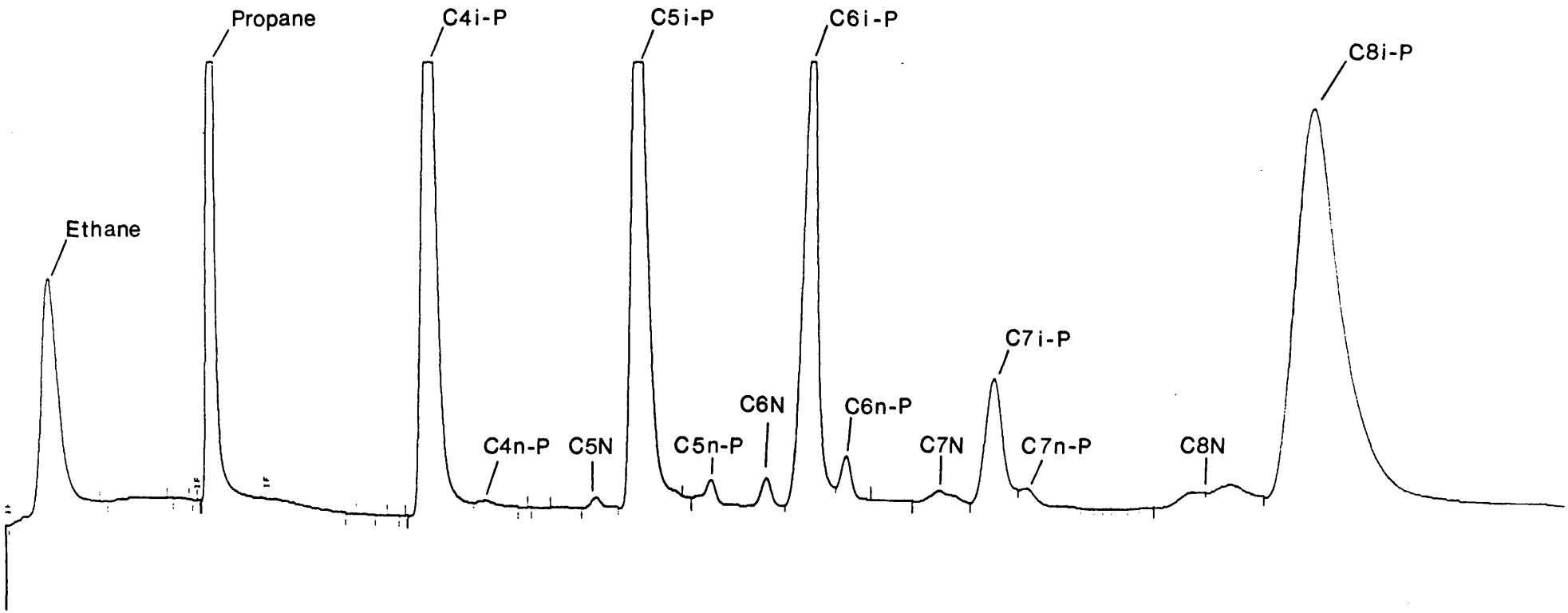

Figure 4.14 - Typical Chromatogram of Paraffin Reformate Products.

4.1.5.3 PNA System Temperature Programming and Carrier Gas Regulation

The PU4500 chromatograph, as supplied, had no temperature programming facilities. The heating element within the oven was therefore disconnected from the PU4500 and combined with an FGH temperature programmer (Model no. K-P200) used in conjunction with a 10A solid state relay. Oven temperature was monitored using a Cr/Al thermocouple connected to the 6 channel digital thermometer described in section 4.1.4.1.

Helium carrier gas was delivered by a 2-stage APO cylinder head. A Negretti Zambra precision pressure regulator (Model no. R182) was used for the fine control of helium pressure. Delivery pressure to the system was set at 80 psig. Pressure was measured on a Budenberg gauge (0-300 psig) (Fig. 4.12 D). Nupro fine metering needle valves 2 and 3 (models' no. SS-SS2) were used to establish the helium flow rate at 40 ml min^{-1} through, respectively, the TCEP and 5A/13X molecular sieve columns. The different column packings and temperature regimes required that the needle valves were set at different values to realize the same flow rates. A Whitey 3 way tap (Valve 11, model no. SS-41SX2) enabled the helium flow to be directed through either needle valve as required.

It was found that the carrier gas flow rate through the 5A/13X column decreased with increasing temperature. This manifested itself as a rising baseline in the non-aromatic chromatograms. In order to attenuate this effect, the reference helium gas flow was directed through a second 5A/13X molecular sieve column which

was identical to the first. Initial flow through this second column was set using a further Nupro fine metering needle valve (needle valve no. 4).

All metal tubing interconnecting the gas sampling valve and the various columns was heated by Electrothermal heating tape. This in turn was lagged with high temperature insulating tape. The temperature of the heating tape was maintained at 160°C by a Variac transformer.

4.1.5.4 Summary of PNA Columns

1. CEF — Allows elution of aliphatics < C10, before benzene, (90°C). Cyano ethyl formamide, 22.5% w/w on acid washed Chromosorb P (60-80 mesh). Stainless steel column, i.d. = 1.8mm, length = 2.0m.

2. TCEP — Aromatics separation, (90°C). Tris cyano ethoxy propane, 5% w/w on acid washed Chromosorb P (60-80 mesh). Stainless steel column, i.d. = 2.4mm, length = 2.0m.

3. 13X Trap — Entrapment of non-aromatics, 13X molecular sieve (60-80 mesh). Stainless steel column, i.d. = 1.8mm, length = 15 cm
Ambient → 450°C

4. 5A/13X — Separation of paraffins by carbon number and by bulk hydrocarbon type.

5A molecular sieve section (60-80 mesh), length = 30 cm.

13X molecular sieve section (60-80 mesh), length = 90 cm.

Both sections contained within one length of stainless steel column, i.d. = 1.8mm.

150°C → 450°C @ 3°/minute.

Columns 3 and 4 were initially activated by heating to 100°C and holding at this temperature for half an hour. The temperature was then ramped to 450°C at 3° min^{-1} and held at this temperature for a further 4 hours. Carrier gas flow was set at 40 ml min^{-1}.

4.1.5.5 Hydrocarbon Detection and Calibration

A thermal conductivity detector and a Hewlard Packard computing integrator (Model no. HP 3396 A) were used for the identification, measurement and display of chromatographic peaks.

The retention times and response factors of all potential reaction products were determined by making unique injections of a known volume of each component into the PNA system. Liquid hydrocarbon samples were introduced via a chromatographic injection port situated after the gas sampling valve. This was enclosed by the heated box described in section 4.1.4.4. Injections were made using an S.G.E. 10μl

graduated liquid tight microsyringe (Type 10A-N). Gaseous hydrocarbon samples were introduced via the gas sampling valve. The calibration procedure was repeated until at least 4 reproducible results were obtained and, therefore, all retention times and response factors represent average values. The retention times of methane and all aromatic hydrocarbons were measured from the point of injection; the retention times of non-aromatic hydrocarbons were measured from the point at which gas flow was directed through the molecular sieves by the 6-port switching valve.

Table 4.1 shows the retention times and response factors of all compounds relevant to this study.

Table 4.1 Chromatographic Retention Times and Response Factor

Compound	Retention Time (minutes)	Response Factor (Area Units x 10^{-13} mol^{-1})
Methane	2.0	10.30
Benzene	7.1	2.76
Toluene	10.5	2.31
Ethylbenzene	14.8	2.08
m/p-Xylene	16.0	1.99
o-Xylene	21.1	2.09
Ethane	4.3	5.44
Propane	20.4	4.16
Iso-butane	42.3	4.17
n-Butane	46.4	3.17
Cyclopentane	59.4	1.79
Iso-pentane	63.4	1.62
n-Pentane	70.9	1.50
Cyclohexane	78.6	1.45
Iso-hexane	82.6	1.24
n-Hexane	86.7	1.14
Cycloheptane	96.1	1.19
Iso-heptane	101.6	1.03
n-Heptane	104.7	0.82
Cyclooctane	123.5	1.09
Iso-octane	133.1	0.91
n-Octane	145.4	0.77

4.1.6 Materials

4.1.6.1 n-Octane

The n-octane used throughout the course of this study was Gold Label n-octane as supplied by the Aldrich Chemical Company Ltd. The purity, as measured by gas chromatography was > 99%. It was used without further purification.

4.1.6.2 Hydrogen

Cylinder hydrogen (B.O.C. Ltd) was used without further purification.

4.1.6.3 Air

Cylinder air (B.O.C. Ltd) was used without further purification.

4.1.6.4 Nitrogen

Cylinder nitrogen (B.O.C. Ltd) was used without further purification.

4.1.6.5 Helium

Cylinder helium (B.O.C. Ltd) was used without further purification.

CHAPTER 5

RESULTS

5.1 n-OCTANE REFORMING EXPERIMENTS

The reaction of n-octane and hydrogen on three different catalysts, GHI, EUROPT 3 and EUROPT 4 was investigated. Reforming experiments, using 0.5g of catalyst sample, were performed at a pressure of 110 psig and a temperature of either 450 or 500°C. The various experimental conditions used for each catalyst are listed in table 5.1. The catalyst were activated using the standard procedures detailed in section 3.1.

Spent catalyst samples were removed after each experiment and analysed for surface carbon deposits and residual chlorine content using the techniques described in section 3.3. The results from analysis of the spent catalysts are summarised in table 5.2.

5.1.1 Yield, Conversion and Selectivity Calculations

The yield, conversion and selectivity values quoted throughout this work are defined as follows:-

Yield:- the amount of a given reaction product related to the amount of the starting component, expressed as a percentage. Thus, for a product i, the yield is expressed by the relationship,

$$(\%)\ \text{yield} = \frac{n_i\,(M_i)}{N\,(X)} \times \frac{100}{1} \qquad \text{.....(1)}$$

Table 5.1 - Experimental Conditions for n-Octane Reforming

Catalyst	GHI	EUROPT3	EUROPT4.1	EUROPT4.2
Temperature (^{o}C)	500	500	500	450
Pressure (psig)	110	110	110	110
WHSV (g.n-octane/g.cat/hr)	2	2	2	2
Reaction Time (hours)	40	26	34.5	28

Table 5.2 - Spent Catalyst Analysis

Catalyst	GHI	EUROPT3	EUROPT4.1	EUROPT4.2
Reaction Time (hours)	40	26	34.5	28
Carbon Weight %	1.20	1.20	0.65	0.40
Cl Wt. % (fresh)	1.28	0.95	0.95	0.95
Cl Wt. % (after reduction)	1.01	-	-	-
Cl Wt. % (spent)	0.37	0.71	0.77	0.56

where n_i = the number of carbon atoms in product species i.

M_i = the number of moles of product species i.

N = the number of carbon atoms in the reactant molecule.

X = the number of moles of hydrocarbon reactant.

Conversion:- the amount of a given reaction component transformed into products related to the initial quantity of that same component, expressed as a percentage. This was obtained by summing all the individual product yields. Thus, for j product species,

$$(\%)\ \text{conversion} = \sum_{i=1}^{i=j} \frac{n_i (M_i)}{N (X)} \times \frac{100}{1} \qquad \text{.....(2)}$$

Selectivity:- the amount of a given reaction product related to the amount of starting material converted, expressed as a percentage. Selectivity values for individual product species are calculated by dividing the appropriate yield values by conversion. Selectivity is therefore expressed by the relationship,

$$(\%)\ \text{selectivity} = \frac{n_i (M_i)}{\sum_{i=1}^{i=j} n_i (M_i)} \times \frac{100}{1} \qquad \text{.....(3)}$$

The molar quantity of each individual hydrocarbon species present in a fixed volume of the product gas stream was determined by gas chromatography as described in section 4.1.5. The post reactor gas stream was sampled at regular intervals by a gas

sampling valve maintained at atmospheric pressure and 140°C; the precision gas sample loops each had a volume of 5ml. The number of moles of hydrocarbon reactant, X, is defined as the quantity of n-octane that would have been present in the fixed volume sample loops had no reaction occurred. Knowing the molar ratio of hydrogen to hydrocarbon and the values of pressure, temperature and volume the value of X could readily be calculated.

5.1.2 n-Octane Reforming on Catalyst GHI

The reactant mixture of hydrogen and n-octane was flowed over a sample of catalyst GHI for a total of 40 hours. The catalyst was maintained at 500°C and 110 psig; a hydrogen to n-octane molar ratio of 6 and WHSV of 2 h^{-1} were used throughout the run. Analysis of the post reactor gas stream allowed yield, selectivity and conversion values to be calculated throughout the 40 hours that the catalyst was on-line.

The yield of each individual hydrocarbon species is presented in table 5.3 as a function of time-on-stream. The results from table 5.3 are plotted in figures 5.1 - 5.4.

The conversion to methane, ethane and propane followed a similar pattern with time. The yield was observed to decrease with time-on-stream, the fall becoming progressively less rapid as a stable value of activity was approached (Figure 5.1). Methane was the principal gas produced during the first 18 hours followed,

respectively, by propane and ethane. However, methane also exhibited the largest fall in yield during this time. Consequently, the yield of propane exceeded that of methane by 20 hours-on-stream.

Iso-butane to iso-octane were the only other non-aromatic hydrocarbon products; no normal or cyclic paraffins were detected during the 40 hours-on-stream. Figure 5.2 shows the conversion of n-octane to iso-butane, iso-pentane and iso-hexane. The yield of the most abundant iso-paraffin, iso-butane, decreased steadily with time. In contrast, the conversion to iso-pentane and iso-hexane show smooth maxima at ca. 13 and 24 hours respectively, with iso-hexane displaying the largest increase in yield. There was no detectable iso-heptane and iso-octane produced during the first 10 hours on-line, thereafter, iso-heptane yield increased to a maximum value of ca. 0.5% by 40 hours-on-stream. Iso-octane yield was observed to rise continuously after 17 hours-on-stream and reached a maximum value of 1.3% by the end of the run.

The reforming of n-octane on catalyst GHI gave rise to the full range of anticipated aromatic products. The yields of benzene, toluene, ethylbenzene, meta/para-xylene and ortho-xylene as a function of time-on-stream are plotted in figures 5.3 - 5.4. The yield of toluene was significantly higher than that of benzene. Both benzene and toluene yields decreased with time. The downward trend in benzene and toluene yields was reflected by an increase in the yield of the four remaining aromatic products. Conversion to ethylbenzene meta/para-xylene and ortho-xylene increased substantially with time until a steady level was reached at approximately 40 hours-on-stream. The principal aromatic products at this time were

meta- and para-xylene.

The selectivity of catalyst GHI for individual hydrocarbons versus time-on-stream are shown in table 5.4. The four major reactions, aromatisation, isomerisation, hydrocracking and hydrogenolysis were assessed by considering the selectivity towards individual hydrocarbons or groups of hydrocarbons. Each was regarded as being representative of a particular type of reaction. The four major reactions were assessed on the following basis:

(1) aromatisation - represented by summing the selectivity for all aromatic products,

(2) isomerisation - represented by summing the selectivity for iso-heptane and iso-octane formation,

(3) hydrocracking - represented by summing the selectivity for iso-butane, iso-pentane and iso-hexane formation,

(4) hydrogenolysis - represented by the selectivity toward methane formation.

The selectivity results for the major reactions are summarised in figure 5.5.

The results obtained demonstrate that the selectivity of the catalyst was modified considerably with time and that each major reaction was affected. Hydrogenolysis was one of the reactions most significantly influenced, with selectivity falling by 8.5% in approximately 37 hours. The most rapid fall in hydrogenolysis

selectivity occurred in the early stages of the experiment with a pseudo-stationary level reached by the end of the run. Hydrocracking selectivity fell by 4.1% in the same period of time. Hydrocracking activity differed from hydrogenolysis activity by initially rising to a maxima after 10 hours-on-stream before falling continuously in a linear manner. Hydrocracking activity exceeded that of hydrogenolysis throughout the entire run.

The principal reaction of n-octane on catalyst GHI, throughout the total 40 hours, was aromatisation. The aromatisation reaction also underwent the largest change in selectivity during the experiment, increasing by 13-14%. This increase was not linear and showed the most significant changes during the earlier stages of the experiment. Isomerisation selectivity on catalyst GHI was initially zero before rising steadily to a value of 8.5%.

One method of assessing the relative activities of hydrocracking and hydrogenolysis is to examine the ratio of propane to methane product yields with time. It is widely accepted that the production of methane by hydrogenolysis is closely associated with the metallic component of a bifunctional catalyst. In contrast, the formation of propane, through hydrocracking, is favoured by the acidic component of the catalyst. The ratio of propane to methane (C3/C1) may therefore be used as an approximate relation of the acidic to the metallic activities of the catalyst.

The values of the C3/C1 ratio for catalyst GHI are listed in table 5.6 and plotted as a function of time-on-stream in figure 5.6. Figure 5.6 shows the ratio

C3/C1 increases steadily with time until it reaches a level value of approximately 1.1. The initial increase in the ratio demonstrates convincingly that the metallic function of the catalyst is relatively more deactivated than the acidic function during the first 20 hours of the n-octane/hydrogen reforming reaction on catalyst GHI.

Total conversion of n-octane on the monometallic GHI catalyst was calculated using the method described in section 5.1.1. The conversion versus time data is shown in table 5.6 and plotted in figure 5.7. Total conversion was low for catalyst GHI and never exceeded 23%. An initial fall in conversion was followed by a steady value of catalyst activity which was maintained for the duration of the experiment.

Catalyst GHI had a coke content of 1.20% by weight and a residual chlorine content of 0.37% by weight on completion of the experiment. The chlorine content of the fresh catalyst was 1.68% by weight (Table 5.2).

Time (hours)	Methane	Ethane	Propane	Iso-butane	n-Butane
3.2	3.2	1.9	2.5	3.2	0
5.9	2.5	1.7	2.4	3.1	0
8.7	2.2	1.6	2.2	2.9	0
11.4	2.2	1.5	2.1	2.8	0
14.5	2.0	1.4	2.0	2.7	0
17.2	2.1	1.4	2.0	2.9	0
20.0	1.8	1.3	1.9	2.6	0
22.8	1.7	1.3	1.8	2.6	0
25.5	1.5	1.2	1.6	2.3	0
40.0	1.3	1.0	1.4	1.9	0

Table 5.3 - Yield of Individual Products versus Time-on-Stream for Catalyst GHI

Time (hours)	C5 Napthene	Iso-pentane	n-Pentane	C6-Napthene	Iso-hexane	n-Hexane
3.2	0	1.5	0	0	0.3	0
5.9	0	1.6	0	0	0.6	0
8.7	0	1.6	0	0	0.8	0
11.4	0	1.6	0	0	0.9	0
14.5	0	1.6	0	0	1.0	0
17.2	0	1.7	0	0	1.2	0
20.0	0	1.6	0	0	1.1	0
22.8	0	1.6	0	0	1.2	0
25.5	0	1.4	0	0	1.0	0
40.0	0	1.2	0	0	0.9	0

Table 5.3(cont) - Yield of Individual Products versus Time-on-Stream for Catalyst GHI

Time (hours)	C7-Napthene	Iso-heptane	n-Heptane	C8-Napthene	Iso-octane
3.2	0	0	0	0	0
5.9	0	0	0	0	0
8.7	0	0	0	0	0
11.4	0	0.1	0	0	0
14.5	0	0.2	0	0	0
17.2	0	0.4	0	0	0.1
20.0	0	0.4	0	0	0.5
22.8	0	0.7	0	0	0.5
25.5	0	0.4	0	0	0.6
40.0	0	0.5	0	0	1.3

Table 5.3(cont) - Yield of Individual Products versus Time-on-Stream for Catalyst GHI

Time (hours)	Benzene	Toluene	Ethylbenzene	m/p-Xylene	o-Xylene
3.2	2.2	4.1	0.2	0.9	1.2
5.9	1.7	4.0	0.6	1.1	1.6
8.7	1.5	3.7	0.8	1.2	1.7
11.4	1.3	3.7	1.0	1.4	1.8
14.5	1.1	3.5	1.5	1.8	2.0
17.2	1.0	3.6	2.0	2.2	2.3
20.0	0.9	3.2	2.1	2.3	2.2
22.8	0.8	3.1	2.3	2.5	2.3
25.5	0.7	2.7	2.0	2.3	2.1
40.0	0.6	2.2	2.6	3.0	2.5

Table 5.3(cont) - Yield of Individual Products versus Time-on-Stream for Catalyst GHI

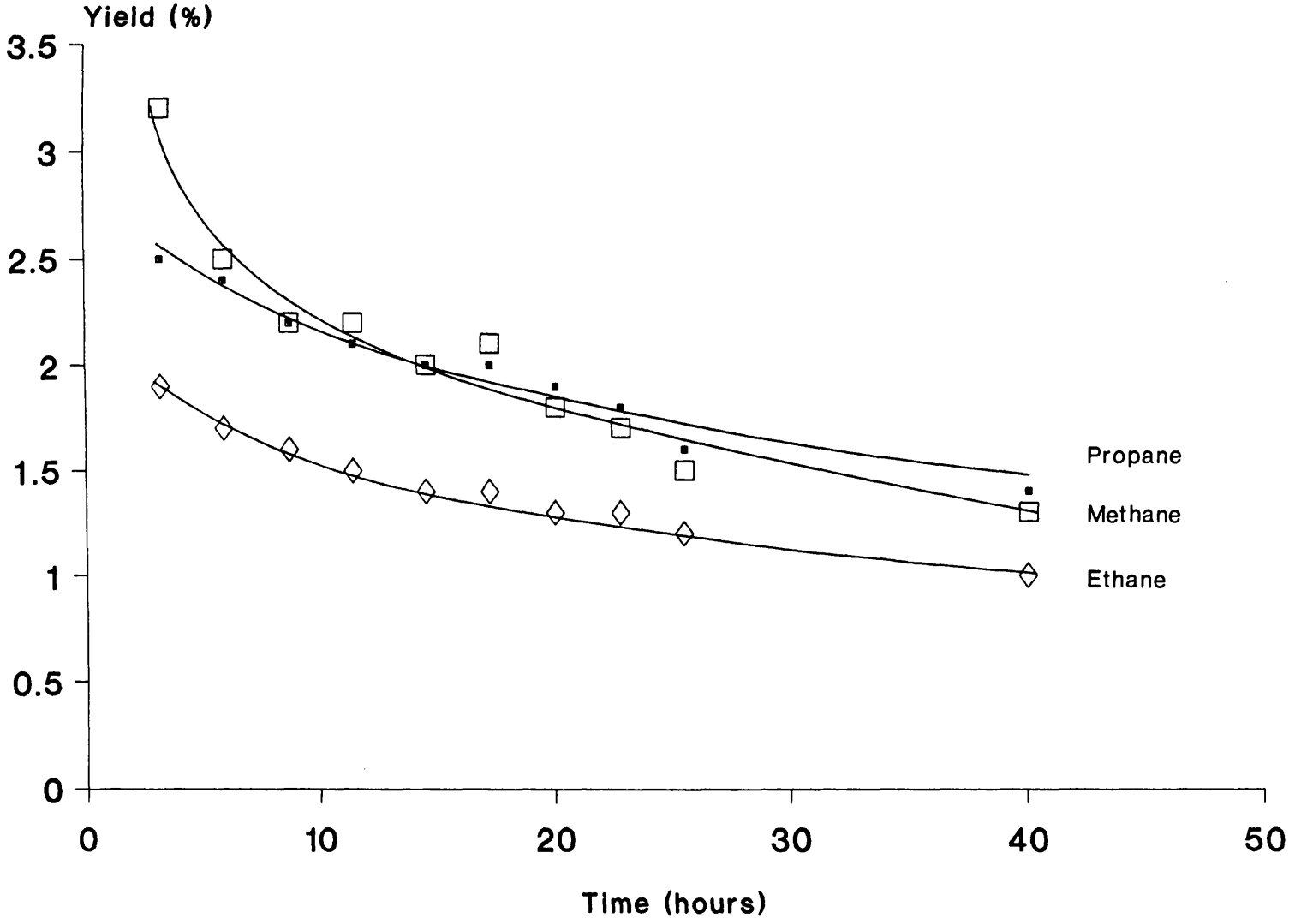

Figure 5.1 - Yield of Methane, Ethane and Propane versus Time-on-Stream for Catalyst GHI

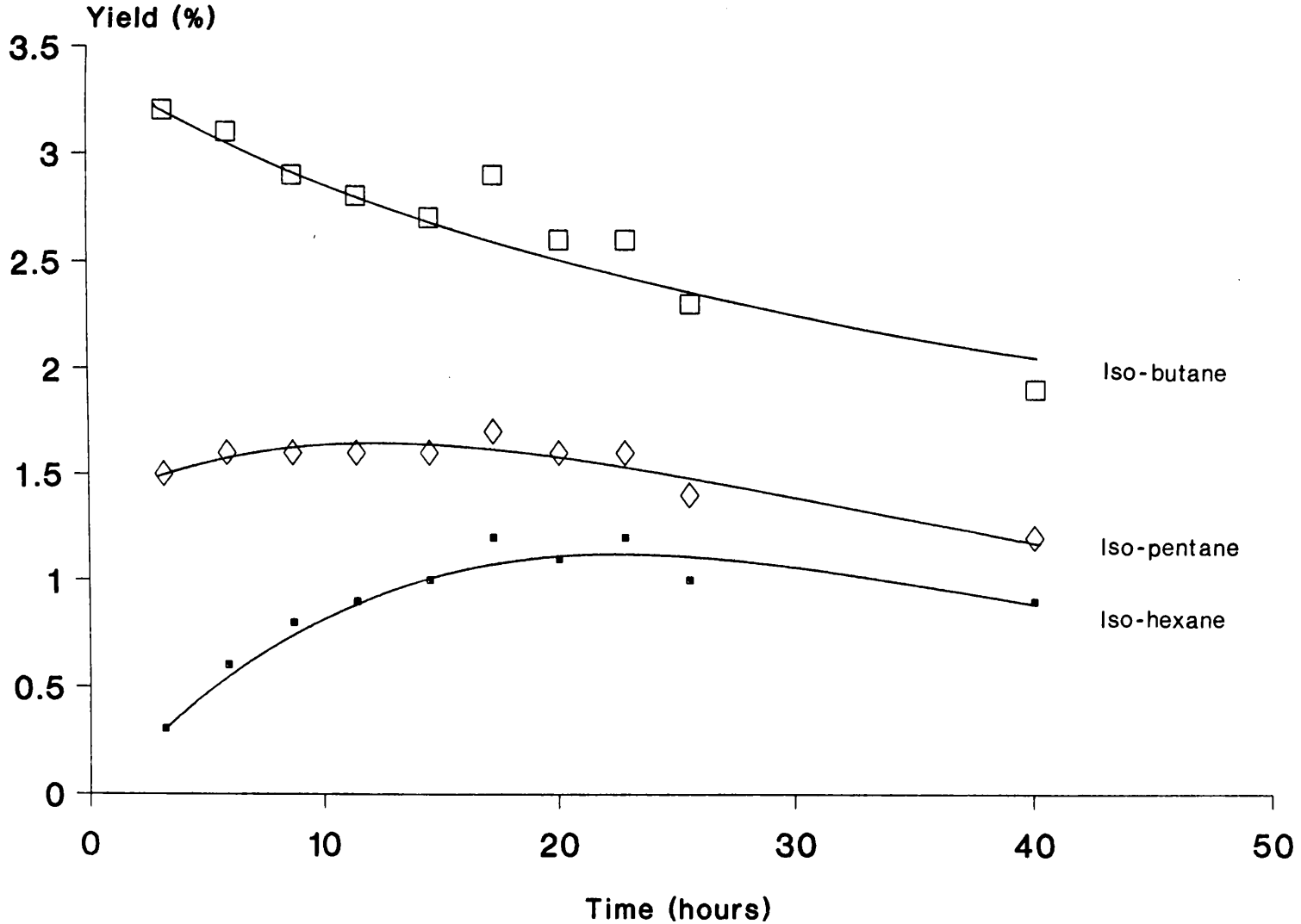

Figure 5.2 - Yield of Iso-butane, Iso-pentane and Iso-hexane versus Time-on-Stream for Catalyst GHI.

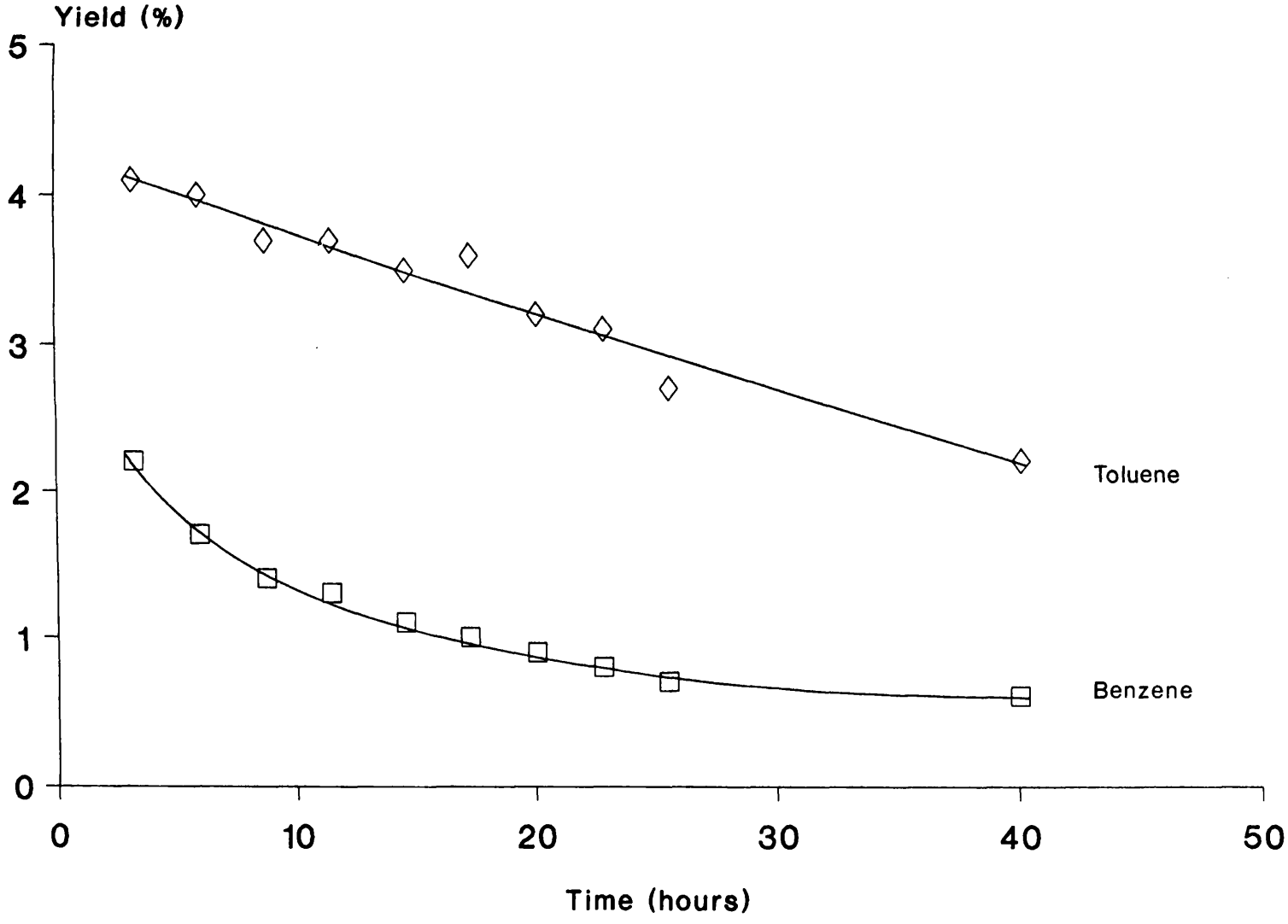

Figure 5.3 - Yield of Benzene and Toluene versus Time-on-Stream for Catalyst GHI.

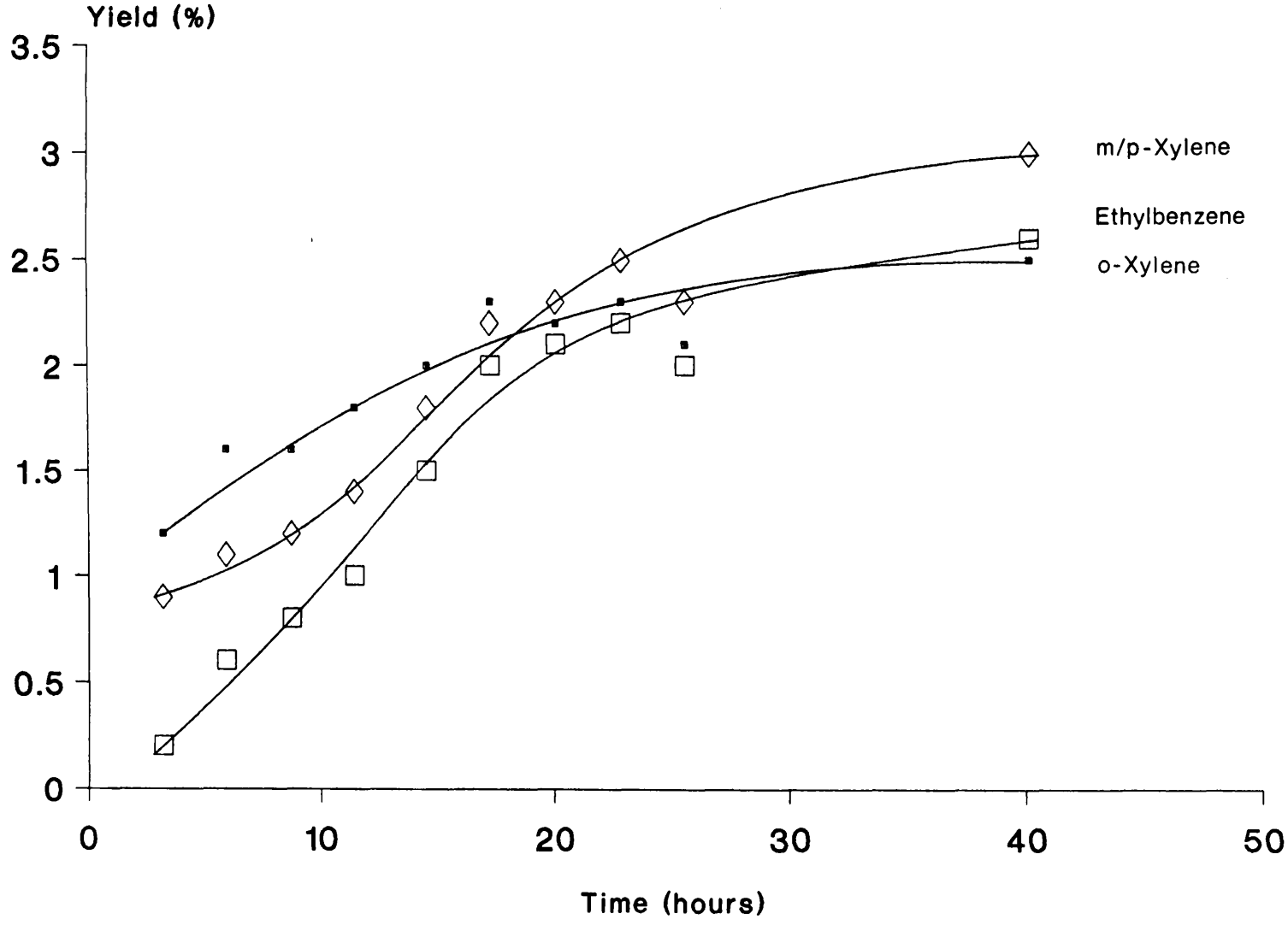

Figure 5.4 - Yield of Ethylbenzene, m/p-Xylene and o-Xylene versus Time-on-Stream for Catalyst GHI.

Time (hours)	Methane	Ethane	Propane	Iso-butane	n-Butane
3.2	14.9	8.9	12.0	15.3	0
5.9	12.1	8.2	11.3	14.8	0
8.7	10.9	8.0	10.8	14.6	0
11.4	10.5	7.5	10.3	13.8	0
14.5	9.4	6.8	9.6	13.2	0
17.2	9.0	6.3	8.9	12.4	0
20.0	8.0	6.0	8.7	12.0	0
22.8	7.6	5.8	8.2	11.5	0
25.5	7.5	5.9	8.2	11.5	0
40.0	6.5	4.7	6.6	9.5	0

Table 5.4 - Selectivity to Individual Products versus Time-on-Stream for Catalyst GHI

Time (hours)	C5 Napthene	Iso-pentane	n-Pentane	C6-Napthene	Iso-hexane	n-Hexane
3.2	0	7.1	0	0	1.5	0
5.9	0	7.6	0	0	2.9	0
8.7	0	7.9	0	0	3.8	0
11.4	0	7.8	0	0	4.3	0
14.5	0	7.7	0	0	4.8	0
17.2	0	7.4	0	0	5.0	0
20.0	0	7.3	0	0	5.2	0
22.8	0	7.2	0	0	5.2	0
25.5	0	6.9	0	0	5.1	0
40.0	0	5.9	0	0	4.5	0

Table 5.4(cont) - Selectivity to Individual Products versus Time-on-Stream for Catalyst GHI

Time (hours)	C7-Napthene	Iso-heptane	n-Heptane	C8-Napthene	Iso-octane
3.2	0	0	0	0	0
5.9	0	0	0	0	0
8.7	0	0.2	0	0	0
11.4	0	0.4	0	0	0
14.5	0	0.9	0	0	0
17.2	0	1.7	0	0	0.6
20.0	0	1.8	0	0	2.1
22.8	0	3.0	0	0	2.3
25.5	0	2.0	0	0	2.9
40.0	0	2.2	0	0	6.2

Table 5.4(cont) - Selectivity to Individual Products versus Time-on-Stream for Catalyst GHI

Time (hours)	Benzene	Toluene	Ethylbenzene	m/p-Xylene	o-Xylene
3.2	10.3	19.3	1.0	4.1	5.4
5.9	8.3	18.9	2.7	5.3	7.7
8.7	7.3	18.5	3.9	6.1	8.2
11.4	6.4	18.0	5.1	7.1	8.8
14.5	5.3	16.9	7.1	8.5	9.6
17.2	4.6	15.6	8.6	9.8	10.0
20.0	4.1	14.7	9.5	10.5	10.1
22.8	3.8	13.8	10.2	11.2	10.4
25.5	3.8	13.8	10.2	11.6	10.6
40.0	2.8	11.1	12.9	14.8	12.2

Table 5.4(cont) - Selectivity to Individual Products versus Time-on-Stream for Catalyst GHI

Time (hours)	Aromatisation	Isomerisation	Hydrocracking	Hydrogenolysis
3.2	40.1	0	24.0	14.9
5.9	42.9	0	25.3	12.1
8.7	44.0	0.2	26.2	10.9
11.4	45.4	0.4	25.9	10.5
14.5	47.4	0.9	25.7	9.4
17.2	48.5	2.3	24.9	9.0
20.0	48.8	4.0	24.6	8.0
22.8	49.3	5.2	23.9	7.6
25.5	50.0	4.9	23.5	7.5
40.0	53.8	8.5	19.9	6.5

Table 5.5 - Selectivity to Major Reactions versus Time-on-Stream for Catalyst GHI

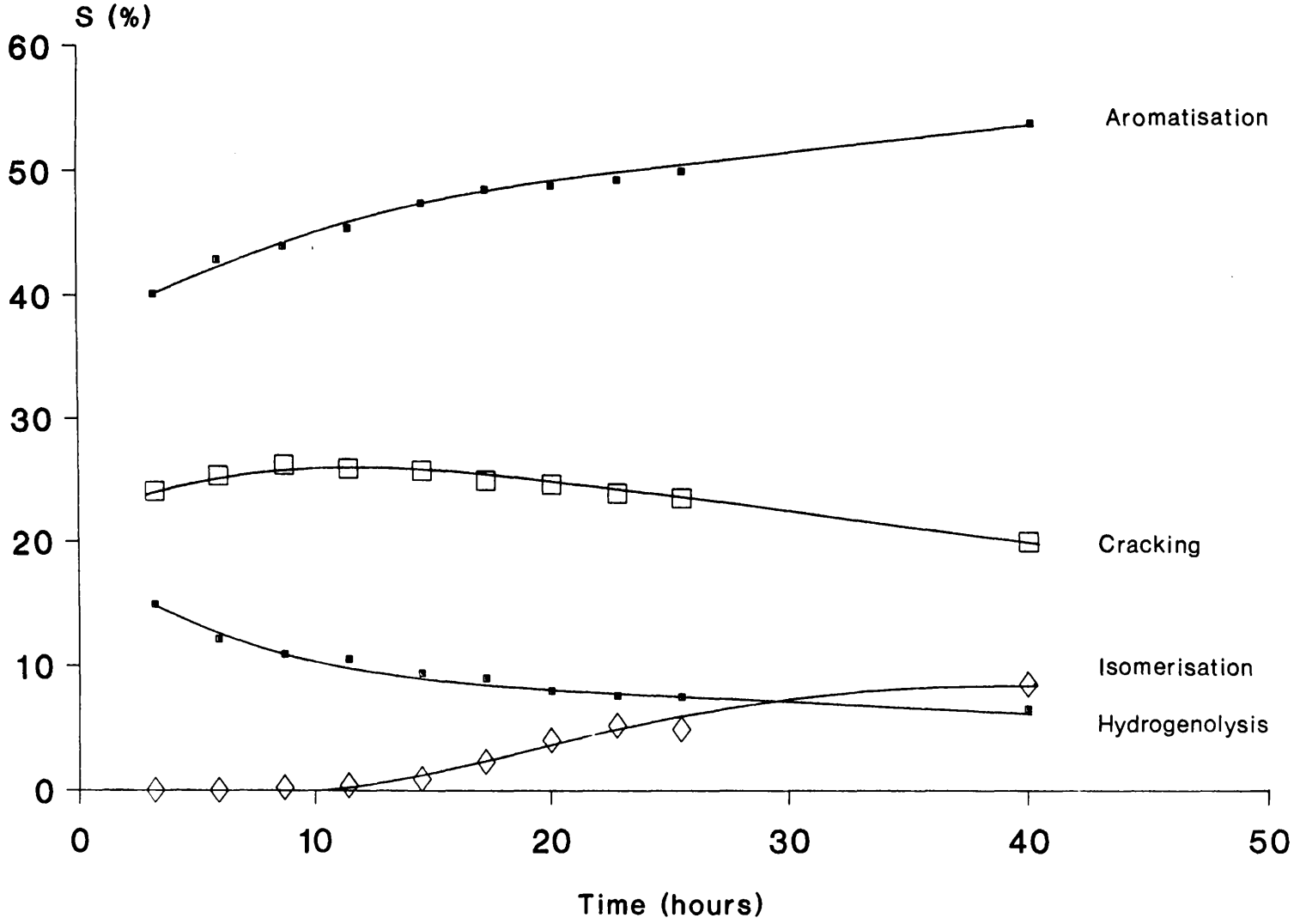

Figure 5.5 - Selectvity Towards Major Reactions versus Time-on-Stream for Catalyst GHI.

Time (hours)	Conversion	C3/C1
3.2	21.2	0.80
5.9	20.8	0.93
8.7	20.0	0.99
11.4	20.6	0.98
14.5	20.7	1.02
17.2	23.0	0.99
20.0	21.9	1.08
22.8	22.2	1.09
25.5	19.7	1.09
40.0	20.2	1.03

Table 5.6 - Conversion and Propane to Methane Ratio versus Time-on-Stream for Catalyst GHI

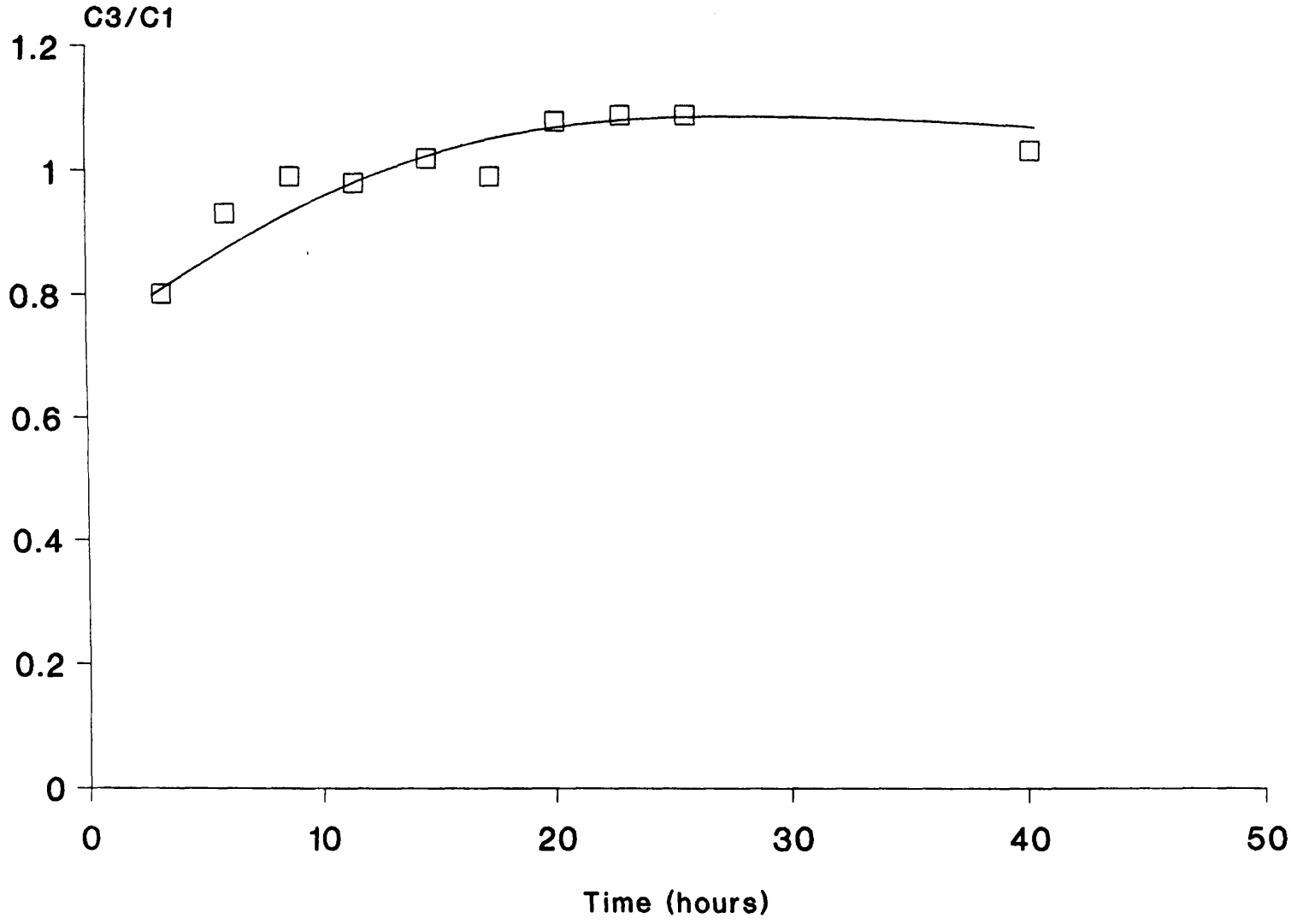

Figure 5.6 - Propane to Methane Ratio versus Time-on-Stream for Catalyst GHI.

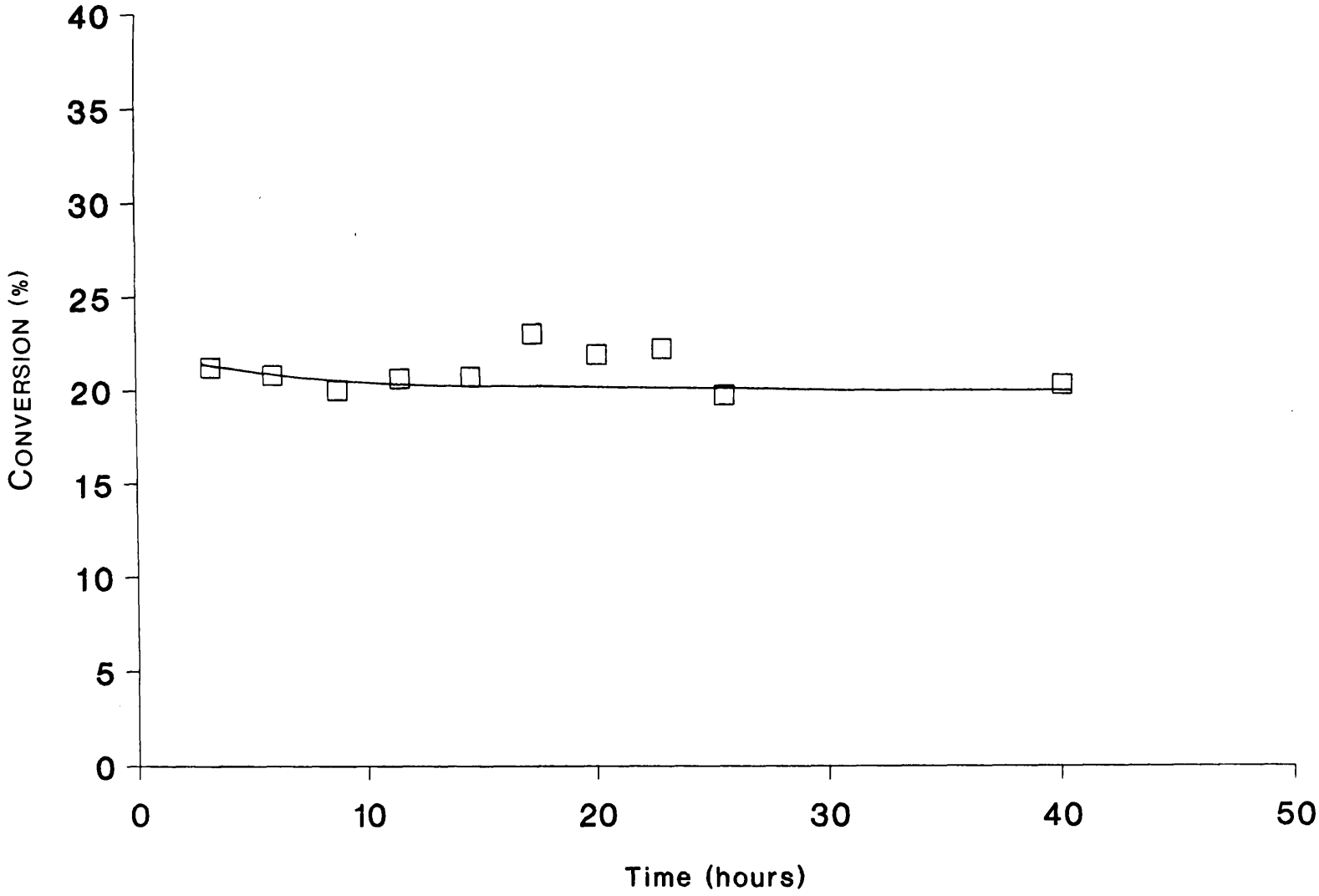

Figure 5.7 - Conversion versus Time-on-Stream for Catalyst GHI.

5.1.3 n-Octane Reforming on Catalyst EUROPT 3

The second monometallic platinum catalyst, EUROPT 3, was studied using conditions identical to those described in section 5.1.2. The reforming reaction of n-octane and hydrogen was investigated for a total of approximately 26 hours.

The yields of individual hydrocarbon species are presented in table 5.7 as a function of time-on-stream and are plotted in figures 5.8 - 5.14. It is apparent from table 5.7 that, with the exception of methane and benzene, the yield of all product species is significantly higher for catalyst EUROPT 3 than for catalyst GHI. The high values of yield are reflected in the conversion data for catalyst EUROPT 3 (Table 5.10). The initial conversion figure calculated at 4.6 hours-on-stream has a value of 84.7%. In contrast, total conversion on catalyst GHI at 3.2 hours-on-stream was only 21.2%.

Despite the differences in activity the behaviour of the two monometallic platinum catalysts is qualitatively similar in several respects. For instance, the most marked changes in yield of methane, ethane and propane occurred during the early stages of the run with a constant level of activity being reached by the end of the experiment.

The importance of central cracking of the n-octane molecule to produce iso-butane is apparent from the results presented in figure 5.9. The yield of individual iso-paraffin species, excluding iso-octane, follow an inverse relationship to carbon

number (Figures 5.9 - 5.10). Conversion to iso-butane and iso-pentane was observed to decrease with time-on-stream. In contrast, the yield of iso-hexane and iso-heptane remained at a constant level. Iso-octane formation was initially low before it increased rapidly and showed no sign of diminishing. The formation of benzene and toluene on EUROPT 3 was quantitatively very similar to that of catalyst GHI. The yield of toluene exceeded that of benzene in each case (Figure 5.13).

Notwithstanding the similarities in n-octane reforming between the two monometallic catalyst there are significant differences which should be noted. Perhaps the most striking is the contrast in the behaviour of the catalysts towards the formation of ethylbenzene, meta/para-xylene and ortho-xylene. All four aromatic hydrocarbons produced on catalyst EUPORT 3 showed a dramatic fall in yield during the first 10 hours-on-stream (Figure 5.14). In contrast, the yields of ethylbenzene, meta- and para-xylene and ortho-xylene were observed to increase with time-on-stream for catalyst GHI. Meta- and para-xylene were the most abundant aromatic products produced using catalyst EUROPT 3.

Propane was the principal gaseous product on catalyst EUROPT 3 followed respectively by ethane and methane (Figure 5.8). The most abundant gas produced on catalyst GHI until approximately 20 hours-on-stream was methane and thereafter propane. Both normal and cycloparaffins were produced in small quantities during the reaction of n-octane on catalyst EUROPT 3 (Figures 5.11 - 5.12).

The selectivity of catalyst EUROPT 3 towards individual hydrocarbons versus

time-on-stream is listed in table 5.8. The selectivity towards the four major reactions, aromatisation, isomerisation, hydrocracking and hydrogenolysis was determined using the procedure detailed in section 5.1.2.; the results are summarised in table 5.9 and presented graphically as a function of time in figure 5.15.

Hydrogenolysis selectively was low on catalyst EUROPT 3 with a maximum value of between 2.5 and 3% during the first 10 hours-on-stream. Hydrogenolysis selectivity decreased steadily and reached a value of 2% by the end of the experiment. Cracking selectivity on catalyst EUROPT 3 was quantitatively very similar to that of catalyst GHI and fell gradually to a steady value of ca. 23%. Isomerisation selectivity, though initially low was always greater than zero. Catalyst activity towards the isomerisation reaction increased steadily with time and a maximum selectivity value of approximately 14% was reached by the end of the run.

The principal reaction of n-octane on both monometallic catalysts was aromatisation. However, in the case of catalyst GHI, the aromatisation reaction showed a large increase in selectivity of approximately 10%. In marked contrast, the selectivity towards the formation of aromatics on catalyst EUROPT 3 decreased by up to 10% during the equivalent time period (Figures 5.5 and 5.15). Aromatisation selectivity on both catalysts experienced the most significant changes during the first hours-on-stream.

The ratio of propane yield to methane yield was calculated for catalyst EUROPT 3 and the results are summarized in table 5.10. The ratio is presented as

a function of time-on-stream in figure 5.16. The high value of the ratio, in excess of 3, is indicative of the diminished importance of methane formation over catalyst EUROPT 3. The value of the C3/C1 ratio remained essentially level throughout the entire run.

Total conversion of n-octane on catalyst EUROPT 3 as a function of time is presented in figure 5.17. The initial conversion figure of ca. 85% fell rapidly and by 7.6 hours-on-stream a value of ca. 66% was reached. This value remained constant for the duration of the experiment.

Catalyst EUROPT 3 had a coke content of 1.20% by weight and a residual chlorine content of 0.71% by weight on completion of the experiment. The chlorine content of the fresh catalyst was 0.95% by weight (Table 5.2).

Time (hours)	Methane	Ethane	Propane	Iso-butane	n-Butane
4.6	1.8	3.6	6.1	11.4	0
7.6	1.9	3.4	5.7	10.1	0
10.6	1.7	3.1	5.2	9.5	0
13.6	1.6	3.2	5.2	8.8	0
16.6	1.3	2.6	4.8	9.0	0
19.6	1.4	2.5	4.8	8.3	0
22.6	1.4	2.5	4.6	8.1	0
25.6	1.4	2.5	4.5	8.0	0

Table 5.7 - Yield of Individual Products versus Time-on-Stream for Catalyst EUROPT 3

Time (hours)	C5 Napthene	Iso-pentane	n-Pentane	C6-Napthene	Iso-hexane	n-Hexane
4.6	0.05	5.9	0	0.1	3.2	0.2
7.6	0.05	5.0	0	0.1	3.1	0.2
10.6	0.05	4.8	0	0.1	3.1	0.2
13.6	0.05	4.5	0	0.1	3.0	0.2
16.6	0.07	4.9	0.1	0.2	3.6	0.2
19.6	0.06	4.5	0.1	0.2	3.3	0.2
22.6	0.06	4.3	0.1	0.1	3.2	0.2
25.6	0.06	4.3	0.1	0.2	3.4	0.2

Table 5.7(cont) - Yield of Individual Products versus Time-on-Stream for Catalyst EUROPT 3

Time (hours)	C7 Napthene	Iso-heptane	n-heptane	C8-Napthene	Iso-octane
4.6	0	0.8	0	0.3	1.3
7.6	0	0.7	0	0.4	1.7
10.6	0	0.9	0	0.4	2.3
13.6	0.1	0.9	0	0.5	3.7
16.6	0.1	1.2	0	0.8	7.3
19.6	0.2	0.9	0	0.8	8.2
22.6	0.2	1.1	0	0.6	8.3
25.6	0.2	1.1	0	0.7	6.5

Table 5.7(cont) - Yield of Individual Products versus Time-on-Stream for Catalyst EUROPT 3

Time (hours)	Benzene	Toluene	Ethylbenzene	m/p-Xylene	o-Xylene
4.6	1.6	4.7	9.5	22.8	11.6
7.6	1.3	3.4	6.9	15.8	7.2
10.6	1.3	3.1	7.1	16.2	7.4
13.6	1.0	2.9	6.9	16.2	7.5
16.6	0.9	2.9	4.8	18.4	8.6
19.6	0.8	2.9	6.1	14.6	7.4
22.6	0.7	3.0	6.0	15.3	7.2
25.6	1.2	2.3	6.9	17.3	8.0

Table 5.7(cont) - Yield of Individual Products versus Time-on-Stream for Catalyst EUROPT 3

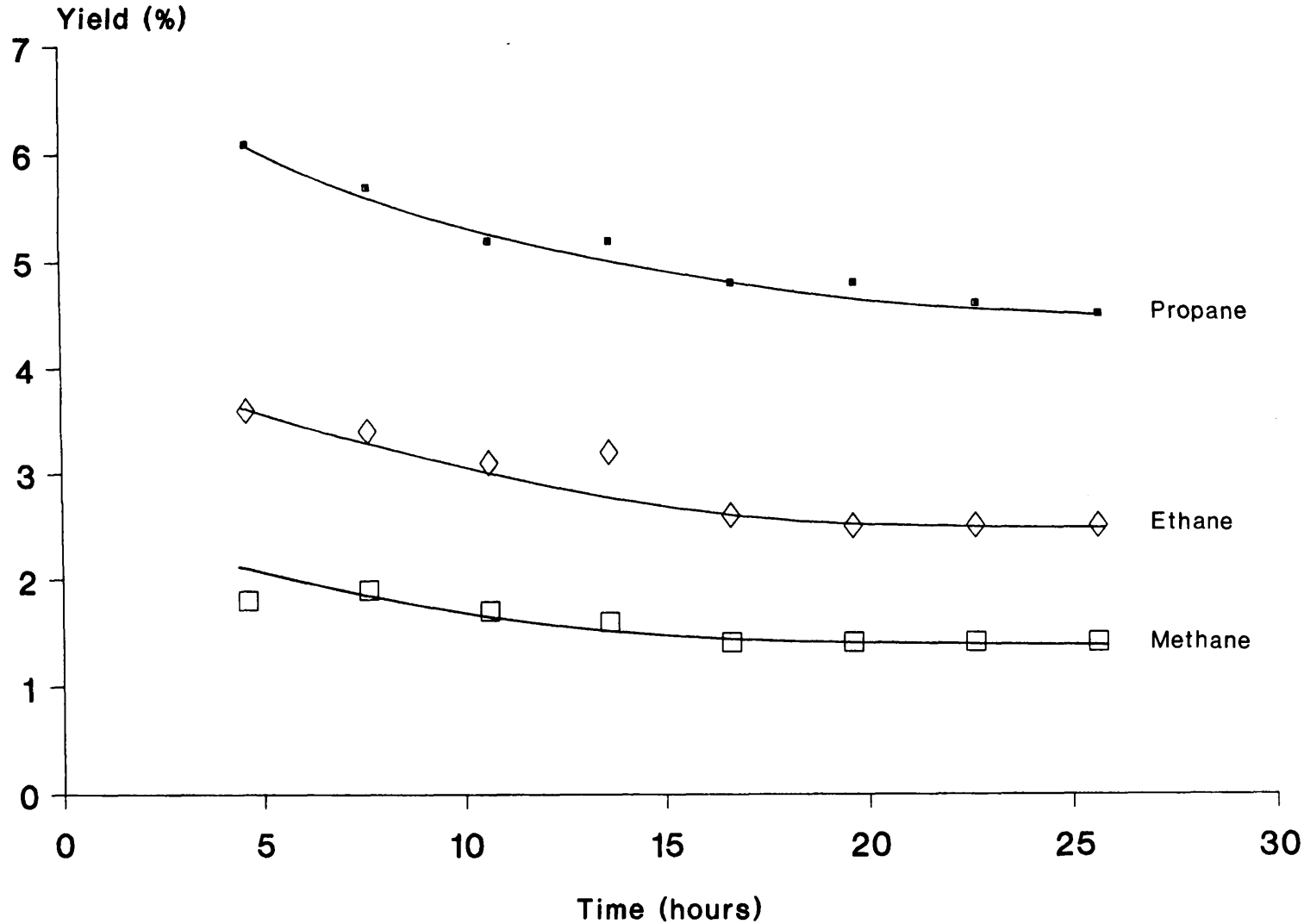

Figure 5.8 - Yield of Methane, Ethane and Propane versus Time-on-Stream for Catalyst EUROPT 3.

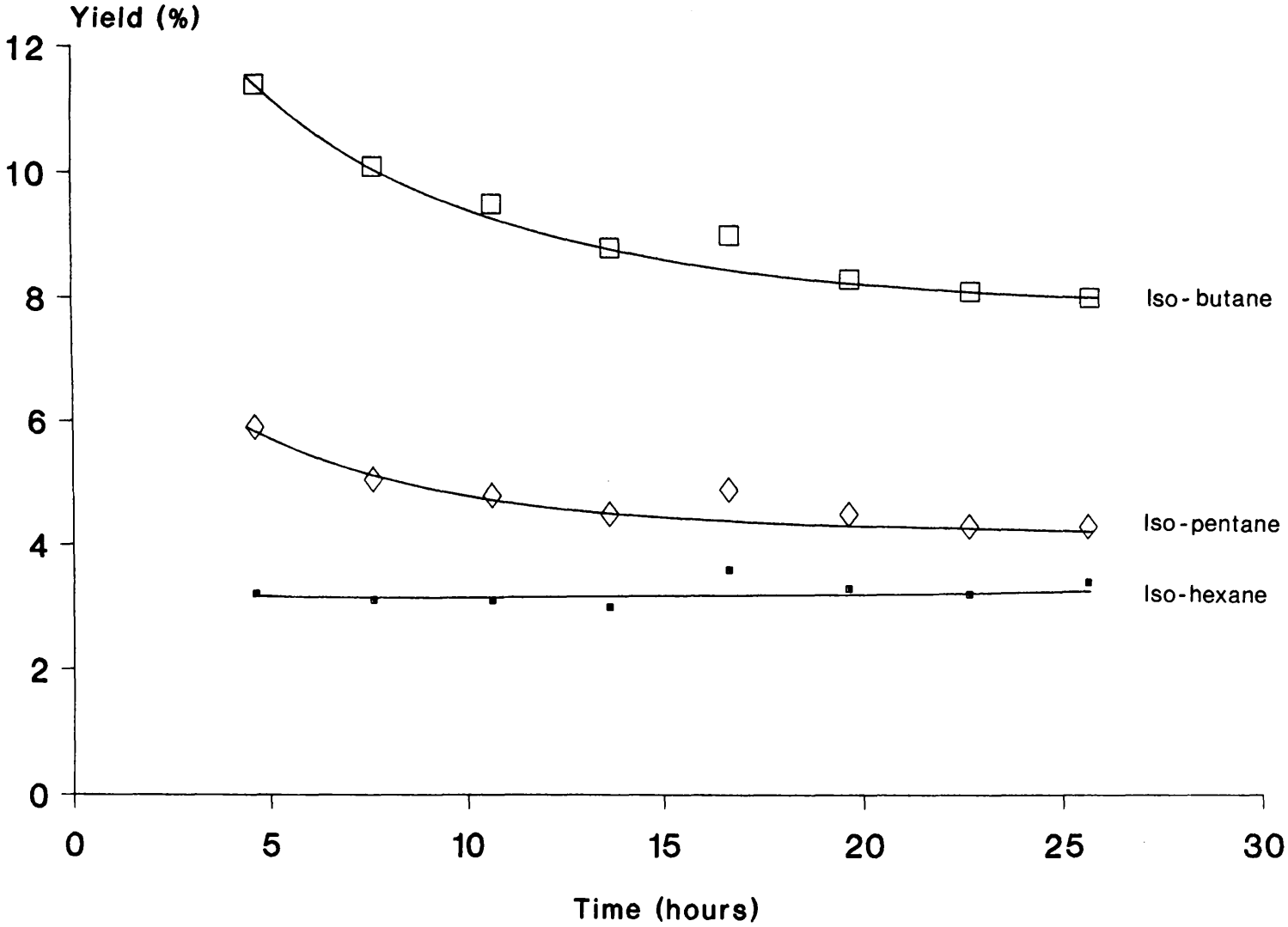

igure 5.9 - Yield of Iso-butane, Iso-pentane and Iso-hexane versus Time-on-Stream for Catalyst EUROPT 3.

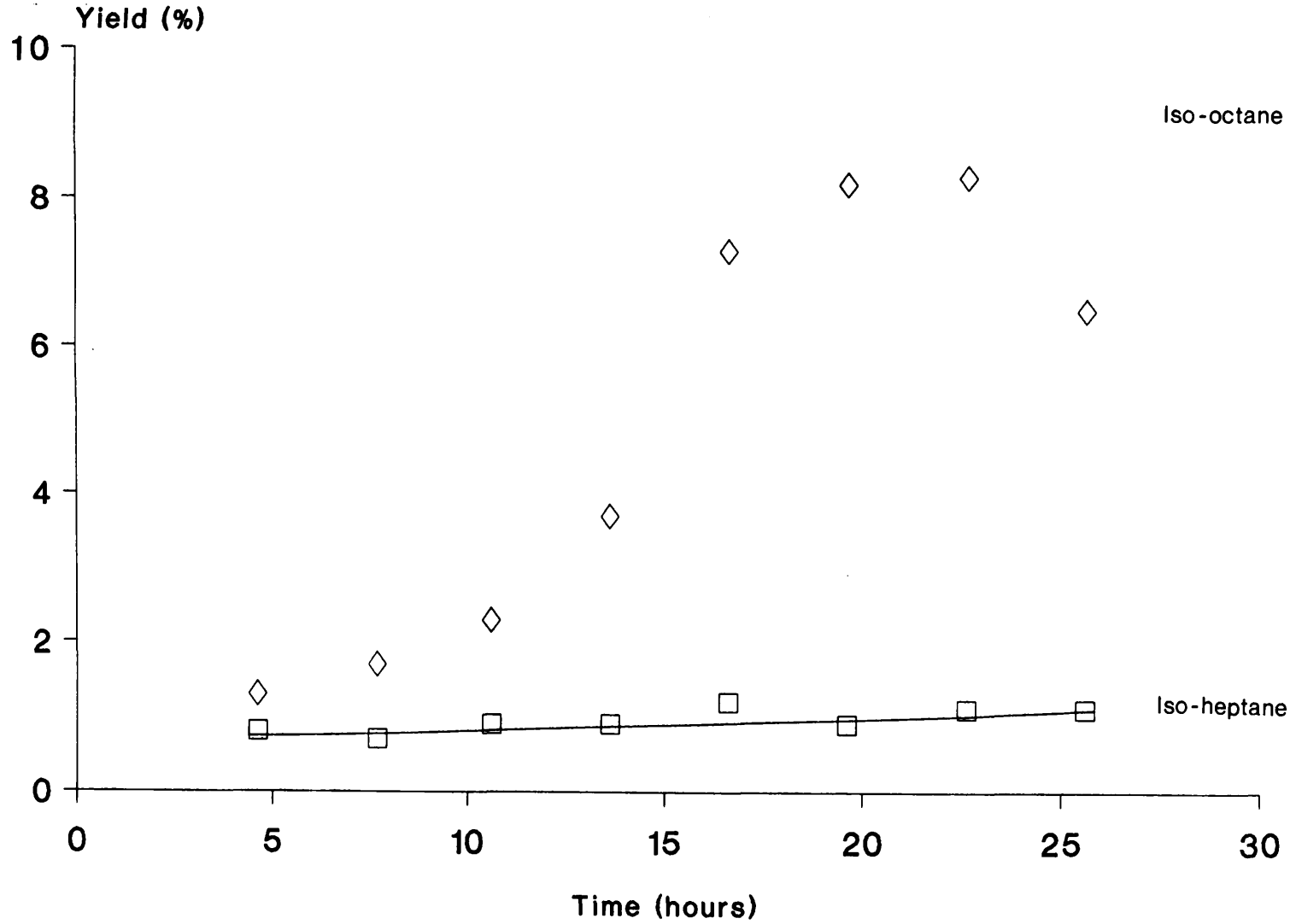

Figure 5.10 - Yield of Iso-heptane and Iso-octane versus Time-on-Stream for Catalyst EUROPT 3.

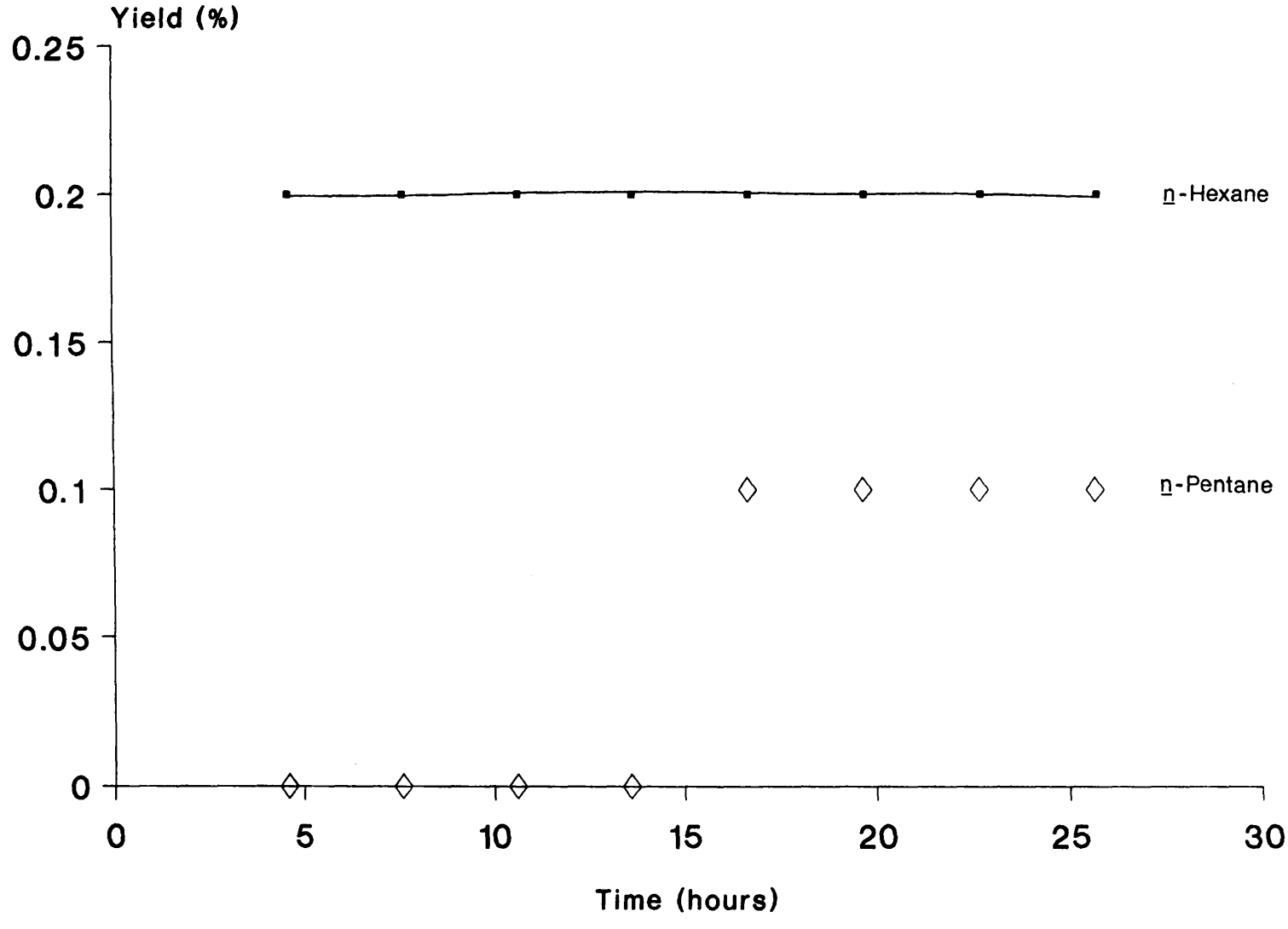

Figure 5.11 - Yield of n-Pentane and n-Hexane versus Time-on-Stream for Catalyst EUROPT 3.

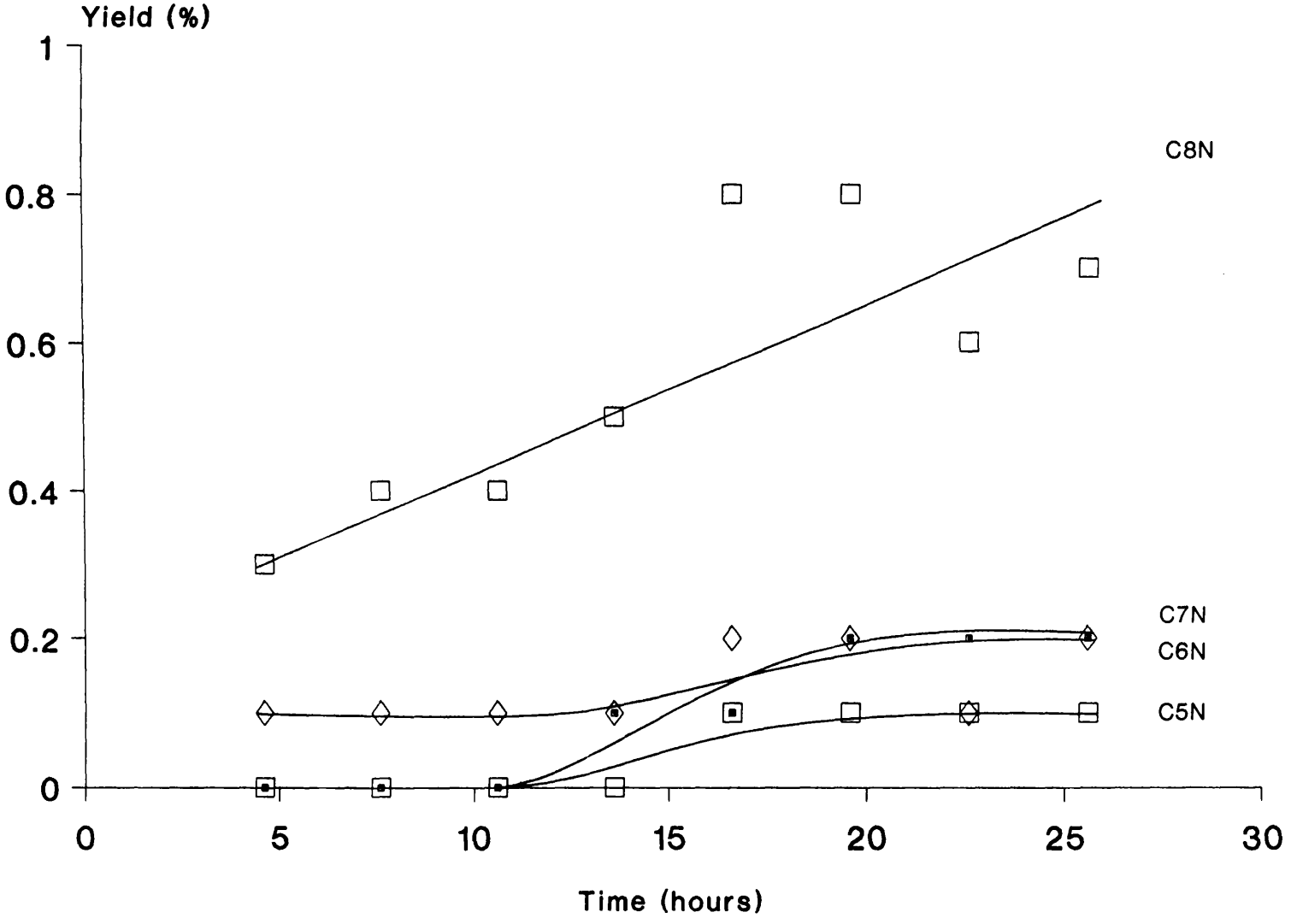

Figure 5.12 - Yield of C5 Napthene, C6 Napthene, C7 Napthene and C8 Napthene versus Time-on-Stream for Catalyst EUROPT 3.

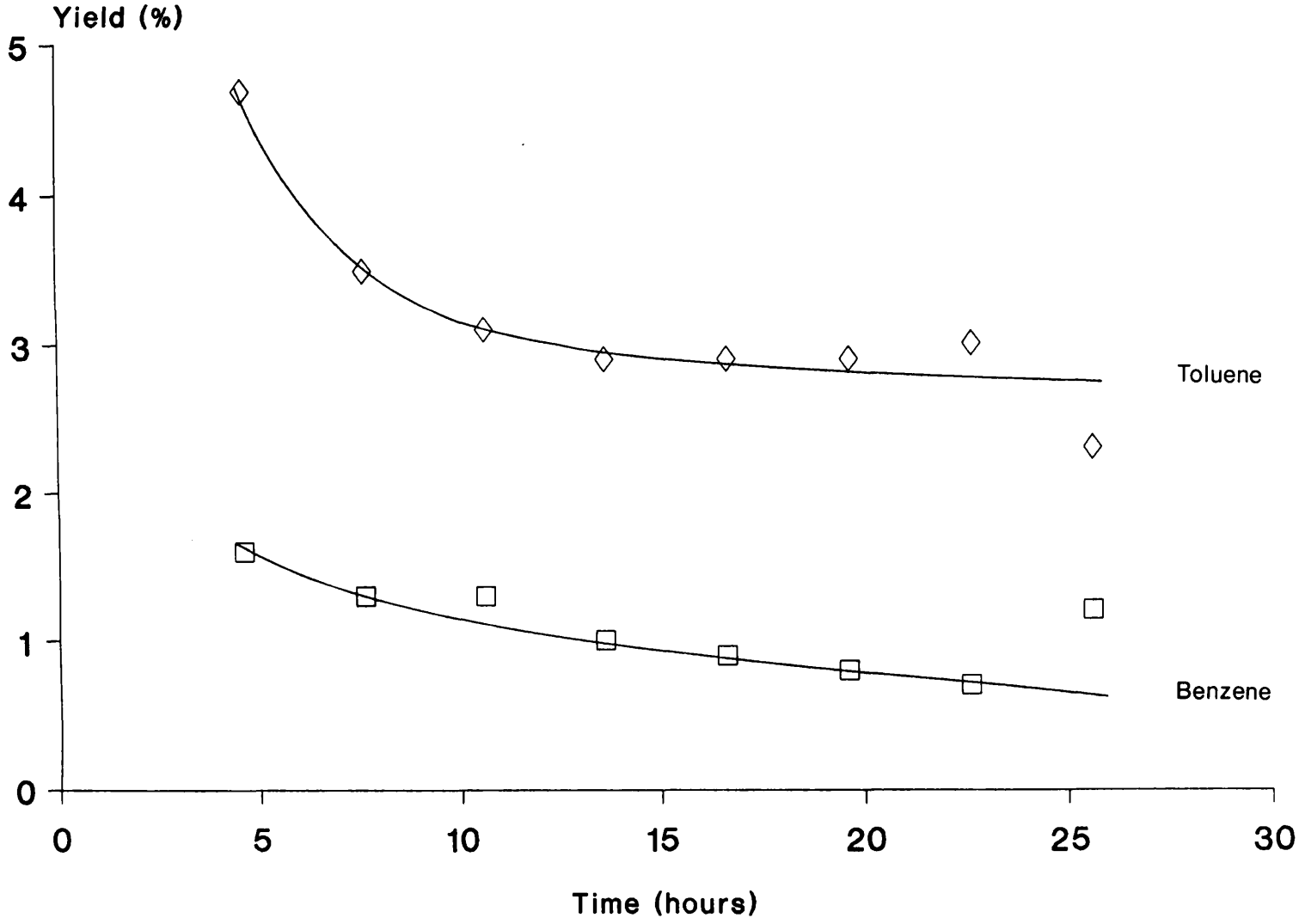

Figure 5.13 - Yield of Benzene and Toluene versus Time-on-Stream for Catalyst EUROPT 3.

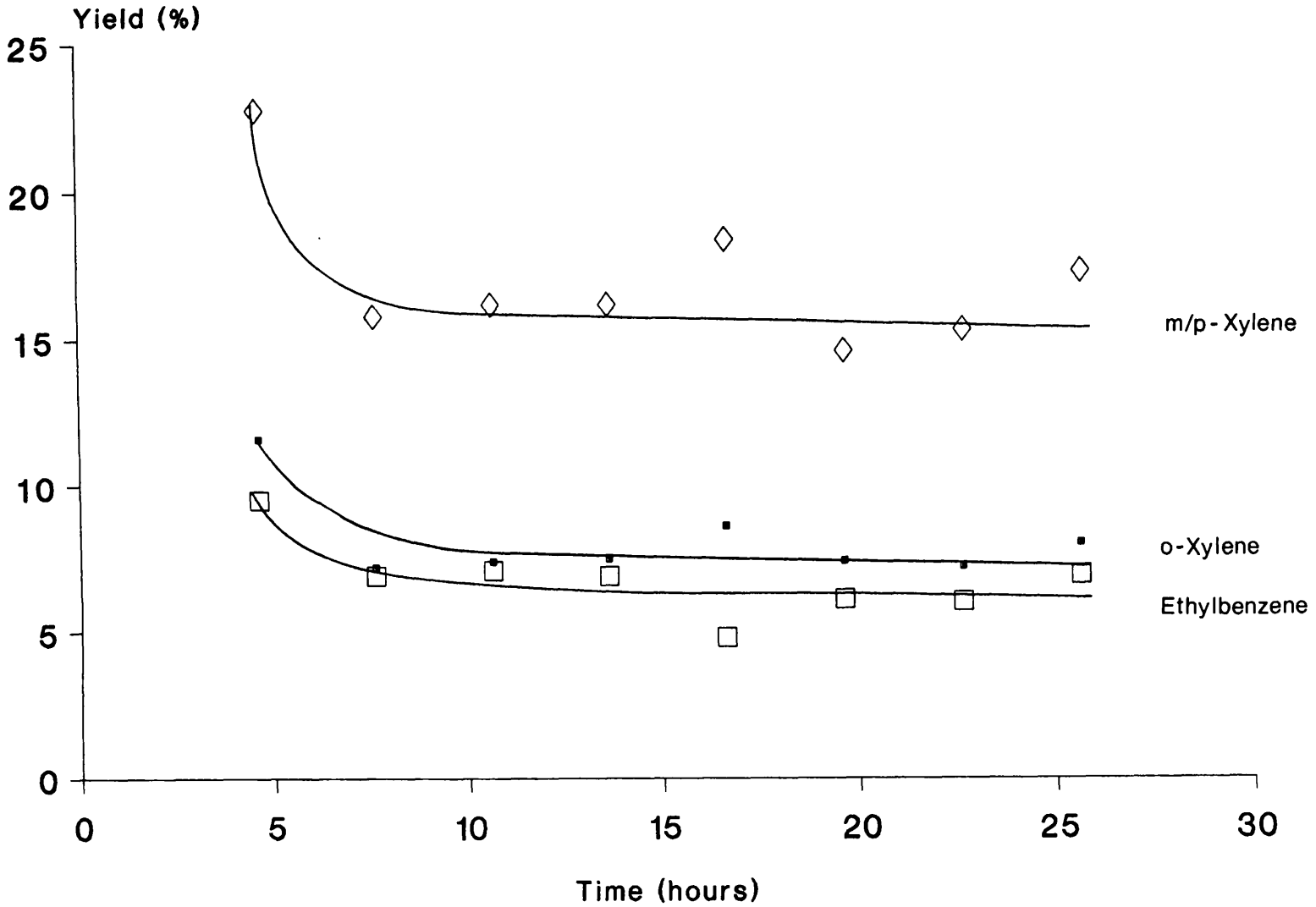

Figure 5.14 - Yield of Ethylbenzene, m/p-Xylene and o-Xylene versus Time-on-Stream for Catalyst EUROPT 3.

Time (hours)	Methane	Ethane	Propane	Iso-butane	n-Butane
4.6	2.4	4.3	7.2	13.4	0
7.6	2.8	5.1	8.5	15.2	0
10.6	2.6	4.7	7.8	14.3	0
13.6	2.3	4.8	7.9	13.4	0
16.6	1.9	3.7	6.7	12.6	0
19.6	2.1	3.8	7.2	12.5	0
22.6	2.1	3.8	6.9	12.2	0
25.6	2.0	3.7	6.6	11.7	0

Table 5.8 - Selectivity to Individual Products versus Time-on-Stream for Catalyst EUROPT 3

Time (hours)	C5 Napthene	Iso-pentane	n-Pentane	C6-Napthene	Iso-hexane	n-Hexane
4.6	0.1	7.0	0	0.1	3.8	0.2
7.6	0.1	7.5	0	0.2	4.7	0.3
10.6	0.1	7.2	0	0.2	4.6	0.3
13.6	0.1	6.8	0.1	0.2	4.6	0.3
16.6	0.1	6.9	0.1	0.3	5.1	0.3
19.6	0.1	6.8	0.1	0.2	5.0	0.4
22.6	0.1	6.5	0.2	0.2	4.8	0.3
25.6	0.1	6.4	0.2	0.2	4.9	0.4

Table 5.8(cont) - Selectivity to Individual Products versus Time-on-Stream for Catalyst EUROPT 3

Time (hours)	C7 Napthene	Iso-heptane	n-heptane	C8-Napthene	Iso-octane
4.6	0	1.0	0	0.3	1.6
7.6	0	1.0	0	0.5	2.5
10.6	0	1.3	0	0.7	3.4
13.6	0.2	1.4	0	0.7	5.6
16.6	0.2	1.7	0	1.2	10.2
19.6	0.2	1.4	0	1.2	12.4
22.6	0.2	1.7	0	0.8	12.5
25.6	0.2	1.6	0	1.0	9.6

Table 5.8(cont) - Selectivity to Individual Products versus Time-on-Stream for Catalyst EUROPT 3

Time (hours)	Benzene	Toluene	Ethylbenzene	m/p-Xylene	o-Xylene
4.6	1.9	5.5	11.3	26.9	13.7
7.6	2.0	5.2	10.4	23.7	10.9
10.6	2.0	4.7	10.8	24.6	11.2
13.6	1.5	4.4	10.5	24.5	11.4
16.6	1.3	4.0	6.8	25.9	12.1
19.6	1.1	4.3	9.1	22.0	11.1
22.6	1.1	4.5	9.0	23.0	10.8
25.6	1.8	3.4	10.1	25.4	11.7

Table 5.8(cont) - Selectivity to Individual Products versus Time-on-Stream for Catalyst EUROPT 3

Time (hours)	Aromatisation	Isomerisation	Hydrocracking	Hydrogenolysis
4.6	59.2	2.5	24.2	2.4
7.6	52.1	3.5	27.3	2.8
10.6	53.2	4.8	26.2	2.3
13.6	52.4	7.0	24.7	2.3
16.6	50.1	11.9	24.5	1.9
19.6	47.7	13.8	24.3	2.1
22.6	48.5	14.2	23.5	2.1
25.6	49.4	14.2	23.0	2.0

Table 5.9 - Selectivity to Major Reactions versus Time-on-Stream for Catalyst EUROPT 3

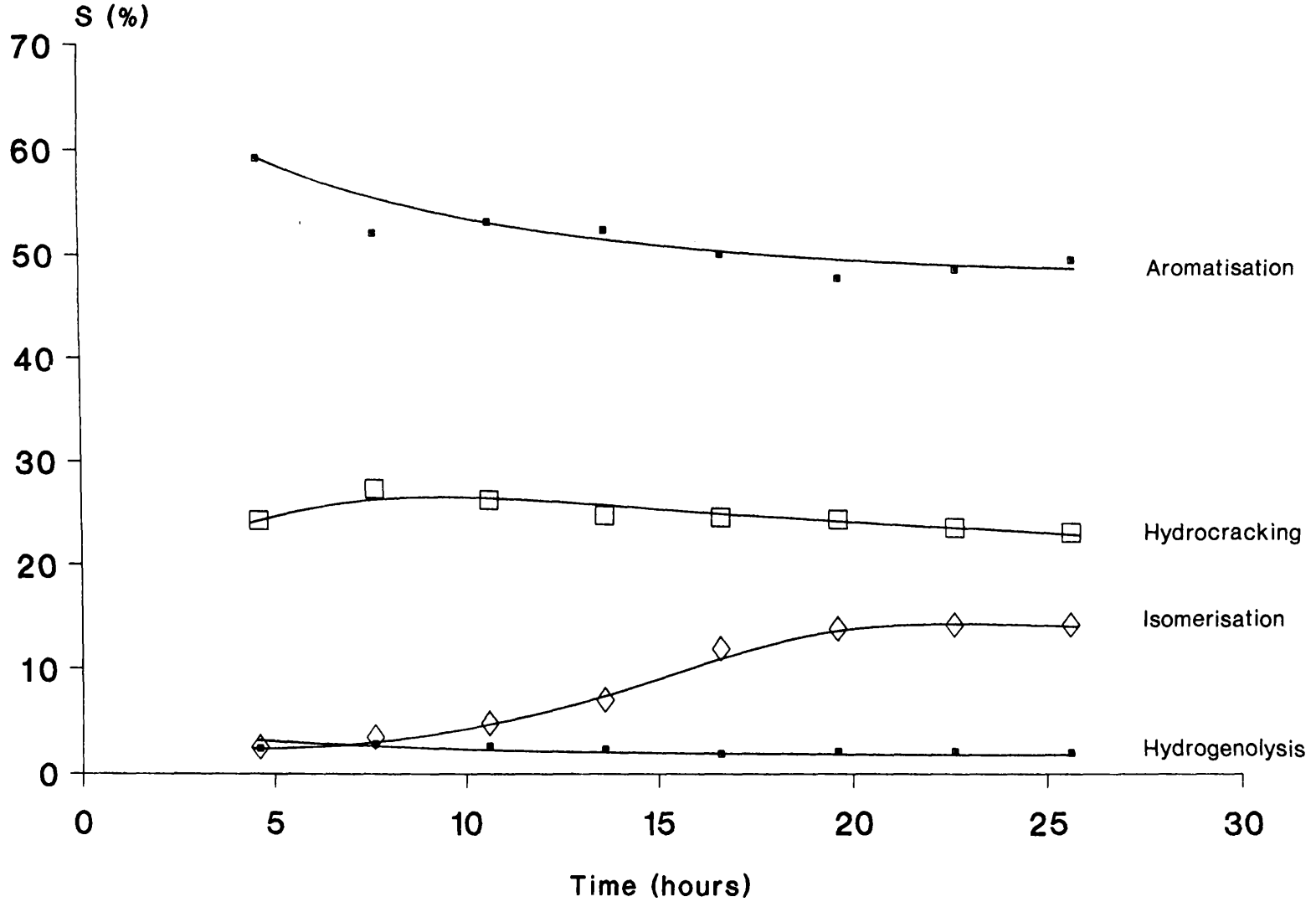

Figure 5.15 - Selectivity Towards Major Reactions versus Time-on-Stream for Catalyst EUROPT 3.

Time (hours)	Conversion	C3/C1
4.6	84.7	3.37
7.6	66.6	3.03
10.6	66.0	3.06
13.6	66.0	3.30
16.6	71.2	3.49
19.6	66.4	3.37
22.6	66.4	3.30
25.6	68.1	3.28

Table 5.10 - Conversion and Propane to Methane Ratio versus Time-on-Stream for Catalyst EUROPT 3

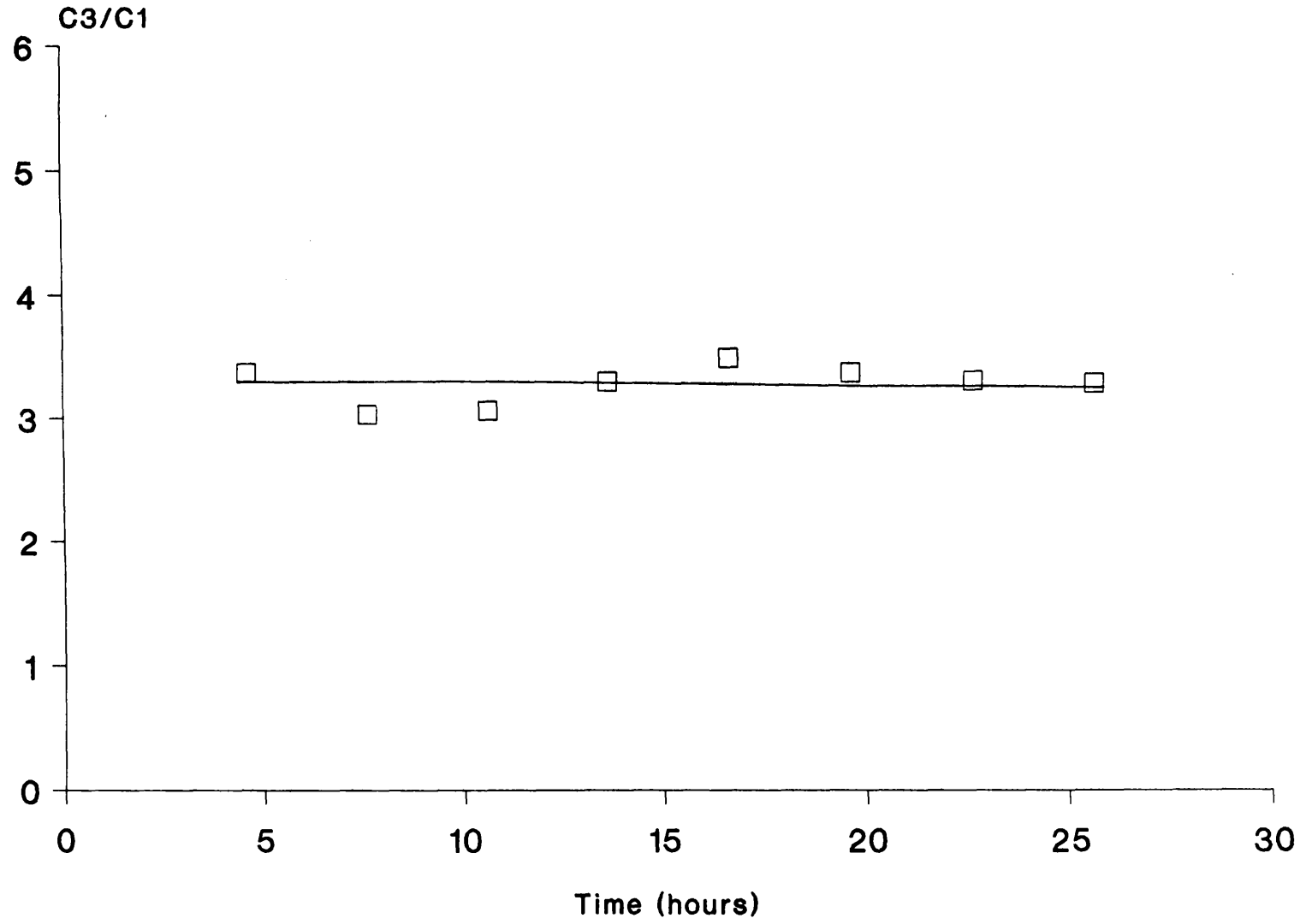

Figure 5.16 - Propane to Methane Ratio versus Time-on-Stream for Catalyst EUROPT 3.

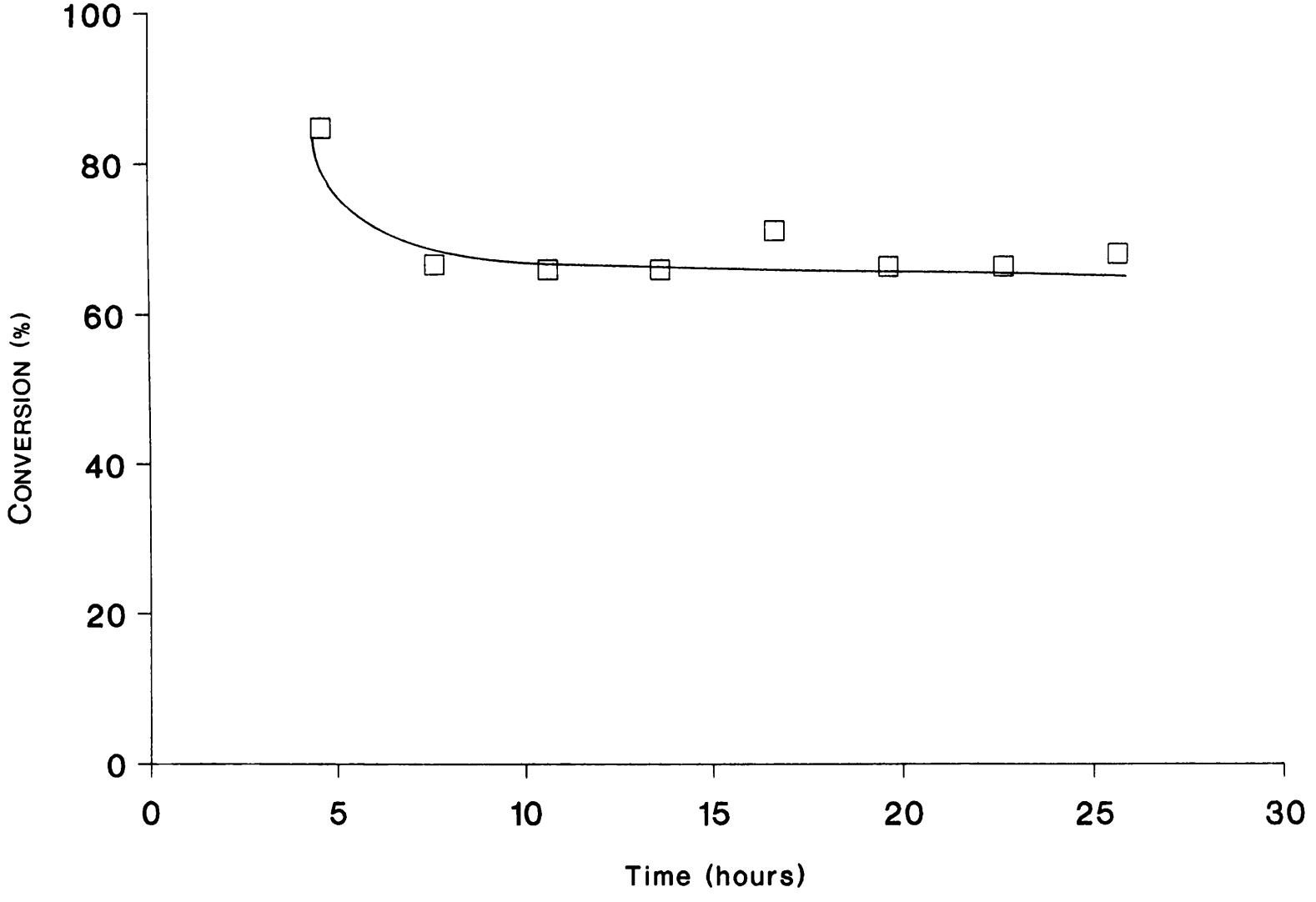

Figure 5.17 - Conversion versus Time-on-Stream for Catalyst EUROPT 3.

5.1.4 Reforming Studies on Catalyst EUROPT 4

n-Octane conversion on the bimetallic Pt-Re/Al_2O_3 catalyst was investigated at two temperatures. Catalysts EUROPT 4.1 and EUROPT 4.2 were studied at 500 and 450°C respectively. Both reactions were performed at 110 psig, space velocity (WHSV) 2^{-1} and molar hydrogen to hydrocarbon ratio 6. The experimental results are of particular interest when compared with those for catalyst EUROPT 3. Catalyst EUROPT 3 and EUROPT 4 were physically identical in all respects except for an additional loading of 0.3% by weight rhenium on catalyst EUROPT 4.

5.1.4.1 n-Octane Reforming on Catalyst EUROPT 4.1

The results from n-octane reforming at 500°C on catalyst EUROPT 4.1 are presented in this section.

Yield, selectivity and conversion results were calculated using the procedure discussed in section 5.1.1. The yields of individual hydrocarbon products are summarized in table 5.11 as a function of time-on-stream and are plotted in figures 5.18 - 5.24. In common with the results presented previously the most marked changes in product yield occurred during the initial stages of the reaction.

Figure 5.18 shows the variation in methane, ethane and propane yield during the 34.5 hours of the experiment. Propane was the principal gas produced followed by methane and ethane respectively. The yield of each was significantly higher on

catalyst EUROPT 4.1 than on either of the monometallic platinum catalysts studied.

The cracking of n-octane to form normal paraffins was a distinctive feature of the reforming reaction on the bimetallic catalyst; the formation of n-butane was particularly favoured and its yield remained constant at ca. 5.2% throughout the run (Figure 5.21). The yield of n-pentane fell slightly then remained at ca. 2.0%. Conversely, the n-hexane yield was observed to rise before reaching a steady level of 1%. No n-heptane was detected in the reaction products.

Iso-paraffin formation on catalyst EUROPT 4.1, from C_4 to C_8, increased with time-on-stream. The production of iso-butane, iso-pentane and iso-hexane followed a similar pattern; after an initial increase during the first 10 hours of the run the yield of each remained at a contant level. Iso-butane was the most abundant iso-paraffin species produced throughout the experiment followed respectively by iso-pentane and iso-hexane. The importance of centre cracking of the n-octane molecule is again apparent from the iso-paraffin product distribution (Figures 5.19 - 5.20). Iso-heptane yield, after the initial stages of the run, increased by only a small fraction in the remaining 25 hours. The production of iso-octane followed a similar trend to that established on the monometallic catalysts and increased throughout the run. The iso-octane yield remained low and never exceeded 1.5%.

The formation of benzene on catalyst EUROPT 4.1 was quantitatively similar to that on catalyst EUROPT 3. Toluene yield however was significantly higher on the bimetallic (Figure 5.23). The most abundant aromatic product on catalyst EUROPT

4.1 was meta-/para-xylene. The maximum yield of meta-/para-xyxlene was approximately 24%. Both meta-/para-xylene and ethylbenzene yields increased with time-on-stream. The ethylbenzene yield reached a steady value of approximately 6% after 15 hours-on-stream. The yield of meta-/para-xylene, on the other hand, continued rising up to 25 hours-on-stream. In contrast, the yield of ortho-xyxlene fell slightly from 10% to 8.5% during the experiment (Figure 5.24). It should be noted that the yield of all aromatic products on catalyst EUROPT 3 decreased without exception.

The selectivity of catalyst EUROPT 4.1 towards individual hydrocarbons is listed in table 5.12. The selectivity towards the four major reactions was determined and the results are shown in table 5.13 and presented as a function of time-on-stream in figure 5.25. It is apparent that hydrogenolysis activity on catalyst EUROPT 4.1 was significantly higher than on the monometallic catalyst EUROPT 3. In contrast, isomerisation and hydrocracking selectivity was considerably lower. Despite the differences in magnitude the selectivity towards the above major reactions followed a broadly similar trend for each catalyst. Hydrocracking selectivity on catalyst EUROPT 4.1 was observed to fall from approximately 15% to 13.5% during the 34.5 hours of the experiment. Hydrogenolysis selectivity decreased from approximately 11% to 5% in the same time interval. Isomerisation selectivity increased with time-on-stream to a maximum value of ca. 3%.

The formation of aromatics was particularly favoured on both EUROPT 3 and EUROPT 4.1 and was the predominant reaction in each case (Tables 5.9, 5.13).

Selectivity towards the aromatisation reaction decreased with time for catalyst EUROPT 3. The selectivity towards aromatics on catalyst EUROPT 4.1 increased throughout the course of the experiment (Figure 5.25).

The behaviour of the propane to methane ratio for catalyst EUROPT 4.1 was very similar to that observed for catalyst GHI, where an initial rise in the ratio preceded a level value (Table 5.14, figure 5.26). The value of the C3/C1 ratio was considerably lower than that determined for catalyst EUROPT 3.

Total conversion of n-octane on catalyst EUROPT 4.1 rose from an initial value of 64% after 3 hours-on-stream to a steady value of approximately 77% by the end of the experiment (Table 5.14, figure 5.27).

Catalyst EUROPT 4.1 had a coke content of 0.65% by weight and a residual chlorine content of 0.77% by weight on completion of the experiment. The chlorine content of the fresh catalyst was 0.95% by weight (Table 5.2).

Time (hours)	Methane	Ethane	Propane	Iso-butane	n-Butane
3.0	7.0	4.6	7.0	4.1	5.2
6.0	4.7	4.0	7.6	4.9	5.8
9.0	4.6	4.0	6.6	4.4	5.4
12.0	4.4	4.1	6.8	4.4	5.3
23.5	4.2	3.9	6.6	4.2	5.3
26.5	4.0	3.8	6.6	4.2	5.2
29.5	4.0	4.0	6.6	4.2	5.2
34.5	4.0	3.8	6.3	4.0	4.9

Table 5.11 - Yield of Individual Products versus Time-on-Stream for Catalyst EUROPT 4.1

Time (hours)	C5 Napthene	Iso-pentane	n-Pentane	C6-Napthene	Iso-hexane	n-Hexane
3.0	0	2.8	2.3	0	1.1	0.2
6.0	0.2	3.8	2.1	0.4	2.5	0.8
9.0	0.2	3.5	2.0	0.3	2.4	0.8
12.0	0.2	3.4	1.9	0.3	2.4	0.8
23.5	0.2	3.5	2.0	0.4	2.6	0.8
26.5	0.2	3.5	1.9	0.3	3.0	0.9
29.5	0.2	3.5	2.0	0.3	2.6	1.0
34.5	0.2	3.3	1.8	0.3	2.5	0.8

Table 5.11(cont) - Yield of Individual Products versus Time-on-Stream for Catalyst EUROPT 4.1

Time (hours)	C7 Napthene	Iso-heptane	n-heptane	C8-Napthene	Iso-octane
3.0	0	0.1	0	0	0
6.0	0	0.6	0	0.7	0.3
9.0	0	0.6	0	0.9	0.5
12.0	0	0.6	0	0.8	0.5
23.5	0	0.8	0	1.2	1.1
26.5	0	0.8	0	1.2	1.3
29.5	0	0.9	0	1.2	1.5
34.5	0	0.8	0	1.2	1.2

Table 5.11(cont) - Yield of Individual Products versus Time-on-Stream for Catalyst EUROPT 4.1

Time (hours)	Benzene	Toluene	Ethylbenzene	m/p-Xylene	o-Xylene
3.0	1.6	9.2	1.7	8.4	9.4
6.0	1.7	5.9	3.6	10.4	10.1
9.0	1.3	6.7	4.7	14.6	8.8
12.0	1.1	6.5	3.4	12.0	9.1
23.5	1.2	7.4	6.2	19.5	8.9
26.5	1.3	7.0	5.7	18.0	8.8
29.5	1.1	7.1	6.0	19.3	8.8
34.5	1.1	5.6	5.0	16.6	8.4

Table 5.11(cont) - Yield of Individual Products versus Time-on-Stream for Catalyst EUROPT 4.1

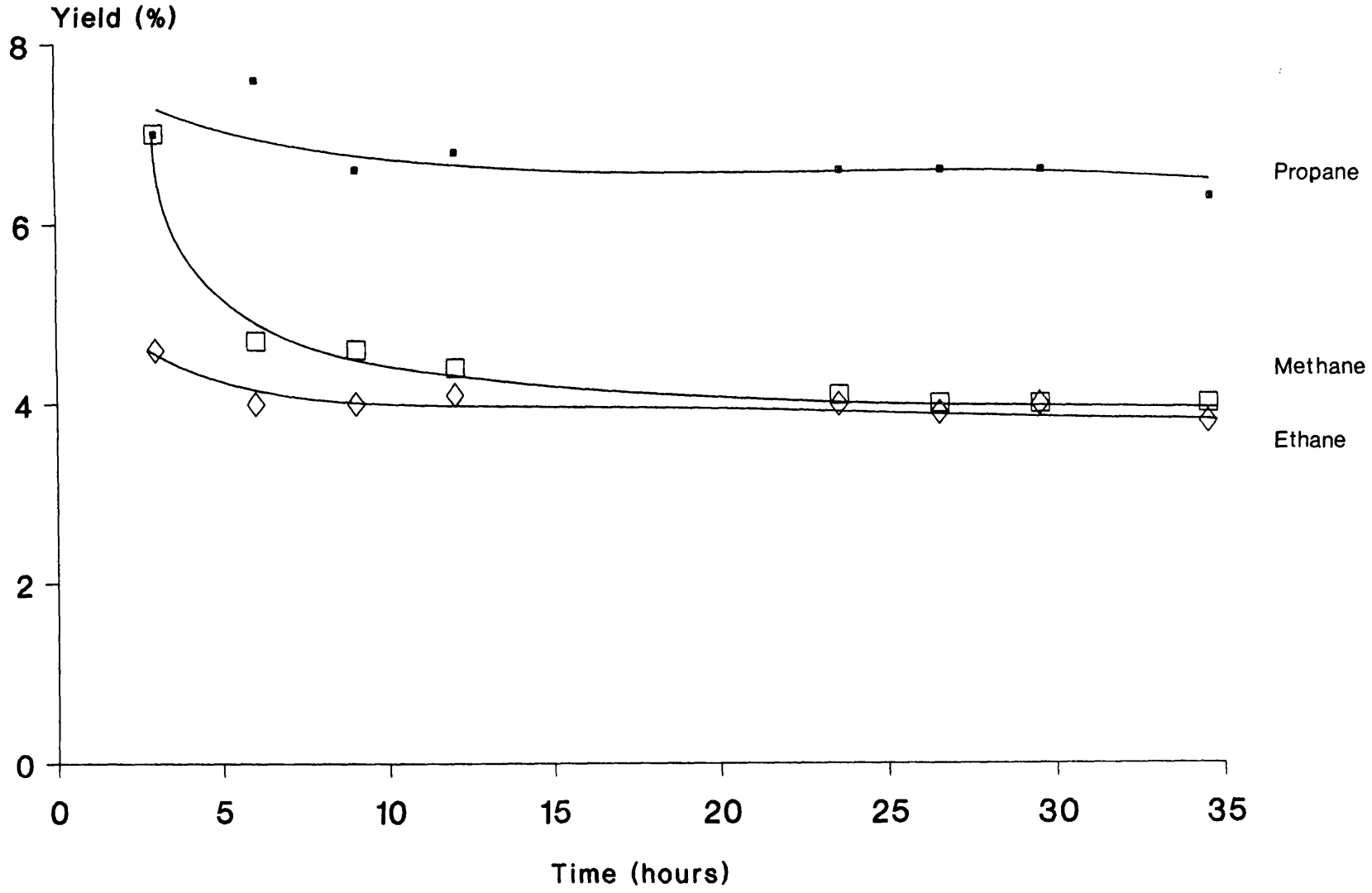

Figure 5.18 - Yield of Methane, Ethane and Propane versus Time-on-Stream for Catalyst EUROPT 4.1.

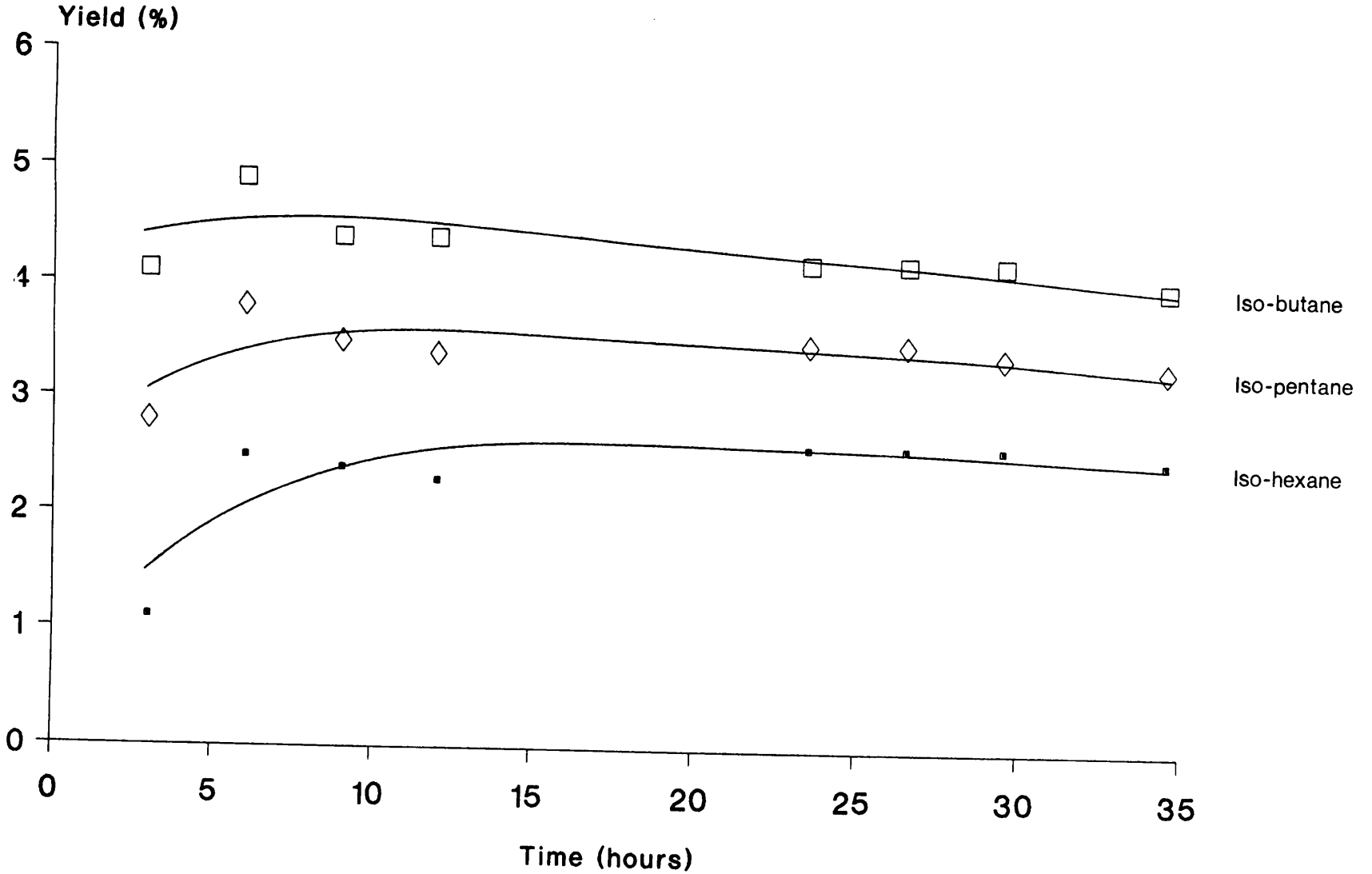

igure 5.19 - Yield of Iso-butane, Iso-pentane and Iso-hexane versus Time-on-Stream for Catalyst EUROPT 4.1.

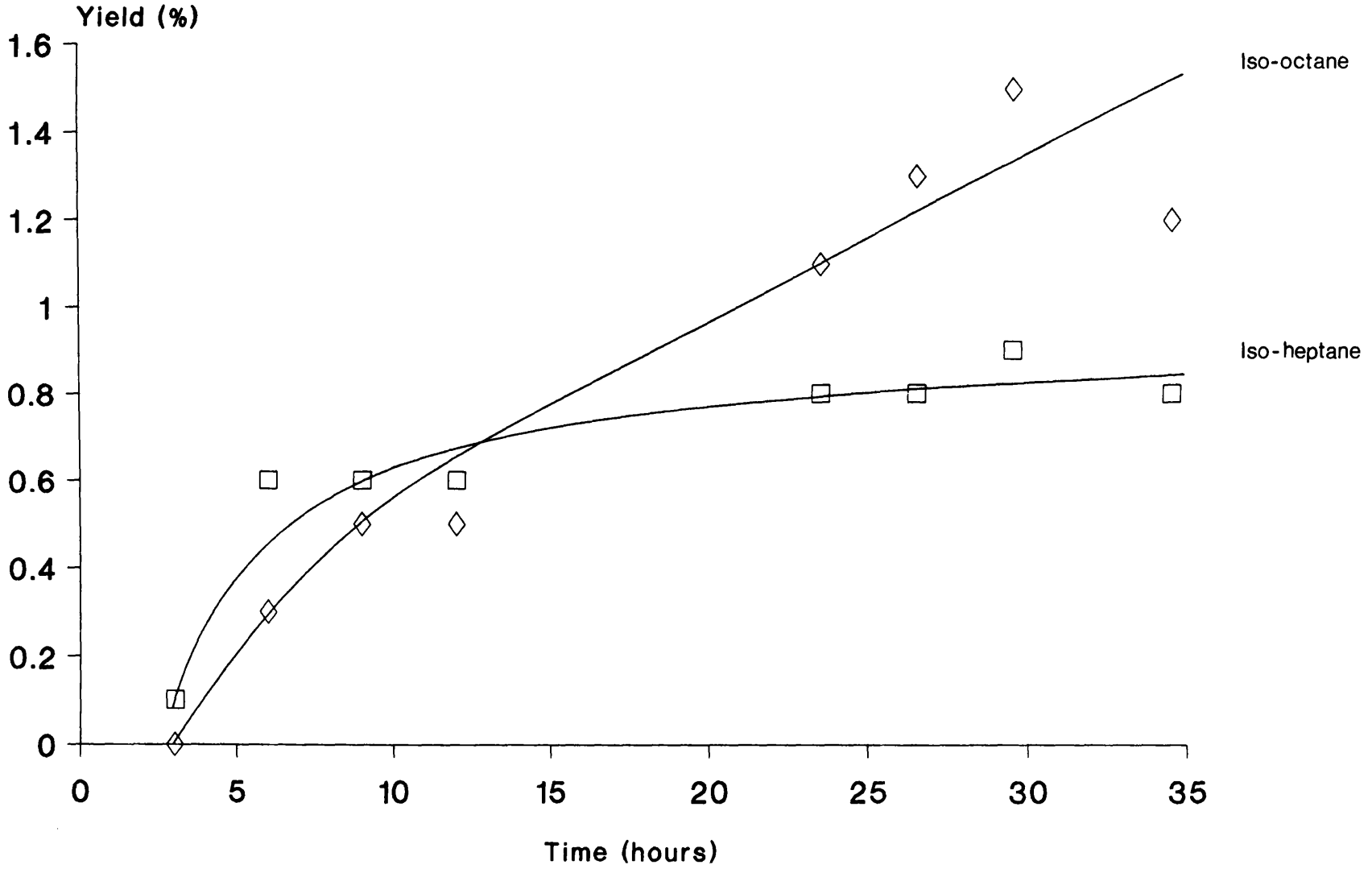

Figure 5.20 - Yield of Iso-heptane and Iso-octane versus Time-on-Stream for Catalyst EUROPT 4.1

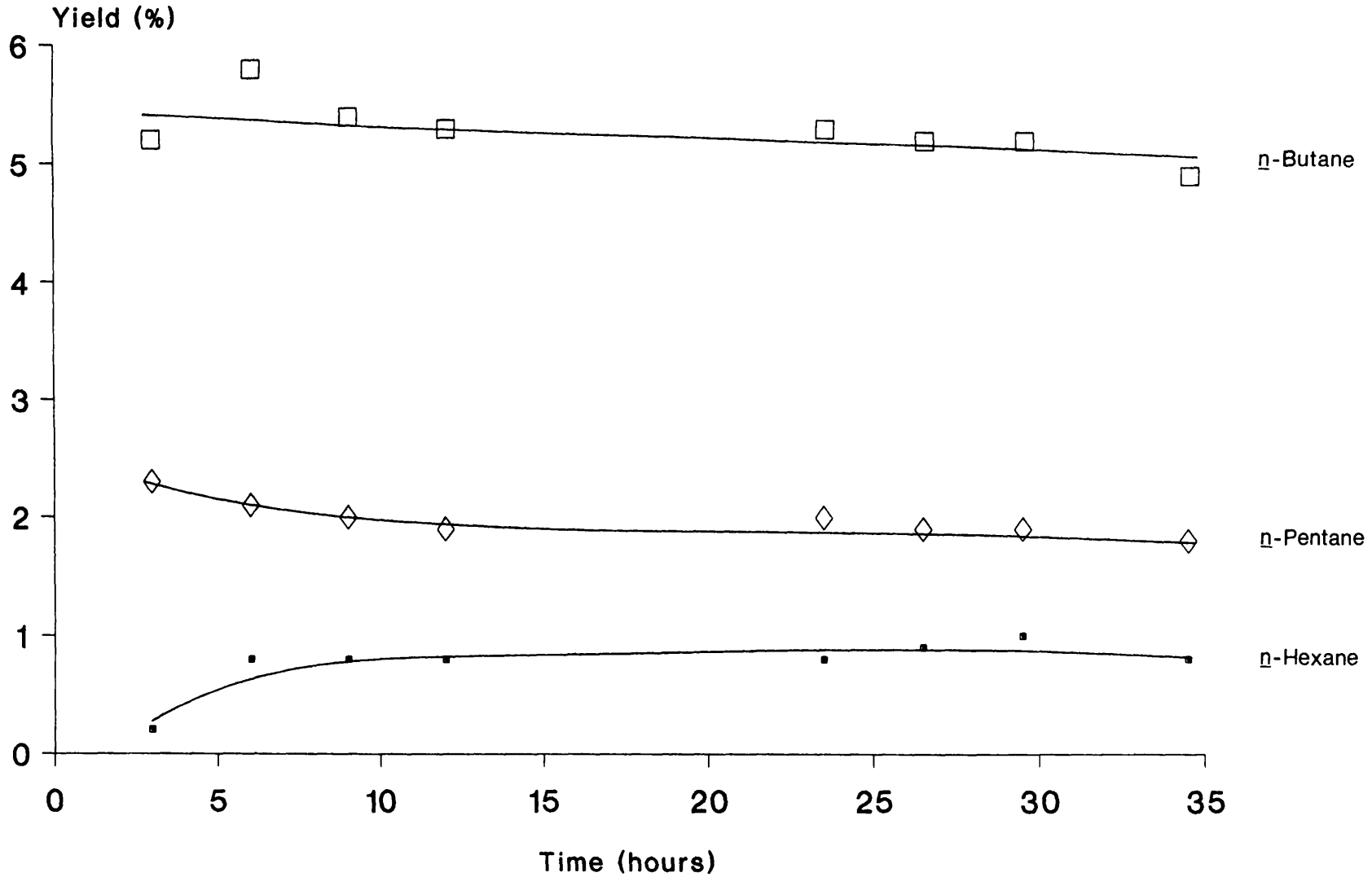

Figure 5.21 - Yield of n-Butane, n-Pentane and n-Hexane versus Time-on-Stream for Catalyst EUROPT 4.1.

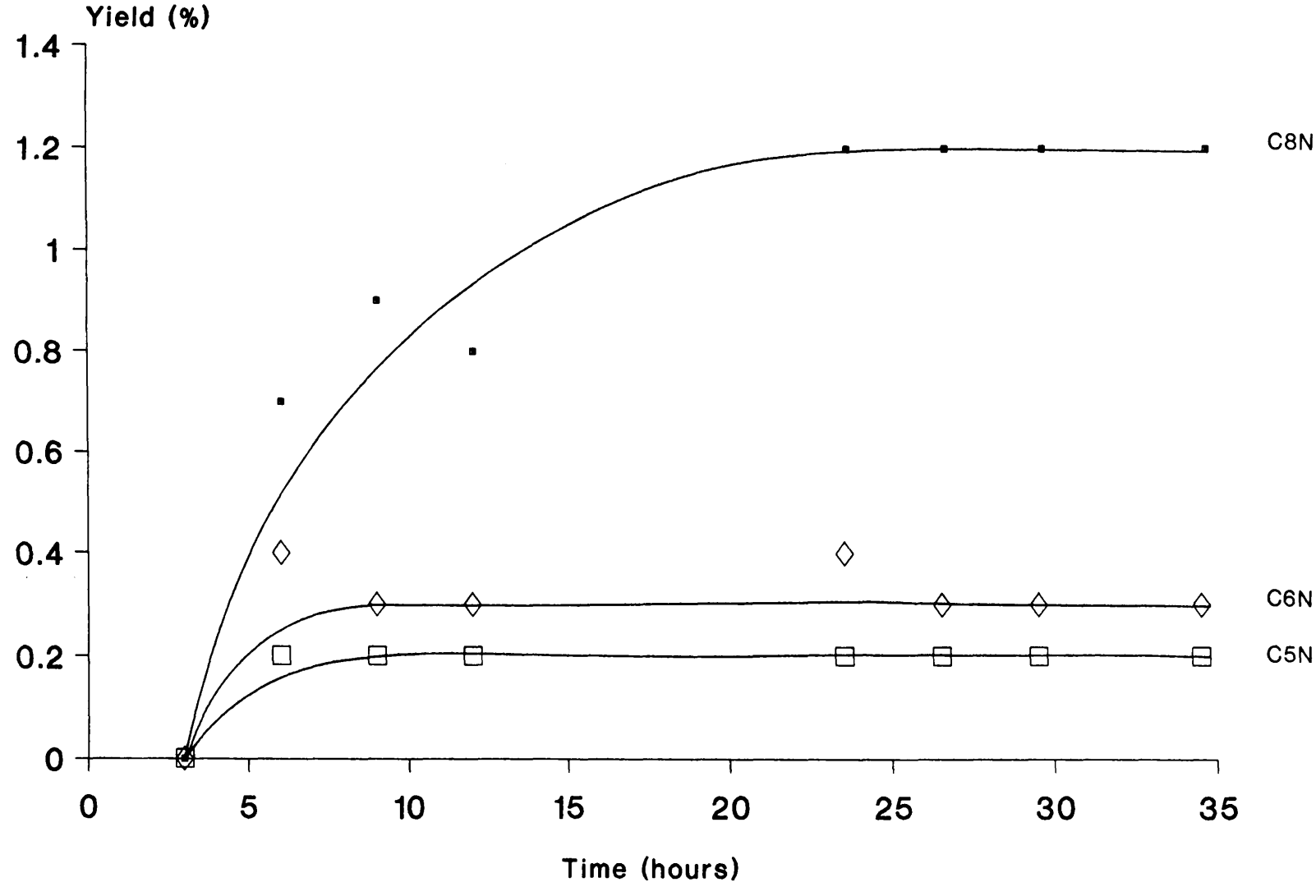

Figure 5.22 - Yield of C5 Napthene, C6 Napthene and C8 Napthene versus Time-on-Stream for Catalyst EUROPT 4.1.

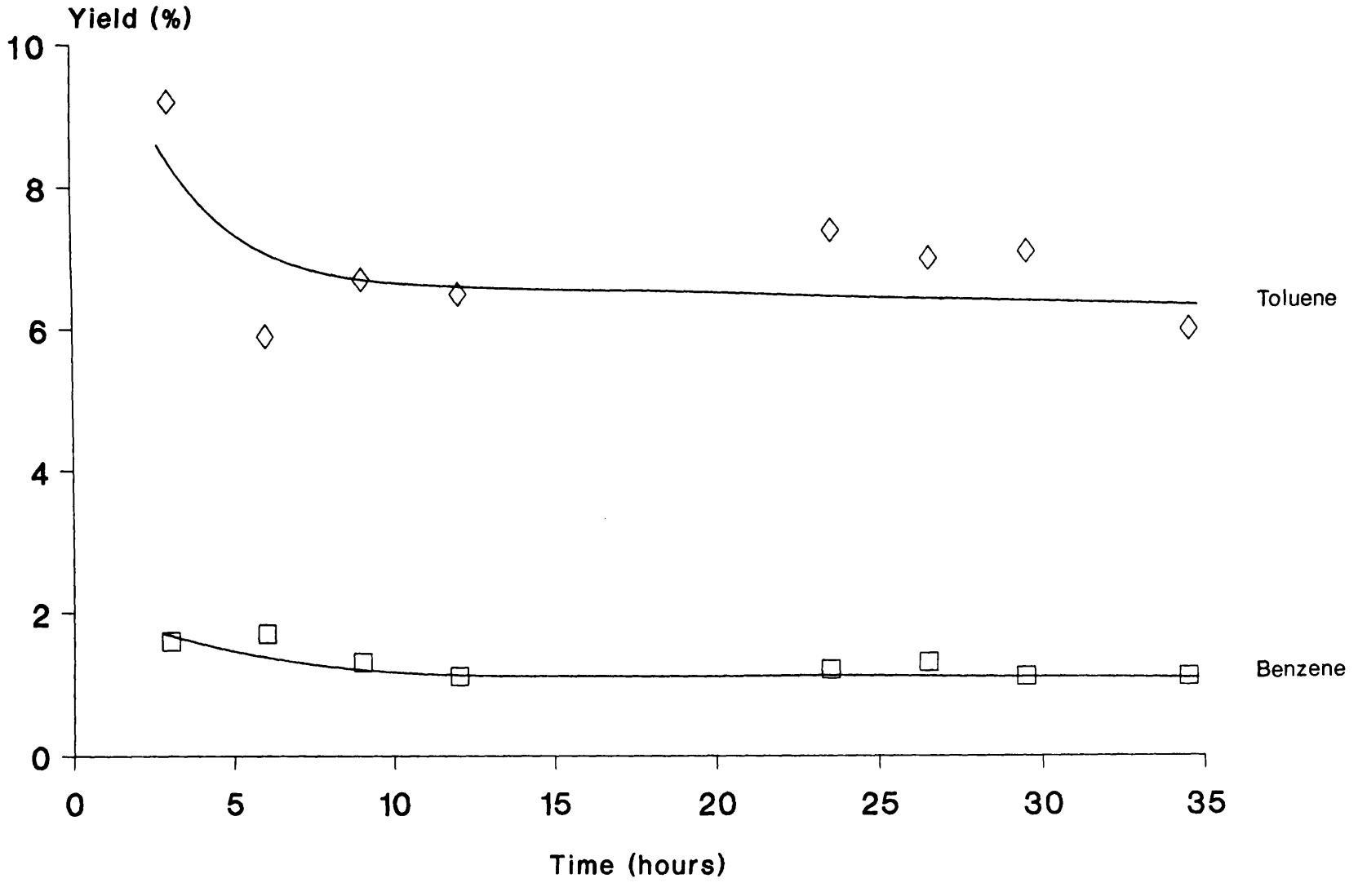

Figure 5.23 - Yield of Benzene and Toluene versus Time-on-Stream for Catalyst EUROPT 4.1.

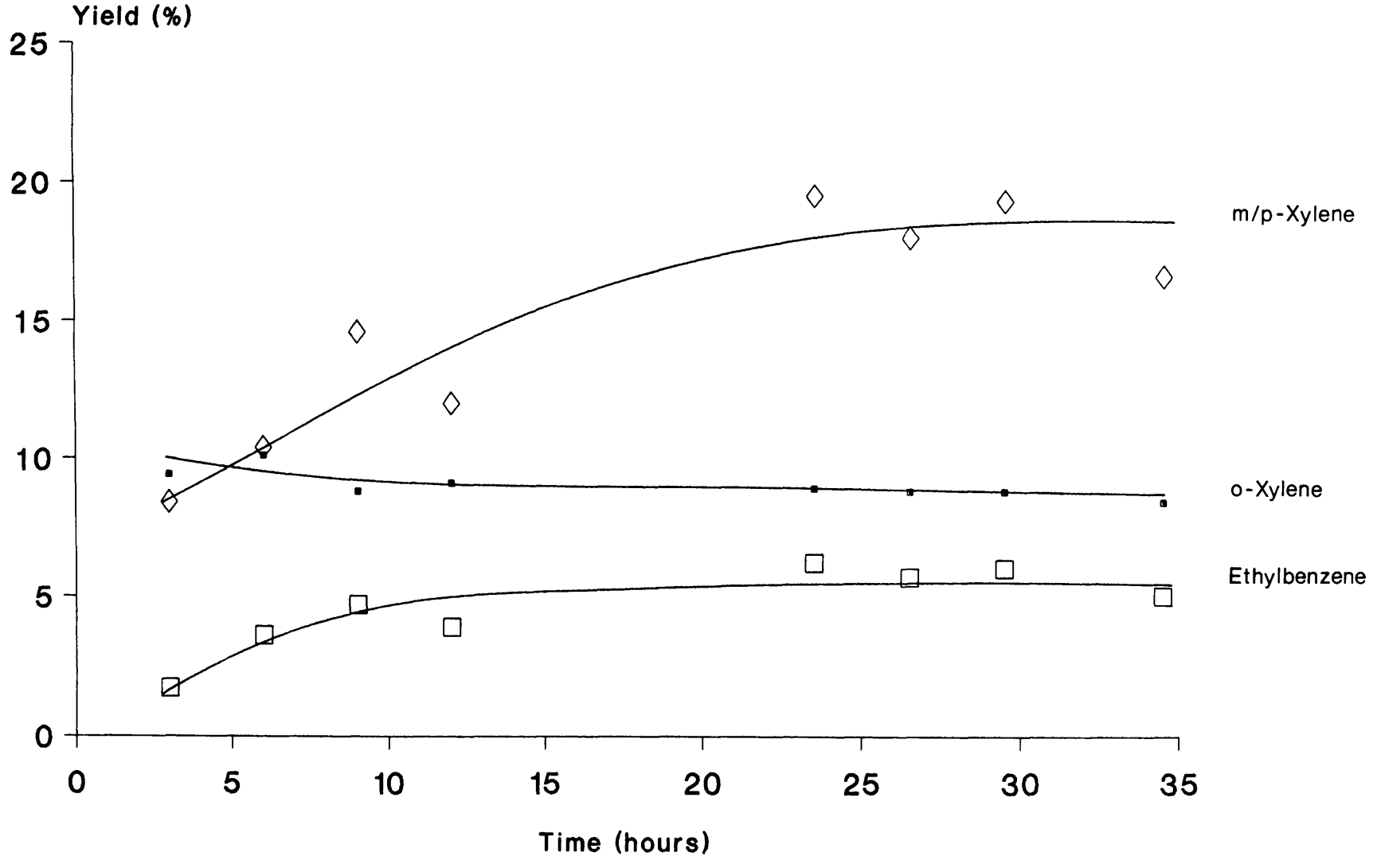

Figure 5.24 - Yield of Ethylbenzene, m/p-Xylene and o-Xylene versus Time-on-Stream for Catalyst EUROPT 4.1.

Time (hours)	Methane	Ethane	Propane	Iso-butane	n-Butane
3.0	10.8	7.1	10.8	6.4	8.0
6.0	6.8	5.8	10.9	7.0	8.4
9.0	6.4	5.6	9.2	6.2	7.5
12.0	6.5	6.0	10.0	6.4	7.8
23.5	5.2	5.0	8.4	5.4	6.7
26.5	5.2	5.1	8.6	5.6	6.8
29.5	5.1	5.0	8.4	5.4	6.7
34.5	5.6	5.3	8.9	5.5	6.8

Table 5.12 - Selectivity to Individual Products versus Time-on-Stream for Catalyst EUROPT 4.1

Time (hours)	C5 Napthene	Iso-pentane	n-Pentane	C6-Napthene	Iso-hexane	n-Hexane
3.0	0	4.4	3.5	0	1.7	0.3
6.0	0.2	5.5	3.1	0.5	3.6	1.1
9.0	0.2	4.9	2.8	0.4	3.3	1.1
12.0	0.2	5.1	2.9	0.5	3.5	1.1
23.5	0.2	4.4	2.5	0.4	3.3	1.1
26.5	0.2	4.6	2.5	0.4	4.0	1.2
29.5	0.2	4.4	2.5	0.4	3.4	1.2
34.5	0.2	4.6	2.5	0.5	3.5	1.2

Table 5.12(cont)-Selectivity to Individual Products versus Time-on-Stream for Catalyst EUROPT 4.1

Time (hours)	C7 Napthene	Iso-heptane	n-heptane	C8-Napthene	Iso-octane
3.0	0	0.1	0	0	0
6.0	0	0.8	0	1.0	0.5
9.0	0	0.9	0	1.3	0.7
12.0	0	0.8	0	1.2	0.7
23.5	0	1.0	0	1.5	1.4
26.5	0	1.1	0	1.6	1.7
29.5	0	1.2	0	1.6	1.9
34.5	0	1.2	0	1.7	1.6

Table 5.12(cont)-Selectivity to Individual Products versus Time-on-Stream for Catalyst EUROPT 4.1

Time (hours)	Benzene	Toluene	Ethylbenzene	m/p-Xylene	o-Xylene
3.0	2.5	14.3	2.7	12.9	14.5
6.0	2.4	8.5	5.2	14.9	14.6
9.0	1.8	9.4	6.6	20.4	12.3
12.0	1.6	9.7	5.7	17.7	13.5
23.5	1.6	9.4	7.9	24.6	11.2
26.5	1.7	9.1	7.5	23.6	11.5
29.5	1.3	9.1	7.7	24.6	11.2
34.5	1.6	8.4	7.1	23.3	11.9

Table 5.12(cont)-Selectivity to Individual Products versus Time-on-Stream for Catalyst EUROPT 4.1

Time (hours)	Aromatisation	Isomerisation	Hydrocracking	Hydrogenolysis
3.0	46.9	0.1	12.4	10.8
6.0	45.7	1.3	16.0	6.8
9.0	50.4	1.6	14.4	6.4
12.0	48.1	1.6	15.0	6.5
23.5	54.7	2.4	13.1	5.2
26.5	53.4	2.8	13.5	5.2
29.5	53.9	3.0	13.2	5.1
34.5	52.2	2.8	13.6	5.6

Table 5.13 - Selectivity to Major Reactions versus Time-on-Stream for Catalyst EUROPT 4.1

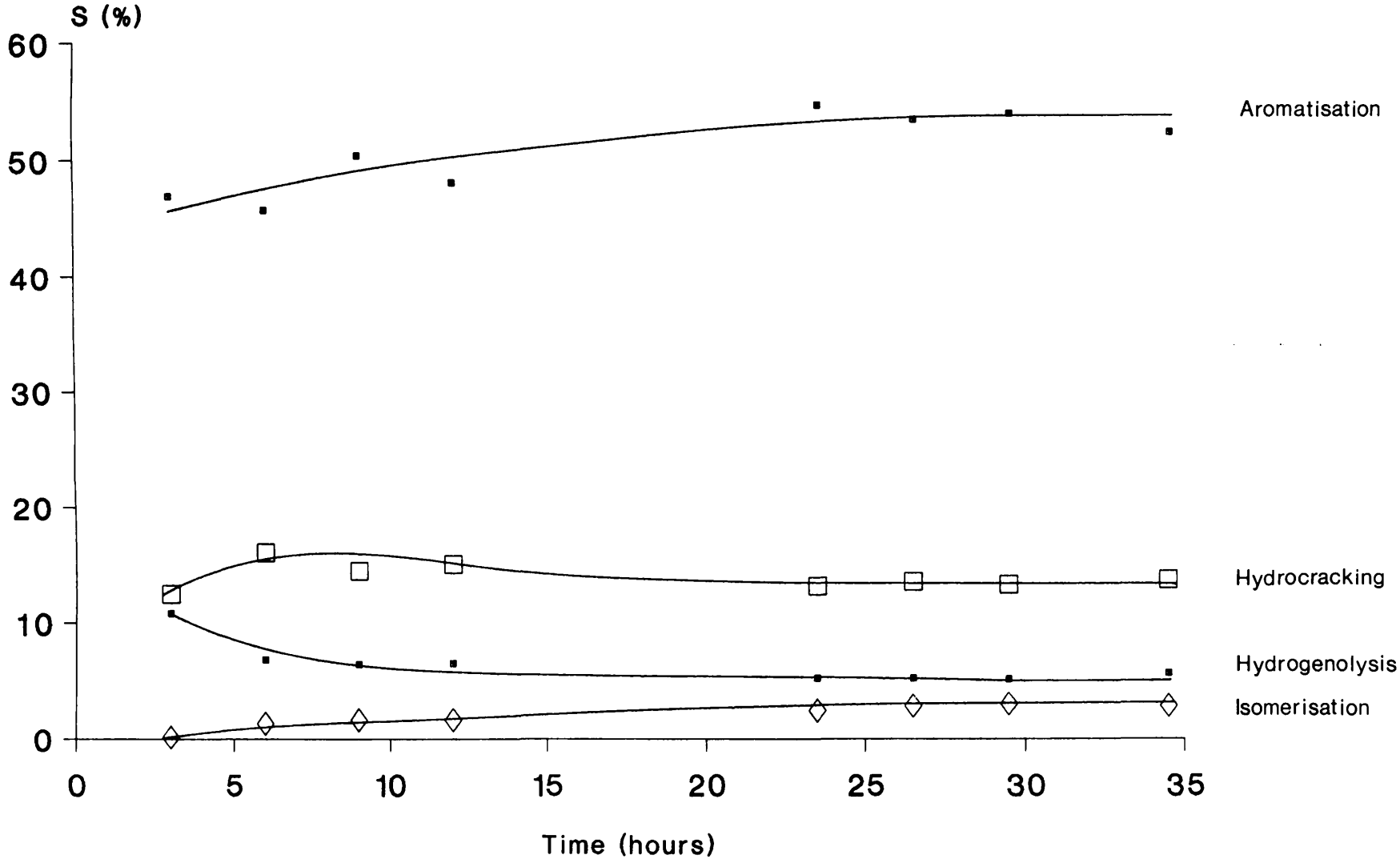

Figure 5.25 - Selectivity Towards Major Reactions versus Time-on-Stream for Catalyst EUROPT 4.1.

Time (hours)	Conversion	C3/C1
3.0	68.5	1.00
6.0	69.5	1.59
9.0	71.5	1.43
12.0	67.6	1.55
23.5	79.1	1.60
26.5	76.4	1.65
29.5	78.4	1.63
34.5	71.2	1.57

Table 5.14 - Conversion and Propane to Methane Ratio versus Time-on-Stream for Catalyst EUROPT 4.1

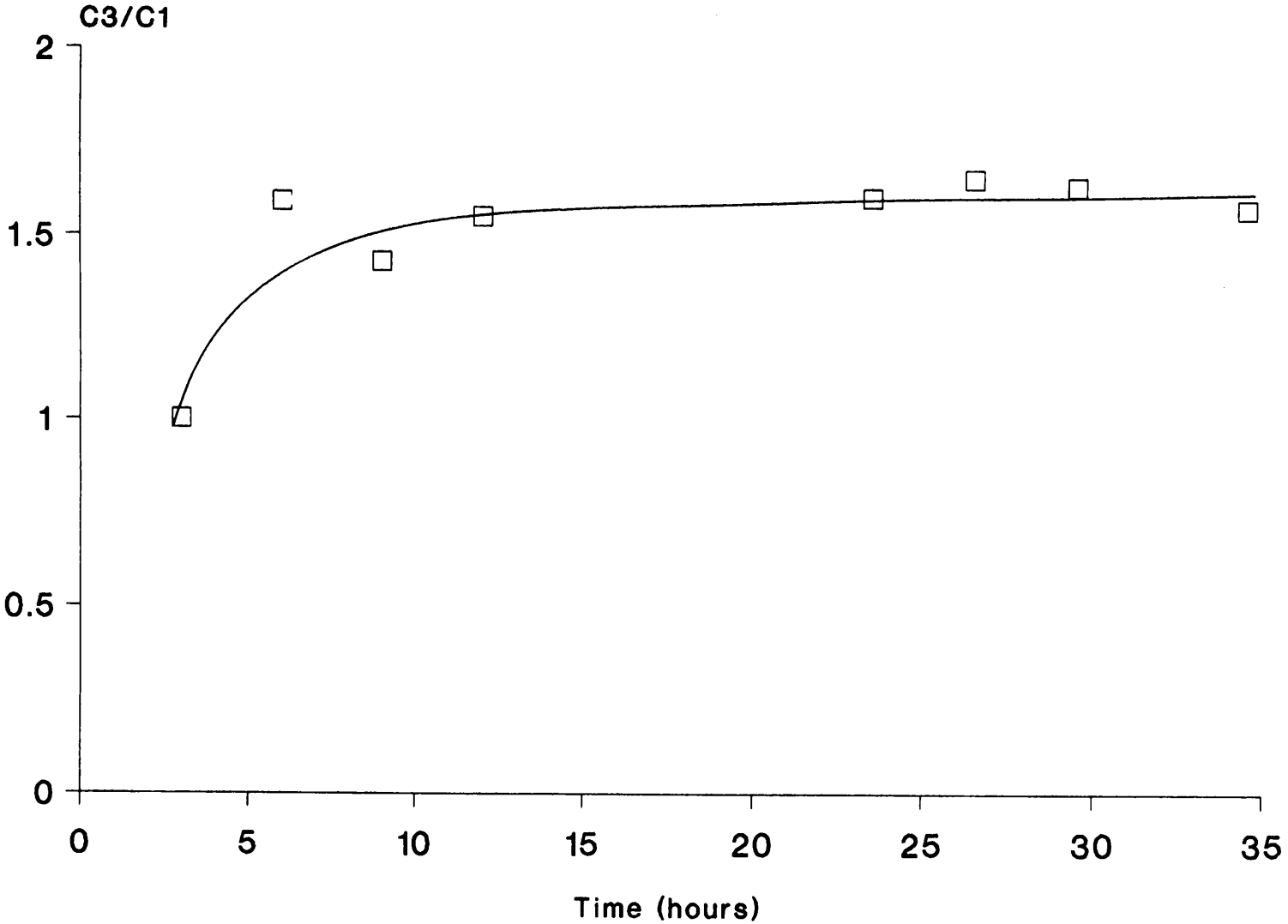

Figure 5.26 - Propane to Methane Ratio versus Time-on-Stream for Catalyst EUROPT 4.1.

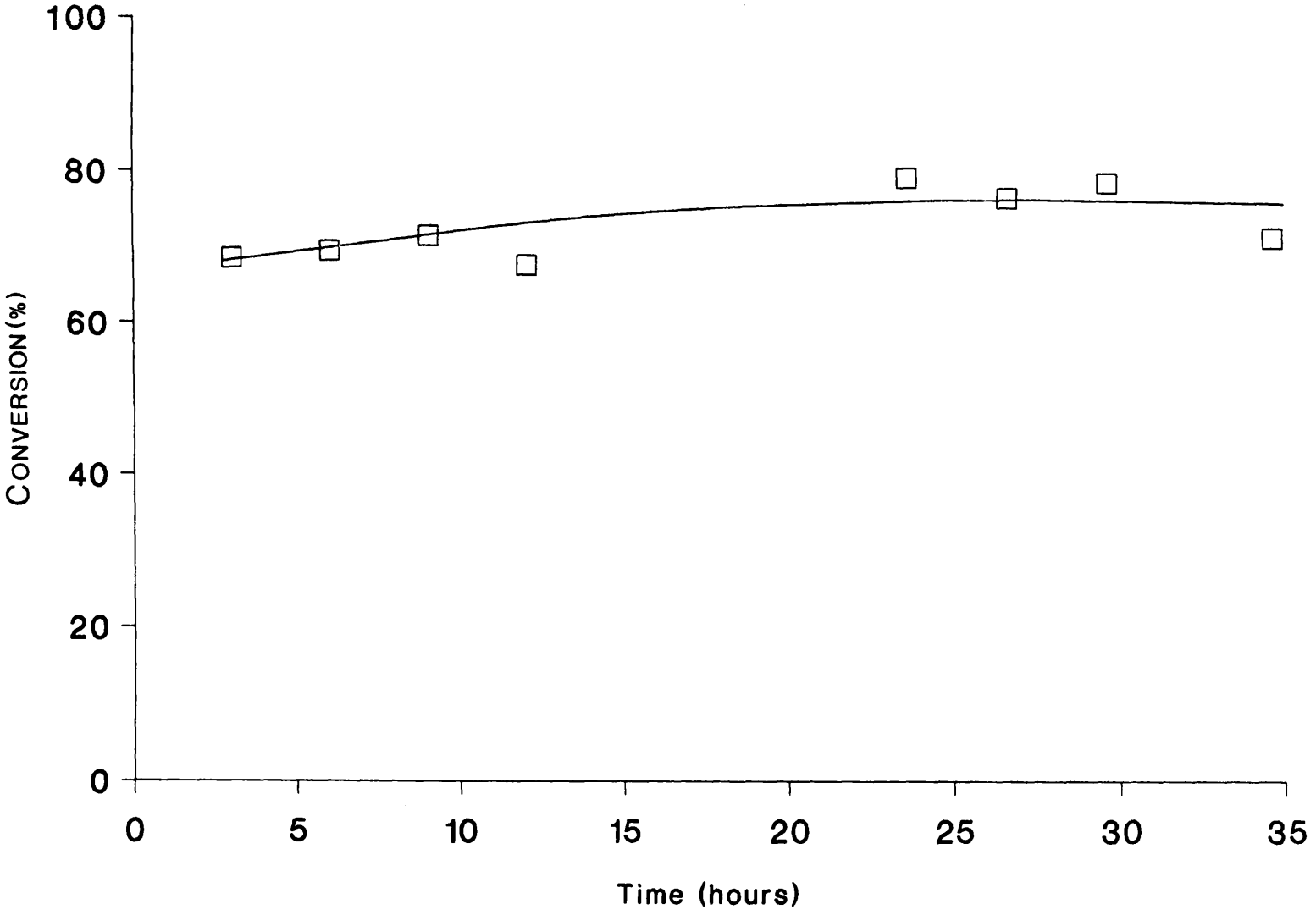

Figure 5.27 - Conversion versus Time-on-Stream for Catalyst EUROPT 4.1.

5.1.4.2 n-Octane Reforming on Catalyst EUROPT 4.2

The reforming reaction of n-octane was investigated at a temperature of 450°C on a second sample of the bimetallic catalyst, designated EUROPT 4.2.

The yields of all product species are given in table 5.15 and are presented as a function of time-on-stream in figures 5.28 - 5.34. The selectivities of the catalyst with respect to both the individual product species and the major reaction types are listed in table 5.16 and table 5.17. The selectivity data contained in table 5.17 is presented graphically in figure 5.35.

Figure 5.28 shows the variation in methane, ethane and propane yield throughout the 28 hours of the reaction. Methane, not propane as in the case of catalyst EUROPT 4.1, was the principal gas produced. It can be seen that the yield of methane, ethane and propane was significantly higher on the bimetallic catalyst at the lower reaction temperature (Tables 5.11, 5.15). The yield of each gas decreased steadily in a linear manner.

Iso-paraffin production on catalyst EUROPT 4.2 followed two distinct trends. The yield of both iso-heptane and iso-octane was observed to increase with time. Iso-octane, in particular, showed a sharp rise in yield between 15 and 22 hours-on-stream (Figure 5.30). In contrast, the yield of each of the three remaining iso-paraffin products had decreased by the end of the experiment (Figure 5.29). Of particular interest in the iso-paraffin product distribution was the reduced importance of centre

cracking of the n-octane molecule to produce iso-butane. It can be seen from figure 5.29 that the yield of iso-hexane exceeded that of iso-pentane and iso-butane throughout the entire run. The distribution of the iso-paraffins in the C_4-C_6 range was therefore the inverse of the pattern established in the three previous studies (Sections 5.1.2 - 5.1.4.1). The pattern was, however, maintained in the product distribution of the normal paraffins, where n-butane was the main species present followed by n-pentane and n-hexane respectively. The yield of both normal and iso-paraffins was consistently higher on the bimetallic catalyst at the lower reaction temperature.

Cycloparaffin species were produced on both catalysts EUROPT 4.2 and EUROPT 4.1; in each case their yield followed a broadly similar trend (Figures 5.22, 5.32). C_8 napthene was the dominant cycloparaffin species on both catalysts, exceeding the yield of C_6 and C_5 napthenic species respectively. The yield of the C_5 and C_6 napthenic species remained essentially level after several hours-on-stream. In contrast, the yield of C_8 napthenic species increased and reached a maximum value of 1.2% on catalyst EUROPT 4.1 and 2.2% on catalyst EUROPT 4.2. No C_7 cycloparaffins were produced by either catalyst.

Toluene was the principal aromatic species produced by catalyst EUROPT 4.2 for much of the experiment and its yield was only exceeded by that of meta-/para-xylene during the last 7 hours of the run (Figures 5.23, 5.24). The yield of all C_8 aromatic hydrocarbons increased with time-on-stream. Toluene yield decreased to a pseudo-stationary level of ca. 4.1% whilst that of benzene remained at a steady value of 0.3 - 0.4%.

Despite the qualitative differences in product yield between catalysts EUROPT 4.1 and EUROPT 4.2 total conversion was comparable for much of the experiment (Figures 5.27, 5.37). Conversion of n-octane at the lower reaction temperature did not increase during the time interval analysed, if anything, a slight fall was observed (Table 5.18).

The selectivity of catalyst EUROPT 4.2 towards the four major reactions reflected the differences in product yield noted above. The most important reaction for much of the experiment was hydrogenolysis. Hydrogenolysis selectivity had a maximum value of between 18 and 19% at the start of the run. This declined to a value of 15.5% by 28 hours-on-stream (Figure 5.35).

In contrast, aromatisation selectivity increased slightly with time from approximately 15% to 18% (Figure 5.35). Consequently the major reaction at 21 hours-on-stream and thereafter was aromatisation. Whilst hydrocracking selectivity was very similar at both reaction temperatures, catalyst EUROPT 4.2 exhibited a much higher selectivity towards isomerisation activity which increased from 7% to 15.5% during the experiment (Figure 5.35).

The propane to methane ratios calculated for catalyst EUROPT 4.2 as a function of time-on-stream are summarized in table 5.18 and presented graphically in figure 5.36. The ratio fell slightly from a value of 0.8 calculated at 6 hours-on-stream. The low value of the ratio reflects the very high hydrogenolysis activity of the catalyst.

Catalyst EUROPT 4.2 had a coke content of 0.40% by weight and a residual chlorine content of 0.56% by weight on completion of the experiment (Table 5.2).

Time (hours)	Methane	Ethane	Propane	Iso-butane	n-Butane
6.0	14.3	8.5	11.1	2.8	9.0
9.0	14.1	6.6	11.1	3.1	9.4
12.0	13.7	8.0	10.1	2.6	7.9
15.0	13.2	7.7	10.1	2.6	8.6
18.0	13.5	7.8	9.9	2.5	8.2
21.0	12.4	7.2	9.2	2.5	8.0
25.0	11.6	6.6	8.6	2.2	7.6
28.0	11.8	6.8	8.8	2.1	7.7

Table 5.15 - Yield of Individual Products versus Time-on-Stream for Catalyst EUROPT 4.2

Time (hours)	C5 Napthene	Iso-pentane	n-Pentane	C6-Napthene	Iso-hexane	n-Hexane
6.0	0	3.6	3.8	0.6	3.9	1.8
9.0	0.2	3.5	3.7	0.7	4.2	2.0
12.0	0.2	3.4	3.3	0.6	4.7	2.0
15.0	0.2	3.4	3.6	0.5	4.0	2.1
18.0	0.2	3.2	3.1	0.5	3.5	1.9
21.0	0.2	3.2	3.4	0.6	3.8	2.4
25.0	0.2	2.9	3.3	0.6	3.6	2.4
28.0	0.2	2.8	3.4	0.6	3.6	2.6

Table 5.15(cont) - Yield of Individual Products versus Time-on-Stream for Catalyst EUROPT 4.2

Time (hours)	C7 Napthene	Iso-heptane	n-heptane	C8-Napthene	Iso-octane
6.0	0	2.3	0	1.1	3.0
9.0	0	2.8	0	1.2	3.2
12.0	0	2.8	0	1.3	3.4
15.0	0	3.0	0	1.4	3.5
18.0	0	3.1	0	1.1	3.5
21.0	0	3.7	0	2.2	7.1
25.0	0	3.5	0	2.2	6.9
28.0	0	4.0	0	1.8	7.7

Table 5.15(cont) - Yield of Individual Products versus Time-on-Stream for Catalyst EUROPT 4.2

Time (hours)	Benzene	Toluene	Ethylbenzene	m/p-Xylene	o-Xylene
6.0	0.3	4.7	1.0	3.1	2.3
9.0	0.3	4.4	1.2	3.7	2.5
12.0	0.4	4.2	1.1	3.5	2.4
15.0	0.4	4.5	1.2	3.9	2.7
18.0	0.4	4.4	1.2	3.6	2.4
21.0	0.4	4.1	1.8	4.6	3.0
25.0	0.3	4.1	1.8	4.5	3.0
28.0	0.3	4.0	1.8	4.4	3.0

Table 5.15(cont) - Yield of Individual Products versus Time-on-Stream for Catalyst EUROPT 4.2

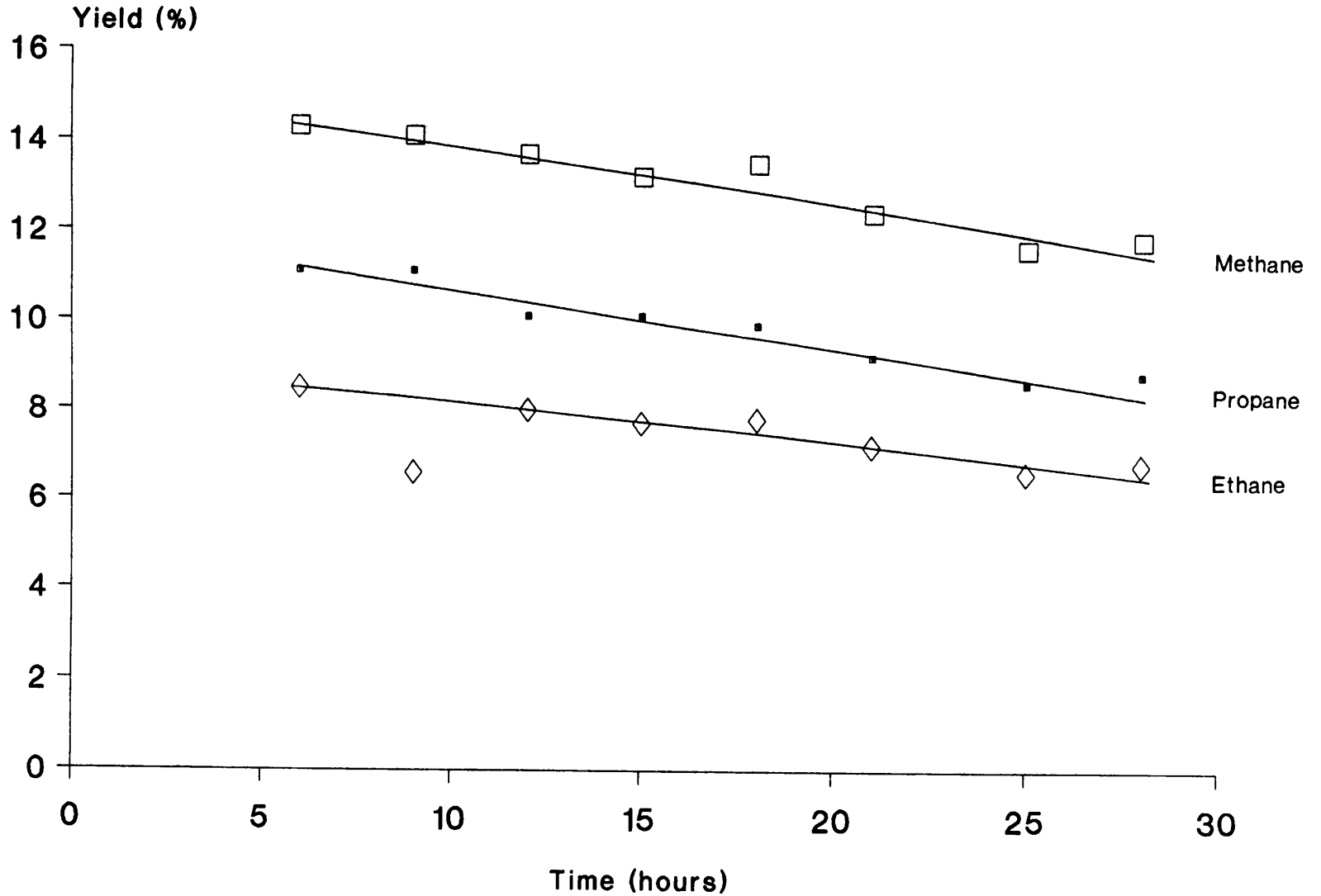

Figure 5.28 - Yield of Methane, Ethane and Propane versus Time-on-Stream for Catalyst EUROPT 4.2.

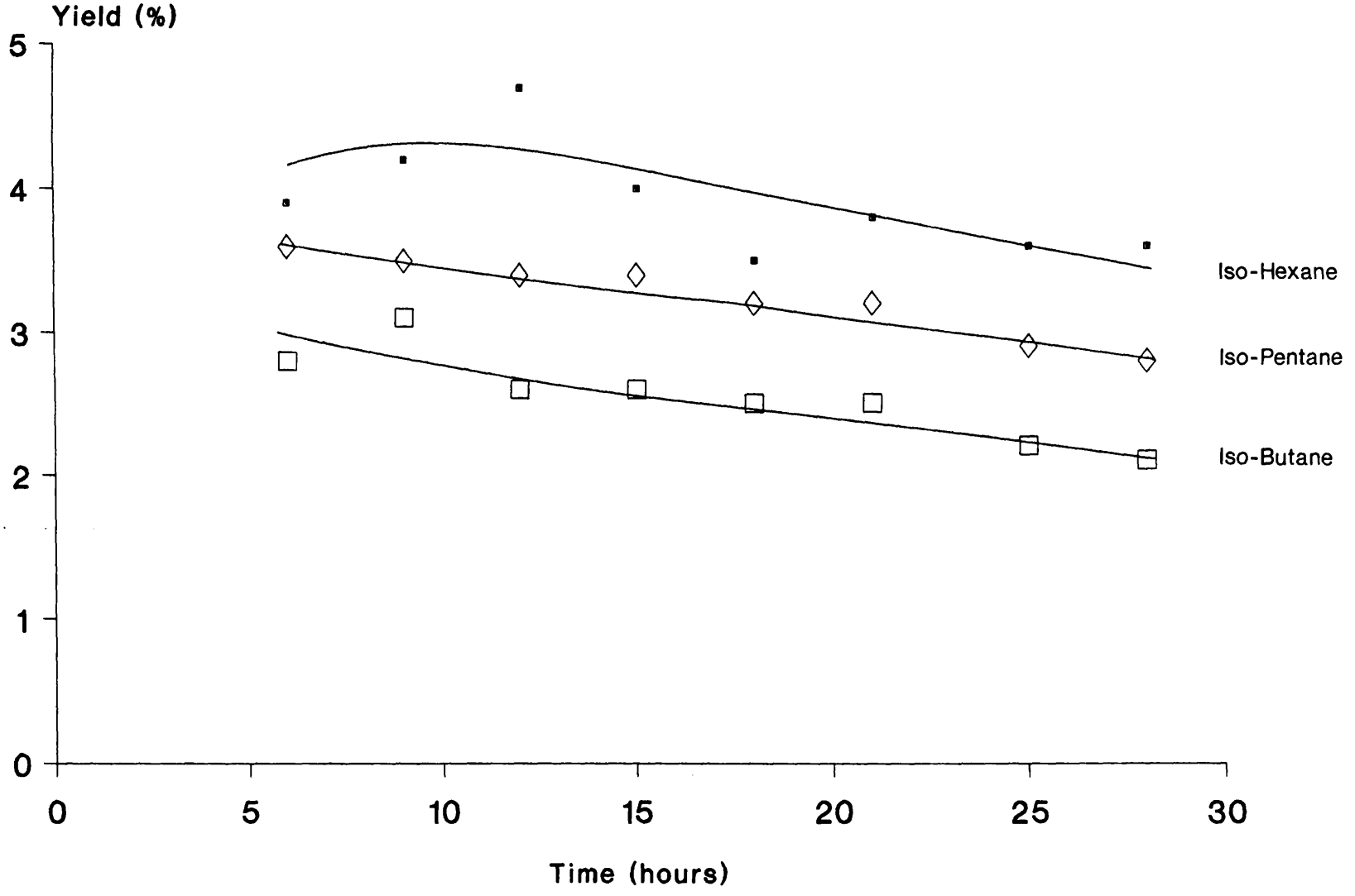

igure 5.29 - Yield of Iso-butane, Iso-pentane and Iso-hexane versus Time-on-Stream for Catalyst EUROPT 4.2.

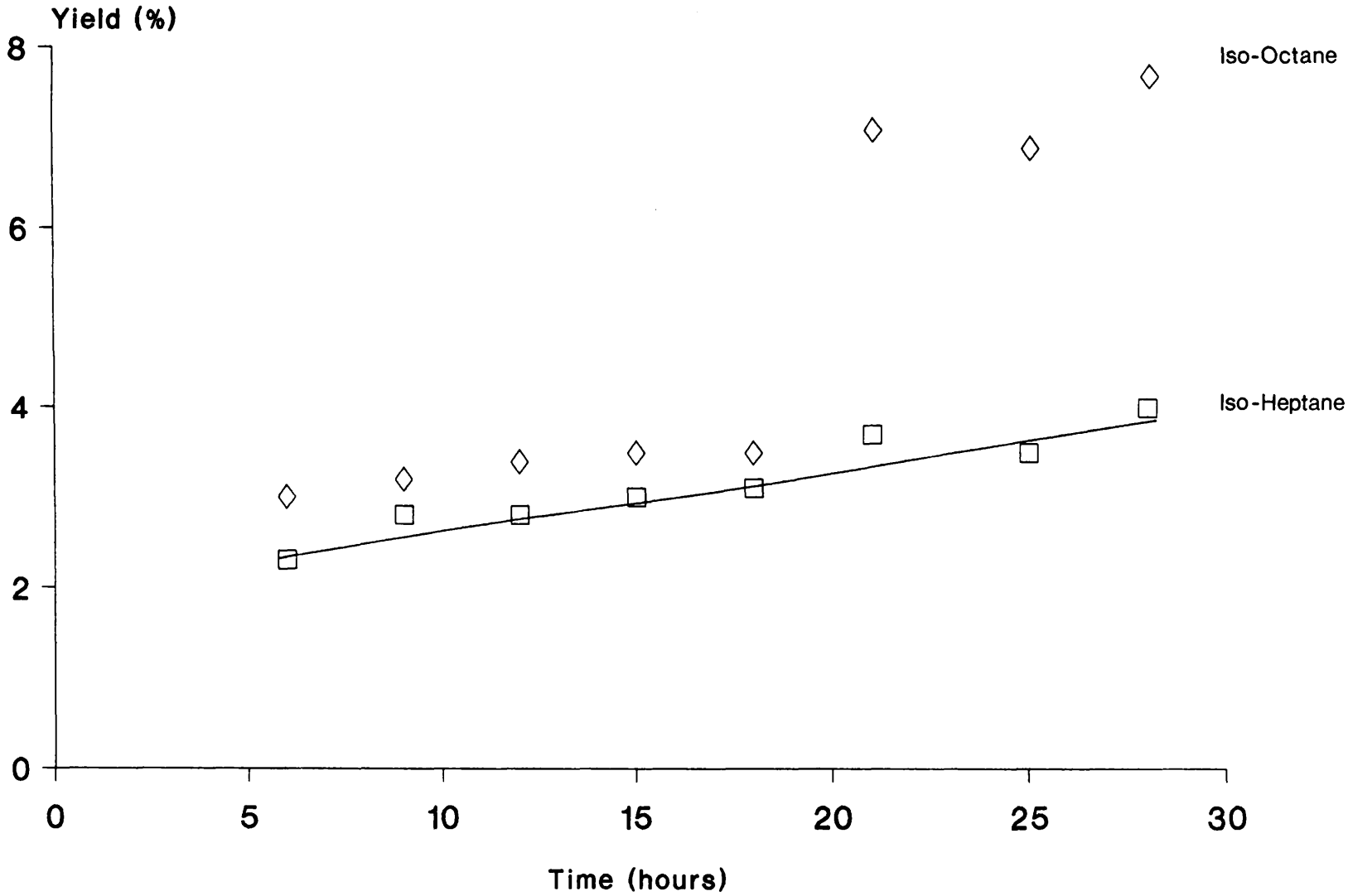

Figure 5.30 - Yield of Iso-heptane and Iso-octane versus Time-on-Stream for Catalyst EUROPT 4.2.

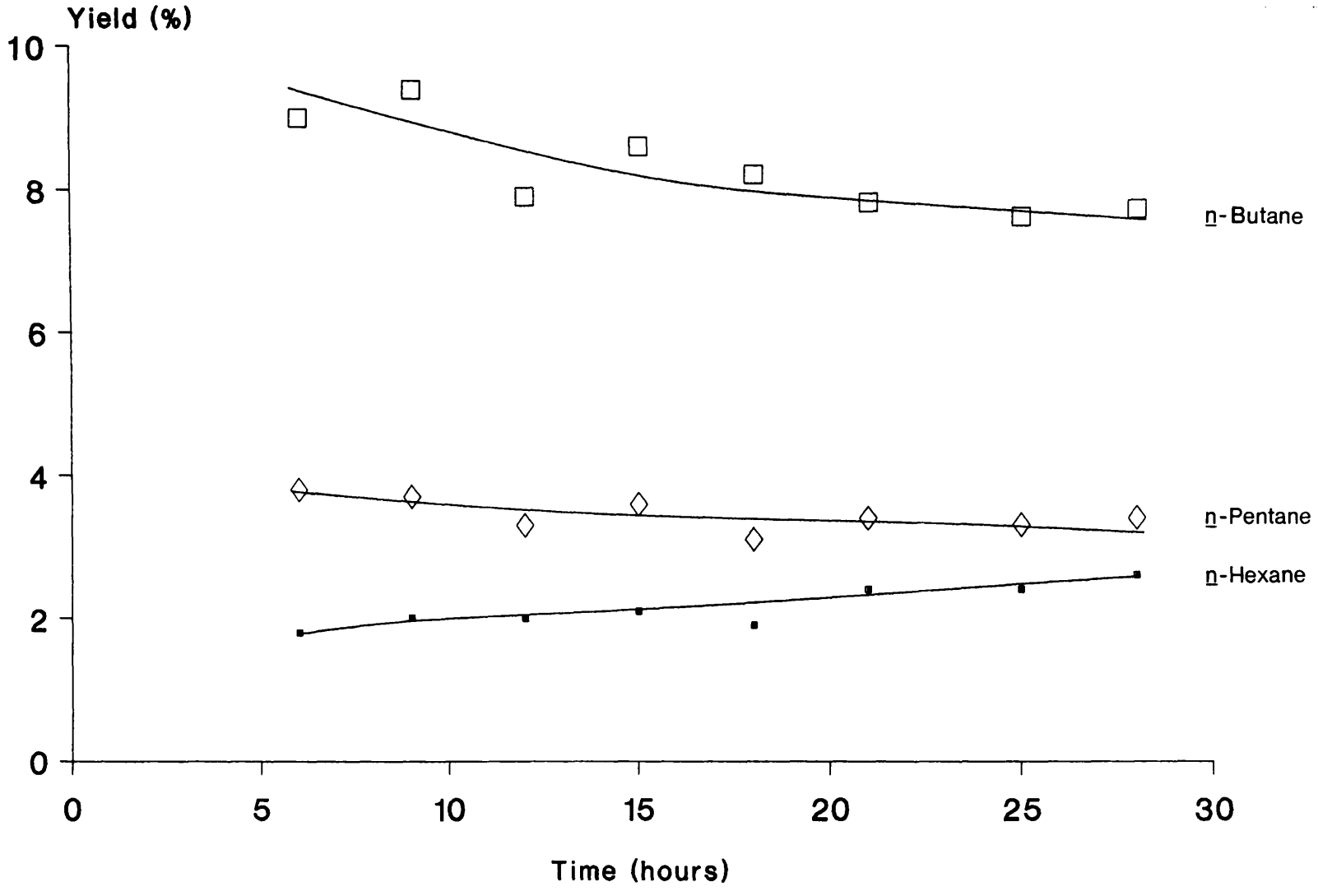

Figure 5.31 - Yield of n-butane, n-pentane and n-hexane versus Time-on-Stream for Catalyst EUROPT 4.2.

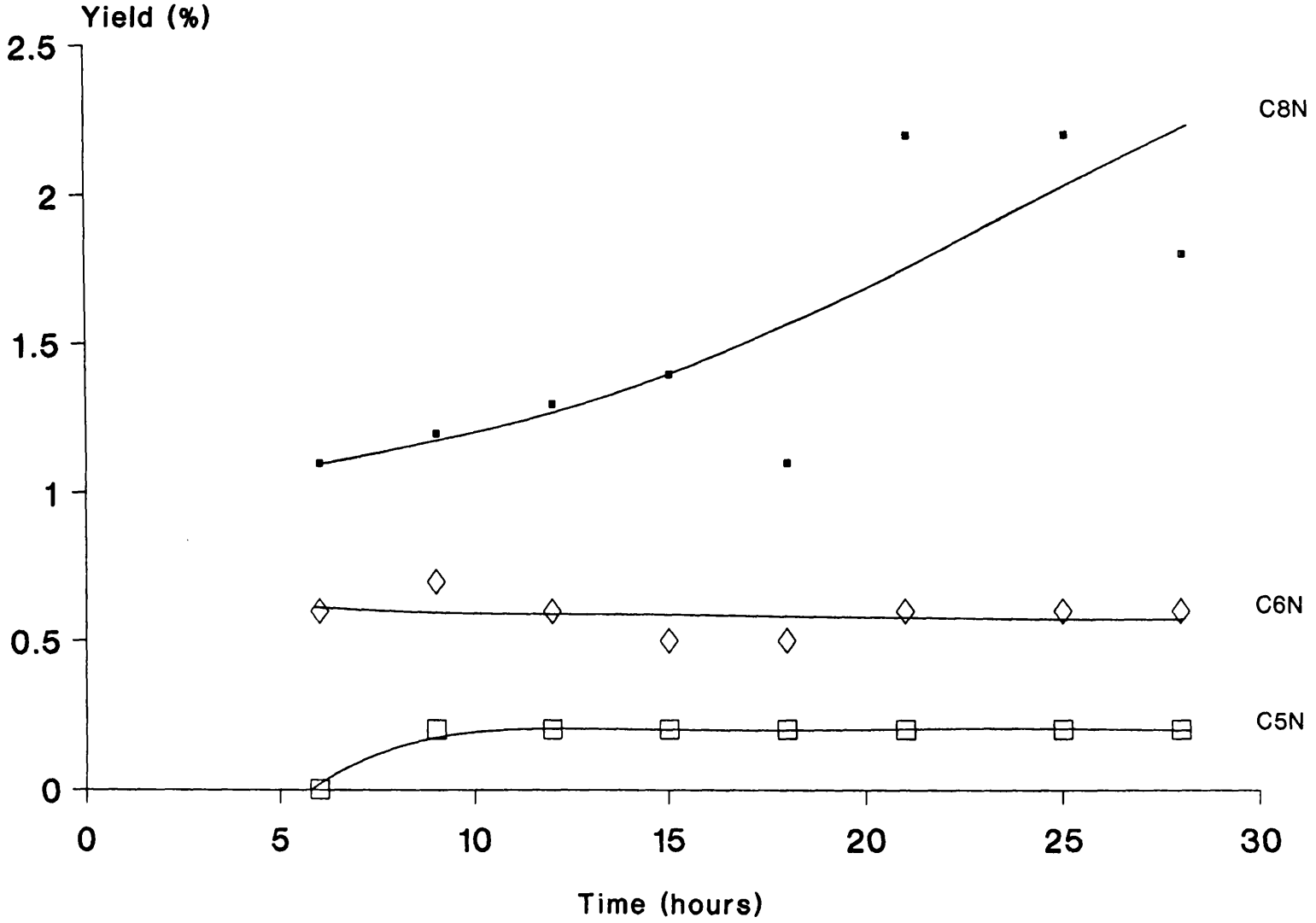

Figure 5.32 - Yield of C5 Napthene, C6 Napthene and C8 Napthene versus Time-on-Stream for Catalyst EUROPT 4.2.

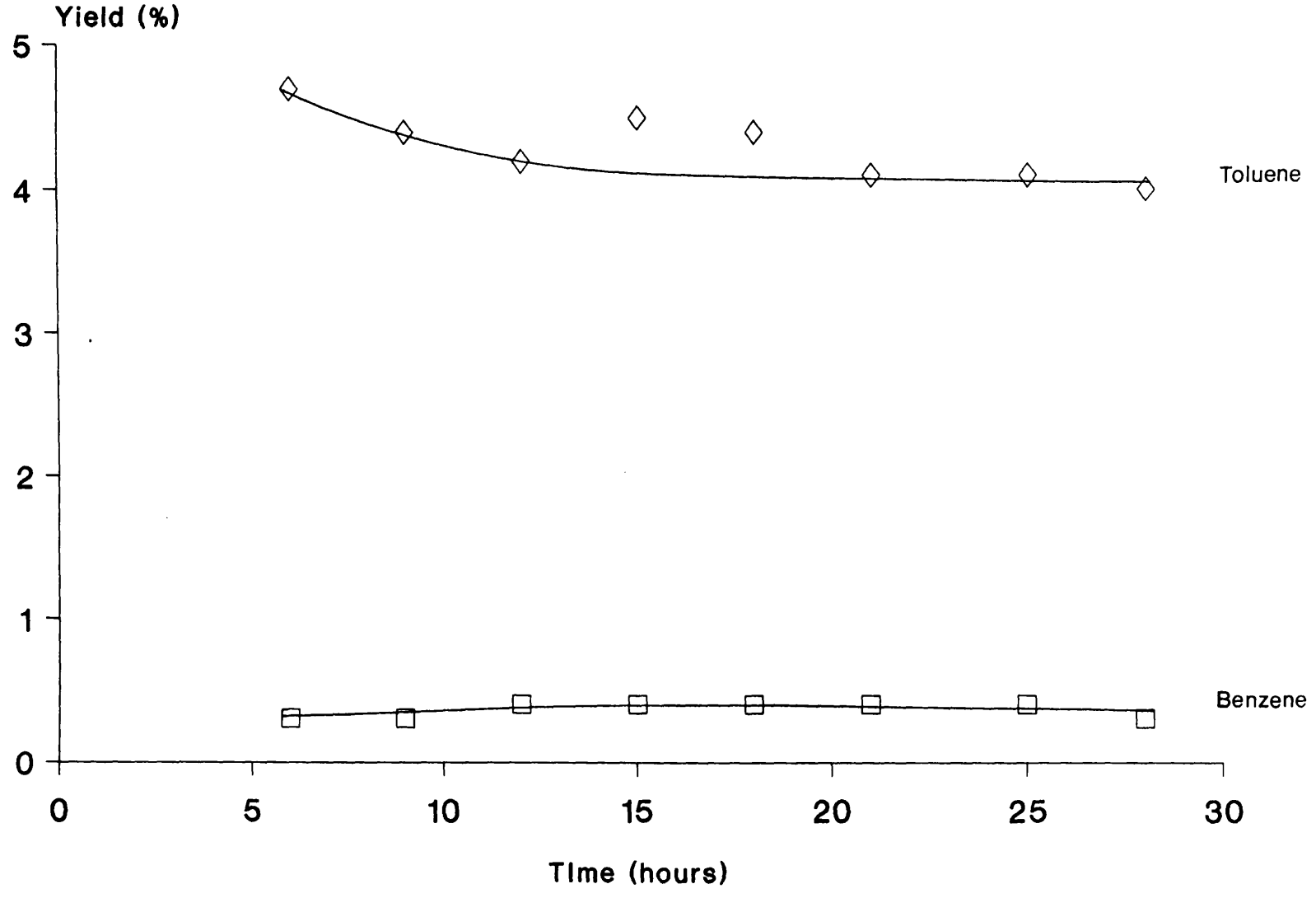

Figure 5.33 - Yield of Benzene and Toluene versus Time-on-Stream for Catalyst EUROPT 4.2.

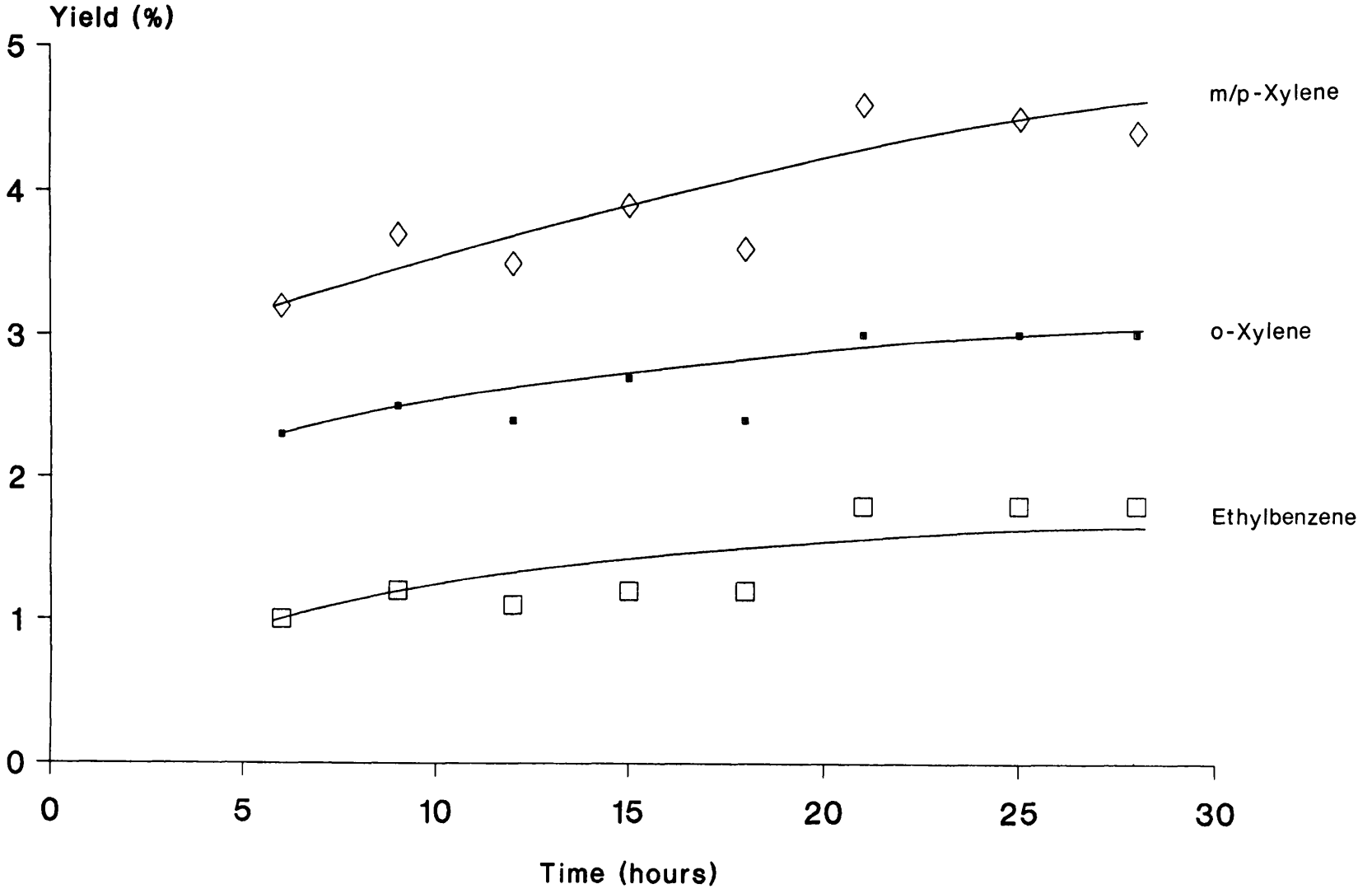

Figure 5.34 - Yield of Ethybenzene, m/p-Xylene and o-Xylene versus Time-on-Stream for Catalyst EUROPT 4.2.

Time (hours)	Methane	Ethane	Propane	Iso-butane	n-Butane
6.0	18.7	11.2	14.5	3.6	11.7
9.0	18.4	8.6	14.5	4.0	12.2
12.0	18.4	10.7	13.6	3.5	10.6
15.0	17.5	10.2	13.3	3.5	11.5
18.0	18.5	10.7	13.6	3.5	11.2
21.0	15.8	9.2	11.8	3.2	10.2
25.0	15.7	8.9	11.6	3.0	10.3
28.0	15.5	8.9	11.6	2.8	10.1

Table 5.16 - Selectivity to Individual Products versus Time-on-Stream for Catalyst EUROPT 4.2

Time (hours)	C5 Napthene	Iso-pentane	n-Pentane	C6-Napthene	Iso-hexane	n-Hexane
6.0	0.1	4.7	4.9	0.8	5.1	2.4
9.0	0.2	4.6	4.8	0.9	5.5	2.6
12.0	0.2	4.6	4.4	0.8	6.3	2.7
15.0	0.2	4.5	4.8	0.7	5.3	2.8
18.0	0.2	4.3	4.3	0.7	4.8	2.6
21.0	0.3	4.0	4.4	0.8	4.8	3.1
25.0	0.3	4.0	4.4	0.8	4.8	3.2
28.0	0.3	3.7	4.5	0.8	4.7	3.4

Table 5.16(cont)-Selectivity to Individual Products versus Time-on-Stream for Catalyst EUROPT 4.2

Time (hours)	C7 Napthene	Iso-heptane	n-heptane	C8-Napthene	Iso-octane
6.0	0	3.1	0	1.5	3.9
9.0	0	3.7	0	1.6	4.2
12.0	0	3.7	0	1.7	4.6
15.0	0	4.0	0	1.8	4.7
18.0	0	4.2	0	1.5	4.8
21.0	0	4.8	0	2.8	9.1
25.0	0	4.8	0	3.0	9.3
28.0	0	5.3	0	2.4	10.1

Table 5.16(cont)-Selectivity to Individual Products versus Time-on-Stream for Catalyst EUROPT 4.2

Time (hours)	Benzene	Toluene	Ethylbenzene	m/p-Xylene	o-Xylene
6.0	0.4	6.2	1.4	4.2	3.0
9.0	0.4	5.6	1.6	4.8	3.2
12.0	0.6	5.7	1.5	4.7	3.2
15.0	0.5	5.9	1.6	5.2	3.5
18.0	0.6	6.0	1.6	4.9	3.3
21.0	0.6	5.3	2.3	5.9	3.9
25.0	0.5	5.6	2.4	6.0	4.1
28.0	0.4	5.3	2.4	5.8	4.0

Table 5.16(cont)-Selectivity to Individual Products versus Time-on-Stream for Catalyst EUROPT 4.2

Time (hours)	Aromatisation	Isomerisation	Hydrocracking	Hydrogenolysis
6.0	15.4	6.9	13.6	18.7
9.0	15.8	7.9	14.1	18.4
12.0	15.6	8.3	14.4	18.4
15.0	16.8	8.7	13.3	17.5
18.0	16.1	9.0	12.5	18.5
21.0	18.0	13.8	12.2	15.8
25.0	18.5	14.1	11.8	15.7
28.0	18.0	15.4	11.2	15.5

Table 5.17 - Selectivity to Major Reactions versus Time-on-Stream for Catalyst EUROPT 4.2

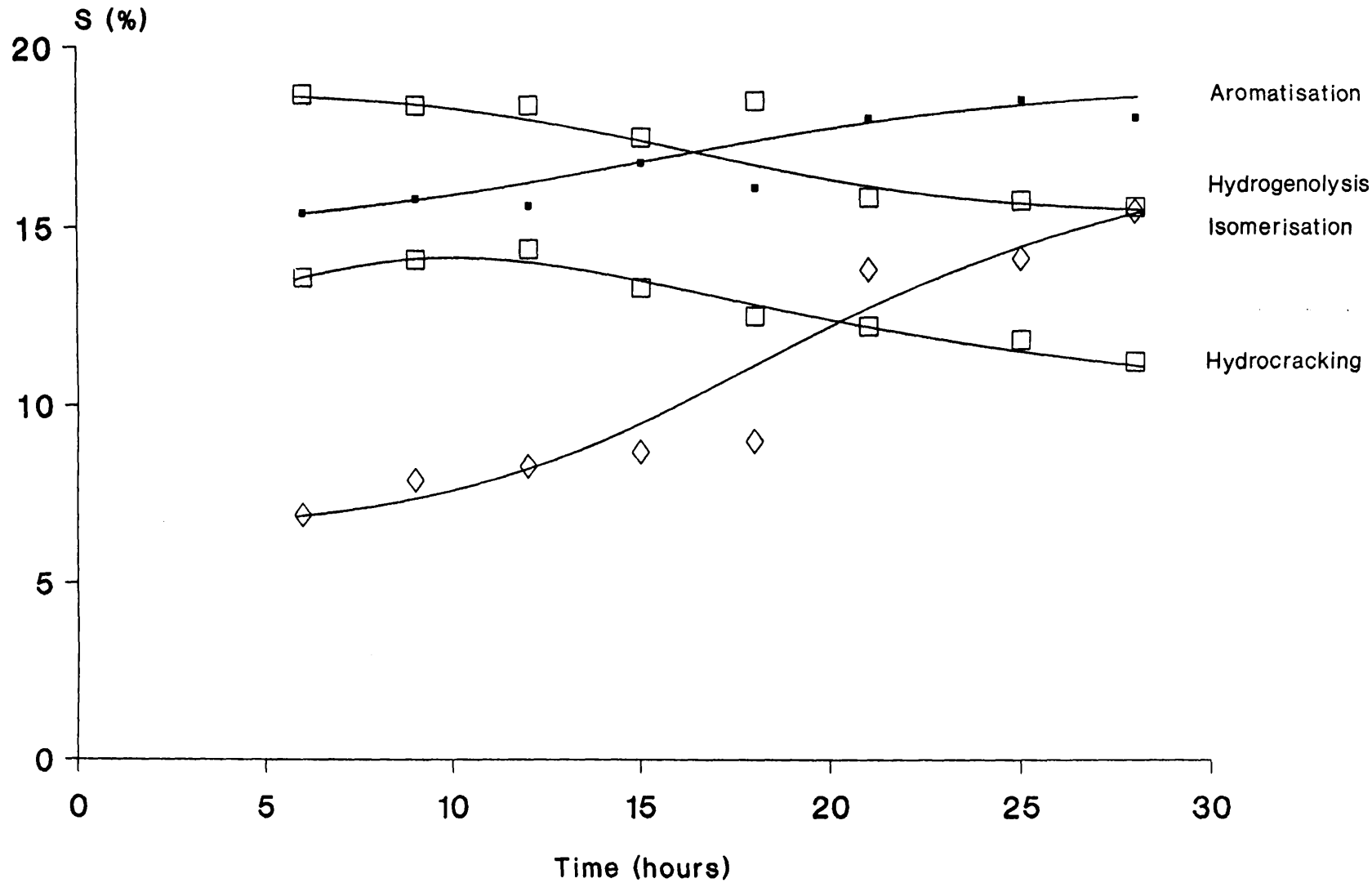

Figure 5.35 - Selectivity Towards Major Reactions versus Time-on-Stream for Catalyst EUROPT 4.2.

Time (hours)	Conversion	C3/C1
6.0	76.5	0.78
9.0	76.8	0.79
12.0	74.4	0.74
15.0	75.5	0.76
18.0	73.1	0.73
21.0	78.0	0.75
25.0	73.8	0.74
28.0	75.8	0.75

Table 5.18 - Conversion and Propane to Methane Ratio versus Time-on-Stream for Catalyst EUROPT 4.2

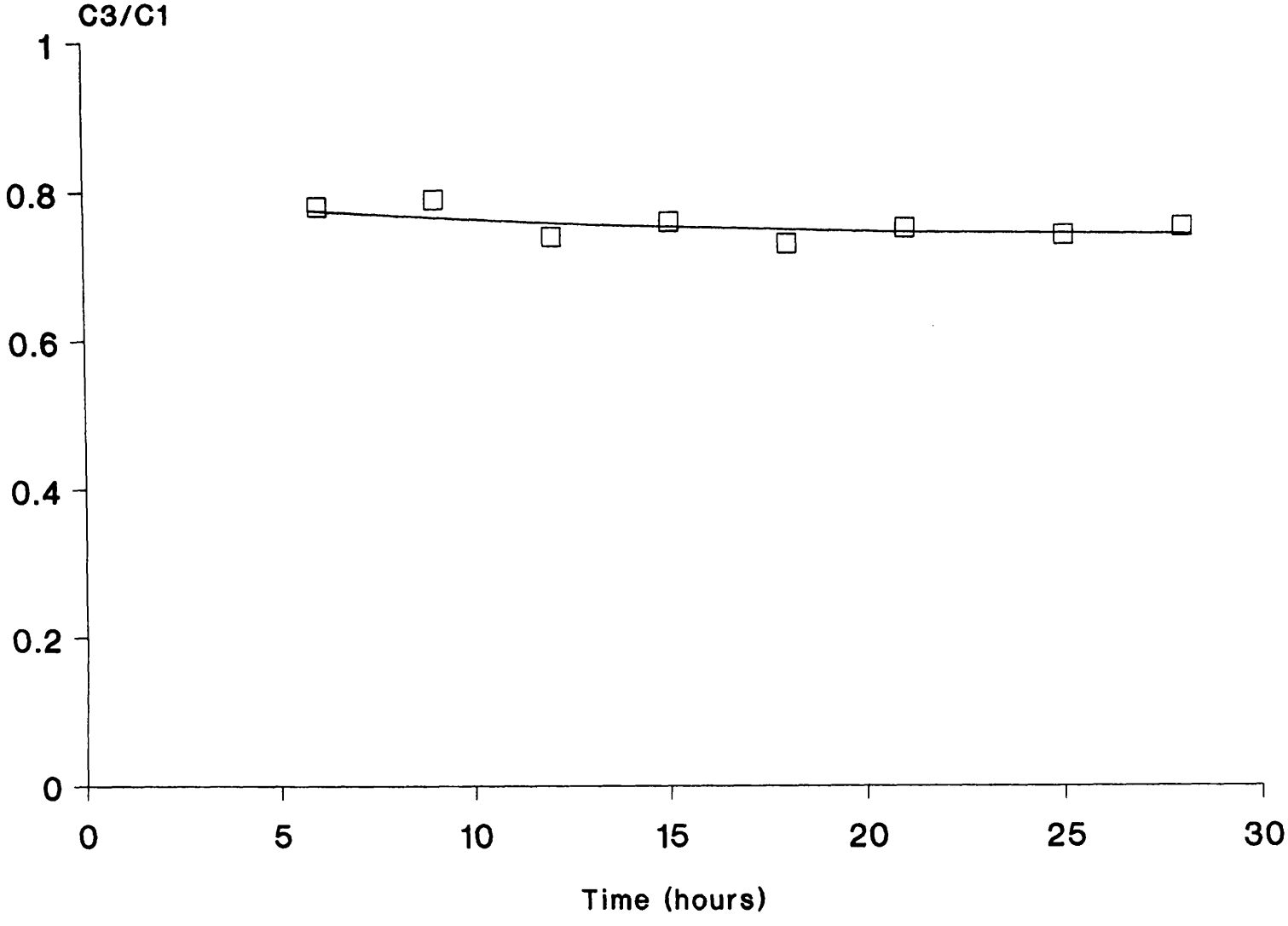

Figure 5.36 - Propane to Methane Ratio versus Time-on-Stream for Catalyst EUROPT 4.2.

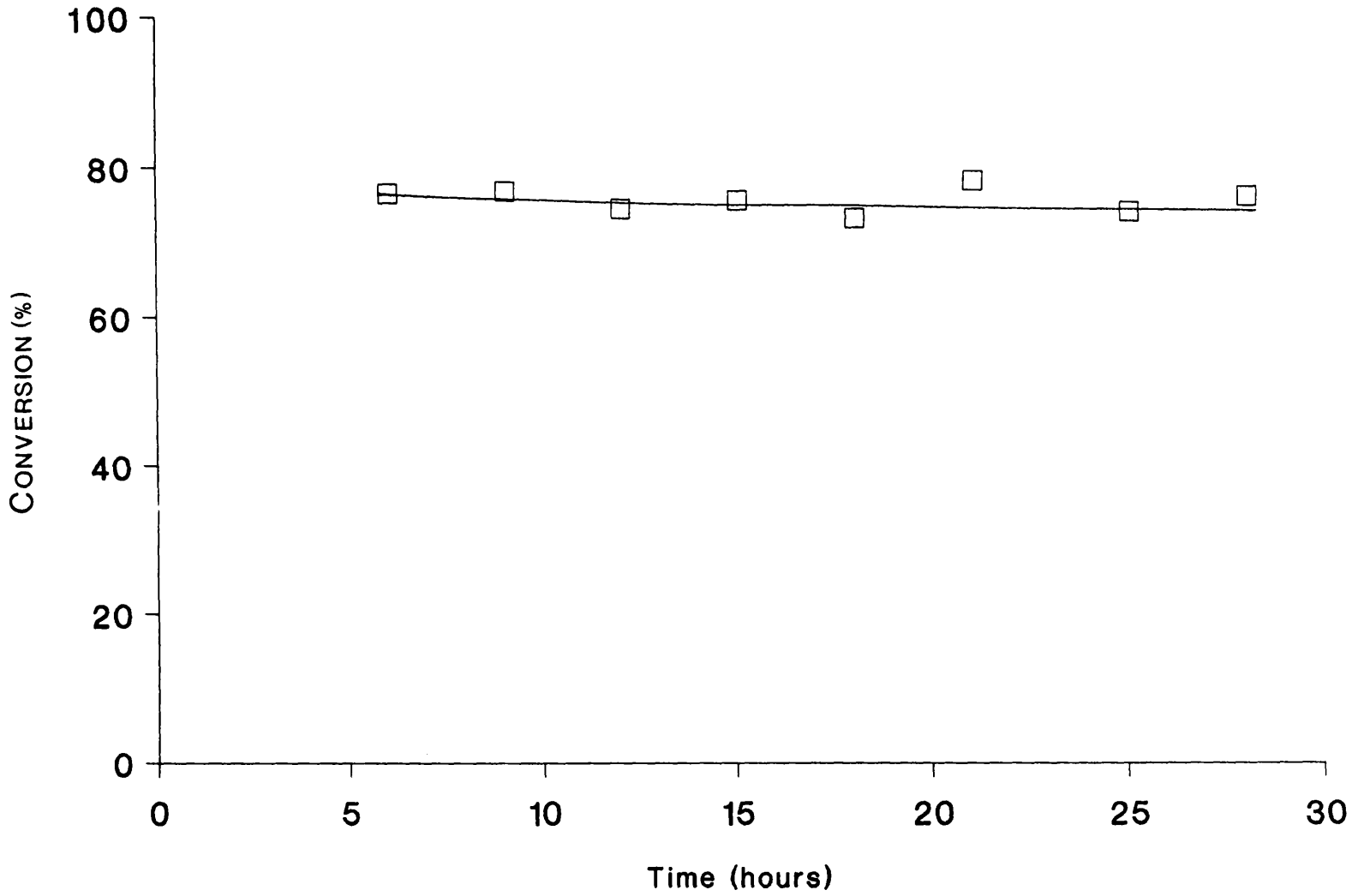

Figure 5.37 - Conversion versus Time-on-Stream for Catalyst EUROPT 4.2.

CHAPTER 6

DISCUSSION

6.1 TEMPERATURE-PROGRAMMED REDUCTION

TPR profiles for the Pt/Al_2O_3 catalyst, EUROPT 3, show a complex relation between hydrogen uptake and temperature, resulting in two well defined peaks at ca. 240 and 340°C (Figure 3.1). In addition, the isothermal region of the TPR profile contains a further 3 overlapping peaks at 550°C. Total hydrogen consumption, given in table 3.3, is in excess of the calculated value expected for the reduction process $Pt^{4+} \rightarrow Pt^0$. It would therefore appear that the platinum in the catalyst is completely reduced to the metal, in agreement with other reports (26, 27, 32). Comparison of TPR results with those reported in the literature is difficult due to the many factors which influence the reduction process and hence the resultant TPR profile (Section 1.1.2). However, there is a general agreement that Pt/Al_2O_3 catalysts reduce in a single step with a maximum reduction rate corresponding to temperatures between approximately 250 and 300°C (26,27). Other workers have also reported the presence of reduction tails up to ca. 500°C (32).

It is evident from figure 3.1 that catalyst EUROPT 3 does not undergo reduction in one step, but is reduced in several distinct stages. The importance of the thermal pretreatment step in determining catalyst reduction profiles has been noted in several studies and particular attention has been drawn to the enhanced interaction of the metal oxides with the Al_2O_3 support at higher oxidation temperatures (32). Indeed, Malet, Munuera and Caballero (131), investigating the temperature-programmed reduction of several Pt/Al_2O_3 catalysts, demonstrated that, even when using inert helium, increasing pretreatment temperatures induced a change in the high temperature

reduction peak which became broader and less well defined. Of particular interest in the study by Malet, Munuera and Caballero are the TPR results reported for catalyst EUROPT 3. After calcination in air at 450°C the resultant TPR profile was reported to show two well resolved peaks at ca. 325 and 505°C. Experimental conditions in this work were essentially identical to those used in the present study, with one exception. In the study by Malet et al., the thermal treatment prior to the TPR consisted of heating to 450°C and maintaining this temperature for 1 hour. In the present work, the pretreatment step involved heating in synthetic air at a 5°/min ramp rate to 400°C and maintaining this temperature for the longer period of 4 hours. It is apparent then, that the extended calcination period at the temperature of 400°C has intensified the interaction of platinum oxide with the increasingly dehydroxylated alumina surface. Peak maxima are more numerous and, with the exception of the peak at ca. 240°C, are consistently higher in temperature than those reported by Malet et al. (131) and other workers (26-28, 32).

A typical TPR profile measured for catalyst EUROPT 4 is shown in figure 3.2. The profile shows several reduction steps consisting of one well resolved peak with a maximum rate of hydrogen uptake at 260°C and several poorly defined peaks at ca. 340, 395 and 415°C. In common with catalyst EUROPT 3, the isothermal region contains 3 further overlapping peaks at 550°C. By comparison with the TPR profile for the Pt/Al_2O_3 catalyst (Figure 3.1) the only peaks that can be unambiguously assigned to reduction of rhenium are those at ca. 395 and 415°C. Despite the high temperature of the calcination step prior to reduction, resulting in dehydroxylation of the catalyst surface, no evidence is found for exclusive reduction of the two metals at

separate temperatures, contrary to the results of other workers (27, 131). Certainly, the increased uptake of hydrogen at ca. 260 and 340°C compared with catalyst EUROPT 3, apparent from figures 3.1 and 3.2, would indicate significant reduction of rhenium occurring simultaneously with platinum. According to Bolivar et al. (28), the lowering of monometallic rhenium's reduction temperature from values in excess of 500°C may be attributed to catalysis by platinum. A corrolary of this is the possibility of alloy formation between platinum and rhenium (Section 1.1.2). It should be noted that the increased hydrogen uptake evident in figure 3.2 and attributed to reduction of rhenium, occurs across the complete TPR spectrum and encompasses all peaks previously identified in the reduction profile of monometallic EUROPT 3. With the exception of the reduction steps at ca. 395 and 415°C, it is apparent that the reduction of platinum and rhenium is occurring concurrently.

Total hydrogen consumption determined for catalyst EUROPT 4 was higher than the expected value for complete reduction of the metallic precursors (Table 3.3). Similar results have been reported by Malet et al. (131). Hydrogen consumption by the Al_2O_3 support was considered by Malet and co-workers to account for this but was dismissed after TPR profiles recorded on pure Al_2O_3 (CK300) revealed no hydrogen uptake in the temperature range 25-700°C. One possible explanation for the excessive hydrogen consumption measured for both catalysts EUROPT 3 and EUROPT 4 is the reduction of impurities in the catalysts.

6.2 CARBON MONOXIDE CHEMISORPTION

The measurement of platinum surface areas by the adsorption of carbon monoxide poses several difficulties. It is accepted that both one and two site adsorption can occur, corresponding to adsorption of the gas in a linear or a bridged configuration (25, 132). The extent to which either of these surface species predominates depends upon several factors. It has been demonstrated by Dorling and Moss (126) that the linear form of carbon monoxide is the dominant species on highly dispersed silica supported platinum catalysts. Wells (133) considers that it is most likely that the carbon monoxide: platinum ratio is 1:1 when the degree of metal dispersion is 60-65%. Accordingly, following the work of Wells and that of Davis, Zaera and Somorjai on single crystals (90), the carbon monoxide results presented in tables 3.4-3.7 were calculated assuming linear adsorption of CO on the metal.

A metal dispersion of 81.2% was determined for catalyst EUROPT 3 from pulse carbon monoxide chemisorption measurements, indicating that the standard activation technique was particularly effective (Table 3.4). The calculated surface area, 0.7 m^2/g catalyst, was correspondingly large and the mean crystallite face diagonal of 1.5 nm correspondingly small. In comparison, static carbon monoxide chemisorption results for catalyst EUROPT 3 gave a significantly lower metal dispersion of 70.5% (Table 3.6). A similar relationship was found between static and pulse chemisorption results for catalyst EUROPT 4 (Tables 3.4, 3.6). The lower dispersion figures were not expected using the static method of chemisorption. Indeed, it is widely accepted that the pulse method, rather than the static method of

chemisorption, gives rise to lower measured gas uptakes due to the removal of weakly chemisorbed adsorbate by the flowing carrier gas used in the former technique (134). It is unlikely that there is any simple explanation for these results unless there was either insufficient time or insufficient pressure of carbon monoxide for true surface-gas phase equilibrium to be established. Alternatively, contamination due to backstreaming of oxygen or pump oil molecules in the Micromeritics 2800 instrument may have reduced the number of measurable platinum surface atoms.

The metal dispersion for catalyst EUROPT 4 was calculated assuming that both platinum and rhenium adsorb carbon monoxide. Total metal dispersion, calculated from pulse chemisorption was only 40.7% (Table 3.4). However, for both static and pulse chemisorption the quantity of carbon monoxide adsorbed was virtually identical for catalysts EUROPT 3 and EUROPT 4, each containing 0.3% by weight platinum. Contrary to the TPR hydrogen consumption results, if it is accepted that rhenium is not in fact completely reduced or, alternatively that rhenium metal is not adsorbing CO, then the metal dispersion may be calculated for platinum only. In this context, it is interesting to note that Bolivar and co-workers (25), investigating a Pt-Re/Al_2O_3 catalyst, demonstrated that Re-CO bonds were present only when the weight % of rhenium was greater than 60%. Assuming no Re-CO interaction, pulse chemisorption results give 83.3% platinum dispersion and a platinum surface area of 0.7 m^2/g catalyst. The high dispersion of metal implied in these figures is in accordance with TEM results for catalyst EUROPT 4 in which no metal particles were observed (Section 3.2.6).

6.3 CATALYST SURFACE AREA AND POROSITY

The nitrogen isotherms determined for the catalysts GHI, EUROPT 3 and EUROPT 4 exhibit Type IV adsorption according to the Brunauer classification (135).

Type IV isotherms are considered to be characteristic of mesoporous materials (pore diameter 2-50 nm). Furthermore, the hystersis loops associated with the isotherms for EUROPT 3 and EUROPT 4 are of type H1 in which the two branches are almost vertical and nearly parallel over an appreciable range of gas partial pressures. Type H1 hysteresis loops are associated with porous materials known to have a narrow distribution of pore sizes (136). The isotherm shape for catalyst GHI, predominantly of type H1, differed slightly from those determined for catalysts EUROPT 3 and EUROPT 4. In particular, the plateau region in the nitrogen adsorption branch was less conspicuous (Figure 3.3 (c)). Excellent, linear BET plots were afforded by the adsorption isotherms within the p/p^0 range of 0.05 to 0.21 (Figure 3.4), allowing calculated surface areas to be quoted with confidence. The BET surface areas determined for EUROPT 3 and EUROPT 4 were 193.2 ± 0.8 and 195.8 ± 0.5 m^2/g respectively (Table 3.8). As both materials use a common Al_2O_3 support in their manufacture the good agreement in results is not surprising. These values compare favourably with the specific surface area of 199.7 m^2/g for the pure support as determined by Figoli and co-workers (18) and indicate that little if any surface area has been lost during the catalyst preparation. The specific surface area of 95.5 m^2/g determined for catalyst GHI (Table 3.8) was significantly lower than that of EUROPT 3 and EUROPT 4. Catalyst GHI was prepared using Aluminium Oxide C, a

commercial γ-alumina produced by flame hydrolysis of anhydrous aluminium chloride (129). Degussa AG, the manufacturers of Aluminium Oxide C, claim that flame hydrolysis creates an alumina absent of pores but retaining a large surface area. Pure Aluminium Oxide C is reported to have a specific surface area of 100±15 m^2/g (129).

Figures 3.5 (a) and 3.5 (b) show that the BET pore area distribution is very narrow for each of the catalysts manufactured using the Ketjen CK300 alumina and is centred at ca. 7.4-7.6 nm. It is apparent from figure 3.5 (c) that the average pore diameter calculated for catalyst GHI is larger and, furthermore, that the pore area distribution is wider, ranging from ca. 6.0 nm to 24.9 nm.

Catalyst EUROPT 3 has a calculated cumulative pore volume of 0.505 cc/g, virtually identical to the value calculated for the maximum volume adsorbed (0.500 cc/g). The values calculated for catalyst EUROPT 4 are slightly lower at 0.490 cc/g and 0.485 cc/g respectively (Table 3.9). The equivalence in maximum volume adsorbed and cumulative pore volume values confirms that the assumptions made in the BJH calculation are valid. Good agreement is also observed in the results for catalyst GHI (Table 3.9) which show that an amount of nitrogen equivalent to 0.46-0.48 cc/g was adsorbed.

Mercury porosimetry results for the alumina support, CK300, and catalyst GHI are presented in table 3.10. A total pore volume of 0.540 cc/g and a total pore area of 203.7 m^2/g was obtained for the pure alumina support, implying that a slight loss of both surface area and internal volume occurred during preparation of EUROPT 3

and EUROPT 4 (Tables 3.8-3.10). Total pore volume determined for catalyst GHI was in good agreement using the two different methods. On the other hand, the calculated value for surface area was slightly lower when determined by mercury porosimetry (93.6 m^2/g vs. 95.5 m^2/g). This may be attributed to the uncertainty associated with mercury porosimetry at the lower end of the mesopore range, resulting in an underestimation of total surface area (137).

Examination of the mercury porosimetry plots of cumulative volume versus applied pressure for both CK300 and catalyst GHI reveals non-closure of the hysteresis loops (Figures 3.6 (a) - (b)). This phenomenon is often encountered in mercury porosimetry and is explained by the entrapment of liquid mercury in the pore structure of the materials investigated (137). It is apparent that the entrapment of liquid mercury in catalyst GHI is significantly higher than that observed for the CK 300 alumina. This may well be indicative of an irregular pore structure or a poorly defined three-dimensional array of cavities interconnected by narrow channels or necks.

Regarding the structure of catalyst GHI, it has already been noted that the Aluminium Oxide C support is claimed to be non-porous. It is clear from the nitrogen adsorption and mercury porosimetery results that significant differences exist between the two support materials used in the catalyst preparation. However, it has also been demonstrated that, far from being non-porous, catalyst GHI has an internal volume almost equivalent to that of catalysts EUROPT 3 and EUROPT 4. Degussa, the manufacturers of Aluminium Oxide C, state that the material is characterised by a

small particle diameter of average size 20 nm. The formation of a close-packed aggregate of these small particles, creating a network of interstices, would readily account for the pore volume determined for catalyst GHI. In this context, the nitrogen adsorption hysteresis associated with catalyst GHI, which may be regarded as being intermediate between type H_1 and type H_3, is of particular interest (Figure 3.3 (c)). Type H_3 loops, which do not exhibit any limiting adsorption at high p/p^0 are often observed with aggregates of plate-like particles (136).

6.4 n-OCTANE REFORMING ON MONOMETALLIC Pt/Al_2O_3

A summary of major reaction selectivities and conversions determined for catalysts GHI, EUROPT 3 and EUROPT 4 after 5 and 25 hours-on-stream is presented in Table 6.1.

On examining Table 6.1 it is evident that the most significant reaction on catalyst GHI during this reaction period is aromatisation. Catalyst selectivity for the dehydrocyclisation reaction increases steadily and after 40 hours-on-stream has reached a value of approximately 54% (Figure 5.5). The increase in aromatisation selectivity is accompanied by a fall in hydrogenolysis selectivity. From an examination of figures 5.3 and 5.4 it is apparent that the increase in yield of ethylbenzene and xylenes is responsible for the rise in aromatisation selectivity. The increase in C_8-aromatic products may be largely attributed to the fall in yield of benzene and toluene. It would appear that benzene and toluene are produced mainly

Table 6.1 - Summary of Major Reaction Selectivity and Conversion at 5 and 25 hours-on-stream.

Catalyst	Aromatisation	Isomerisation	Hydrocracking	Hydrogenolysis	Conversion
GHI ($500^{o}C$)	Increases from 42% to 50%	Increases from zero to 5%	Increases from 25% then falls to 24%	Falls from 13% to 7%	Falls from 21% to 20%
EUROPT 3 ($500^{o}C$)	Falls from 59% to 49%	Increases from 3% to 14%	Increases from 25% then falls to 23%	Falls from 3% to 2%	Falls from 75% to 67%
EUROPT4.1 ($500^{o}C$)	Increases from 46% to 54%	Increases from 1% to 3%	Increases from 15% then falls to 13%	Falls from 8% to 5%	Increases from 69% to 76%
EUROPT4.2 ($450^{o}C$)	Increases from 15% to 18%	Increases from 7% to 14%	Increases from 13% then falls to 12%	Falls from 19% to 16%	Falls from 77% to 74%

as a result of dealkylation of C_8-aromatics on platinum, a result similar to that obtained by Beltramini and Trimm (119). The reduced likelihood of any C_8-aromatic undergoing two successive demethylation reactions would explain why toluene is the more prevalent species.

The very rapid fall in yield of methane and ethane (Figure 5.1), also produced by carbon-carbon bond cleavage on the metal function, mirrors that of benzene and toluene. The rapid decrease observed in hydrogenolysis activity is in accordance with the results of a number of authors (105, 116, 117) and is believed to be caused by a reduction in the number of suitable ensembles for this reaction, due to site blocking by coke deposition.

Hydrocracking selectivity on catalyst GHI is significant and was second only to that of aromatisation (Figure 5.5.). The conversion of n-octane to hydrocracking products shows a broad maximum in selectivity of ca. 26% at approximately 11 hours-on-stream. The maximum is caused by the conversion of n-octane to iso-pentane and iso-hexane as the conversion to iso-butane, the main cracking product, decreases continuously with time (Figure 5.2). The decline in hydrocracking selectivity coincides with a steady increase in isomerisation selectivity. Analogous results have been reported by Parera and co-workers (105) and were interpreted in terms of carbon laydown on the alumina surface.

Both hydrocracking and isomerisation reactions are known to be controlled by the acid sites of reforming catalysts (Section 1.1.4). Furthermore, it is well established

that isomerisation requires less acidic sites than hydrocracking (2, 117). From the observed changes in hydrocracking and isomerisation selectivity over catalyst GHI (Figure 5.5) it is apparent that after approximately 10 hours-on-stream the strongest acid sites are blocked preferentially by coke deposition and, as a consequence, hydrocracking is reduced. Reactions occurring on less acidic sites become relatively more important with the result that isomerisation selectivity is observed to increase. However, the removal of chlorine from the catalyst surface during the course of the reaction must also be considered. Catalyst GHI had a chlorine content of 1.28% by weight prior to use. This was reduced to 0.37% by weight after reduction and 40 hours of reaction (Table 5.2). Any decrease in the chlorine content whilst the catalyst was on-stream is likely to have affected the acid-catalysed reactions. Figoli et al. (18) have established that increasing chlorine content on reforming catalysts increases hydrocracking and diminishes isomerisation. It follows that the observed decrease in hydrocracking activity and accompanying increase in isomerisation activity over catalyst GHI implies the preferential removal of chlorine from the more acidic sites on the catalyst surface. The change in yield and selectivity of hydrocracking and isomerisation reactions on catalyst GHI should therefore not be interpreted solely in terms of coke deposition but rather in terms of a combination of coke deposition and removal of catalyst chlorine.

The low conversion exhibited by catalyst GHI compared unfavourably with that determined for the monometallic catalyst, EUROPT 3 (Figures 5.7, 5.17). Overall conversion at 5 hours-on-stream was 21% for catalyst GHI compared with approximately 75% for catalyst EUROPT 3 (Table 6.1). It has been shown in section

1.1.4 that isomerisation and dehydrocyclisation reactions, though predominantly catalysed by a bifunctional mechanism, may also occur on the metal function alone. Sinfelt and co-workers (55) have established that the rate of isomerisation is independent of metal content above 0.1% by weight, the rate of dehydrocyclisation, however, was enhanced when the platinum content of a bifunctional catalyst was increased from 0.1% to 0.6% by weight. Taking the two monometallic catalysts and assuming that all other aspects were equal, the higher metal loading (0.9% vs. 0.3% by weight) and the corresponding higher metal surface area of catalyst GHI (Tables 3.1, 3.5) should have been expected to result in a higher conversion of n-octane compared to that of catalyst EUROPT 3. The low conversion of n-octane on catalyst GHI must therefore be attributed to the acidic function of the catalyst. The chlorine content of unreduced samples of catalysts GHI and EUROPT 3 were determined by neutron activation analysis to be 1.28 and 0.95% by weight respectively (Table 3.1). According to Jackson et al. (121) the chlorine content of catalyst GHI is reduced to 1.01% by weight after the standard reduction technique detailed in section 3.1. No information is available on the loss of chlorine from catalyst EUROPT 3 during its activation. However, when we consider that the chlorine content of catalyst EUROPT 3 was 0.71% by weight after not only activation but also 26 hours of reaction, the loss of chlorine during the activation procedure could not have been great (Table 5.2). It would appear, therefore, that there was no substantial difference in the chlorine content of catalysts GHI and EUROPT 3 prior to the n-octane reforming reaction.

Both mercury porosimetry and nitrogen BET results confirm that the surface area of catalyst GHI is approximately 50% of that for catalyst EUROPT 3. Specific

surface areas determined by nitrogen adsorption, for example, were 95.5 and 193.2 m^2/g respectively (Table 3.8). It can be concluded that the poor conversion on catalyst GHI is related to the lower surface area of the alumina support and hence a decreased availability of acid sites required for the bifunctional mechanism. The possibility that the lower conversion on catalyst GHI may be accounted for by the high hydrogenolysis activity of the catalyst, resulting in rapid carbiding of the catalyst surface may be discounted when we consider that catalyst EUROPT 3 displayed a much higher rate of coking (Table 5.2).

The combined yield of methane, ethane and propane on catalyst EUROPT 3 was significantly higher than that on catalyst GHI. Propane yield, for example, was far in excess of that determined for the GHI catalyst. Nevertheless, despite the lower overall conversion on catalyst GHI, the yield of methane was consistently higher than that on EUROPT 3 (Tables 5.3, 5.7). The relative importance of metal catalysed carbon-carbon bond scission can be assessed from the hydrogenolysis selectivity given in table 6.1. At 5 hours-on-stream, selectivity towards the hydrogenolysis reaction on GHI was ca. 13%. In contrast, hydrogenolysis selectivity on EUROPT 3 was only ca. 3%. It is well established that hydrogenolysis is a metal catalysed reaction (8, 82). In accordance with the results of other workers (72, 138), the increased hydrogenolysis activity on catalyst GHI is consistent with the larger platinum particles on the catalyst (d = 1.7 nm vs. 1.5 nm).

The influence of the acid support on catalyst EUROPT 3 combined with the higher metal dispersion is best demonstrated by a comparison of the propane to

methane ratios determined for the two monometallic catalysts (Figures 5.6, 5.16). The C_3/C_1 ratio for catalyst GHI increases from 0.8 at 3.2 hours-on-stream to a value of close to 1.1 at 25 hours. In contrast, the value of the C_3/C_1 ratio for catalyst EUROPT 3 is at least three times higher, remaining relatively constant at between 3 and 3.5 (Figure 5.16). This difference in behaviour is a result of the lower yield of methane on catalyst EUROPT 3 and the larger surface area of the alumina support, leading to increased production of propane. Propane is known to be an additional product of acid catalysed hydrocracking (120).

The most important reaction of n-octane on EUROPT 3 was aromatisation and, in this respect, its behaviour was similar to that of catalyst GHI. Furthermore, the principal aromatic products on both catalysts after 20 hours-on-stream were meta- and para-xylene (Figures 5.4, 5.14) In the case of catalyst EUROPT 3 meta- and para-xylene were the dominant aromatic species throughout the reaction, whereas, with catalyst GHI, the meta- and para-xylene yield exceeded that of ortho-xylene only after 20 hours.

Fogelberg and co-workers have established that virtually no isomerisation of C_8-aromatics occurs on bifunctional reforming catalysts after formation of the six-membered ring (139). Thus, isomerisation of aromatics cannot account for the composition of C_8-aromatics observed. The presence of C_8-aromatics, not allowed by direct six-membered ring formation on the metal function, such as meta- and para-xylene, can be accounted for by an isomerisation step prior to ring closure (139, 140). It is known that isomerisation is a primary reaction on reforming catalysts and that the

products may undergo subsequent conversion (141). The results on catalysts EUROPT 3 and GHI support this view. Formation of iso-octane is seen to increase as secondary reactions such as hydrocracking, hydrogenolysis and dehydrocyclisation either decrease in importance or reach a pseudo-stationary level (Tables 5.3, 5.7).

The validity of the metal aromatisation mechanism is not in doubt. However, the bifunctionally catalysed aromatisation mechanism may also account for the observed composition of C_8-aromatics. Davis (66), for example, has demonstrated that n-propylcyclopentane, one of the five-membered ring isomers formed from n-octane, can form large amounts of meta- and para-xylene on bifunctional Pt/Al_2O_3 catalysts. In addition, in a more recent paper, Swasanker and Padalkar (142) conclude that both the metal and acid functions of reforming catalysts are important in determining the composition of C_8-aromatic isomers from n-octane reforming. Consequently, it is likely that both mechanisms are active in the reforming of n-octane on catalysts GHI and EUROPT 3. However, the results of the present study do not allow for any conclusions to be drawn on which is the dominant reaction pathway.

Any similarities in product distribution arising from dehydrocyclisation on each catalyst end when we consider the greater yield of aromatics on catalyst EUROPT 3 (eg. ca. 31% vs. 10.7% at 20 hours-on-stream) and, more importantly, the changes in yield with time. The increase in ethylbenzene, ortho-xylene and meta- and para-xylene yields on catalyst GHI has already been discussed above. In marked contrast, the yield of C_8-aromatics decreased with time over catalyst EUROPT 3 (Figure 5.14). Decreasing aromatic yields during hydrocarbon reforming have been widely reported

in the literature and have been attributed to coke deposition on the bifunctional catalyst (82, 105, 115, 116). According to Shum, Butt and Sachtler (143) and Christoffel and Paál (116) the initial suppression of dehydrocyclisation activity may be explained by deactivation of the metal function as a result of coking. Dehydrocyclisation activity on catalyst EUROPT 3 undergoes its most significant decline during the first 10 hours-on-stream and thereafter falls only slightly (Figures 5.13, 5.14). Accepting that dehydrocyclisation activity on EUROPT 3 is catalysed by a combination of monofunctional (metal) and bifunctional (metal + acid) mechanisms, the initial fall in yield of aromatics may be interpreted in terms of severe coke deposition on the metal function. This is in agreement with work by Querini, Figoli and Parera (120), where it has been established that, although long-term laydown of carbonaceous residues is restricted to the Al_2O_3 support, the initial rapid deposition of coke is on the metal function.

The second most important reaction on catalyst EUROPT 3, as with catalyst GHI, was hydrocracking. Hydrocracking selectivity is quantitatively the same for both GHI and EUROPT 3; increasing from 25% before falling to 23% and 24% respectively, between 5 and 25 hours-on-stream (Table 6.1, Figures 5.5, 5.15). The yield of hydrocracked products on catalyst EUROPT 3, considering the difference in catalyst conversion, is of course much higher. As with propane production this may be ascribed to a greater availability of acid sites on the higher surface area alumina support.

Iso-butane is the most abundant product of hydrocracking on each catalyst, demonstrating the importance of central cracking of the reactant molecule (Figures 5.2, 5.9). It is of particular interest that, with the exception of propane, branched paraffins were the only products of hydrocracking on catalyst GHI. Similarly, catalyst EUROPT 3 yielded no n-butane and insignificant quantities of other straight-chain paraffins (Table 5.7). The predominance of iso-compounds is in agreement with observations in the literature and may be explained by cracking via a carbonium ion mechanism, in which the more stable tertiary alkyl cations are formed by intra-molecular rearrangements (1,144). Assuming that primary cracking of n-octane may lead to the following pairs per mole of n-octane: $C_4 + C_4$ and $C_5 + C_3$, it is not surprising that butanes are the main cracking products. The sequential cracking of butanes by a further β-scission would generate unstable primary cations and in consequence is severely inhibited (144).

The rate of coking on catalyst EUROPT 3 was significantly higher than that on GHI. Catalyst GHI was on-stream for a total of 40 hours. The coke content of the spent catalyst was determined as 1.20% by weight. Despite being on-stream for a shorter period of 26 hours, under identical conditions to those of the GHI catalyst, the coke content of EUROPT 3 was also 1.20% by weight (Table 5.2). Assuming the metal function of the catalysts is instrumental in determining the overall level of coking then, following Lankhorst et al. (108) and Somorjai and co-workers (90), catalyst GHI, with its lower dispersion and higher metal loading would be expected to show a higher rate of coking than catalyst EUROPT 3. The present results strongly suggest that the acidic function of the two catalysts is responsible for the contrast in

the rates of coking.

Barbier (117) and Figoli et al. (18) state that coking levels increase with the acidity or chlorine levels of reforming catalysts. Since the results of neutron activation analysis indicated that, after reduction, both monometallic catalysts have similar levels of chlorine (Table 5.2), any difference in the strength of the acidic function of catalysts GHI and EUROPT 3 must be related to the different alumina supports. It is also likely that the more extensive activation method used for catalyst EUROPT 3 compared with that for catalyst GHI, would give rise to a more dehydrated surface and hence greater Lewis acidity. According to Parera and co-workers (88) coke formation on bifunctional reforming catalysts may be attributed to a Diels-Alder mechanism catalysed by Lewis acid sites. EUROPT 3 was calcined in air at 400°C for 4 hours before reduction at 400°C for a further 2 hours. No calcination step was involved in the activation of catalyst GHI which was simply reduced at 300°C for 1 hour prior to heating to the required reaction temperature of 500°C. Unfortunately, quantitative measurement of catalyst acidity was not a feature of the present study.

6.5 n-OCTANE REFORMING ON BIMETALLIC Pt-Re/Al_2O_3 AT 500°C

n-Octane reforming on catalyst EUROPT 4.1 produced striking differences in reaction selectivity and coke formation compared with catalyst EUROPT 3. As both

catalysts were investigated under identical reaction conditions and are physically indistinguishable, excepting the addition of rhenium, the changes observed may be directly attributed to the presence of the second metal.

The first result of relevance is the high specificity of the Pt-Re catalyst for methane formation. For example, the methane yield on catalyst EUROPT 4.1 at 5 hours-on-stream is more than double that determined for catalyst EUROPT 3 (ca. 5% vs. 2%) and remains consistently higher (Figures 5.8, 5.18). The increased yield of methane, produced on the metal sites of the bimetallic catalyst, relative to the acid catalysed production of propane results in a low value of C_3/C_1 ratio. In consequence, the C_3/C_1 ratio for catalyst EUROPT 4.1 at 6 hours-on-stream and thereafter is approximately half that determined for catalyst EUROPT 3 (Tables 5.10, 5.14). As with the monometallic catalyst, methane production on catalyst EUROPT 4.1 decreases with time, presumably due to coke deposition on the metallic sites.

Significantly, the influence of rhenium is not restricted to enhancing methane formation as can be seen from the greatly increased yield of normal paraffins (Figures 5.11, 5.21). Indeed, n-butane, a product not observed during n-octane reforming on catalyst EUROPT 3, is produced in such quantities by catalyst EUROPT 4.1 that its yield exceeds that of iso-butane throughout the reaction (Table 5.11).

The high selectivity of the Pt-Re/Al_2O_3 catalyst for carbon-carbon bond scission is in good agreement with the results of other workers (46, 72, 111-113, 120). The increased yield of methane and normal paraffins can be explained by multiple fission

of the reactant n-octane on Pt-Re particles as proposed by Shum, Butt and Sachtler (111). According to these workers, high methane selectivity and high levels of multiple fission of hydrocarbons are characteristic of Pt-Re alloy formation. In an earlier publication the same authors rationalised this phenomenon by accepting that Re forms stronger bonds to carbon than does Pt (143). Accordingly, the likelihood of forming chemisorption bonds with more than one carbon atom of the same molecule would increase in the following order: Re ensembles > mixed ensembles > Pt ensembles. According to Ponec (145), multiple adsorption is likely to precede hydrogenolysis and it follows that mixed ensembles will have a higher hydrogenolysis selectivity than Pt ensembles. Indeed, Haining et al. (146) have found that a maximum in n-butane hydrogenolysis activity exists for Pt-Re/Al_2O_3 catalysts in which the metal loading is 60% rhenium. It was further demonstrated that the catalytic activity could not be represented by a linear combination of the platinum and rhenium indicating that there was an interaction between the two metals.

Isomerisation and hydrocracking selectivity on catalyst EUROPT 4.1 is qualitatively similar to that on catalyst EUROPT 3. Isomerisation selectivity, for example, is observed to increase during the reaction, whereas hydrocracking selectivity declines after an initial rise (Figures 5.15, 5.25). Iso-butane is again the principal product of hydrocracking. Compared to catalyst EUROPT 3 the behaviour of the bimetallic catalyst with respect to these two reactions may be explained in an analogous manner, namely increasing laydown of carbonaceous material and decreasing chlorine levels. However, in quantitative terms it is apparent that the yield of isomerisation and hydrocracked products is significantly lower on EUROPT 4.1

(Tables 5.7, 5.11). Iso-octane yield, for example, reaches its optimum value of 1.5% at 29.5 hours-on-stream (Table 5.11). Even at the shorter time-on-stream of 22.6 hours the yield of iso-octane using the monometallic catalyst is several orders of magnitude greater at 8.3% (Table 5.7). In a similar manner the yields of iso-butane, iso-pentane and iso-hexane are consistently lower for catalyst EUROPT 4.1 throughout the reaction (Figures 5.9, 5.19).

The lower yield of iso-octane is consistent within which, once formed, it readily undergoes carbon-carbon bond fission on the Re component of the catalyst. Similar results have been reported by Parera and co-workers (46) investigating the role of Re in the Pt-Re/Al_2O_3 catalysed reforming of n-hexane. It might have been expected that the product yields of acid catalysed hydrocracking reactions would have been similar between catalysts EUROPT 3 and EUROPT 4.1. The lower yields of hydrocracked products must therefore be a consequence of the presence of Re. Successive hydrogenolysis steps either before or after the hydrocracking reaction, which is known to be slow (8), is one possible explanation for the attenuation in the yield of light iso-paraffins.

One of the most significant differences in behaviour between catalysts EUROPT 3 and EUROPT 4.1 is in their activity for the dehydrocyclisation reaction. Total conversion to aromatics over each catalyst is quantitatively similar at certain stages. For example, at 13.6 hours-on-stream the aromatic yield on catalyst EUROPT 3 is 34.5% compared to a yield of 32.6% on catalyst EUROPT 4.1 at 12 hours-on-stream (Tables 5.7, 5.11). However, while the aromatic yield decreases with time on

the monometallic catalyst, the converse occurs on catalyst EUROPT 4.1. Ethylbenzene and meta- and para-xylene yields all increase by a considerable amount (Figure 5.24). In consequence, by 34.5 hours-on-stream the total yield of aromatics on the Pt-Re catalyst has risen to 37.1%. Although a similar effect was seen for catalyst GHI, this could largely be explained by a corresponding fall in the yields of benzene and toluene. This is not the case with catalyst EUROPT 4.1. Benzene and toluene yields decline by only 3.8% during the 34.5 hours-on-stream, which is significantly less than the 10.6% increase in the yield of C_8-aromatics (Table 5.11). This is a surprising result when compared with the published literature on the reforming behaviour of Pt-Re/Al_2O_3 catalysts. It has been widely reported that bimetallic Pt-Re/Al_2O_3 catalysts lose dehydrocyclisation activity with time-on-stream due to increasing levels of coke (82, 120, 147). However, the observed increase in yield of aromatics is not without precedence. Beltramini and Trimm (119), investigating the catalytic reforming of n-heptane over an unsulphided Pt-Re/Al_2O_3 catalyst of similar properties to that used in the present study, have found that toluene yield increased with time-on-stream, although no explanation was given by the authors for this effect.

Many theories have been proposed which attempt to explain the different behaviour of Pt-Re catalysts as compared with Pt catalysts. Ludlum et al. (148) and Bertolacini and Pellet (36) favour a mechanism whereby Re influences the deposition of carbon on the acidic support (long-term deactivation). The function of Re, either in the oxidic or metallic form, is to promote the fission or removal of coke precursors, thus inhibiting catalyst deactivation. Considering the importance of aromatic and

polycyclic ring compounds as intermediates in the formation of graphitic coke (88, 92) (Section 1.1.2), it is conceivable that Re- catalysed fission of these carbonaceous residues would give rise to aromatic products in addition to methane and other paraffins, as proposed by Margitfalvi et al. (149). Why this should be restricted to the increased formation of ethylbenzene and meta- and para-xylene only, is not clear (Figure 5.24).

That Re is playing an active role in attenuating coke formation is very clear when the weight % of carbon on the spent catalyst is considered. After 34.5 hours-on-stream the coke content of EUROPT 4.1 was only 0.65% by weight (Table 5.2). This figure is almost half that determined for catalyst EUROPT 3 despite the fact that the Pt-Re catalyst was on-stream for an additional 8.5 hours. These results are in disagreement with those of Sachtler (150) who stated that equivalent Pt and Pt-Re catalysts produce equal amounts of coke. Many other authors, however, have reported lower levels of coking on Pt-Re/Al_2O_3, consistent with the results presented in this work (81, 82, 119). Regarding coke formation, if Pt and Re were acting independently on catalyst EUROPT 4.1, Pt would produce the same amount of coke on catalyst EUROPT 3 or on catalyst EUROPT 4.1 because both have the same Pt concentration. The lower levels of coke produced on the Pt-Re catalyst would suggest that some form of interaction between the two metals is extant and that the Re is active in the removal of pre-graphitic coke deposits.

6.6 n-OCTANE REFORMING ON BIMETALLIC Pt-Re/Al_2O_3 AT 450°C

n-Octane reforming on catalyst EUROPT 4 at the lower reaction temperature of 450°C resulted in significant changes in product yield and selectivity.

At 6 hours-on-stream, for example, the yield of methane on catalyst EUROPT 4.2 showed a three-fold increase over that determined for catalyst EUROPT 4.1 (14.3% vs. 4.3%) and remained higher throughout the reaction. Similarly, the production of ethane was significantly increased at the lower reaction temperature (Tables 5.11, 5.15). The importance of hydrogenolysis activity on catalyst EUROPT 4.2 is best demonstrated by considering the selectivity towards the reaction. Between 5 and 25 hours-on-line, hydrogenolysis selectivity on catalyst EUROPT 4.2 had a maximum value of 19% before falling to 16%. In comparison, the maximum value determined for hydrogenolysis selectivity on catalyst EUROPT 4.1 was only 8% (Table 6.1). As a result of the increased hydrogenolysis activity, methane is the principal gaseous product produced by EUROPT 4.2, rather than propane as in the case of catalyst EUROPT 4.1 (Figures 5.18, 5.28). The C_3/C_1 ratio determined for catalyst EUROPT 4.2 reflects these changes and is approximately half that determined for EUROPT 4.1 throughout the reaction (eg. 0.78 vs. 1.59 at 6 hours-on-stream) (Tables 5.14, 5.18).

This data is not in accord with the results of Parera et al. (151) who reported that hydrogenolysis activity on Pt-Re/Al_2O_3 increased with increasing temperature. According to Kugelmann (152) hydrogenolysis is not restricted by thermodynamics

and is dependent only on kinetic factors. Regarding the kinetics of hydrogenolysis, Le Page (3) states that the reaction has a high activation energy and is therefore favoured by increasing temperatures. It has been demonstrated that coke formation and hydrogenolysis occur on the same active metal sites in reforming (48). It is also known that coke formation increases with temperature (2). Regarding the two competitive reactions occurring on the metal sites, the lower hydrogenolysis activity of catalyst EUROPT 4.1 at 500°C would suggest there was a critical temperature beyond which coke deposition became predominant. Similar results have been reported by Bond (153) for Pt-Re/Al_2O_3 catalysts, where the loss of hydrogenolysis activity with increasing temperature was attributed to coke deposition.

Isomerisation activity was significantly greater at the lower reaction temperature. At six hours-on-stream, for example, the yield of iso-octane on EUROPT 4.2 showed a ten-fold increase over that determined for catalyst EUROPT 4.1 (3.0% vs. 0.3%). Similarly, the difference in yield of iso-heptane over each catalyst, though less pronounced, was still considerable(eg. 2.3% vs. 0.6% at 6 hours-on-stream) (Tables 5.11, 5.15). Isomerisation activity remained consistently higher on catalyst EUROPT 4.2 throughout the run. These results are in good agreement with reports in the literature, where the consensus is that the isomerisation reaction is favoured at lower temperatures (3,8,151). According to Ako and Susu (141) and Parera et al. (151), iso-octane may be regarded as an intermediate product which can undergo subsequent conversion. This conversion to aromatics and light paraffins is increased by increasing temperature. The high conversion to iso-octane on catalyst EUROPT 4.2 is even more remarkable when we consider the chlorine content of the spent

catalyst. The chlorine level of catalyst EUROPT 4.2, critical in determining the activity of acid catalysed reactions, was only 0.56% after 28 hours-on-line. In comparison, analysis of the spent catalyst EUROPT 4.1 revealed a chlorine content of 0.77% after 34.5 hours-on-line (Table 5.2). Why catalyst EUROPT 4.2 should have lost more chlorine after a shorter time-on-stream at a lower temperature is unclear.

Hydrocracking activity on catalyst EUROPT 4 was similar at the two different reaction temperatures. At six hours-on-stream the combined yield of iso-butane, iso-pentane and iso-hexane was 8.0% for catalyst EUROPT 4.1 and 10.3% for catalyst EUROPT 4.2. At 29 hours-on-stream the corresponding values were 10.1% and 8.5% respectively (Tables 5.11, 5.15). These figures are surprising when it is considered that hydrocracking is favoured by increasing temperatures due to its high activation energy (2, 151).

Of particular interest in the hydrocracking results is the product distribution of C_4 - C_6 iso-paraffins determined for EUROPT 4.2, which is the reverse of that observed with catalyst EUROPT 4.1. Thus, iso-hexane was the principal iso-paraffin produced at the lower reaction temperature followed by iso-pentane and iso-butane respectively. In contrast, the order for catalyst EUROPT 4.1, at 500°C, was iso-butane, then iso-pentane, then iso-hexane (Figures 5.19, 5.29). The increased hydrogenolysis activity of catalyst EUROPT 4.2 at 450°C offers an explanation in that iso-octane, present in significantly larger quantities at 450°C, may have undergone increased hydrogenolysis at the lower reaction temperature, resulting in larger yields of iso-paraffins than would have been produced by hydrocracking alone. As multiple

hydrogenolysis, leading to light iso-paraffins, would be progressively less likely than single or double demethylation steps, the resultant order of iso-paraffin products from this source should be iso-heptane, iso-hexane, iso-pentane and iso-butane. This second source of iso-paraffin products containing fewer carbon atoms than the reactant could also account for the apparent equivalence in hydrocracking activity (eg. C_4i-P - C_6 i-P products) observed at 450°C and 500°C.

The formation of aromatic hydrocarbons was much attenuated at the lower reaction temperature. After 6 hours-on-stream the total yield of aromatics on catalyst EUROPT 4.2 was 11.1%. In comparison, a total aromatics' yield of 31.7% was determined for catalyst EUROPT 4.1 at the equivalent time-on-stream (Tables 5.11, 5.15). These results are not surprising when it is considered that higher temperatures favour both the kinetics and the thermodynamics of the dehydrocyclisation reaction (Section 1.1.3) (3,8,152).

In comparison with EUROPT 4.1, the principal aromatic product for much of the reaction over catalyst EUROPT 4.2 was toluene. The yield of toluene was exceeded by that of meta- and para-xylene only after a 21 hour reaction time. Toluene was presumably formed by the demethylation of a C_8-aromatic or by the dehydrocyclisation of n-heptane. In either case, the pre-eminence of toluene as an aromatic product on catalyst EUROPT 4.2 demonstrates the importance of the hydrogenolysis reaction at the lower reaction temperature. The increase in yield of C_8-aromatic hydrocarbons with time over catalyst EUROPT 4.1 was discussed earlier. Catalyst EUROPT 4.2 displayed similar behaviour and the yields of all three C_8-

aromatic hydrocarbons increased such that, after 28 hours-on-stream, the total yield of aromatics at 450°C had risen from 11.1% to 13.5%. As with catalyst EUROPT 4.1 it is conceivable that Re- catalysed fission of carbonaceous residues could be responsible for this increased aromatic yield.

According to the literature, conversion increases with reaction temperature (1,3,8,151). However, under the experimental conditions used (Section 5.1.4), catalyst EUROPT 4 did not exhibit a marked increase in conversion at the higher reaction temperature. On the contrary, despite the significant changes in product yield over catalyst EUROPT 4.2, during the first 10-15 hours of the reaction at 450°C, the overall conversion was greater than that determined for EUROPT 4.1 at 500°C. At six hours-on-stream, for example, the respective conversion figures were 76.5 and 68.5% (Tables 5.10, 5.18). Thus, despite the lower aromatisation activity over catalyst EUROPT 4.2, in terms of overall conversion this was compensated for by the greatly increased yield of isomerisation and hydrogenolysis products. The reforming reaction of n-octane on EUROPT 4.2 did not exhibit any increase in conversion as was observed with catalyst EUROPT 4.1. This was largely due to the much smaller increase in yield of aromatic products (eg. 2.1% vs. ca. 10.3% between 6 and 28 hours-on-stream) (Tables 5.10, 5.18). In consequence, after 10-15 hours reaction time, n-octane conversion on catalyst EUROPT 4.2 had declined slightly to 75.8%. In contrast, after 29.5 hours reaction time, n-octane conversion on the bimetallic catalyst at 500°C had increased to 78.4% (Figures 5.27, 5.37).

6.7 GENERAL CONCLUSIONS

Conversion on the GHI catalyst was signficantly lower than that determined on EUROPT 3. At 5 hours-on-stream, for example, total conversion was 21%, less than a third of that determined for catalyst EUROPT 3. The lower activity of the GHI catalyst is attributed to its different alumina support and to the less extensive activation procedure used in its preparation. Aromatisation was the principal reaction occurring on catalyst GHI, followed respectively by hydrocracking, hydrogenolysis and isomerisation. It is proposed that coke deposition on the stronger acid sites of the alumina support coupled with a loss of surface chlorine is responsible for increased isomerisation and reduced hydrocracking activity, whilst the observed decline in hydrogenolysis is believed to be caused by the blocking of active metal sites by coke.

Coke deposition was greater on EUROPT 3 than on the GHI catalyst, despite being on stream for a shorter period of time (26 hours vs. 40 hours). The results of n-octane reforming on the two monometallic Pt/Al_2O_3 catalysts would suggest that the different alumina supports of the catalysts (acidic function) are responsible for not only the greater coke deposition on EUROPT 3 but also the higher hydrocracking activity. The decrease in aromatisation activity observed on catalyst EUROPT 3 may be explained by deactivation of the metal function by coke deposition. Compared with the GHI catalyst, the lower Pt loading and increased metal dispersion of EUROPT 3 resulted in a low selectivity for the hydrogenolysis reaction (ca. 3% vs. ca. 13% at 5 hours). Consequently, the reaction selectivities on EUROPT 3 were in the order, aromatisation > hydrocracking > isomerisation > hydrogenolysis.

Compared with EUROPT 3 the reaction of n-octane on the bimetallic catalyst at 500°C showed important changes in product yields and selectivities . Of greatest significance was the high selectivity of EUROPT 4 for carbon-carbon bond scission. The observed increase in n-octane conversion may be explained by rhenium catalysed fission of carbonaceous residues giving rise to aromatic products. In comparison with EUROPT 3 the lower coke deposition on EUROPT 4 (0.65% w/w after 34.5 hours vs. 1.20% w/w2 after 26 hours) demonstrates that rhenium plays an active role in attenuating coke formation. With catalyst EUROPT 4 at 500°C, after 20 hours-on-stream the selectivities decreased in the order, aromatisation (52%) > hydrocracking (13%) > hydrogenolysis (5%) > isomerisation (2%), whilst at 450°C, the order was; aromatisation (17%) > hydrogenolysis (16%) > isomerisation (13%) > hydrocracking (12%). The higher hydrogenolysis activity of catalyst EUROPT 4 of 450°C is interpreted in terms of competing hydrogenolysis and coking reactions on the metal sites. The reduced aromatisation activity at the lower reaction temperature is compensated for by the increased selectivity towards hydrogenolysis and, in consequence, conversion is similar at 450 and 500°C.

REFERENCES

1. Edmonds, T., "Catalysis and Chemical Processes", (Pearce, R., Patterson, W.R., Eds.) London, Leonard Hill (1981).

2. Franck, J.P. and Martino, G.P., "Deactivation and Poisoning of Catalysts" (Oudar, J., Wise, H., Eds.) New York, Marcel Dekker Inc. (1985).

3. Le Page, J.F., "Applied Heterogeneous Catalysis Design, Manufacture and Use of Solid Catalysts", Paris, Editions Technip (1987).

4. American Petroleum Insititute Research Project 45, Sixteenth Annual Report (1954).

5. Sinfelt, J.H., Catalysis Science and Technology Vol. 1 (Anderson, J.R., Boudart, M., Eds.) New York, Springer-Verlag (1981).

6. Ciapetta, F.G., Dobres, R.H. and Baker, R.W., Catalytic Reforming of Pure Hydrocarbons and Petroleum Napthas. Catalysis Vol.6, p495-692, New York, Reinhold (1958).

7. Hettinger, W.P., Keith, C.D., Gring, J.L. and Teter, J.W., Ind. Eng. Chem. 47 719 (1955).

8. Gates, B.C., Katzer, J.R. and Schuit, G.C., "Chemistry of Catalytic Processes", p184-318, New York, McGraw-Hill (1979).

9. Arai, H., Seiyana, T., Harakawa, M. and Tominga, M., "Catalyst Deactivation" (Delmon, B., Froment, G.F., Eds.) Amsterdam, Elsevier (1980).

10. Guenin, M., Breysse, M. and Frety, R., J. Molec. Catal. 15 119 (1984).

11. Leonard, A.J., van Cauwelaert, F. and Fripiat, J.J., J. Phys. Chem. 71 695 (1967).

12. Peri, J.B. and Hannan, R.B., J. Phys. Chem 64 1526 (1960).

13. Peri, J.B., J. Phys. Chem. 69 220 (1965).

14. Parry, E.P., J. Catal. 2 371 (1963).

15. Pines, H. and Haag, W.O., J. Am. Chem. Soc. 82 2488 (1960).

16. Tanaka, M. and Ogasawara, S., J. Catal. 16 157 (1970).

17. Boehm, H.P., Adv, Catal. 16 179 (1966).

18. Figoli, N.S., Sad, M.R., Beltramini, J.N., Jablonski, E.L. and Parera, J.M. Ind. Eng. Chem. Prod. Res. Dev. 19 545 (1980).

19. Jacobson, R.L., Kluksdahl, H.E., McCoy, C.S. and Davis, R.W., Am. Pet. Inst., Div. Refin. Proc. 34th Midyear Meet, Chicago, 49 504 (1969).

20. Dowden, D.A., Catalysis, 2, Specialist Periodical Reports, 1 (1978).

21. den Hartog, A.J., Rek, P.J.M., Botman, M.J.P., de Vreugd, C. and Ponec, V., Langmuir 4 1100 (1988).

22. Johnson, M.F.L. and Le Roy, V.M., J. Catal. 35 434 (1974).

23. Webb, A.N., J. Catal. 39 485 (1975).

24. Yao, H.C. and Shelef, M., J.Catal. 44 392 (1976).

25. Bolivar, C., Charcosset, R., Frety, R., Primet, M., Tournayan, L., Betizeau, C., Leclercq, G. and Maurel, R., J. Catal. 45 163 (1976).

26. McNicol, B.D., J. Catal. 46 438 (1977).

27. Isaacs, B.H. and Peterson, E.E., J. Catal. 77 43 (1982).

28. Bolivar, C., Charcosset, R., Frety, R., Primet, M., Tournayan, L., Betizeau, C., Leclercq, G. and Maurel, R., J. Catal. 39 249 (1975).

29. Sermon, P.A. and Bond, G.C., Catal. Rev. 8 211 (1973).

30. Kramer, R. and Andre, M., J. Catal. 58 287 (1979).

31. Mieville, R.L., J. Catal. 87 437 (1984).

32. Wagstaff, N. and Prins, R., J. Catal. 59 434 (1979).

33. Jossens, L.W. and Petersen, E.E., J. Catal. 76 265 (1982).

34. Bolivar, C., Charcosset, H., Frety, R., Tournayan, L., Betizeau, C., Leclercq, G. and Maurel, R., J. Catal. 45 179 (1976).

35. Peri, J.B., J. Catal. 52 144 (1978).

36. Bertolacini, R.J. and Pellet, R.J., "Catalyst Deactivation" (Delmon, B., Froment, G.F., Eds.) Amsterdam, Elsevier, 73 (1980).

37. Kelly, M.J., Freed, R.L. and Swartzfager, D.G., J. Catal. 78 445 (1982).

38. Ciapetta, F.G. and Wallace, D.N., Cat. Rev. Sci. Eng. 5 (1) 88 (1971).

39. Kluksdahl, H.E., U.S. Patent 3415737 (1968).

40. Appesteguia, C.R. and Barbier, J., J. Catal. 78 352 (1982).

41. Coughlin, R.W., Hasan, A. and Kawakami, K., J. Catal. 88 163 (1984).

42. Menon, D.G. and Prasad, J., Proc. 6th. Intern. Congr. Catal. (Bond, G.C., Wells, P.B. and Tompkins, F.C., Eds.), p1601, The Chemical Society, London, 1977.

43. Sachtler, W.M.H. and van Santen, R.A., Adv. Catal. 26 69 (1977).

44. Boudart, M., Aldag, A., Benson, J.E., Dougharty, N.A. and Harkins, C.G., J. Catal 6 92 (1966).

45. Apesteguia, C.R., Brema, C.E., Garetto, T.F., Borgna, A. and Parera, J.M., J. Catal. 89 52 (1984).

46. Parera, J.M., Beltramini, J.N., Querini, C.A., Martinelli, E.E., Churin, E.J., Aloe, P.E. and Figoli, N.S., J. Catal. 99 39 (1986).

47. Sachtler, W.M.H. and Biloen, P., Div. Pet. Chem., Am. Chem. Soc., Seattle Meeting, March 20-25, 1983.

48. Barbier, J., Corro, G., Zhang, Y., Bournville, J.P. and Franck, J.P., App. Catal. 16 169 (1985).

49. Antos, G.J., Hayes, J.C. and Mitsche, R.T., U.S. Patent 4178268 (1979).

50. Dautzenberg, F.M., Helle, J.N., Bileon, P. and Sachtler, W.M.H., J. Catal. 63 119 (1980).

51. Rossini, F.D., Pitzer, K.S., Arnett, R.L., Braum, R.M. and Pimental, G.C., Selected values of physical and thermodynamic properties of hydrocarbons and related compounds. API Res. Project 44. Pittsburgh, Carnegie Press Inc. 1953.

52. Mills, G.A., Heinemann, H., Milliken, T.H. and Oblad, A.G., Ind. Eng. Chem. 45 134 (1953).

53. Weisz, P.B. and Swegler, E.W., Science 126 31 (1957).

54. Sinfelt, J.H., Hurwitz, H. and Rohrer, J.C., J. Phys. Chem. 64 892 (1960).

55. Sinfelt, J.H., Hurwitz, H. and Rohrer, J.C., J. Catal. 1 481 (1962).

56. Starnes, W.C. and Zabor, R.C., Symp. Div. Petrol. Chem. Am. Chem. Soc., Boston, Mass., April 5-10, 1959.

57. Corolleur, C., Corolleur, S. and Gault, F.G., J. Catal. 24 385 (1972).

58. Anderson, J.R., Adv. Catal. 23 1 (1973).

59. Anderson, J.R. and Avery, N.R., J. Catal. 7 315 (1967).

60. Rooeny, J.J., McKervey, M.A. and Samman, N.G., J. Catal. 30 330 (1973).

61. Gault, F.G., Adv. Catal. 30 1 (1981).

62. Sinfelt, J.H. and Rohrer, J.C., J. Chem. Eng. Data 8 (1) 109 (1963).

63. Sinfelt, J.H., Hurwitz, H. and Rohrer, J.C., J. Phys. Chem. 65 1458 (1961).

64. Silverstri, A.J., Naro, P.A. and Smith, R.L., J. Catal. 14 386 (1969).

65. Dautzenberg, F.M. and Platteeuw, J.C., J. Catal. 19 41 (1970).

66. Davis, B.H., Proc. 8th Intern. Congr. Catal. Vol.2, p469 (1984).

67. Pollitzer, E.L., Hayes, J.C. and Haensel, V., Am. Chem. Soc. Refining Petrol. Chem. Symp., New York, Sept. 7-12, 1969.

68. Barron, Y., Maire, G., Muller, J.M. and Gault, F.G., J. Catal. 5 428 (1966).

69. Sinfelt, J.H., Adv. Catal. 23 91 (1973).

70. Anderson, J.R. and Avery, N.R., J. Catal. 5 446 (1966).

71. Sinfelt, J.H., Catal. Rev. 9 (1) 147 (1974).

72. Augustine, S.M. and Sachtler, W.M.H., J. Catal. 106 417 (1987).

73. McKervey, M.A., Rooney, J.J. and Samman, N.G., J. Catal. 30 330 (1973).

74. Schaik, J.R.H. van, Dessing, R.P. and Ponec, V., J. Catal. 38 273 (1975).

75. Blakely, D.W. and Somorjai, G.A., J. Catal. 42 181 (1976).

76. Myers, C.G. and Munn, G.W., Ind. Eng. Chem. 50 1727 (1958).

77. Greensfelder, B.S., Voge, H.H. and Good, G.M., Ind. Eng. Chem. 41 2573 (1949).

78. Daniels, L.J., Sperling, P. and Rouquier, A.G., Oil Gas J., May 8, 78 (1972).

79. Parera, J.M., Figoli, N.S. and Traffano, E.M., J. Catal. 79 481 (1983).

80. Barbier, J., Marecot, P., Martin, N., Elassal, L. and Maurel, R., "Catalyst Deactivation" (Delmon, B., Froment, G.E., Eds.) Amsterdam, Elsevier, 93 (1980).

81. Barbier, J., "Catalyst Deactivation" (Delmon, B., Froment, G.E., Eds.) Amsterdam, Elsevier, 1 (1987).

82. Biswas, J., Bickle, G.M., Gray, P.G., Do, D.D. and Barbier, J., Cat. Rev. Sci. Eng. 30(2) 161 (1988).

83. Krebs, H.J. and Bonzel, H.P., Surf. Sci. 99 570 (1980).

84. Wolf, E.E. and Petersen, E.E., J. Catal. 46 190 (1977).

85. Davis, S.M. and Somorjai, G.A., Chem. Phys. Solid Surf. p217 (1982).

86. Salmeron, M. and Somorjai, G.A., J. Phys. Chem. 86 341 (1982).

87. Parmaliani, A., Frusteri, F., Nesterov, G.A., Paukshtis, E.A. and Giordano, N., "Catalyst Deactivation" (Delmon, B., Froment, G.E., Eds.) Amsterdam, Elsevier, 197 (1987).

88. Beltramini, J.N., Parera, J.M., Figoli, N.S, Churin, E.J. and Cabrol, R.A., Proceedings, 8th Int. Congress on Catalysis, Berlin, 1984. Berlin, Verlag Chemie, 593 (1984).

89. Barbier, J., Churin, E., Marecot, P. and Menezo, J.C., App. Catal. 36 277 (1988).

90. Davis, S.M., Zaera, F. and Somorjai, G.A., J. Catal. 77 439 (1982).

91. Espinat, D., Dexpert, H., Freund, E. and Martino, G., App. Catal. 16 343 (1985).

92. Trimm, D.L., App. Catal. 5 263 (1983).

93. Appleby, W.G., Gibson, J.W. and Good, G.M., Ind. Eng. Chem. Process. Des. Dev. 1 102 (1962).

94. Mackor, E.L., Hofstra, A. and Van der Waals, Trans. Faraday Soc. 54 66 (1958).

95. Trimm, D.L., "Deactivation and Poisoning of Catalysts" (Oudar, J., Wise, H., Eds.) New York, Dekker, 151 (1985).

96. Maire, G., Luck, F. and Aeinjach, S., Proceedings 8th Int. Congress on Catalysis, Berlin, 1984. Berlin, Verlag Chemie, 1984.

97. Levinter, M.E., Bortkevich, M.I., Zabotin, L.I. and Berkovie, L.M., Kinet, Katal., 16 221 (1975).

98. Wojciechowski, B.W., John, T.M. and Pachovsky, R.A., Adv. Chem. Ser. 133 422 (1974).

99. Margitfalvi, J., Göbölös, S., Talas, E., Hegedus, M. and Szedlacsek, P., "Catalyst Deactivation" (Delmon, B., Froment, G.E., Eds.) Amsterdam, Elsevier, 147 (1987).

100. Shum, K., Butt, J.B. and Sachtler, W.M.H., App. Catal. 11 151 (1984).

101. Biswas, J., Gray, P.G. and Do, D.D., App. Catal. 32 249 (1987).

102. Figoli, N.S., Beltramini, J.M., Martinelli, E.E., Sad, M.R. and Parera, J.M., App. Catal. 5 19 (1983).

103. Zhorov, Y.M., Panchekov, G.M. and Kartashev, Y.N., Kinet Katal. 21 (3) 776 (1980).

104. Cooper, B.J. and Trimm, D.L., "Catalyst Deactivation (Delmon, B., Froment, G.F., Eds.) Amsterdam, Elsevier, 63 (1980).

105. Beltramini, J.N., Martinelli, E.E., Churin, E.J., Figoli, N.S. and Parera, J.M., App. Catal. 7 43 (1983).

106. Franck, J.P. and Martino, G.P., "Deactivation and Poisoning of Catalysts" (Oudar, J., Wise, H., Eds.) Elsevier, Amsterdam, 43 (1980).

107. Barbier, J, Corro, G. and Zhang, Y., App. Catal. 13 245 (1985).

108. Lankhorst, P.P., de Jongste, H.C. and Ponec, V., "Catalyst Deactivation" (Delmon, B., Froment, G.F., Eds.) Elsevier, Amsterdam, 43 (1980).

109. Somorjai, G.A. and Blakely, D.W., Nature 258 580 (1975).

110. Bishara, A., Murad, K.M., Stanislaus, A., Ismail, M. and Hussain, S.S., App. Catal., 7 337 (1983).

111. Shum, V.K., Butt, J.B. and Sachtler, W.M.H., J. Catal. 99 126 (1986).

112. Carter, J.L., McVicker, G.B., Weissman, W., Kinak, W.S. and Sinfelt, J.H., App. Catal. 3 327 (1982).

113. Barbier, J., Marecot, P. and Churin, E., J. Catal. 126 228 (1990).

114. Margitfalvi, J. Göbölös, S., Kwaysser, E., Hegedus, M., Nagy, F. and Koltai, L., React. Kinet. Catal. Lett., 24 315 (1984).

115. Burch, R. and Mitchell, A.J., App. Catal. 6 121 (1983).

116. Christoffel, E.G. and Paal, Z., J. Catal. 73 30 (1982).

117. Barbier, J., App. Catal. 23 225 (1986).

118. Beltramini, J. and Trimm, D.L., App. Catal. 31 113 (1987).

119. Beltramini, J. and Trimm, D.L., App. Catal. 32 71 (1987).

120. Parera, J.M., Querini, C.A. and Figoli, N.S., App. Catal. 52 249 (1989).

121. Jackson, S.D., Willis, J., McLellan, G.D., Webb, G., Keegan, M.T., Moyes, R.B., Simpson, S., Wells, P.B. and Whyman, R., Part 1. Submitted for publication to J. Catalysis.

122. Hurst, N.W., Gentry, S.J. and Jones, A., Catal. Rev. Sci. Eng., 24 (2) 233 (1982).

123. Robertson, S.D., McNicol, B.D., Debaos, J.H., Kloet, S.C. and Jenkins, J.W., J. Catal. 37 424 (1975).

124. Spenadal, L., and Bondart, M., J. Phys. Chem. 64 204 (1960).

125. Dorling, T.A. and Moss, R.L., J. Catal. 5 111 (1966).

126. Dorling, T.A. and Moss, R.L., J. Catal. 7 378 (1967).

127. Jackson, S.D., Glanville, B.M., Willis, J., McLellan, G.D., Webb, G., Moyes, R.B., Simpson, S., Wells, P.B. and Whyman, R., Part II. Submitted for publication to J. Catalysis.

128. Barrett, E.P., Joyner, L.G. and Halenda, P.P., J. Am. Chem. Soc. 73 373 (1951).

129. Technical Bulletin Pigments No. 56, Degussa AG, Inorganic Chemical Products Division.

130. Carberry, J.J., "Chemical and Catalytic Reaction Engineering", New York, McGraw-Hill (1976).

131. Malet, P., Munuera, G. and Caballero, A., J. Catal. 115 567 (1989).

132. Gruber, H.L., J. Phys. Chem. 66 48 (1962).

133. Wells, P.B., App. Catal. 18 259 (1985).

134. Lemaitre, J.L., Menon, P.G. and Delannay, F., "Characterisation of Heterogeneous Catalysts", (Delanny, F., Ed.) New York, Marcel Dekker Inc. (1984).

135. Sing, K.S.W., "Characterisation of Catalysts", (Thomas, J.M., Lambert, R.M., Eds.) Chicester, John Wiley and Sons (1980).

136. Sing, K.S.W., Everett, D.H., Haul, R.A.W., Moscou, L., Pierotti, R.A., Rouquérol, J. and Siemieniewska, T., Pure and Appl. Chem. 57 (4) 603 (1985).

137. Gregg, S.J. and Sing, K.S.W., "Adsorption, Surface Area and Porosity" (Second Edition), London, Academic Press (1982).

138. Boudart, M., Aldag, A.W., Ptak, L.D. and Benson, J.E., J. Catal. 11 35 (1968).

139. Fogelberg, L., Gore, R. and Ranby, B., Acta Chem. Scand. 21 2041 (1967).

140. Davis, B.H. and Venuto, P.B., J. Catal. 15 363 (1969).

141. Ako. C.T. and Susu, A.A., J. Chem. Biotechnol. 36 519 (1986).

142. Sivasanker, S. and Padalkar, S.R., App. Catal. 39 123 (1988).

143. Shum, V.K., Butt, J.B. and Sachtler, M.H., J. Catal. 96 371 (1985).

144. Pines, H., "The Chemistry of Catalytic Hydrocarbon Conversions", New York, Academic Press (1981).

145. Ponec, V., Adv. Catal. 32 149 (1983).

146. Haining, I.H.B., Kemball, C. and Whan, D.A., J. Chem, Res. (M) 2056 (1977).

147. Van Trimpont, P.A., Marin, G.B. and Froment, G.F., App. Catal. 17 161 (1985).

148. Ludlum, L.H., Eischens, R.P., Prepr. - Am. Chem. Soc. Div. Pet. Chem., 375 (1976).

149. Margitfalvi, J., Hegedus, M., Göbölös, S., Kwaysser, E., Koltai, L. and Nagy, F., Acta Chim. Acad. Sci. Hung. 111 573 (1982).

150. Sachtler, W.M.H., J. Molec. Catal. 25 1 (1984).

151. Parera, J.M., Querini, C.A., Beltramini, J.N. and Figoli, N.S., App. Cat. 32 117 (1987).

152. Kugelmann, A.M., Hydrocarbon Processing, p95, January 1976.

153. Bond, G.C., Faraday Trans 1, 85 (11) 3767 (1989).